ABSTRACT

KWAG, SHINYOUNG. Probabilistic Approaches for Multi-Hazard Risk Assessment of Structures and Systems. (Under the direction of Dr. Abhinav Gupta.)

Performance assessment of structures, systems, and components for multi-hazard scenarios has received significant attention in recent years. However, the concept of multi-hazard analysis is quite broad in nature and the focus of existing literature varies across a wide range of problems. In some cases, such studies focus on hazards that either occur simultaneously or are closely correlated with each other. For example, seismically induced flooding or seismically induced fires. In other cases, multi-hazard studies relate to hazards that are not dependent or correlated but have strong likelihood of occurrence at different times during the lifetime of a structure. The current approaches for risk assessment need enhancement to account for multi-hazard risks. It must be able to account for uncertainty propagation in a systems-level analysis, consider correlation among events or failure modes, and allow integration of newly available information from continually evolving simulation models, experimental observations, and field measurements. This dissertation presents a detailed study that proposes enhancements by incorporating Bayesian networks and Bayesian updating within a performance-based probabilistic framework. The performance-based framework allows propagation of risk as well as uncertainties in the risk estimates within a systems analysis. Unlike conventional risk assessment techniques such as a fault-tree analysis, a Bayesian network can account for statistical dependencies and correlations among events/hazards. The proposed approach is extended to develop a risk-informed framework for quantitative validation and verification of high fidelity system-level simulation tools. Validation of such simulations can be quite formidable within the context of a multi-hazard risk assessment in nuclear power plants. The efficiency of this approach lies in identification of critical events, components, and systems that contribute to the overall risk. Validation of any event or component on the critical path is relatively more important in a risk-informed environment. Significance of multi-hazard risk is also illustrated for uncorrelated hazards of earthquakes and high winds which may result in competing design objectives. It is also illustrated that the number of computationally intensive nonlinear simulations needed in performance-based risk assessment for external hazards can be significantly reduced by using the power of Bayesian updating in conjunction with the concept of equivalent limit-state.

Probabilistic Approaches for Multi-Hazard Risk Assessment of Structures and Systems

by
Shinyoung Kwag

A dissertation submitted to the Graduate Faculty of
North Carolina State University
in partial fulfillment of the
requirements for the Degree of
Doctor of Philosophy

Civil Engineering

Raleigh, North Carolina

2016

APPROVED BY:

Dr. Nam Dinh	Dr. Mervyn Kowalsky
Dr. Kumar Mahinthakumar	Dr. Shamim Rahman

Dr. Abhinav Gupta
Chair of Advisory Committee

DEDICATION

Firstly, to My LORD GOD

Lastly, to my father, mother, wife and daughter

BIOGRAPHY

Shinyoung was born on October 28th, 1981 in Gwangju, South Korea. He received a Bachelor's of Civil Engineering from Sungkyunkwan University, South Korea in 2005 and a Master of Science degree from the Department of Civil Engineering at Seoul National University in 2010. During the Master's program, he also worked as an instructor at Awassa TVET College in Ethiopia for three years as part of KOICA (Korea International Cooperation Agency) volunteer program. Following the graduation from Master's program, he worked for four years at the research reactor division of KAERI (Korea Atomic Energy Research Institute) as a senior researcher. In August 2013, he joined the graduate school at NC State University to pursue a doctoral degree. During his time at NC State University, he worked as a research assistant in the CNEFS (Center for Nuclear Energy Facilities and Structures), a teaching assistant for "CE527: Structural Dynamics", and an instructor for "CE324: Structural Behavior and Measurements Laboratory". Upon graduation, he plans to continue working for KAERI. Shinyoung's research interests include structural dynamics, probabilistic risk assessment, engineering optimization, earthquake engineering, Bayesian statistics and Bayesian network.

ACKNOWLEDGEMENTS

″Being confident of this, that he who began a good work in you will carry it on to completion until the day of Christ Jesus (Philippians 1:6).”

Most of all, I praise my LORD GOD by giving me an opportunity to conduct doctoral level research and work towards satisfactory completion of all requirements. You are the one who start and finish such endeavors in my life. If compliments and honor are bestowed upon me, all belong to you GOD.

This research was supported by the Center for Nuclear Energy Facilities and Structures (CNEFS) at North Carolina State University. Resources for the center come from dues paying member organizations, Department of Civil, Construction and Environmental Engineering (CCEE) and College of Engineering at NCSU. I really appreciate the assistance of the Center by providing me with a good learning environment and the facilities throughout my time in graduate school. I would also like to thank all the staff members of the CCEE department for their help and support over the years.

I would like to express sincere appreciation for my advisor, Dr. Abhinav Gupta, for giving me the opportunity to pursue my graduate studies at NCSU and the freedom to explore and discover new areas in structural engineering research. This research would not have become a reality without his invaluable guidance and inspiration throughout my graduate studies. I would like to thank Dr. Nam Dinh, Dr. Shamin Rahman, Dr. Mervyn Kowalsky and Dr. Kumar Mahinthakumar for graciously agreeing to serve on my doctoral

committee and for their valuable suggestions. I would like to thank friends, colleagues and all my professors who helped me learn during my time in graduate school. These include Dr. Buseog Ju, Dr. Yonghee Ryu, Dr. Minho Kwon, Dr. Hyun-Su Kim, Dr. John Baugh, Payel Chatterjee, Harleen Sandhu, Saran Bodda, Ankit Dubey, Sugandha Singh, Vivek Samu, Heramb Mahajan and Greg Adams. I wish to thank my former advisor at Seoul National University, Professor Hyun-Moo Koh and my academic mentor at Hankyong National University, Professor Seung-Yong Ok for their support and guidance. I would like to thank Dr. Jinho Oh, PI Jong-Min Lee, Dr. Jeong-Soo Ryu and Vice President Young-Ki Kim at KAERI for allowing me to pursue a PhD degree at NCSU. I would like to thank all the members of Nehemiah and Saem-mul communities at Duraleigh Presbyterian Church.

I am indebted to my family for their selfless support. I would like to express my deepest gratitude to my parents (Hangi Kwag and Youngja Seol), parents in law (Namsik Lee and Bongsan Kim), and other family members (Miyoung Kwag, Buil Kim, Youngjin Lee, Hankwon Kim, and Younghwa Lee) for their unconditional love, prayer, sacrifices, support, and encouragement in my pursuit.

Last but not the least, I would really like to thank my wife. My journey through this doctoral degree would not have been possible without her unconditional love and wonderful support. Youngsun, your continuous encouragement to do my best inspired me and motivated me all along. My lovely daughter Yena, you are not old enough to read this since you are baby now, but later, you may realize that you too contributed to my achievements as a family member.

TABLE OF CONTENTS

LIST OF TABLES

PART II: Probabilistic Risk Assessment Framework for Structural Systems under Multiple Hazards using Bayesian Statistics

PART III: Probabilistic Risk Assessment Based Model Validation Method using Bayesian Network

PART IV: Efficient Seismic Fragility Analysis of Coupled System using Equivalent Elastic Limit State Concept and Bayesian Updating

LIST OF FIGURES

PART II: Probabilistic Risk Assessment Framework for Structural Systems under Multiple Hazards using Bayesian Statistics

PART III: Probabilistic Risk Assessment based Model Validation Method using Bayesian Network

PART IV: Efficient Seismic Fragility Analysis of Coupled System using Equivalent Elastic Limit State Concept and Bayesian Updating

PART V: Significance of Multi-Hazard Risk in Design of Buildings under Earthquake and Wind Loads

PART I

INTRODUCTION

1. Introduction

In United States, NIST (2007) specified that natural hazards either directly or indirectly result in approximately $55 billion of annual economic loss. FEMA (2008) estimated that hurricanes and earthquakes can annually cause direct economic loss of about $5.4 billion and $4.4 billion, respectively. The detailed quantitative estimation of casualties and economic loss for various hazards are outlined in Li et al. (2012). External hazards can be categorized into natural hazards and human induced hazards. Natural hazards include earthquakes, high winds (hurricane, cyclone, typhoon, and tornado), floods, wild fires, snow storms, volcanic activity, hail, lightning strike, heavy precipitation, and so on. The human induced hazards consist of military action, industrial sabotage, terrorist attacks, vehicle collision, aircraft crash, etc. This study relates primarily to risk assessment for multiple external natural hazards such as those due to earthquakes, high winds, and flooding.

2. Background

2.1 Probabilistic risk assessment under multiple hazards

The comprehensive procedure to calculate the risk metrics under a certain external hazard is called as probabilistic safety assessment (PSA) or probabilistic risk assessment (PRA) (USNRC, 1983; IAEA, 1992; EPRI, 1994; Ellingwood, 2001). Risk metric for a specific hazard is evaluated by convolution of fragility and hazard curve. The hazard curve expresses the annual probability of exceedance as a function of the intensity measure employed to

characterize the hazard. The fragility curve is expressed in terms of the conditional probability of failure as a function of the intensity measure for a given hazard and is evaluated by considering uncertainties in the mechanistic model of a component or system through the use of empirical, experimental, and/or numerical data. Specifically, US Nuclear Regulatory Commission and International Atomic Energy Agency have issued guidelines for conducting a full scope PRA (EPRI 1994, IAEA 1992). In this methodology, the plant level risk is calculated by a combining the component and subsystem fragility curves through a systems analysis. Typically, fault and event trees are used for conducting the systems analysis to combine the fragilities and convoluting with the hazard curve. Existing guidelines consider each external hazard independently. The existing approach can be applied directly to a multi-hazard scenario only under the assumption of statistically independent and mutually exclusive events.

Only a few studies have been conducted to consider multi-hazard scenario in structural design or risk-assessment. Ellingwood (2001) proposed a framework to calculate risk due to competing hazards based on total probability theorem. Subsequently, Ayyub et al. (2007) suggested the critical asset and portfolio risk analysis framework for evaluating risks under multiple hazards. Li and Ellingwood (2009) conducted multi-hazard risk assessment for wood-frame structures subjected to earthquake and hurricane. Beavers et al. (2009) studied the overall risk to bridges due to earthquakes, storm surge, and ship collision. Kameshwar and Padgett (2014) proposed a multi-hazard risk assessment for bridges subjected to earthquake and hurricane. In all these studies, risk is calculated for each

individual hazard using the traditional approach wherein the hazard curve is convoluted with the fragility data. The effect of multiple hazards on the overall risk is computed by using the total probability theorem. The fundamental assumption in using the total probability theorem is that individual hazards are statistically independent, mutually exclusive, and collectively exhaustive. Therefore, this approach cannot be used for assessment of risks associated with multi-hazard scenarios such as seismically induced internal flooding or flooding induced fires in which the undesirable response of the plant to one hazard acts as the initiator of another hazard making them correlated events/hazards.

2.2 Validation of system-level simulation models

Given the events at Fukushima-Daiichi nuclear power plant, there is an increased emphasis on using high fidelity simulation tools to evaluate the vulnerability of nuclear facilities subjected to external hazards. Availability of sophisticated computer models capable of simulating multi-physics multi-scale phenomena has increased the need for verification and validation of such high fidelity simulations. In the current practice of model validation, a graphical comparison is employed to determine the degree of agreement between the simulation predictions and the actual observations in the component level. The statistical approaches using confidence bounds, hypothesis testing and inference have been explored as quantitative approaches. In most cases and particularly in nuclear power plants, it is not only impractical but almost impossible to conduct system-level experiments. The recommended approach for validation of such large-scale system simulations is to use a building block

approach (AIAA Guide, 1998; Oberkampf and Smith, 2014). Some studies (Mahadevan and Rebba, 2005; Jiang and Mahadevan, 2007) have used reliability and Bayesian statistics to validate the computational system model when the system behavior can be characterized by mechanics based mathematical equations. A general framework to validate computer model for crashworthiness (Bayarri et al., 2005) is based on Bayesian hierarchical modeling. Bayesian approach has also been applied to the validation of agent-based simulation modeling (Korb et al., 2013). In the context of the various existing studies, the validation problem continues to be a challenging one due to few different reasons. First, the existing definitions of a quantitative validation metric need significant improvement especially for addressing validation problems that have large degree of uncertainties associated with them. Second, the existing studies are restricted to problems in which the system level simulation model is characterized mathematically. Such a mathematical description is neither available nor possible especially for evaluating the performance of nuclear systems subjected to external hazards. In addition to these restrictions, current approaches do not identify whether or not an improvement in the validation of a given component or subsystem is important/critical with respect to system level performance.

2.3 Equivalent linearization methods in seismic fragility analysis

Theoretically, a seismic fragility curve can be developed through a large amount of empirical, experimental, or simulation data. In reality, the experience or experimental data for large systems is usually not available or available in a very limited sense. Therefore, seismic

fragility is evaluated by conducting probabilistic simulations in which multiple nonlinear time history analyses of a large-scale simulation model are performed at different levels of seismic intensity parameter. A large number of computationally rigorous nonlinear time history analyses makes this process highly inefficient. Consequently, equivalent linearization approach can be highly efficient for calculating seismic fragility. Many equivalent linearization methods have been developed over the years. Proppe et al. (2003) and Crandall (2006) provide a good summary of existing methods which can be broadly categorized into following:

- Equivalent viscous damping method
- Elastic strain energy method
- Empirical method
- Stochastic linearization method
- Secant stiffness method
- Equivalent elastic limit state method

Most researches in equivalent linearization methods have analytically or empirically focused on how to linearize the system model by minimizing the average error between the responses of nonlinear and the linearized system. In this regard, Tadinada and Gupta (2016) proposed a novel concept of equivalent limit-state (ELS) to reduce the computational effort needed in such fragility studies. However, their approach considered only a bilinear curve to model

nonlinearities. This methodology needs enhancements to account for uncertainties, more realistic hysteretic nonlinear models, and effect of non-classical damping.

2.4 Multi-hazard risk assessment for earthquake and wind in tall building

The research on the design and retrofit of buildings subjected to multiple hazards of earthquake and wind have mostly focused on mitigating the effects of each hazard independently which is also implemented in the codes and standards especially in favor of designing the building for a single hazard that corresponds to higher load. The premise for such an approach is that these two hazards are not dependent or correlated but have strong likelihood of occurrence at different times during the lifetime of a structure. Recent studies have identified limitations of such an approach. Wen and Kang (2001) illustrate that even if a single hazard (earthquake or wind) dominates the design loads, the less dominant hazard can contribute significantly to the overall design. Duthinh and Simiu (2009) and Crosti et al. (2010) show that ASCE 7-05 requirements are not risk consistent. They illustrate that the overall risk for combined earthquake and wind loads in regions susceptible to both strong earthquakes and extreme winds can be more than twice of that calculated by considering only a single dominant hazard. Subsequently, these studies propose modifications to ASCE 7-05. Chen (2012) considered mid- to high-rise buildings to study the inherent wind resistance of a building designed for earthquake loads as well as the inherent seismic resistance of a building designed for wind loads. It illustrates that certain solutions to ensure safety against a single dominant hazard, such as wind, can create competing design objectives with respect to the

other hazard, such as earthquake. Li et al. (2012) also shows that the design and retrofit strategies to improve a structure's performance for withstanding a single hazard can make the structure more vulnerable to the other non-dominant hazards.

3. Research Objectives

The primary objective of this research is to develop a new probabilistic risk assessment (PRA) framework for structural systems subjected to multiple hazards. This framework aims to amalgamate existing PRA risk assessment approach and the system risk analysis technique of Bayesian network including Bayesian inference. Within this PRA framework, a related objective is to propose a PRA based model validation method combining the Bayesian network based PRA approach with a probabilistic index as a degree of validation in order to quantitatively assess and efficiently improve the validation metric of system-level simulation. An additional objective is to develop an efficient seismic fragility analysis method for the coupled structure-equipment-piping systems in order to reduce the number of nonlinear analyses of coupled structural systems under earthquake hazard for calculating the seismic fragility curve. Lastly, another objective is to develop a performance-based approach to determine whether the performance of a building is governed by a multi-hazard scenario for earthquake and high wind loads or only by a single dominant hazard.

4. Proposed Research

The following specific research tasks are proposed to achieve the objectives of this research.

4.1 Probabilistic risk assessment framework for structural system under multiple hazards using Bayesian statistics

The specific steps needed to address this aspect of the proposed research are:

- Study the existing PRA methodologies for multiple hazard risk assessment.
- Identify limitations of the current approaches:
    - Existing studies are conducted for only a single hazard or combine risks from multiple hazards by using total probability theorem which considers each hazard as a statistically independent mutually exclusive event. Statistical correlations and conditional relationships among events and hazards cannot be accounted for in existing approaches.
    - Incorporation of newly observed data or scenario for vulnerabilities beyond design basis is not directly possible in existing approaches.
- Introduce fault tree analysis (FTA) for a system-level reliability or system sequence analysis. Some of the limitations in FTA are:
    - It cannot consider uncertainties in basic events.
    - It characterizes relationships between events through logic gates. It cannot accommodate newly observed data or vulnerabilities beyond design basis.

- Incorporate Bayesian network and Bayesian inference concepts in order to address the limitations of current PRA and fault tree analysis.
- Illustrate the effectiveness of the proposed framework by application to simple representative and realistic examples. The purpose would be to illustrate that the proposed framework can consider statistical dependencies and correlations among events, include the additional information at any level, and even allow analysis for vulnerabilities beyond the design basis.

4.2 PRA based model validation method using Bayesian network

It is proposed to develop a quantitative approach to validation of high fidelity system-level simulations within a risk-informed performance based decision environment. The main tasks needed to accomplish the objectives of this research consist of three main phases: (1) Probabilistic risk assessment based on Bayesian network and identification of critical sequences for the system risk, (2) Select important component-level simulation models within the identified critical path from Bayesian network based PRA, (3) Calculate a system-level quantitative validation metric by introducing the concept of overlapping coefficient. Bayesian updating is employed to revalidate by incorporating enhanced simulation results or new experimental data. Specific tasks needed in this research are outlined as follows:

- Study the current model validation approaches.
- Identify the failure modes for system.

- Construct Fault Tree (FT) for system risk analysis.
- Map fault tree into Bayesian network.
- Evaluate the upper level risks based on component level risks, and identify the most critical scenario/path for the system risk.
- Select simulation models from the identified critical path.
- Introduce an overlapping coefficient (OC) as a quantitative validation metric.
- Calculate OCs at component-level using simulation & experimental data.
- Establish the relationship between lower level and upper level events using either mechanistic models or generating response surface.
- If new data is available at any levels, update OCs at all levels based on this data.
- Evaluate system-level OCs by propagating component level fragilities through the Bayesian network.
- Compare the system-level OC with a desired predefined acceptance criterion.
- Illustrate the effectiveness of this method by application to several examples.

4.3 Efficient simulation based seismic fragility assessment by using equivalent limit state concept and Bayesian updating

The specific tasks needed to achieve the objectives of this research are:

- Introduce equivalent limit-state (ELS) concept and Bayesian updating in the context of seismic fragility assessment.

- Incorporate a numerical model for representing nonlinear hysteretic behavior of secondary system.
- Demonstrate the efficiency of ELS concept using simple coupled systems.
- In order to generalize the efficiency of ELS concept, consider several different coupled systems having different tuning ratios between primary and secondary system, nonlinearities, ductility and damping ratios of the secondary system.
- Propose a modified closed-form equation for ELS.
- Application of the methodology using the closed-form equation and Bayesian updating to increase the efficiency.
- Demonstrate the effectiveness of the proposed methodology through applications to different configurations of primary-secondary systems. Illustrate that the proposed methodology can significantly reduce the computational efforts and also arrive at accurate seismic fragility curve compared to that calculated from comprehensive nonlinear time history analyses.

4.4 Significance of multi-hazard risk in design of buildings under earthquake and wind loads

In this research, we propose a novel performance-based framework. The proposed framework uses (a) site-dependent hazard intensity for a given site, (b) the building configuration/height, and (c) performance criteria that governs the design of building for each individual hazard. This framework can be used to determine if a particular building

structure requires any retrofitting especially in cases where both the earthquake and the wind hazards govern the design and performance of a building whose initial design may not have necessarily considered such a multi-hazard scenario. In addition, a retrofit strategy using energy dissipation devices is introduced and optimal design of these is investigated. The specific tasks needed are outlined below:

- Study the current practice for the design of buildings in a multi-hazard region.
- Identify the limitations of current approaches.
- Develop a probabilistic framework that combines the performance functions with the multi-hazard intensity measures to enable a graphical representation of the problem.
- As an application of the proposed framework, consider multiple geographical sites, and obtain the design hazard information of earthquake and wind at these sites.
- Develop the input time history loadings corresponding to design information on earthquake and wind hazard.
- Define a tall building structure as a target structure of interest.
- Identify the performance limits and formulate the performance functions.
- Evaluate the performance functions for the designated sites and develop the multiple hazard (both earthquake and high wind) based graphical representation for the target building structure.

- To illustrate the differences in solutions for a multi-hazard risk scenario, two adjacent buildings are considered as a target structure and the two buildings are connected by supplemental damping devices as a retrofit solution.
- Finally, compare the optimal damper design considering a single hazard with a multi-hazard scenario.

5. Organization

This dissertation primarily consists of four manuscripts which will be submitted for possible publications in peer reviewed journals. The first manuscript (Part II) of the dissertation presents the probabilistic risk assessment (PRA) framework for structural systems under multiple hazards using Bayesian statistics. The second manuscript (Part III) in this dissertation discusses the PRA based model validation method. The third manuscript (Part IV) in this dissertation addresses the development of efficient seismic fragility assessment for the coupled building-equipment-piping system using equivalent limit state concept. The fourth manuscript (Part V) in this dissertation describes the framework for characterizing the significance of multi-hazards in design of buildings under earthquake and wind loads. The last part (Part VI) of this dissertation gives a summary and conclusions of this research and the anticipated future research associated with these topics.

References

AIAA, "Guide for the verification and validation of computational fluid dynamics simulations," *American Institute of Aeronautics and Astronautics*, AIAA-G-077-1998, Reston, VA, 1998.

ASCE, Minimum design loads for buildings and other structures, ASCE/SEI 7-05/-10, Reston, VA, US.

Ayyub BM, McGill WL, and Kaminskiy M, "Critical asset and portfolio risk analysis: An all-hazards framework." *Risk Analysis*, 27(4), 789–801, 2007.

Bayarri MJ, Berger JO, Kennedy MC, Kottas A, Paulo R, Sacks J, Cafeo JA, Lin, CH, and Tu J, "Bayesian validation of a computer model for vehicle crashworthiness," *National Institute of Statistical Sciences (NISS)*, Technical Report Number 163, 2005.

Beavers JE, "Multihazard issues in the central United States: Understanding the hazards and reducing the losses." *ASCE Council on Disaster Risk Management Monograph No. 3*, Reston, VA, US, 2009.

Chen EY, *Multi-hazard design of mid- to high-rise structures*, M.S. thesis, Univ. of Illinois, Urbana-champaign, IL, 2012.

Crandall SH, "A half-century of stochastic equivalent linearization," *Structural Control and Health Monitoring*, 13(1), 27-40, 2006.

Crosti C, Duthinh D, and Simiu E, "Risk consistency and synergy in multihazard design," ASCE Journal of Structural Engineering, 137(8), 844-9, 2010.

Duthinh D and Simiu E, "Safety of structures in strong winds and earthquakes: multihazard considerations," *ASCE Journal of structural engineering*, 136(3), 330-3, 2009.

Ellingwood BR, "Acceptable risk bases for design of structures." *Progress in Structural Engineering and Materials*, 3(2), 170–179, 2001.

EPRI, "Methodology for developing seismic fragilities," *TR-103959*, Electric Power Research Institute, 1994.

FEMA, "HAZUS-MH estimated annualized earthquake losses for the United States," *FEMA 366*, Federal Emergency Management Agency, 2008.

IAEA, "Procedures for conducting probabilistic safety assessments of nuclear power plants (Level 1)," *Safety Series No. 50-P-4*, International Atomic Energy Agency, 1992.

Jiang X and Mahadevan S, "Bayesian risk-based decision method for model validation under uncertainty," *Reliability Engineering & System Safety*, 92(6), 707-718, 2007.

Kameshwar A, and Padgett JE, "Multi-hazard risk assessment of highway bridges subjected to earthquake and hurricane hazards," *Engineering Structures*, 78, 154-166, 2014.

Korb KB, Geard N, and Dorin A, "A Bayesian approach to the validation of agent-based models," *Epistemology, & Teleology for Model. & Simulation*, ISRL 44, 255-269, 2013.

Li Y and Ellingwood BR, "Framework for multihazard risk assessment and mitigation for wood-frame residential construction." *ASCE Journal of Structural Engineering*, 135(2), 159–168, 2009.

Li Y, Ahuja A, and Padgett J, "Review of methods to assess, design for, and mitigate multiple hazards," *ASCE Journal of Performance of Constructed Facilities*, 26(1), 104–117, 2012.

Mahadevan S and Rebba R, "Validation of reliability computational models using Bayes networks," *Reliability Engineering & System Safety*, 87(2), Pages 223-232, 2005.

NIST, *Measurement sciences for disaster-resilient structures and communities*, National Institute of Standards and Technology, 2007.

Oberkampf WL and Smith BL, "Criteria for assessing fluid dynamics validation experiments," *American Society of Mechanical Engineers Third Annual Symposium on Verification and Validation*, Las Vegas, Nevada, 6 – 8 May, 2014.

Proppe C, Pradlwarter HJ, and Schuëller GI, "Equivalent linearization and Monte Carlo simulation in stochastic dynamics," *Probabilistic Engineering Mechanics*, 18(1), 1-15, 2003.

Tadinada SK and Gupta A, "Structural fragility of large-scale piping systems using equivalent elastic time-history simulations," *Structural Safety, submitted.*

US NRC, "PRA Procedure Guide – A guide to the performance of probabilistic risk assessments for nuclear power plants," *NUREG/CR-2300*, US Nuclear Regulatory Commission, 1983.

Wen YK and Kang YJ, "Minimum building life-cycle cost design criteria. I: Methodology," *ASCE Journal of Structural Engineering*, 127(3), 330-337, 2001.

PART II

PROBABILISTIC RISK ASSESSMENT FRAMEWORK FOR STRUCTURAL SYSTEMS UNDER MULTIPLE HAZARDS USING BAYESIAN STATISTICS

Shinyoung Kwag and Abhinav Gupta

ABSTRACT

Conventional probabilistic risk assessment (PRA) methodologies (USNRC, 1983; IAEA, 1992; EPRI, 1994; Ellingwood, 2001) conduct risk assessment for different external hazards by considering each hazard separately and independent of each other. The risk metric for a specific hazard is evaluated by a convolution of the fragility and the hazard curves. The fragility curve for basic event is obtained by using empirical, experimental, and/or numerical simulation data for a particular hazard. Treating each hazard as an independent mutually exclusive event can be inappropriate in some cases as certain hazards are statistically correlated or dependent. Examples of such correlated events include but are not limited to flooding induced fire, seismically induced internal or external flooding, or even seismically induced fire. In the current practice, system level risk and consequence sequences are typically calculated using a Fault Tree Analysis (FTA) that uses logic gates to express the causative relationship between events. Furthermore, the basic events in an FTA are considered as independent. Therefore, conducting a multi-hazard PRA using a Fault Tree is quite impractical. In some cases using an FTA to conduct a multi-hazard PRA can even be inaccurate because an FTA cannot account for uncertainties in probabilistic distributions of basic events by itself and the use of logic gates ("AND" and "OR" gates) limits the consideration of statistical correlations or dependencies between the events. An additional limitation of an FTA based PRA lies in its inability to easily accommodate newly observed data and calculation of updated risk or accident scenarios under the newly available

information. Finally, FTA is not best suited for addressing beyond design basis vulnerabilities. In this paper, we present the results from a study on multi-hazard risk assessment that is conducted using a Bayesian network (BN) with Bayesian inference. The framework can consider general relationships among risks from multiple hazards, allows updating by considering the newly available data/information at any level, and evaluate scenarios for vulnerabilities due to beyond design bases events.

1. Introduction

In a probabilistic safety assessment (PSA) or probabilistic risk assessment (PRA) (USNRC, 1983; IAEA, 1992; EPRI, 1994; Ellingwood, 2001), the risk metric for a specific hazard is evaluated by convolution of fragility and hazard curves. The hazard curve expresses the annual probability of exceedance as a function of the intensity measure employed to characterize the hazard. The fragility curve of basic event is expressed in terms of the conditional probability of failure as a function of the intensity measure for a given hazard and is obtained by considering uncertainties in the available physical model of a component or system through the use of empirical, experimental, and/or numerical data. US Nuclear Regulatory Commission and International Atomic Energy Agency have issued guidelines for conducting a full scope PRA (EPRI 1994, IAEA 1992). In this methodology, the plant level risk is calculated by a combining the component and subsystem fragility curves through a systems analysis. Typically, fault and event trees are used for conducting the systems analysis to combine the fragilities and convoluting with the hazard curve.

The currently used methodology is focused on addressing the risk associated with each external hazard separately. Multi-hazard scenarios have not been considered in a traditional PRA study because the possibility of simultaneous occurrence of two different extreme events such as earthquake and hurricane or earthquake and floods is extremely rare and almost impossible. However, there have been several instances of closely-related multiple hazards that have resulted in significant damage or a major disaster. Seismically

induced flooding due to tsunami following the great Tohoku earthquake caused the disaster at Fukushima Daiichi nuclear plant (Aoki and Rothwell, 2013). One may argue that such a multi hazard scenario though very recent is also quite rare and limited to very specific regions in the world. On the other hand, there are many instances of significant damage or a major disaster due to seismically induced internal flooding such as those due to failure of fire piping or tanks in a hospital or other industrial facilities. Seismically induced fires are widely acknowledged. Similarly, hurricane induced storm surge flooding and high winds pose simultaneously occurring multiple hazards that can have a significant impact on not only the design of a nuclear plant but also on the accident management and emergency response.

Only a limited number of studies have been conducted to consider multi-hazard scenario in the design or risk-assessment. Ellingwood (2001) proposed a framework to calculate risk due to competing hazards based on total probability theorem. Subsequently, Ayyub et al. (2007) suggested the critical asset and portfolio risk analysis framework for evaluating risks under multiple hazards. Li and Ellingwood (2009) conducted multi-hazard risk assessment for wood-frame structures subjected to earthquake and hurricane. Beavers et al. (2009) studied the overall risk to bridges due to earthquakes, storm surge, and ship collision. Kameshwar and Padgett (2014) proposed a multi-hazard risk assessment for bridges subjected to earthquake and hurricane. The common theme in all these studies is that the risk is calculated for each individual hazard using the traditional approach wherein the hazard curve is convoluted with the fragility data. The effect of multiple hazards on the overall risk is computed by using the total probability theorem.

The fundamental assumption in using the total probability theorem is that individual hazards are statistically independent, mutually exclusive, and collectively exhaustive. Therefore, it cannot be used for assessment of risks associated with multi-hazard scenarios such as seismically induced internal flooding or flooding induced fires in which the undesirable response of the plant to one hazard acts as the initiator of another hazard making them correlated events. It can be argued that a well designed plant should not exhibit such failures. Traditional PRAs do not exhibit such correlated events because failures of these nature are not encountered in a plant that is well designed to withstand the design basis events. On the contrary, identifying and suppressing such events are the primary reason for the strong emphasis in recent years on evaluating vulnerability beyond design basis. The response of a plant's structures, systems, and components to beyond design basis events is quite different from that to the events at or below the design basis levels. Consequently, there is need for developing multi-hazard risk assessment methodologies to account such correlated events beyond the design basis levels and to determine a plant's vulnerability. As additional studies are conducted and new data becomes available, such methodologies should allow easy and continued updating of plant risk.

A systems analysis is typically used to consider the various aspects mentioned above. Some of the typical tools used for conducting such systems analysis are fault tree analysis (FTA), event tree analysis, Petri net, PNET, logic tree, decision tree, etc. Out of these, a typical PRA in a nuclear power plant relies heavily on FTA for modeling and assessment of system level failure. The system-level failure is typically referred to as the "top event (TE)."

A fault-tree based approach can be broadly divided into two parts: (1) a qualitative development of the logic diagram which is then used to write an expression for the TE and determine the minimal cut-sets; (2) a quantitative evaluation based on probabilities of occurrence of basic events to determine the probability of occurrence of the TE (and of any intermediate-level events) together with a determination of the importance measure for each minimal cut-set. The importance measures are used to identify critical events contributing significantly to the probability of system failure and to identify the weak links. A traditional implementation of fault-tree analysis is quite static in nature and some of its limitations are: (1) it does not allow an explicit consideration of uncertainties in the probabilities of basic events, (2) the events are related through logic gates (AND/OR gates) which prohibits consideration of statistical dependencies and correlated events, and (3) it was not developed to consider and identify updated scenarios due to availability of new data/information particularly for events beyond design basis.

The limitations in FTA mentioned above are generally overcome by combining it with other techniques. For example, the uncertainties in basic event probabilities are considered by implementing an FTA in conjunction with Monte-Carlo simulation (Rasmussen, 1975) or Fuzzy set theory (Tanaka et al., 1983; Singer, 1993; etc.). Consideration of the statistical correlations and relationships among events beyond what can be represented by logical gates is possible by converting a fault-tree into a Bayesian network (BN). The concept of Bayesian Network was developed to directly manage various statistical dependencies that cannot otherwise be represented by a fault-tree. Bobbio et al. (2001)

proposed the mapping method which converts a fault tree into a corresponding Bayesian network (BN). Finally, Bayesian updating has been found to be quite effective for accommodating the new data/information (Hamada et al., 2004; Wilson et al., 2007; Kelly and Smith, 2009). Consequently, in this paper we explore the use of a Bayesian Network and Bayesian Inference based approach for multi-hazard risk assessment so as to account for statistical dependencies. The premise is to explore if this framework can allow identification of critical events for both the design basis risk as well as for the beyond design basis vulnerabilities. Illustrative examples are used to identify differences in possible solutions evaluated from the traditional FTA methodology compared to a Bayesian Network based risk assessment.

2. Summary of Current PRA Methodology

In the current methodology, the overall risk (i.e. annual probability of failure) for an individual hazard is evaluated by convolution of hazard curve and the corresponding fragility as following:

$$P_f = \int P_{f|\lambda} \cdot \left| \frac{dH(\lambda)}{d\lambda} \right| d\lambda \qquad (1)$$

in which λ is a hazard intensity parameter, $P_{f|\lambda}$ is the fragility curve, and $H(\lambda)$ represents the hazard curve. The hazard curve expresses the probability of annual exceedance in a domain of the intensity measure used for characterizing the external hazard. The fragility curve for

basic events is obtained by using empirical, experimental, and/or numerical simulation data. It represents the conditional probability of failure under each hazard's intensity. The system-level risk is calculated by employing either a series-parallel system as a simplistic representation of the complete system or by conducting a fault tree analysis in which the events are assumed to be statistically independent, mutually exclusive, and collectively exhaustive.

2.1 Probabilistic Hazard Analysis

In order to develop a hazard curve, the hazard is characterized in terms of an engineering design parameter which also characterizes the intensity of the hazard. For example, the intensity measures that have been used to characterize earthquake intensities are one or a combination of its magnitude (M_w), peak ground acceleration (PGA) or spectral acceleration (SA). Similarly, the wind hazard is typically characterized in terms of maximum wind velocity and flood hazard by the elevation of water levels for a specified return period. If multiple sources can initiate the hazard at a given site, then a probabilistic analysis is conducted to identify and integrate the hazard from each source, their relative size, propagation characteristics from source to the site, prediction model, etc. The end result is a hazard curves (H (λ)).

Seismic Hazard: The probabilistic seismic hazard analysis (PSHA) focuses on quantifying uncertainties in the sources, size, distance, and ground motion characteristics of future earthquakes and incorporating this information to produce a complete description of the

distribution of possible ground motions that can occur at a site of interest. The end result of the PSHA is represented by seismic hazard curves where the annual rates of exceedance are plotted against a ground motion intensity parameter such as moment magnitude (M_w), peak ground acceleration (PGA) or spectral acceleration (SA). A detailed description for conducting PSHA is described in McGuire (2002). The US Geological Survey (USGS, http://earthquake.usgs.gov/hazards/products/) provides hazard information and hazard curves at any site of interest.

Wind Hazard: A probabilistic wind hazard analysis (PWHA) expresses the annual rates of exceedance with respect to average wind speed during a gust of 3 second or less in the open terrain at a 10 m height. A PWHA is based on extrapolation from various return period of tropical cyclones (typhoons and hurricanes) and wind field models developed from recorded data. The detailed guidelines are represented in IAEA safety guide SSG-18 (IAEA, 2011). Specifically for hurricanes, several wind models have been proposed to estimate wind speeds corresponding to different return periods. A Weibull distribution is revealed to be an appropriate model for hurricane wind speeds (Batts et al., 1980; Georgiou, 1985; Peterka and Shahid, 1998; Vickery et al., 2000). Li and Ellingwood (2006) obtained the parameters for the Weibull distribution at three different geographical locations namely, southern Florida, Charleston, SC, and Boston MA.

Flood Hazard: A probabilistic flood hazard analysis (PFHA) evaluates the annual exceedance probabilities for different external flood severities in terms of a site-specific probabilistic model using available data. The hazard curves gives the annual exceedance

probabilities with respect to flood levels (median, mean and other confidence levels). The various methodologies used for conducting a PFHA can be mainly categorized into two groups: the simple statistical methods and the detailed probabilistic methods. The statistical methods utilize extrapolation of historical data and estimates probabilities for flood events that have annual exceedance of 1e-2 or 5e-3. The detailed probabilistic methods combine hydrologic and statistical models as well as the corresponding uncertainties. The detailed description for PFHA is given in the IAEA safety guide (IAEA, 2011) and the corresponding technical report (IAEA, 2015).

2.2 Fragility Analysis

The fragility of a structure, system, or component (SSC) is defined as the conditional failure probability, $P_{f|\lambda}$, to attain or exceed a specified performance function, G, under a given measure of specific intensity parameter λ. Mathematically,

$$P_{f|\lambda} = P\left(G < 0 \mid \lambda\right) \tag{2}$$

G is a function of the random variables representing uncertainties in material properties, physical and mechanistic models, and loading conditions. It can be described in a simplistic form as:

$$G\left(S, R\right) = S - R \tag{3}$$

where *S* represents the "strength" or "capacity" corresponding to the specified loading condition and *R* represents the "maximum response" or "demand" corresponding to the given hazard intensity parameter. Eq. (3) can be written in terms of various different approaches such as physics or mechanics based models, experimentally obtained data, empirical relations, simulations, or a combination of these. The Eq. (3) can then be solved in many different ways such as Monte Carlo simulation, First/Second order reliability methods, random vibration based approach, statistical inference approach, etc. In most implementations, the fragility curves are represented as the cumulative distribution function for a log-normal distribution.

3. Summary of Fault Tree Analysis and Bayesian Representation

3.1 Fault Tree Analysis (FTA)

A fault tree diagram is a graphical decomposition of an undesirable event representing system failure (denoted as top event TE) into intermediate events and basic events through the use of logical gates (AND and OR gates). The basic events are characterized by Boolean states that represent "failure" or "safe" states. The basic events are considered to be statistically independent as well. The basic events are connected through the logic gates to characterize intermediate events which are also connected through the logic gates.

To begin with, a qualitative evaluation is used to develop the logical expression for the TE. Boolean algebra is used to obtain the minimal cut-sets. The order of a minimal cut-set is a number of basic events that contributes to the particular minimal cut-set. For

illustration purposes, let us consider the example of a simple fault tree shown in Fig. 1. In this figure, x1, x2, x3 and x4 represent the four basic events. The IE1 and IE2 are the intermediate events produced through combination of basic events by logic gates. Therefore, we can write a logical expression for the top event as: $\mathrm{TE} = (\mathrm{x1} \cap \mathrm{x2}) \cup (\mathrm{x3} \cup \mathrm{x4})$. The corresponding Boolean algebra is $\mathrm{TE} = (\mathrm{x1} \cdot \mathrm{x2}) + (\mathrm{x3} + \mathrm{x4})$ and a total of 3 minimal cut-sets exist namely, x1·x2, x3, and x4. The minimal cut-sets x3 and x4 are of first order and the minimal cut-set x1·x2 is the second order. Finally, a quantitative analysis is conducted to compute the probability of occurrence of the TE and determine the importance measure for each minimal cut-set. The probability of occurrence of the TE is calculated by using following equation:

$$\begin{aligned} P(TE) &= P\left(\bigcup_{i=1}^{n} M_i\right) \\ &= \sum_{i=1}^{n} P(M_i) - \sum_{i<j=2}^{n} P(M_i M_j) + \sum_{i<j<k=3}^{n} P(M_i M_j M_k) \\ &\quad + \cdots + (-1)^{n-1} P(M_1 M_2 \cdots M_n) \end{aligned} \tag{4}$$

where M_1, M_2, …, M_n represents the minimal cut-sets and n is the total number of minimal cut-sets. The importance measure (*IM*) analysis calculates the contribution of the minimal cut-sets to the occurrence of TE and accordingly identifies the critical events. Various methods for assessing the *IM*s are: Birnbaum, Criticality, Fussell-Vesely, Risk-Reduction Worth and Risk-Achievement Worth measures of importance (Modarres et al., 1999). In this

study, the importance measure of minimal cut-set of Fussell-Vesely (1975) is employed according to which:

$$IM = F\left(M_i\right) / F\left(\mathbf{M}\right) \qquad (5)$$

where F (**M**) is the total risk from all minimal cut-sets; F (M_i) is the risk from minimal cut-sets which contain minimal cut-set M_i. These *IM*s compute the overall percent contributions of minimal cut sets to the total risk.

3.2 Bayesian Network (BN)

In contrast to a fault-tree, a Bayesian Network (BN), also referred to as a Bayesian Belief Network (BBN), is a more general form that can account for the statistical relationships among the events. It is a graphical representation of a set of conditionally independent assumptions and accordingly requires a joint probability distribution between random variables. This generality makes it a powerful tool for the structure/system reliability, risk management, accident analysis, artificial intelligence, etc. A Bayesian Network is a directed acyclic graph (DAG) which is represented using the nodes (or vertices) represented by circles, arrows (or arcs), and the conditional probability table (CPT). Each node defines either a discrete or a continuous random variable. In this study, we consider only discrete variables. An intermediate node serves as a parent as well as a child node. The nodes which have arrows directed to other nodes are parent nodes and nodes that have coming from other nodes are called as child nodes A node that do not have any arrow coming from another node is

called as root node and it does not have any parent node. Arrows represent direct relationships between interconnected parent and child nodes. The CPTs assigned to nodes describe the quantitative relationships between interconnected nodes.

The BN analysis is basically performed based on the conditional probability as per Eq. (6) and conditional independence assumption, i.e. P(x,y|z) = P(x|z) P(y|z) if and only if $X \perp Y|Z$. The joint probability distributions can be expressed using conditional probability as:

$$P\left(X_1, X_2, \cdots, X_n\right) = \prod_{i=1}^{n} P\left(X_i \mid X_1, \cdots, X_{i-1}\right) \tag{6}$$

The conditional independence assumption simplifies Eq. (6) further as:

$$P\left(X_1, X_2, \cdots, X_n\right) = \prod_{i=1}^{n} P\left(X_i \mid \text{Parent}\left(X_i\right)\right) \tag{7}$$

Parent (X_i) is parent nodes for X_i; P(X_i | Parent (X_i)) is the CPT of X_i and n is the number of nodes in the network. For illustration, let us consider a simple network shown in Fig. 2 in which X_1, X_2, X_3 and X_5 are the root nodes. X_4 is the child node of X_1 and X_2, and parent node of X_6 and X_7. X_6 is the child node of X_3 and X_4. X_7 is the child node of X_4 and X_5.

A Bayesian network can also be used as an inference tool to evaluate beliefs of events when new information also called as “evidence” becomes available. The evidence is typically represented by binary states: occurrence of event by “1” and non-occurrence by “0”. For evidence e, the joint probability of all the nodes can be inferred as

$$P(X_1, X_2, \cdots, X_n \mid e) = \frac{P(X_1, X_2, \cdots, X_n, e)}{P(e)} = \frac{P(X_1, X_2, \cdots, X_n, e)}{\sum_{X_1, \cdots, X_n} P(X_1, X_2, \cdots, X_n, e)} \qquad (8)$$

This equation can be adopted for two types of probabilistic reasoning - the predictive analysis as well as updating analysis.

3.3 Mapping algorithm

In general, it is not straightforward to start with creating a Bayesian network directly. It is relatively much easier to create a fault tree. Therefore, a mapping algorithm is needed to transform a fault tree into a Bayesian network. The mapping involves two steps, graphical representation and numerical computation. First, all events in a fault tree - the basic, intermediate, and top events - are converted into the nodes of Bayesian network. The basic events map into the root nodes of a BN and the intermediate events map to child nodes of the root nodes. The top event of a fault tree maps into a child node of basic and intermediate events. For numerical computation, the probabilities of the basic events in a fault tree are assigned to the marginal probabilities of the root nodes of BN. For the intermediate and top events of fault tree defined by gates, the CPTs are established at corresponding child nodes of BN. For illustration, let us consider the fault tree that was shown in Fig. 1 which is mapped into a BN as shown in Fig. 3. The CPTs of IE1 and IE2 nodes of BN which are represented as “AND” and “OR” gates in FT are given in tables located besides these nodes. In this

Figure, “0” and “1” represent non-occurrence and occurrence of event, respectively. A detailed discussion of mapping algorithm is given in Bobbio et al. (2001). It is noteworthy that the mapped BN from the fault tree have the specific conditional probabilities consisting of binary values 0 and 1, which is a special case of BN. Unlike the fault tree, the BN can be extended to more general problem by using non-binary values in the CPT within the same BN structure or creating arcs among the nodes for representing the correlation of events. Also, though each root node has the binary outcomes, the marginal probability corresponding to the either binary value (for example, P(x1 = 1)) can have uncertainties which can be represented by an appropriate probability distribution (for example, P(x1 = 1) ~ Normal Distribution). Since the root nodes are described by the probability distributions, the other nodes are also evaluated as probability distributions after accounting for the CPT relations.

3.4 Bayesian Inference

The inference considered by Eq. (8) above is binary in nature. Therefore, Bayes’ theorem or Bayesian inference can be employed in accordance with Eq. (9) in order to account for non-binary data, different levels of discrete data , and uncertainties (Hamada et al., 2004; Wilson and Huzurbazar, 2007).

$$f\left(\mathbf{p}\,|\,\mathbf{D}\right)=\frac{f\left(\mathbf{D}\,|\,\mathbf{p}\right)f\left(\mathbf{p}\right)}{f\left(\mathbf{D}\right)}=\frac{L\left(\mathbf{D},\mathbf{p}\right)f\left(\mathbf{p}\right)}{\int L\left(\mathbf{D},\mathbf{p}\right)f\left(\mathbf{p}\right)d\mathbf{p}} \qquad (9)$$

$f(\mathbf{p}|\mathbf{D})$ is the posterior distribution; $f(\mathbf{D}|\mathbf{p})$ is the likelihood function which is also expressed as $L(\mathbf{D},\mathbf{p})$; $f(\mathbf{p})$ is the prior distribution; $\mathbf{p}$ is the probabilities corresponding to root nodes X_i consisting of p_{X1}, p_{X2}, …, p_{Xn}; and $\mathbf{D}$ is the data. The prior and posterior distributions are typically represented as probability density functions (PDFs). The likelihood function to incorporate multi-level discrete data is typically formulated as a binomial distribution:

$$L(\mathbf{D},\mathbf{p}) \propto {p_{X1}}^{n_f}\left(1-p_{X1}\right)^{n_t-n_f}\cdots {p_{Xn}}^{n_f}\left(1-p_{Xn}\right)^{n_t-n_f} \\ {p_{IE1}}^{n_f}\left(1-p_{IE1}\right)^{n_t-n_f}\cdots {p_{IEm}}^{n_f}\left(1-p_{IEm}\right)^{n_t-n_f}\ {p_{TE}}^{n_f}\left(1-p_{TE}\right)^{n_t-n_f} \tag{10}$$

where n_t is the total number of data corresponding to each event; n_f is the number of failure/occurrence of each event; n and m are the total number of the basic and intermediate events; and p_{Xi}, p_{IEi} and p_{TE} are the occurrence probabilities of basic events (X_i), intermediate events (IE_i) and top events (TE), respectively.

As the size of the problem increases, the solution of Eq. (9) becomes formidable. In such cases, MCMC (Markov Chain Monte Carlo) methods such as Metropolis-Hastings algorithm, Slice sampling, Extended Kalman Filter, Gibbs sampling, etc. are employed. In this study, we use MCMC method with Gibbs sampling algorithm which is implemented through the use of JAGS of R code (Plummer, 2003). For the quantitative convergence diagnostics, the Deviance Information Criteria (DIC), auto correlation plot of the samples, the effective sample size, Gelman stat, etc. are utilized (Gelman et al., 2014).

4. Multi-Hazard PRA and Vulnerabilities Beyond Design Basis

The Bayesian approaches presented above provide the basis for a very powerful environment to conduct PRA studies for multi-hazard scenarios and for exploring vulnerabilities beyond design basis. As discussed earlier, a multi-hazard PRA requires consideration of correlated events which can be accounted through a Bayesian network. In fact, even a single hazard PRA performed in a Bayesian environment can provide greater insights than a conventional PRA using a fault-tree approach because it can consider correlations among multiple failure modes of various structures, systems, and components (SSC). In addition, any newly available data can be easily accommodated through Bayesian inference.

Assessment of vulnerability beyond design basis is a significant undertaking that requires enormous time and cost especially under the conventional PRA approaches. A bottom-up approach in a conventional fault-tree cannot be used because different components and systems have different degree of margins before failure for loads beyond design basis. In fact, much of the information on failure of systems beyond design basis is not even available. Many of the past studies have focused on evaluating and improving a systems performance at design basis levels. Consequently, a significant effort is needed in assessment of vulnerability beyond design basis and the effort may even be impractical as such if one has to evaluate the vulnerabilities of each and every component/system in a plant in order to determine a plant's performance for beyond design basis events. It is precisely in this context that a Bayesian network together with Bayesian inference can be quite effective

in reducing the scope of such exploration. In order to explain this argument further, let us consider a Bayesian network shown in Fig. 3. The critical path in this network corresponding to the design basis would be very different compared to a critical path for vulnerability beyond design basis. However, it is not possible to identify the vulnerability related critical path in bottom-up approach without a complete understanding of how each component and system performs for loads beyond design basis. Yet, a Bayesian approach can use a top-down approach to determine the critical path, i.e. a vulnerability of the plant can be characterized as the occurrence of TE even if we do not know the path that leads to the TE. The probability of the TE to occur in such a scenario is equal to unity. With this as the starting point (available information), Bayesian inference can be employed to traverse from top to down in the network and identify the critical path that leads to this condition. Identification of the new critical path can then help engineers and decision makers in focusing their effort to determine the true vulnerabilities or the performance of components and systems that lie on this critical path. Once this information is available then the process can be repeated.

5. Application Examples

5.1 Enhancements to a Single Hazard PRA

In this section, we use a simple representative example to illustrate the benefits of using a Bayesian framework for a single-hazard PRA. For this purpose, we consider a building-piping structural system subjected to an earthquake. In order to consider the probabilistic hazard information, the location for this site is taken as Charleston, SC. The reason to select

this location is because it has significantly higher hazards due to earthquakes as well as high winds during hurricanes and flooding due to storm surges. The location serves as a good selection for consideration of multiple hazards which is discussed in the next section. For simplicity, we consider a low-rise building structure, safety-related equipment, piping supports, and piping joints in this model. A total of four basic failure modes are considered: (i) Building failure is governed by "excessive story drift," (event denoted by C1), (ii) loss of circulation due to failure of safety related equipment such as a pump (event denoted by C2), (iii) loss of coolant from piping initiated by failure of pipe supports (denoted by event C3), and (iv) loss of coolant from piping due to leakage at pipe joints (denoted by event C4). Fig. 4 shows the fault tree for this scenario. As seen in this figure, the two intermediate events are defined as: Loss of circulation (IE1) and Loss of coolant (IE2). The system failure (S) is defined with respect to IE1 and IE2.

The probabilistic seismic hazard curves for Charleston, SC are calculated in accordance with the methodology described in section 2.1 and shown in Fig. 5. As seen in this figure, the annual probability of exceedance is calculated in terms of spectral accelerations at two different periods T = 0.2 seconds and T = 0 seconds which is representative of the peak ground acceleration (PGA). The mean seismic fragility curves for all four basic events C1, C2, C3 and C4 are assumed to follow log-normal distributions. Event C1 is characterized by spectral acceleration at T = 0.2 seconds which corresponds to the natural period of oscillation for the building structure. The median and logarithmic standard deviation for the lognormal distribution of C1 are taken as 2.0g and 0.5, respectively,

based on the information provided in (Li and Ellingwood, 2009). For the remaining three basic events (C2, C3, and C4), the fragility is characterized in terms of lognormal distributions for PGA values. Event C2 has a_m = 1.6 g and β = 0.35, C3 is characterized as LN(a_m = 2.0g, β = 0.5) and C4 as LN(a_m = 0.5g, β = 0.55) in accordance with Ju and Gupta (2015), respectively. In practice, the fragility information is developed for a specific plant based on actual analysis of plant's SSC. In this study, the fragility information given above is taken from prior studies on such systems conducted by other researchers (Li and Ellingwood, 2009; Ju and Gupta, 2015). The seismic hazard curves and the fragility information together can be used to calculate the mean risks associated with the four basic events as per Eq. (1). The risk for C1 is calculated as 0.000310, for C2 as 0.000200, for C3 as 0.000163 and for C4 as 0.000727. In addition to the mean annual risk values, the uncertainties are considered by treating the annual risk values to be normally distributed with c.o.v. for each event being 0.3.

To begin with, a conventional fault tree analysis is conducted by using only the mean risk values for basic events. The logical expression for event S of this fault tree is given by $S = (C1 \cup C2) \cup (C3 \cup C4)$ and the corresponding Boolean expression is $S = (C1 + C2) + (C3 + C4)$. The mean risk of S calculated using Eq. (4) is 0.0014. The risks for intermediate events IE1 and IE2 and the importance measures (IMs) of minimal cut-sets computed using Eq. (5) are summarized in Table 1. As seen in this table, the critical basic event contributing to the overall risk of S is the basic event C4. Next, we consider uncertainties in the fault tree analysis through the use of MCMC method (Gibbs sampling as

implemented in JAGS in R). A total of 100,000 samples are used including 10,000 burn-in samples. The results are summarized in Table 1.

Verification using Boolean Relationships: Next, we create a Bayesian network for this application example by using the mapping algorithm presented in section 3.3. Fig. 6 shows the corresponding Bayesian network along with the CPT information for each arc. The distributions of all events are calculated using MCMC. To being with, the CPTs are all Boolean in nature and there the Bayesian network gives exactly the same results as those obtained from the fault tree analysis.

Effect of Non-Boolean Relationships: Once the Bayesian network with Boolean values of CPTs is verified by comparison with corresponding fault tree analysis, we illustrate the effect of considering non Boolean information through CPTs. Let us consider certain scenarios to do so. The basic event C1 which represents excessive story drift may not necessarily represent a system failure in certainty but rather only partially. In some cases, failure of structure through excessive story drift may not result in any loss of coolant or loss of circulation. Similarly, the basic event of support failure in piping (C3) may not necessarily result in a loss of coolant or circulation because a piping systems often have redundant supports and failure of one support may not directly influence in any loss of coolant or circulation. In addition, while a loss of circulation (IE1) effects cooling, it would not necessarily result in a system failure as partial circulation can continue for a certain time thereby giving ample time for undertaking actions to remedy the problem. This information or scenarios can be directly incorporated in a Bayesian network by adjusting the CPTs. Fig. 7

gives modified values of CPTs taken in this study to represent these non Boolean scenarios. The distribution of risk calculated for each event in this case along with the 95% confidence limit is given in Table 2. Fig. 8 compares the PDF and CDF of system level risk calculated in this case with that calculated from the fault tree analysis. It can be seen that the mean risk calculated from this modified Bayesian network is less than that corresponding value from the fault tree analysis. The mean risk from the Bayesian analysis is about 0.00107 compared to the 0.00140 from the fault tree analysis. However, the coefficient of variation increases to 0.21 compared to 0.18 from the fault tree analysis. Risk goals are typically defined by a high confidence low probability of failure (HCLPF) value which is defined as 5% probability of failure at the 95% confidence level. The HCLPF value calculated from the Bayesian analysis is 0.00033 compared to 0.00058 from the fault tree analysis.

Effect of Correlated Events: Next, we illustrate the effect of correlations among basic events. The scenario considered in this study represents a situation wherein a possibility exist that the event C1 which represents excessive story drift can also lead to a failure of pipe support attached to the particular story. Therefore, event C3 is then initiated by and correlated to event C1. In addition, a failure of pipe support can results in large deformations at pipe joints leading to a leakage failure which is represented by event C4. This scenario can be investigated by considering a correlation between events C3 and C4. The modified Bayesian network with additional dependencies and the corresponding CPTs are shown in Fig. 9. The information on distributions calculated for all the nodes of the modified network is given in Table 3. The PDF and CDF of system level risk as calculated from the modified network are

compared to the original values calculated from the fault tree analysis in Fig. 10. As seen in Fig. 10, the differences between the two sets of results increase significantly. The mean risk, c.o.v. and HCLPF for system failure in this case are 0.000583, 0.23, and 0.00015, respectively.

Updating to Incorporate New Data: Lastly, we illustrate the concept of updating to incorporate new data into a PRA. For this purpose, we start with the Bayesian network shown in Fig. 6. Let us consider that new data is available on the performance of this system through any of a multiple possible sources such as experiments, simulation studies, or even experience data. The new data is characterized in terms of failure rates for intermediate event IE1 and the corresponding system failure S. We assume that IE1 failure occurs about twice in a 40 year of operating experience and S occurs only once over the same period. This additional information is incorporated into the Bayesian network by using Bayesian inference and updating the prior distributions for all events. Given this data, the likelihood function of Eq. (10) takes the following form:

$$L(\mathbf{D},\mathbf{p}) \propto {p_{IE1}}^{2}\left(1-p_{IE1}\right)^{38}\ {p_S}^{1}\left(1-p_s\right)^{39} \tag{11}$$

where p_{IE1} is the risk of IE1, and p_s is the risk of S. Table 4 provides a summary of the posterior distributions. Fig. 11 shows the prior and posterior distributions for system failure. It is observed that the mean risk is increased and uncertainties are reduced due to the additional evidence. The mean risk, c.o.v. and HCLPF for system failure in this case are 0.000149, 0.16, and 0.00068, respectively.

5.2 Application to Multi-Hazard PRA

In this section, we consider the same building-piping system as discussed for a single hazard PRA but we consider that it exhibits multiple hazards due to earthquake, hurricane winds, and flooding loads. The fault tree for the multi-hazard scenario is shown Fig. 12. The mean wind hazard curves for Charleston, SC are shown in Fig. 13. The mean wind fragility curves of basic events B1, B2 and B3 are assumed to follow lognormal distributions having medians and logarithmic standard deviations as LN(a_m = 68, β = 0.15), LN(a_m = 45, β = 0.08), and LN(a_m = 50, β = 0.12), respectively. Computation of the mean wind hazard curve and fragilities is described in details by Li and Ellingwood (2006). For flooding risk, US Bureau of Reclamation for Dams (1998) provides the risks associated with various failure modes in dams as evaluated from risk studies and using historical data. In this study, we adopt these risk values which in turn serve as the flooding hazard initiated by the failure of a flood defense structure nearby or a dam upstream of a plant. Since other events such as pump, sump, battery components, etc. are not related to the specific hazard and fragility, these risks are represented as annual failure probabilities. The mean annual risks for all basic events are given in parenthesis under the event labels in Fig. 12. The c.o.v. for each normally distributed event is taken as 0.3.

To begin with, the conventional FTA not considering the uncertainties but using mean risks of basic events is executed. The qualitative approach of FTA obtains total 18 minimal cut-sets as A1, A2, A3, A4, A5, A6·A7, A8, A9, A10·A11, B1, B2·B3, C1·C2·C3,

C1·C2·C4, C5, C6, C7, C8 and C9. The quantitative approach of FTA evaluates the mean risk of S as about 0.0302. The importance measures (IMs) of minimal cut-sets are summarized in Table 5. From the IM results, we can determine the critical minimal cut-sets contributing risk of S most as A10·A11. Then, the Bayesian network is constructed for the scenario of system risk of this structure under multiple hazards as shown in Fig. 14. The developed BN is exactly matched to fault tree of Fig. 12 as we define the CPTs of intermediate nodes to just express logic gates of the FTA. So, this BN produces the same results of FTA considering uncertainties. The detailed results of this including the scenarios of the non-Boolean relation and having new additional data are represented in the Appendix.

Vulnerability Beyond Design: Next, we illustrate the concept to using the updating to identify critical events that are most likely to result in a system level vulnerability. This can be accommodated by simply starting with the assumption that the system failure occurs which can be represented by the probability for event S to be equal to unity. Starting with this information, updating is performed to calculate the posterior distributions. The posterior mean risks for this example are summarized in Table 6 and the modified importance measures of minimal cut-sets induced from this accident are given in Table 7 which can then be used to identify the most critical event and accordingly evaluate the scenarios for vulnerabilities due to beyond design bases events. Fig. 15 graphically illustrates the critical path and corresponding events under this accident scenario. As shown in this figure, the red solid lines and circles represent critical path for vulnerability beyond design basis which is different from the critical path for the design basis condition which is shown with blue

dashed lines and circles. Specifically, we can see that the identified critical path and events of A10·A11 under the design event are changed to the other critical scenario and event of B1 under the beyond design basis accident. It means that there is most likely that the earthquake induces the failure in system during design condition, but under the beyond design accident situation, the hurricane causes the system failure. This also makes the important components for system risk be different. Accordingly, for the design purpose, the risks of pumps of piping triggered from an earthquake event (A10 and A11) are the most important, but for the accident situation perspective, the risk of failure of roof structure caused by a hurricane hazard (B1) is the most significant. This information can be finally used for the plan for mitigating the system risk subjected to multiple external hazards. This scenario under the beyond design accident is the one that the conventional FTA can never discover.

Correlated multi-hazard - seismically induced internal flooding scenario: Lastly, we discuss the scenario that the pipe break induced from the seismic event initiates the internal flooding. This correlated multi-hazard scenario .i.e. seismically induced internal flooding can be easily captured within the graphical representation of BN. The Fig. 16 illustrates this scenario by creating arcs between (1) A8 and C1, (2) AI3 and C2, and (3) AI3 and C5, and defining the corresponding CPTs. The reason that this representation is quite plausible is that the piping joint leakage failure caused form the earthquake (A8) can firstly bring about the water intrusion to the basement sump system (C1), and subsequently the EDG failure can induce the primary pump failure (C2) and the event that exceeds pump capacity (C5). This additional correlation information representing the seismic induced internal flooding scenario

can be only realized within the BN formulation. Fig. 17 compares the PDF for the risk of basement flooding event (CI5) from FT and BN. The PDF and CDF of system level risk as calculated from the BN are compared to the original values calculated from the FT analysis in Fig. 18. It is observed that the mean risk of the basement flooding and system level risk is increased due to the additional scenario of seismically induced internal flooding. The mean risk, c.o.v. and HCLPF for system failure considering this scenario are 0.0331, 0.09, and 0.0229, respectively.

6. Conclusions

This study focuses on the development of Bayesian framework for Probabilistic Risk Assessment (PRA) of structural systems under multiple hazards. The concepts of Bayesian network and Bayesian inference are combined by mapping the traditionally used fault trees into a Bayesian network. Unlike traditional fault tree analysis, such a mapping allows for consideration of dependencies as well as correlations between events. This is essential in risk assessment for multi-hazard scenarios especially when correlated events are possible. Furthermore, Bayesian inference facilitates updating of prior information of all events based on new information or data that might become available from experimental studies, field observations, or high fidelity simulations. The primary conclusion of this study can be summarized as:

- The proposed Bayesian framework can consider statistical dependencies and correlations among different events and hazards in a relatively straightforward manner.
- Consideration of correlated events in the Bayesian framework allows appropriate treatment of multi-hazard scenarios.
- Application to simple examples for single as well as multi-hazard scenarios illustrate that consideration of dependencies and correlations can result in a reduction of overall risk estimates both for mean as well as HCLPF values.
- Incorporation of Bayesian inference permits a novel way for exploration of vulnerability beyond design events.
- The proposed approach for vulnerability beyond design basis assists in identification of events and the corresponding SSC that would lie on a critical path with respect to system level vulnerability.
- The critical path for vulnerability beyond design basis can be quite different from that corresponding to the design basis as calculated from a conventional PRA. Availability of this information can be quite useful in managing the costs without compromising the safety by restricting additional studies on vulnerability to the SSC on critical path.

Acknowledgements

This research was partially supported by the Center for Nuclear Energy Facilities and Structures at North Carolina State University. Resources for the Center come from the dues paid by member organizations and from the Civil, Construction, and Environmental Engineering Department and College of Engineering in the University.

References

Aoki M and Rothwell G, "A comparative institutional analysis of the Fukushima nuclear disaster: Lessons and policy implications," *Energy Policy*, 53, 240-7, 2013.

Ayyub BM, McGill WL, and Kaminskiy M, "Critical assest and portfolio risk analysis: An all-hazards framework." *Risk Analysis*, 27(4), 789–801, 2007.

Batts ME, Cordes MR, Russell LR, Shaver JR, and Simiu E, "Hurricane wind speeds in the United States," Rep. no. BSS-124. Washington (DC), National Bureau of Standards, US Department of Commerce, 1980.

Beavers JE et al., "Multihazard issues in the central united states: Understanding the hazards and reducing the losses." *ASCE Council on Disaster Risk Management Monograph No. 3*, Reston, VA, 2009.

Bobbio A, Portinale L, Minichino M, and Ciancamerla E, "Improving the analysis of dependable systems by mapping fault trees into Bayesian networks," *Reliability Engineering & System Safety*, 71(3), 249-260, 2001.

Ellingwood BR, "Acceptable risk bases for design of structures." *Progress in Structural Engineering and Materials*, 3(2), 170–179, 2001.

EPRI, "Methodology for Developing Seismic Fragilities," *TR-103959*, Electric Power Research Institute, 1994.

Fussell J, "How to Hand Calculate System Reliability and Safety Characteristics," *IEEE Transaction on Reliability*, 24(3), 1975.

Gelman A, Carlin JB, Stern HS and Rubin DB, *Bayesian data analysis*, Chapman & Hall/CRC, Boca Raton, FL, USA, 2014.

Georgiou PN, *Design wind speeds in tropical cyclone-prone regions*, PhD thesis, Faculty of Engineering Science, University of Western Ontario, Canada, 1985.

Hamada M, Martz HF, Reese CS, Graves T, Johnson V, and Wilson AG, "A fully Bayesian approach for combining multilevel failure information in fault tree quantification and

optimal follow-on resource allocation," *Reliability Engineering & System Safety*, 86(3), 297-305, 2004.

IAEA, "Assessment of External Flooding (excluding Tsunami) and High Wind Hazards in Site Evaluation for Nuclear Installations," IAEA Safety Report, International Atomic Energy Agency, Vienna, 2015.

IAEA, "Meteorological and Hydrological Hazards in Site Evaluation for Nuclear Installations," Specific Safety Guide SSG-18, International Atomic Energy Agency, Vienna, 2011.

IAEA, "Procedures for Conducting Probabilistic Safety Assessments of Nuclear Power Plants (Level 1)," *Safety Series No. 50-P-4*, International Atomic Energy Agency, 1992.

Ju BS and Gupta A, "Seismic fragility of threaded Tee-joint connections in piping systems," *International Journal of Pressure Vessels and Piping*, 132, 106-118, 2015.

Kameshwar S and Padgett JE, "Multi-hazard risk assessment of highway bridges subjected to earthquake and hurricane hazards," *Engineering Structures*, 78(1), 154-166, 2014.

Kelly DL and Smith CL, "Bayesian inference in probabilistic risk assessment-The current state of the art," *Reliability Engineering & System Safety*, 94(2), 628-643, 2009.

Li Y and Ellingwood B, "Framework for Multihazard Risk Assessment and Mitigation for Wood-Frame Residential Construction," *ASCE Journal of Structural Engineering*, 135(2), 159-168, 2009.

Li Y and Ellingwood BR, "Hurricane damage to residential construction in the US: Importance of uncertainty modeling in risk assessment," *Engineering structures*, 28(7), 1009-1018, 2006.

McGuire RK, "Probabilistic seismic hazard analysis and design earthquakes: closing the loop," *Bulletin of the Seismological Society of America*, 85(5), 1275-1284, 1995.

Modarres M, Kaminskiy MP, and Krivtsov V, *Reliability engineering and risk analysis: a practical guide*, CRC press, 1999.

Peterka JA and Shahid S, "Design gust wind speed in the United States," *ASCE Journal of Structural Engineering*, 124(2), 207-14, 1998.

Plummer M, "JAGS: A program for analysis of Bayesian graphical models using Gibbs sampling," *Proceedings of the 3rd international workshop on distributed statistical computing*, 124, Technische Universit at Wien, 2003.

Rasmussen NC, "Reactor safety study," WASH-1400, NUREG-75/014, Appendix II, US Nuclear Regulatory Commission, Washington DC, 1975.

Singer D, "A fuzzy set approach to fault tree and reliability analysis," *Fuzzy Sets and Systems*, 34(2), 145-155, 1990.

Tanaka H, Fan LT, Lai FS, and Toguchi K, "Fault-Tree Analysis by Fuzzy Probability," *IEEE Transactions on Reliability*, 32(5), 453-457, 1983.

Tatalovich J, "Comparison of Failure Modes from Risk Assessment and Historical Data for Bureau of Reclamation Dams," Report DSO-98-01, Dam Safety Office, US Bureau of Reclamation, Denver, 1998.

US NRC, "PRA Procedure Guide – A Guide to the performance of probabilistic risk assessments for nuclear power plants," *NUREG/CR-2300*, US Nuclear Regulatory Commission, 1983.

Vickery PJ, Skerlj PF, Steckley AC, and Twisdale LA, "Simulation of hurricane risk in the United States using empirical track modeling technique," *ASCE Journal of Structural Engineering*, 126(10), 1222-37, 2000.

Wilson AG and Huzurbazar AV, "Bayesian networks for multilevel system reliability," *Reliability Engineering & System Safety*, 92(10), 1413-1420, 2007.

Appendix: Additional Scenarios in Example 2

Verification using Boolean Relationships: Table A-1 presents the distribution information of intermediate and system nodes of Bayesian network (BN) constructed by the fault tree of Fig. 12 and mapping algorithm. This case accounts for the uncertainties of basic events. The analysis is performed using MCMC. The result of this is observed as same as the mean risk of system failure of fault tree analysis (FTA) represented in section 5.2.

Effect of Non-Boolean Relationships: Let us think about the scenario which FTA cannot characterize. In this case of the example, EQ induced failure (AI8), Wind induced failure (BI2) and Flood induced failure (CI7) can influence the system failure in part since the basis events of these cannot endanger a complete failure in the system. For example, the excessive story drifts of the system (A2) cannot directly lead to the loss of system function. The functional failure caused from wind (BI1) does not mean the system failure related to the safety function of system. The flood defense structure failure (CI6) cannot also bring the entire damage to the system. This information is only incorporated into the BN by adjusting the CPT of S node. Table A-2 shows the defined CPT of S node which can describe the scenario above. The distribution information of intermediate and system nodes of BN of this case is calculated in Table A-3. Specifically, Fig. A-1 compares the PDF and CDF of risk of system failure (S) from FTA and BN. This figure illustrates that the mean risks and HCLPF of system failure of BN results is reduced compared to those of FTA results since BN reflects the additional scenario the FTA could not handle.

Updating to Incorporate New Data: Let us suppose that we have multi-level binomial discrete data of Table A-4 in BN not considering the effect of non-Boolean relationship. This additional information is incorporated into the BN by associating Bayesian inference and updates the prior distributions of all events. Given these data, the likelihood has the form by using following equation:

$$L(\mathbf{D},\mathbf{p}) \propto p_{\mathrm{A8}}{}^{1}(1-p_{\mathrm{A8}})^{39}\ p_{\mathrm{AI8}}{}^{1}(1-p_{\mathrm{AI8}})^{39}\ p_{\mathrm{BI2}}{}^{3}(1-p_{\mathrm{BI2}})^{37}\ p_{\mathrm{CI7}}{}^{1}(1-p_{\mathrm{CI7}})^{39}\ p_{\mathrm{S}}{}^{5}(1-p_{\mathrm{S}})^{35} \tag{A-1}$$

where p_{A8}, p_{AI8}, p_{BI2}, p_{CI7} and p_S are the risks of A8, AI8, BI2, CI7, and S, respectively. Table A-5 provides a numerical summary of the posterior distributions. Fig. A-2 shows the prior and posterior distributions of the event of system failure. It is observed that the mean risk is increased due to newly observed data of Table A-4.

Table 1: Risks, importance measures, statistics of events for FTA

Minimal cut-sets / Events	Conventional FTA not considering uncertainties		FTA considering uncertainties			
	Mean risks	IM (%)	Mean risks	Standard Deviation	c.o.v	95% CI
C1	0.000310	22	0.000309	9.305e-05	0.30	0.000364
C2	0.000200	14	0.000200	6.003e-05	0.30	0.000235
C3	0.000163	12	0.000163	4.891e-05	0.30	0.000192
C4	**0.000727**	**52**	0.000728	2.181e-04	0.30	0.000856
IE1	0.000510	-	0.000509	1.107e-04	0.22	0.000435
IE2	0.000890	-	0.000891	2.233e-04	0.25	0.000876
S	0.001399	-	0.001400	2.492e-04	0.18	0.000976

Table 2: Risks and statistics of events for BN, effect of non-Boolean events

Basic Events	Mean risks	Standard Deviation	c.o.v	95% CI
C1	0.000310	9.29e-05	0.30	0.000365
C2	0.000200	6.00e-05	0.30	0.000236
C3	0.000163	4.89e-05	0.30	0.000192
C4	0.000727	2.19e-04	0.30	0.000855
IE1	0.000262	6.29e-05	0.24	0.000246
IE2	0.000841	2.21e-04	0.26	0.000867
S	0.001077	2.28e-04	0.21	0.000892

Table 3: Risks and statistics of events for BN, effect of correlated events

Basic Events	Mean risks	Standard Deviation	c.o.v	95% CI
C1	0.000310	9.36e-05	0.30	0.000366
C2	0.000200	6.01e-05	0.30	0.000236
C3	0.000217	6.55e-05	0.30	0.000256
C4	0.000195	5.89e-05	0.30	0.000231
IE1	0.000262	6.30e-05	0.24	0.000248
IE2	0.000347	1.05e-04	0.30	0.000410
S	0.000583	1.33e-04	0.23	0.000523

Table 4: Risks and statistics of events for BN, influence of updating

Basic Events	Mean risks	Standard Deviation	c.o.v	95% CI
C1	0.000347	9.03e-05	0.26	0.000354
C2	0.000215	5.91e-05	0.27	0.000232
C3	0.000164	4.88e-05	0.30	0.000192
C4	0.000759	2.16e-04	0.28	0.000851
IE1	0.000562	1.06e-04	0.19	0.000416
IE2	0.000923	2.21e-04	0.24	0.000869
S	0.001485	2.44e-04	0.16	0.000954

Table 5: IMs of minimal cut-sets, multi-hazard example

Minimal Cut-set	Probability	IM (%)
A1	0.00125	4.1
A2	0.00031	1.0
A3	0.001	3.3
A4	0.001	3.3
A5	0.001	3.3
A6·A7	0.01·0.01	0.3
A8	0.00073	2.4
A9	0.00016	0.5
A10·A11	**0.09·0.09**	**26.5**
B1	0.0076	24.8
B2·B3	0.076·0.049	12.2
C1·C2·C3	0.1·0.01·0.005	0.02
C1·C2·C4	0.1·0.01·0.05	0.2
C5	0.001	3.3
C6	6.38e-6	0.02
C7	3.52e-5	0.1
C8	0.00319	10.4
C9	0.00134	4.4

Table 6: Mean risks of events for BN, multi-hazard example

Basic Events	**A1**	**A2**	**A3**	**A4**	**A5**	**A6**	**A7**	**A8**	**A9**	**A10**
Mean risks	0.04	0.01	0.03	0.03	0.03	0.01	0.01	0.02	0.01	0.33
Basic Events	**A11**	**B1**	**B2**	**B3**	**C1**	**C2**	**C3**	**C4**	**C5**	**C6**
Mean risks	0.33	0.25	0.19	0.16	0.10	0.01	0.01	0.05	0.03	2e-4
Basic Events	**C7**	**C8**	**C9**	**-**	**-**	**-**	**-**	**-**	**-**	**-**
Mean risks	1e-3	0.11	0.04							
Inter. Events	**AI1**	**AI2**	**AI3**	**AI4**	**AI5**	**AI6**	**AI7**	**AI8**	**BI1**	**BI2**
Mean risks	0.07	0.27	0.10	0.003	0.30	0.05	0.40	0.45	0.12	0.37
Inter. Events	**CI1**	**CI2**	**CI3**	**CI4**	**CI5**	**CI6**	**CI7**	**S**	**-**	**-**
Mean risks	0.06	0.002	0.001	0.15	0.03	0.15	0.19	**1.00**		

Table 7: IMs of minimal cut-sets, vulnerability beyond design basis in multi-hazard example

Minimal Cut-set	Probability	IM (%)
A1	0.0400	5.4
A2	0.0100	1.4
A3	0.0300	4.1
A4	0.0300	4.1
A5	0.0300	4.1
A6·A7	0.0001	0.01
A8	0.0200	2.7
A9	0.0100	1.4
A10·A11	0.1089	14.7
B1	**0.2500**	**33.8**
B2·B3	0.0304	4.1
C1·C2·C3	1e-5	0.001
C1·C2·C4	0.0001	0.01
C5	0.0300	4.1
C6	0.0002	0.03
C7	0.0010	0.1
C8	0.1100	14.9
C9	0.0400	5.4

Table A-1: Risks and statistics of events for BN, Boolean relation

Intermediate Events	Mean risks	Standard Deviation	c.o.v	95% CI
AI1	0.001997	4.23E-04	0.21	0.001659
AI2	0.008098	3.81E-04	0.05	0.001487
AI3	0.002996	5.16E-04	0.17	0.002016
AI4	0.000100	4.32E-05	0.43	0.000168
AI5	0.008980	4.41E-04	0.05	0.001729
AI6	0.001558	3.88E-04	0.25	0.001521
AI7	0.012047	6.76E-04	0.06	0.002643
AI8	0.013587	7.76E-04	0.06	0.003040
BI1	0.003718	1.61E-03	0.43	0.006264
BI2	0.011285	2.79E-03	0.25	0.010944
CI1	0.054680	1.51E-02	0.28	0.059086
CI2	0.000055	2.89E-05	0.53	0.000112
CI3	0.000042	1.08E-05	0.26	0.000042
CI4	0.004528	1.04E-03	0.23	0.004071
CI5	0.001056	3.01E-04	0.29	0.001181
CI6	0.004569	1.04E-03	0.23	0.004069
CI7	0.005620	1.08E-03	0.19	0.004226
S	0.030199	3.02E-03	0.10	0.011895

Table A-2: CPT of S node of BN

AI8	BI2	CI7	P(S=1 | AI8, BI2, CI7)	P(S=0 | AI8, BI2, CI7)
0	0	0	0	1
1	0	0	0.8	0.2
0	1	0	0.5	0.5
0	0	1	0.6	0.4
1	1	0	0.9	$0.2 \cdot 0.4 = 0.08$
1	0	1	0.92	$0.2 \cdot 0.4 = 0.08$
0	1	1	0.80	$0.5 \cdot 0.4 = 0.20$
1	1	1	0.96	$0.2 \cdot 0.5 \cdot 0.4 = 0.04$

Table A-3: Risks and statistics of events for BN, Non-Boolean relation

Intermediate Events	Mean risks	Standard Deviation	c.o.v	95% CI
AI1	0.002000	4.22E-04	0.21	0.001655
AI2	0.008086	3.50E-03	0.43	0.013562
AI3	0.002997	5.18E-04	0.17	0.002032
AI4	0.000100	4.33E-05	0.43	0.000168
AI5	0.008968	3.51E-03	0.39	0.013590
AI6	0.001559	3.87E-04	0.25	0.001514
AI7	0.012038	3.54E-03	0.29	0.013673
AI8	0.013578	3.55E-03	0.26	0.013775
BI1	0.003728	1.62E-03	0.43	0.006282
BI2	0.011298	2.78E-03	0.25	0.010942
CI1	0.054782	1.50E-02	0.27	0.058956
CI2	0.000055	2.87E-05	0.53	0.000110
CI3	0.000042	1.07E-05	0.26	0.000042
CI4	0.004533	1.04E-03	0.23	0.004064
CI5	0.001056	3.02E-04	0.29	0.001184
CI6	0.004574	1.04E-03	0.23	0.004066
CI7	0.005626	1.08E-03	0.19	0.004230
S	0.019770	3.19E-03	0.16	0.012516

Table A-4: Observation of failures, multi-hazard example

	S	AI8	A8	BI2	CI7
Observation (/year)	5/40	1/40	1/40	3/40	1/40

Table A-5: Risks and statistics of events for BN, incorporating new data in multi-hazard example

Intermediate Events	Mean risks	Standard Deviation	c.o.v	95% CI
AI1	0.002019	4.25E-04	0.21	0.001662
AI2	0.009917	3.81E-03	0.38	0.014837
AI3	0.003027	5.19E-04	0.17	0.002028
AI4	0.000100	4.35E-05	0.43	0.000169
AI5	0.010868	3.81E-03	0.35	0.014840
AI6	0.001577	3.87E-04	0.25	0.001521
AI7	0.013961	3.83E-03	0.27	0.014879
AI8	0.015516	3.84E-03	0.25	0.014896
BI1	0.004587	1.81E-03	0.39	0.007024
BI2	0.013672	2.68E-03	0.20	0.010494
CI1	0.054870	1.51E-02	0.28	0.059133
CI2	0.000055	2.89E-05	0.53	0.000111
CI3	0.000042	1.07E-05	0.26	0.000042
CI4	0.004794	1.02E-03	0.21	0.003984
CI5	0.001076	3.01E-04	0.28	0.001180
CI6	0.004835	1.02E-03	0.21	0.003983
CI7	0.005906	1.06E-03	0.18	0.004141
S	0.034712	4.58E-03	0.13	0.017946

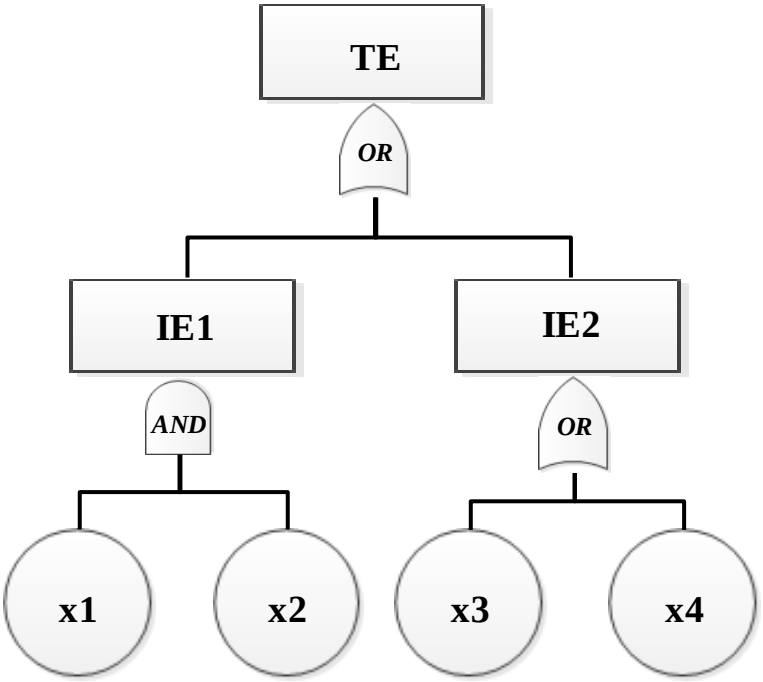

Fig. 1. An example of simple fault tree (FT)

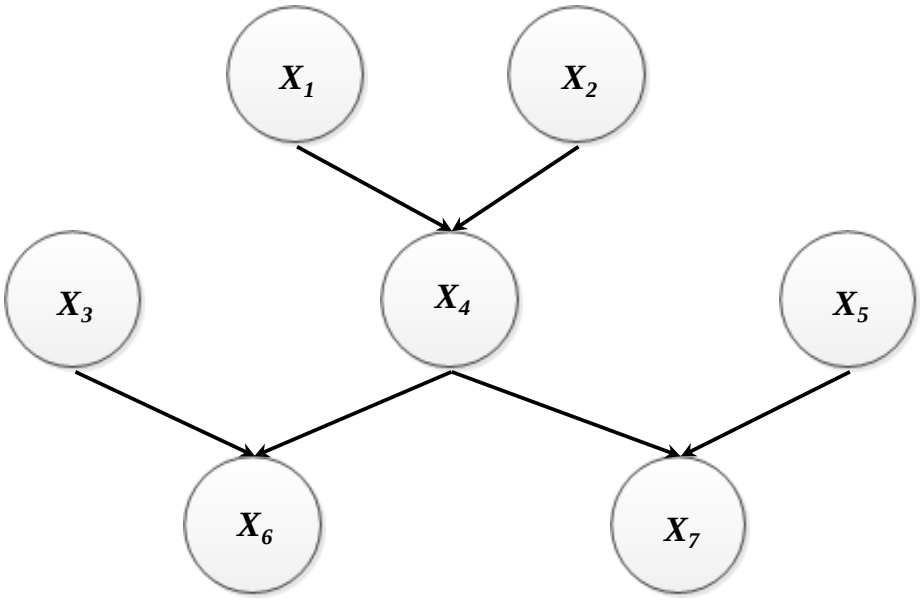

Fig. 2. An example of simple Bayesian network (BN)

CPT of IE1: ***"AND" Node***

x1	x2	P(IE1=1|x1, x2)
0	0	0
0	1	0
1	0	0
1	1	1

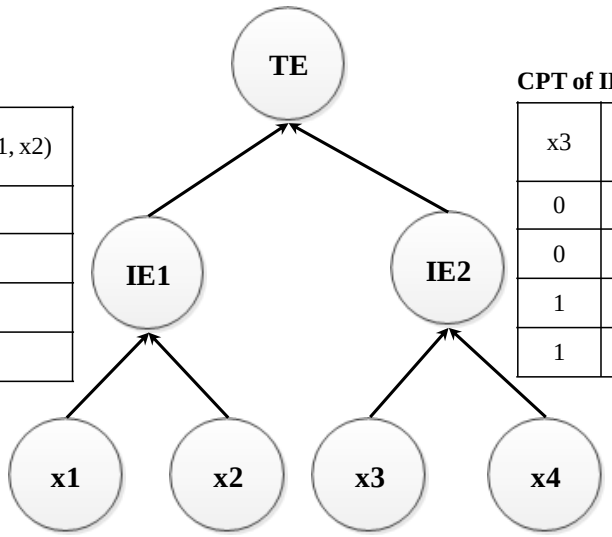

CPT of IE2: ***"OR" Node***

x3	x4	P(IE2=1|x3, x4)
0	0	0
0	1	1
1	0	1
1	1	1

Fig. 3. BN for FT example of Fig. 1 using mapping algorithm

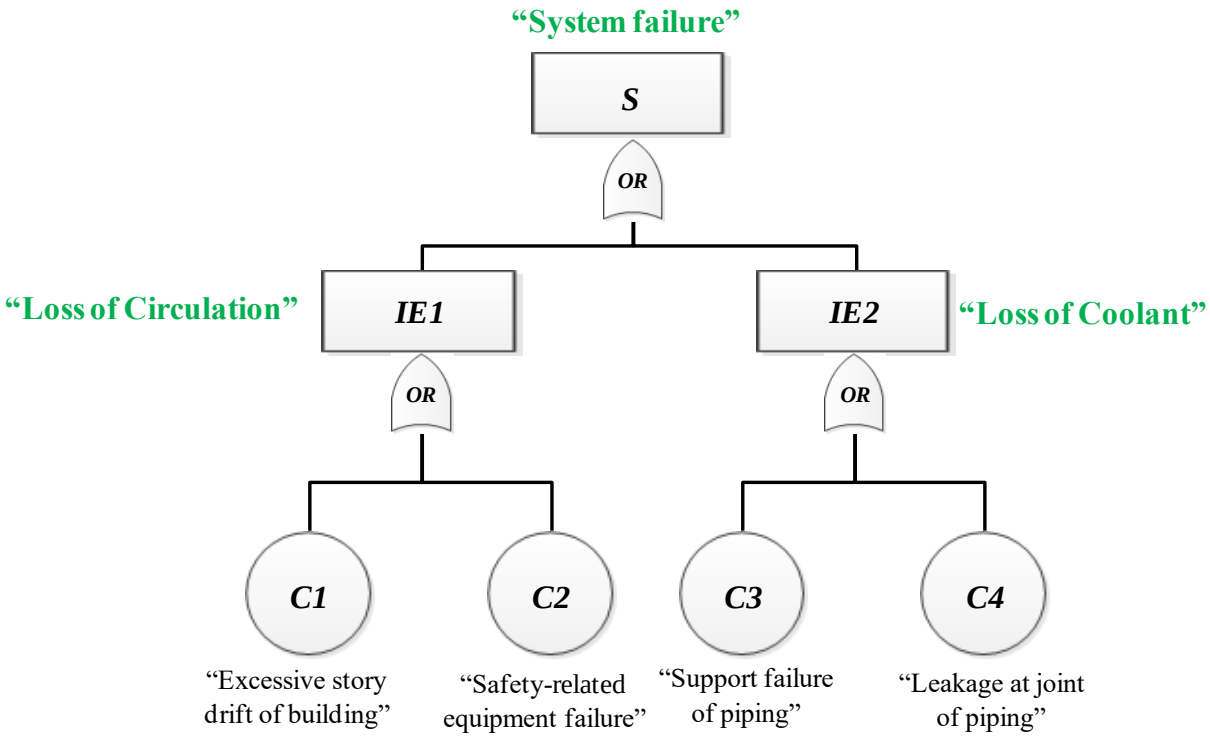

Fig. 4. Fault tree of building-piping structure system risk under an earthquake event

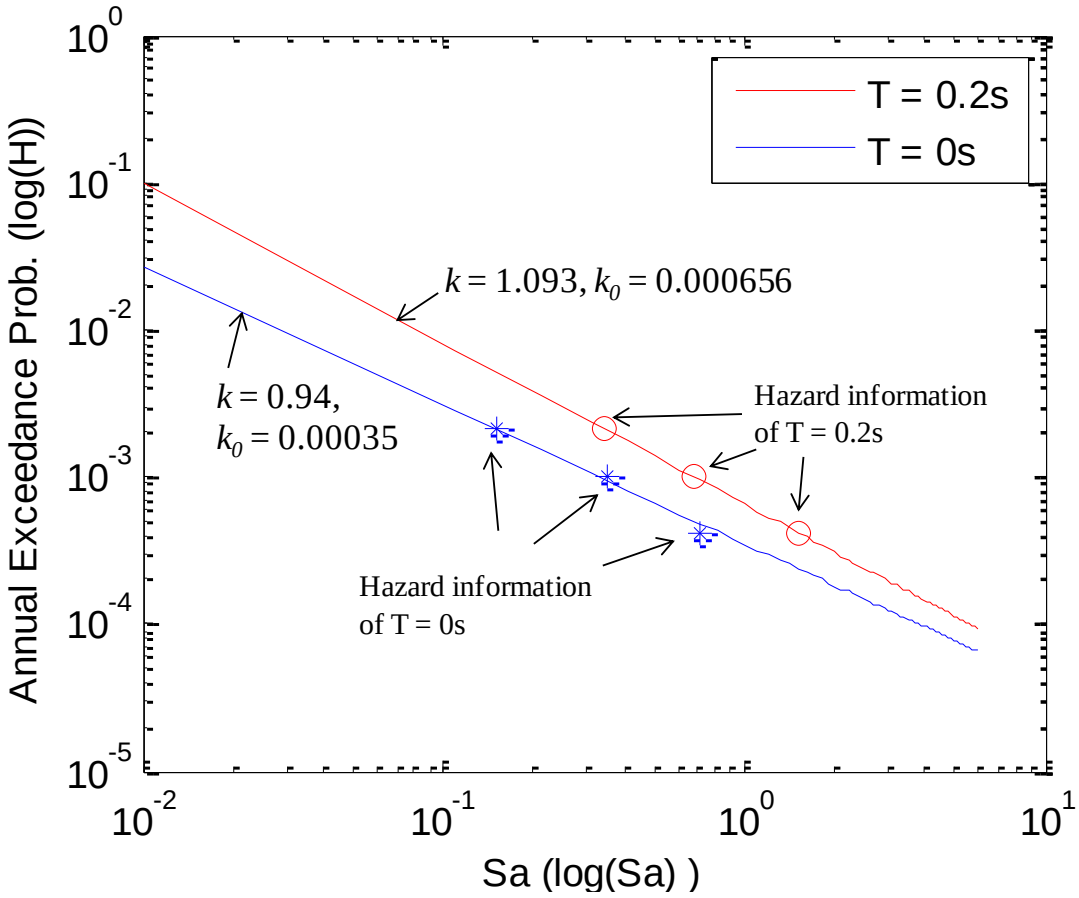

Fig. 5. Mean seismic hazard curves at Charleston (T = 0s and T = 0.2s)

* "0" and "1" mean safe and failure, respectively.

C1	P(C1)
1	**0.000310**
0	1 -0.000310

C2	P(C2)
1	**0.000200**
0	1 -0.000200

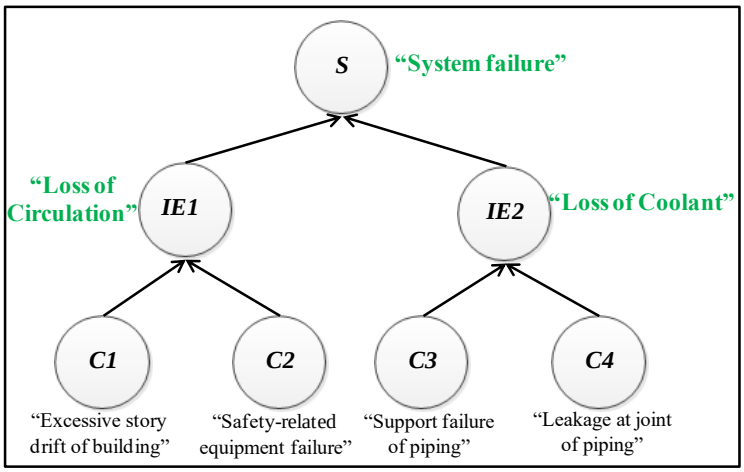

C3	P(C3)
1	**0.000163**
0	1 -0.000163

C4	P(C4)
1	**0.000727**
0	1 -0.000727

CPT of IE1 "OR node"

C1	C2	P(IE1=1|C1,C2)
1	1	**1.00**
1	0	**1.00**
0	1	**1.00**
0	0	**0.00**

CPT of IE2 "OR node"

C3	C4	P(IE2=1|C3,C4)
1	1	**1.00**
1	0	**1.00**
0	1	**1.00**
0	0	**0.00**

CPT of S "OR node"

IE1	IE2	P(S=1|IE1,IE2)
1	1	**1.00**
1	0	**1.00**
0	1	**1.00**
0	0	**0.00**

Fig. 6. BN corresponding to FT of Fig. 4

* “0” and “1” mean safe and failure, respectively.

C1	P(C1)
1	**0.000310**
0	1-0.000310

C2	P(C2)
1	**0.000200**
0	1-0.000200

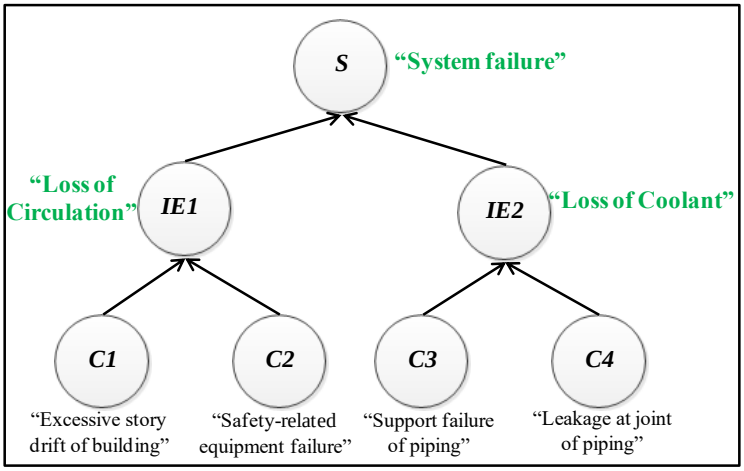

C3	P(C3)
1	**0.000163**
0	1-0.000163

C4	P(C4)
1	**0.000727**
0	1-0.000727

CPT of IE1

C1	C2	P(IE1=1|C1,C2)
1	1	**1.00**
1	0	**0.20**
0	1	**1.00**
0	0	**0.00**

CPT of IE2

C3	C4	P(IE2=1|C3,C4)
1	1	**1.00**
1	0	**0.70**
0	1	**1.00**
0	0	**0.00**

CPT of S

IE1	IE2	P(S=1|IE1,IE2)
1	1	**1.00**
1	0	**0.90**
0	1	**1.00**
0	0	**0.00**

Fig. 7. BN incorporating additional scenario

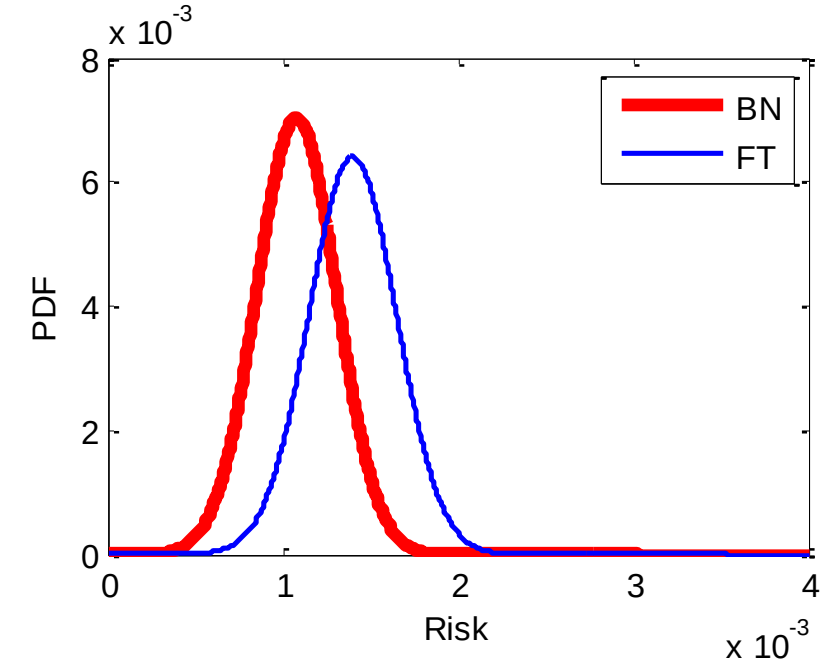

(a) PDF

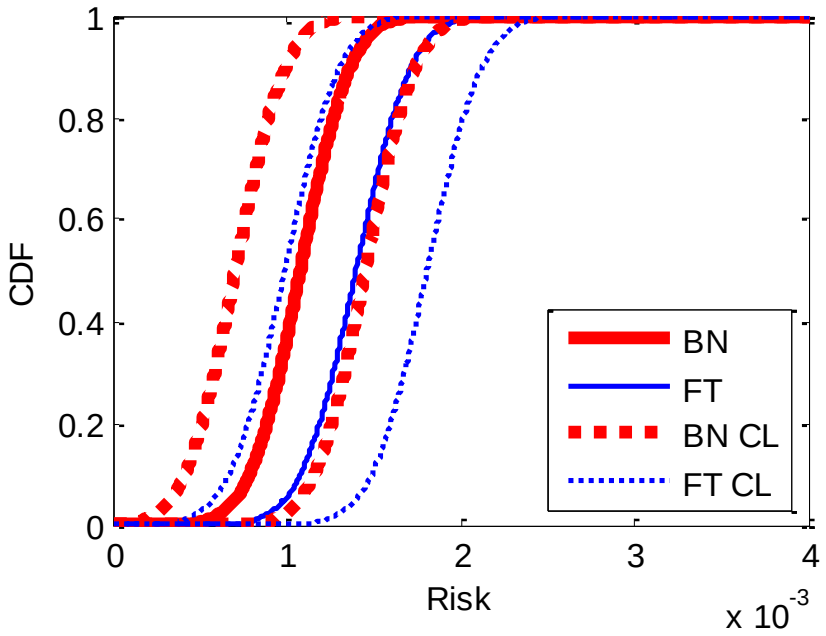

(b) CDF with 5 % and 95 % confidence level

Fig. 8. PDF and CDF of risk of system failure from FTA and BN, single hazard example

* "0" and "1" mean safe and failure, respectively.

C1	P(C1)
1	0.000310
0	1-0.000310

C2	P(C2)
1	0.000200
0	1-0.000200

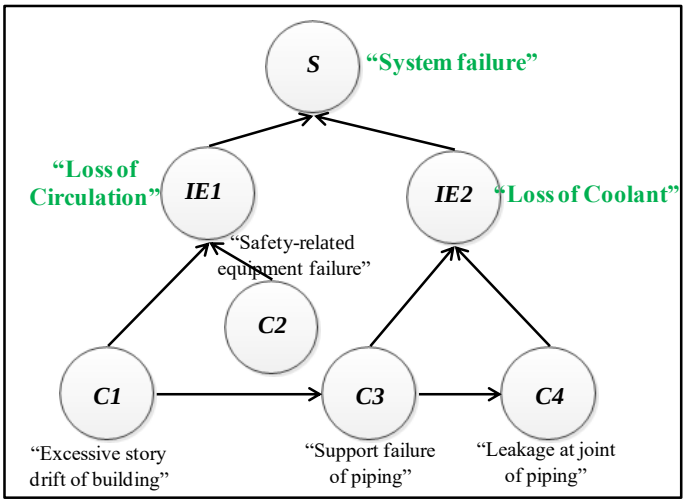

CPT of C3

C1	P(C3=1|C1)
1	0.70
0	0.00

CPT of C4

C3	P(C4=1|C3)
1	0.90
0	0.00

CPT of IE1

C1	C2	P(IE1=1|C1,C2)
1	1	1.00
1	0	0.20
0	1	1.00
0	0	0.00

CPT of IE2

C3	C4	P(IE2=1|C3,C4)
1	1	1.00
1	0	0.70
0	1	1.00
0	0	0.00

CPT of S

IE1	IE2	P(S=1|IE1,IE2)
1	1	1.00
1	0	0.90
0	1	1.00
0	0	0.00

Fig. 9. BN for additional correlation information

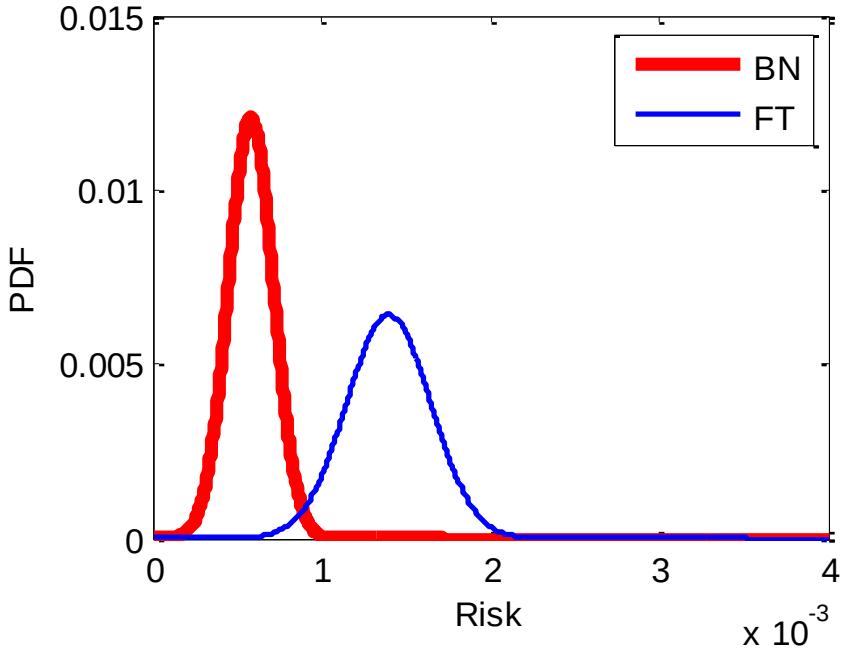

(a) PDF

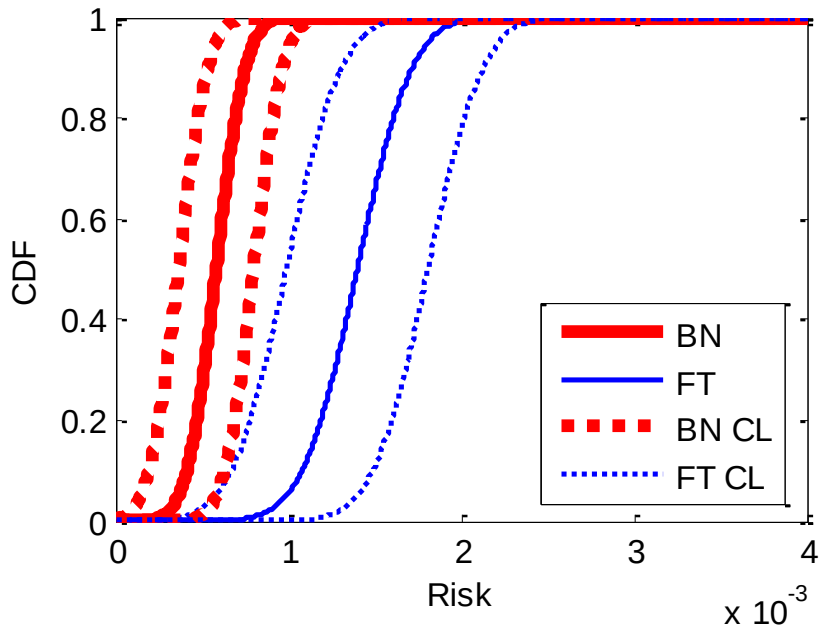

(b) CDF with 5 % and 95 % confidence level

Fig. 10. PDF and CDF of risk of system failure from FTA and BN

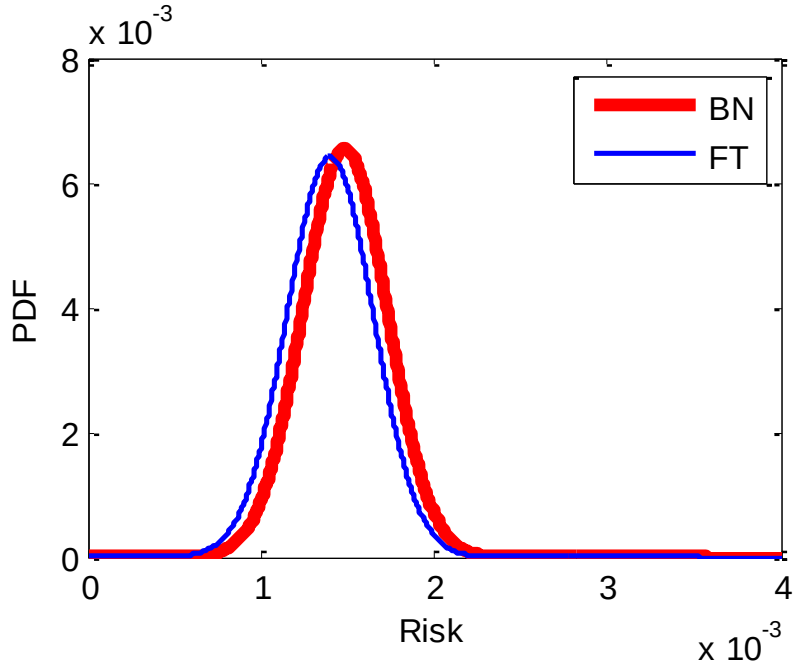

(a) PDF

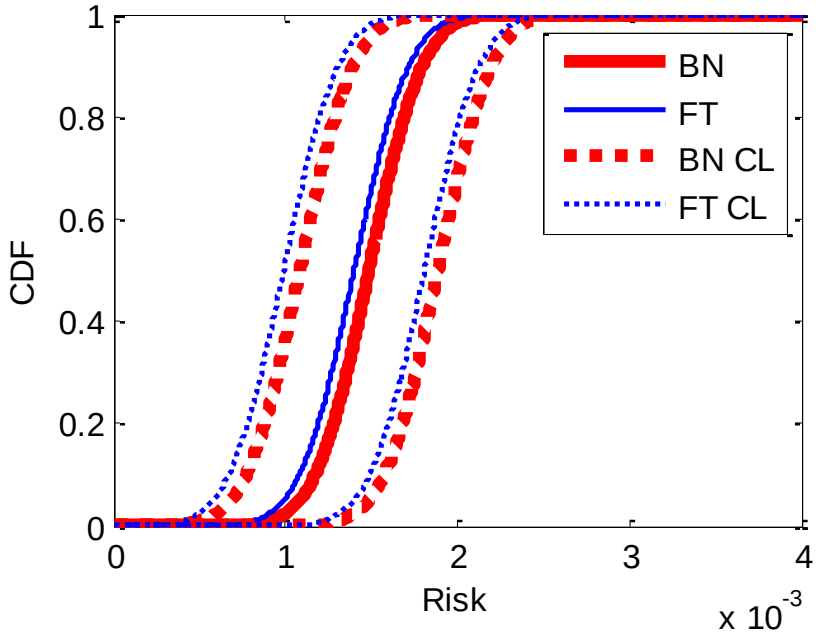

(b) CDF with 5 % and 95 % confidence level

Fig. 11. Prior and posterior distributions of the event of system failure with additional information

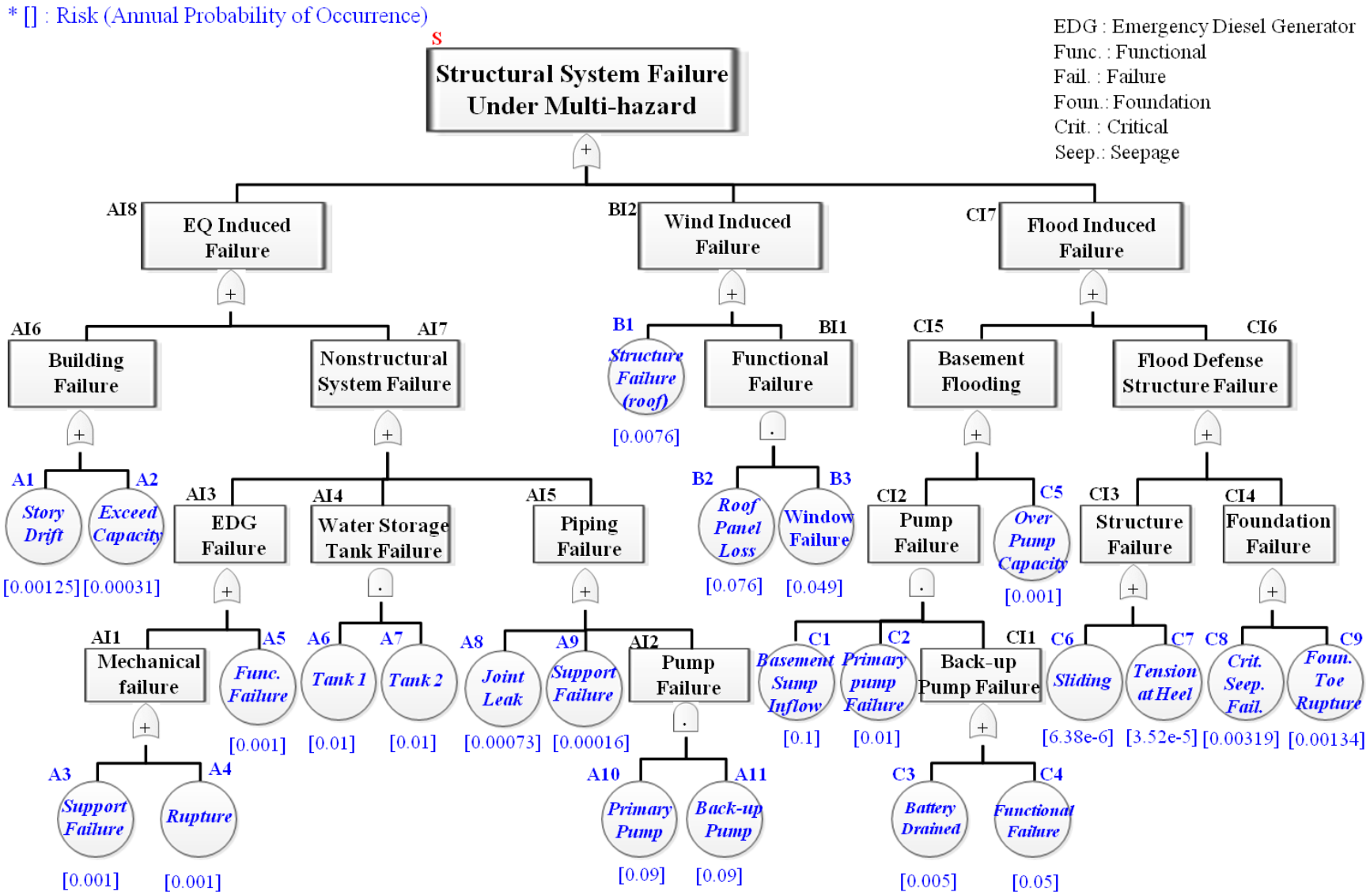

Fig. 12. FT of building-piping structure system risk under multiple hazards

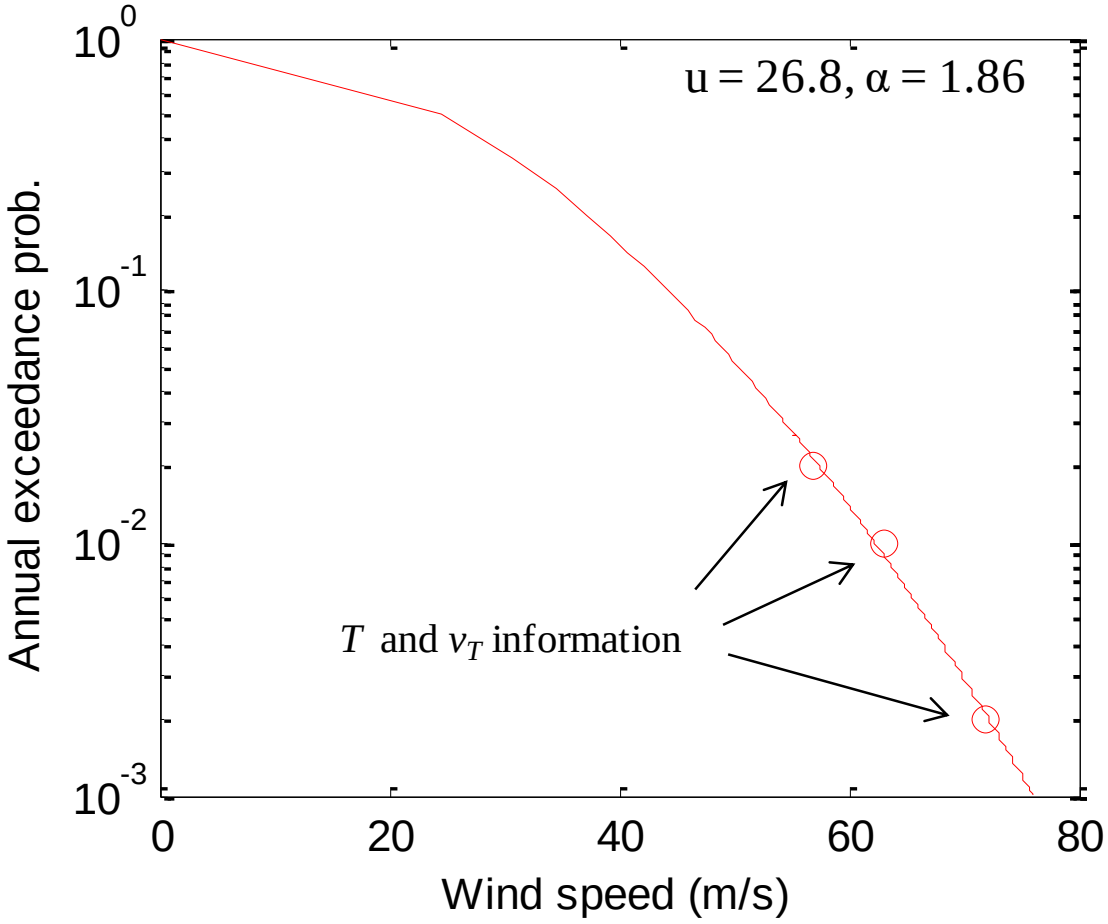

Fig. 13. Wind hazard curves at Charleston

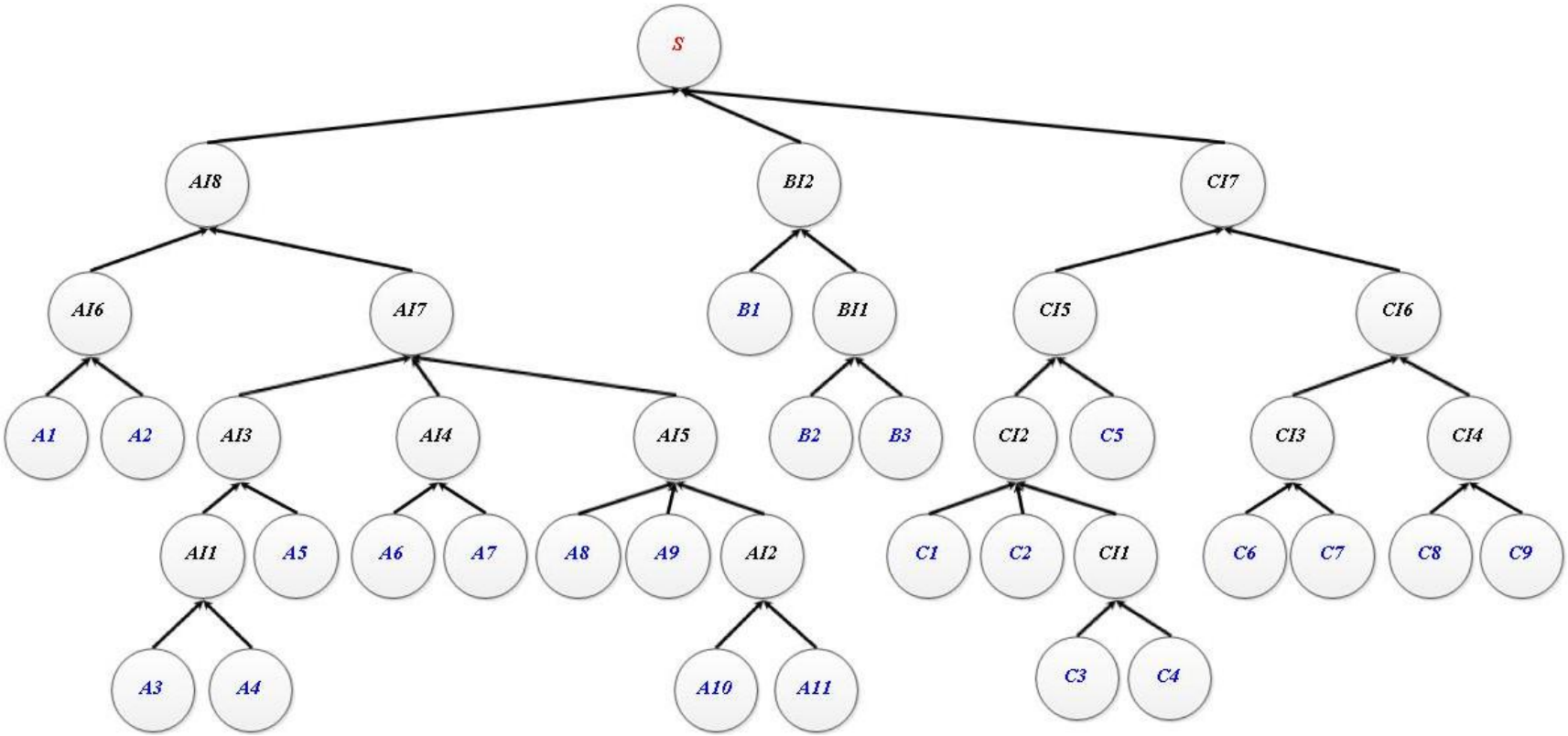

Fig. 14. BN corresponding to FT of Fig. 12

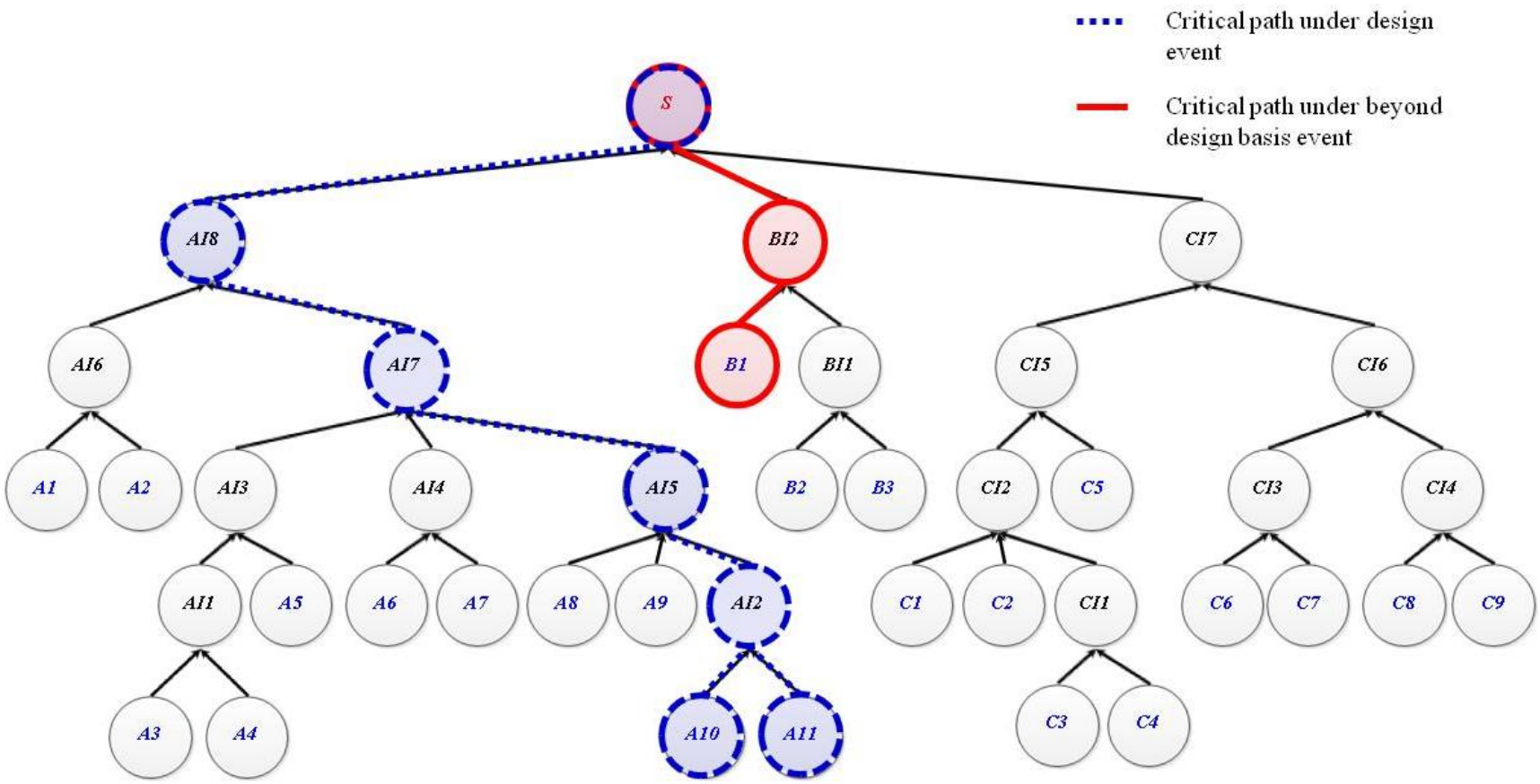

Fig. 15. Scenarios for vulnerabilities due to beyond design basis event

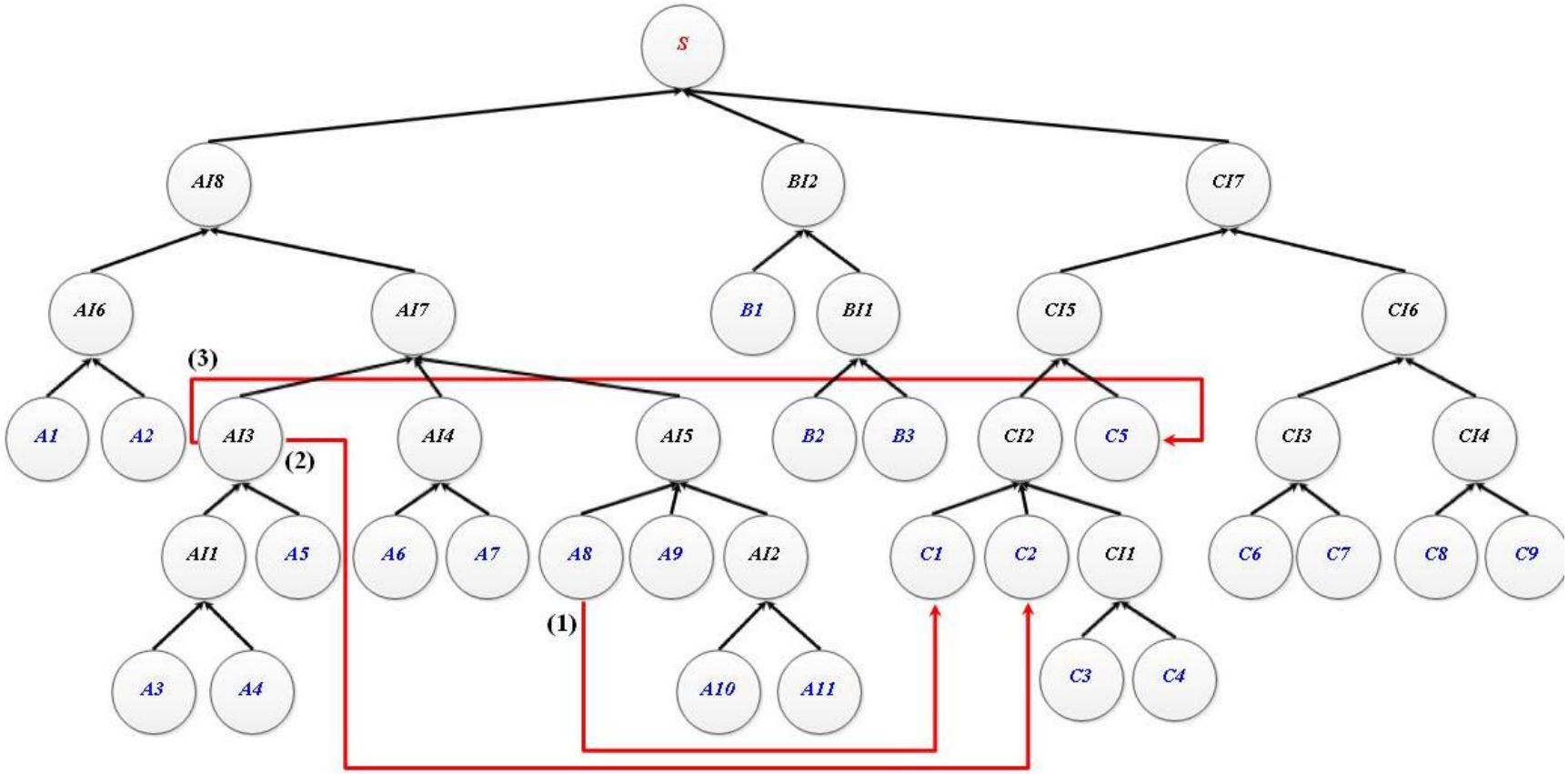

(1)

A8	P (C1=1|A8)
1	**0.90**
0	**0.10**

(2)

AI3	P (C2=1|AI3)
1	**1.00**
0	**0.01**

(3)

AI3	P (C5=1|AI3)
1	**1.00**
0	**0.001**

Fig. 16. Scenarios for seismically induced internal flooding

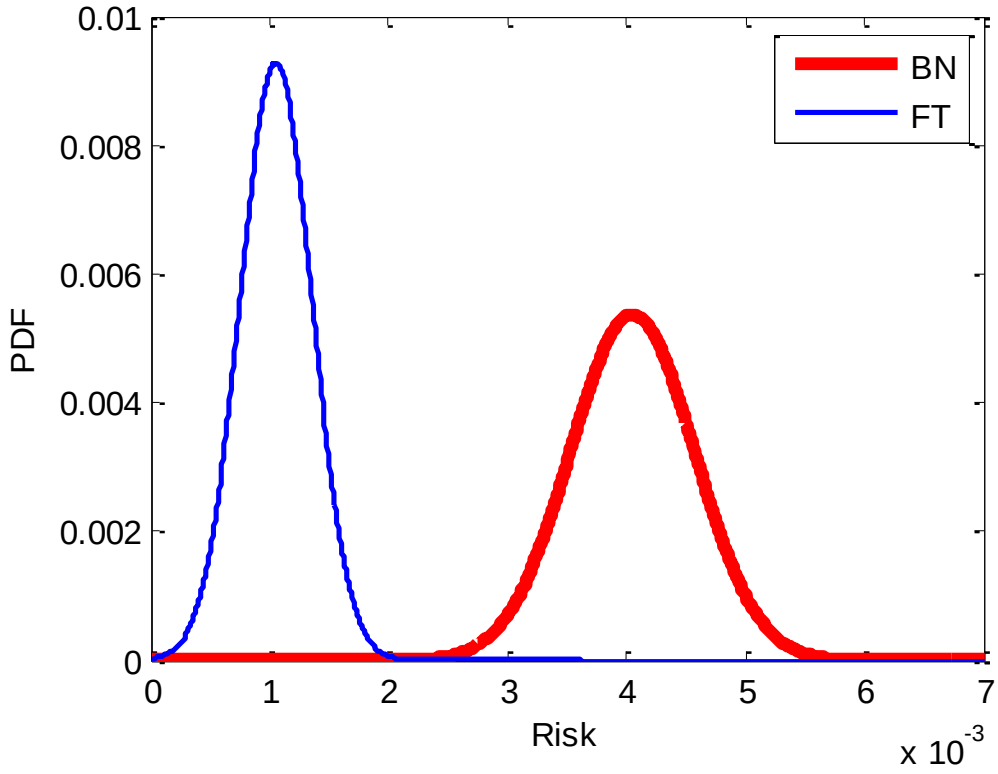

Fig. 17. PDF of risk of basement flooding event (CI5) from FT and BN considering seismically induced flooding scenario

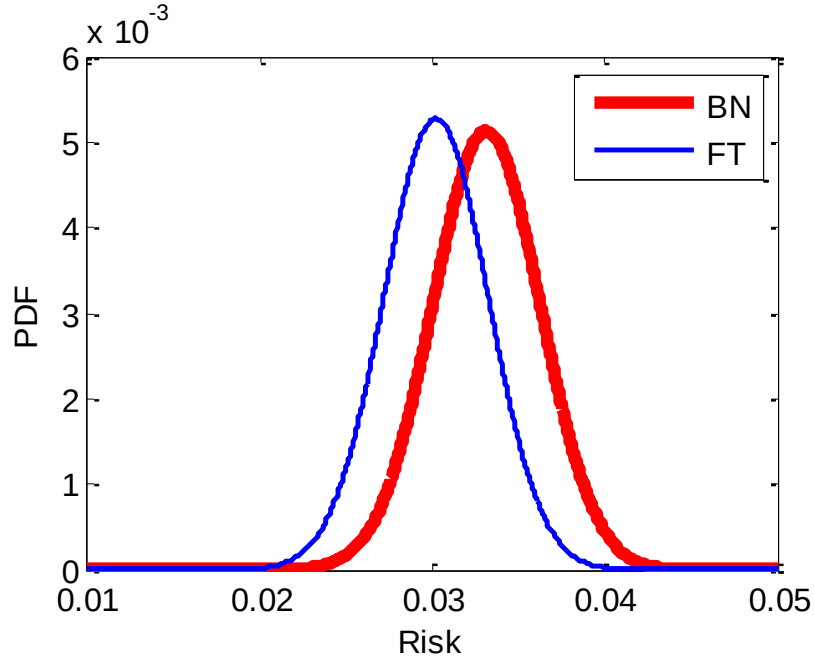

(a) PDF

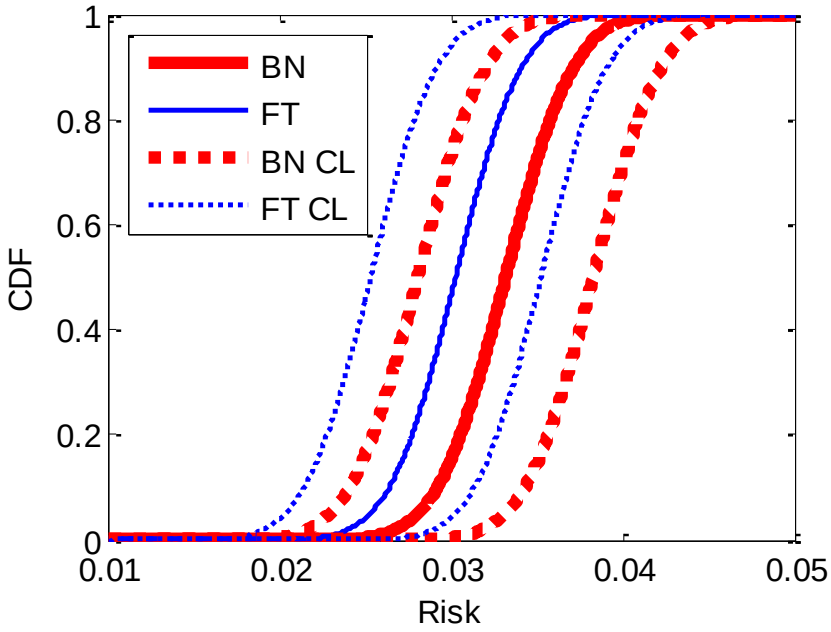

(b) CDF with 5 % and 95 % confidence level

Fig. 18. PDF and CDF of risk of system failure from FT and BN considering seismically induced flooding scenario

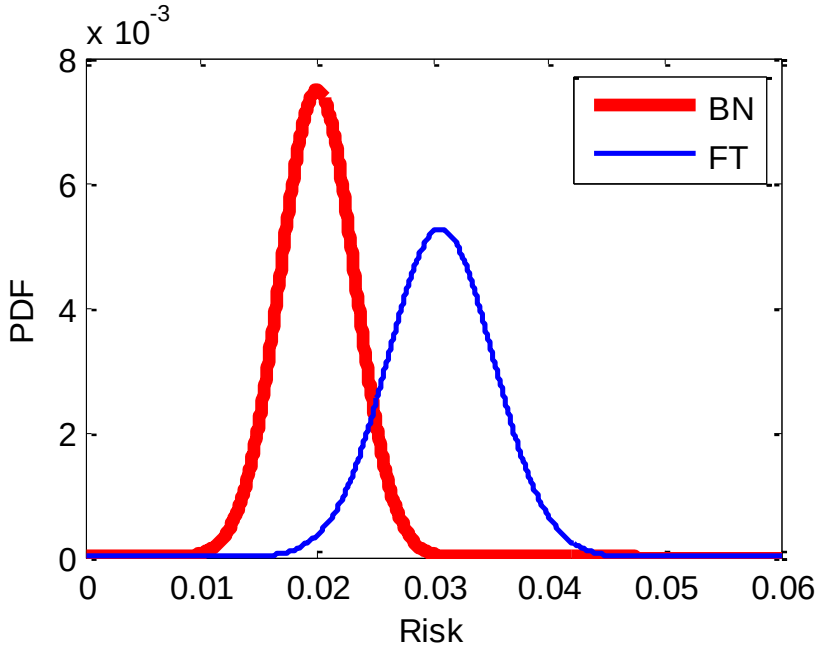

(a) PDF

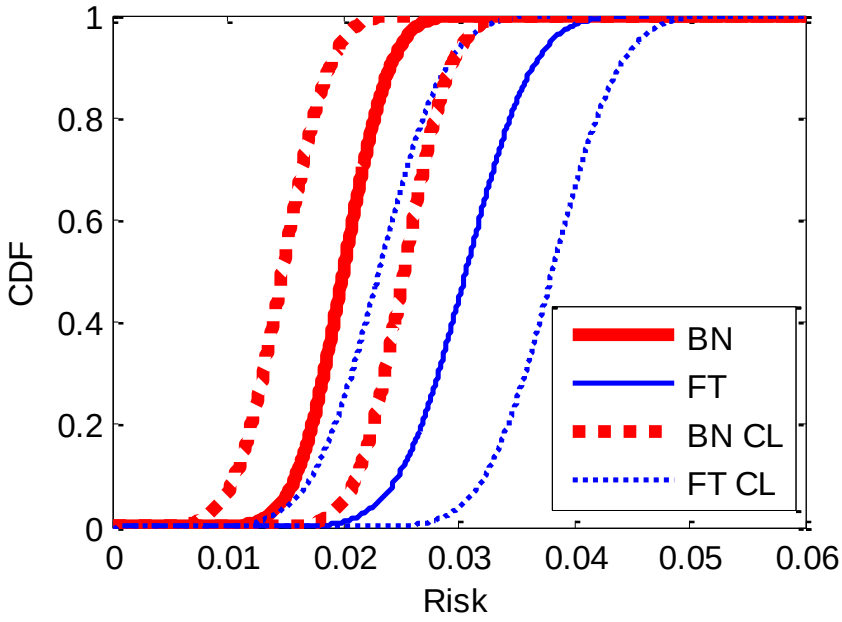

(b) CDF with 5 % and 95 % confidence level

Fig. A-1. PDF and CDF of risk of system failure from FTA and BN (non-Boolean relation)

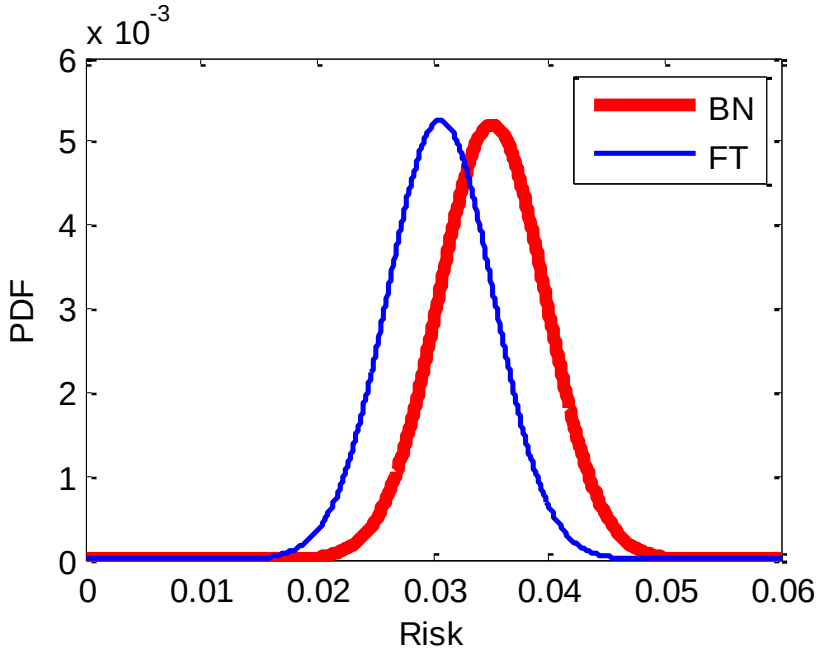

(a) PDF

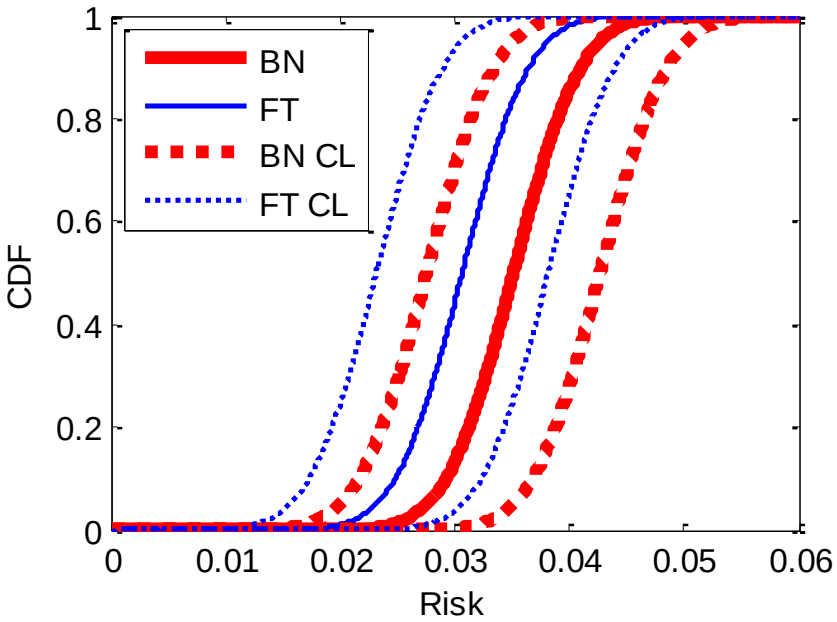

(b) CDF with 5 % and 95 % confidence level

Fig. A-2. Prior and posterior distributions of the event of system failure with additional information

PART III

PROBABILISTIC RISK ASSESSMENT BASED MODEL VALIDATION METHOD USING BAYESIAN NETWORK

Shinyoung Kwag and Abhinav Gupta

ABSTRACT

Past few decades have seen a rapid growth in the availability of computational power and that induces continually reducing cost of simulation. This rapidly changing scenario together with availability of high precision and large-scale experimental data has enabled development of high fidelity simulation tools capable of simulating multi-physics multi-scale phenomenon. At the same time, there has been an increased emphasis on developing strategies for validation and verification of such high fidelity simulation tools. The problem is more pronounced in cases where it is not possible to collect experimental data or field measurements on a large-scale or full scale system performance. This is particularly true in case of systems such as nuclear power plants subjected to external hazards such as earthquakes. In such cases, engineers rely solely on simulation tools but struggle to establish the validity of the system level simulations. Most validation approaches rely heavily on expert elicitation. There is an increasing need of a quantitative approach for validation of high fidelity simulations that is consistent, efficient, and effective. A validation approach should be able to consider uncertainties due to inherent lack of knowledge and randomness in the system's performance as well as in the characterization of external hazard. A new approach to validation is presented in this paper that uses a probabilistic index as a degree of validation and propagates it through the system using the performance-based probabilistic risk assessment (PRA) framework. Unlike traditional PRA approaches, it utilizes the power of Bayesian statistic to account for non-Boolean relationships and correlations among events

at various levels of a network representation of the system. Bayesian updating facilitates evaluation of updated validation information as additional data from experimental observations or improved simulations is incorporated. PRA based framework assists in identifying risk-consistent events and critical path for appropriate allocation of resources to improve the validation.

1. Introduction

Given the events at Fukushima-Daiichi nuclear power plant, there is an increased emphasis on using high fidelity simulation tools to evaluate the vulnerability of nuclear facilities subjected to external hazards. Availability of sophisticated computer models capable of simulating multi-physics multi-scale phenomena has increased the need for verification and validation of such high fidelity simulations. Among the many challenges in this process, the two primary ones are: (1) lack of relevant plant-level data needed for validation of high-fidelity simulations, and (2) non-availability of a rational, consistent, and quantitative approach for validation. While first item above is essential in any validation effort, it is usually restricted by high cost of collecting such data and in some cases inability to conduct large-scale experiments. The confidence in high-fidelity simulations decreases due to excessive reliance on expert opinion for establishing the acceptability of high simulation models.

The uncertainties due to inherent randomness and lack of knowledge about real physical complex systems as well as natural hazards pose significant challenges to the model validation assessment. Fidelity of a system-level computer simulation model is difficult to assess even though a model for each component of the system can be individually validated with available component-level data. The quantitative system-level validation process involves a validation at component level, establish the degree of validation in each case, determine a relationship between component-level and system-level performance, and finally

establish an inference of the degree of validation at system-level. The validation goal is difficult to achieve particularly in a quantitative sense because of the uncertainties in the relationship between different levels as well as in the parameters used for characterizing the performance at both the component and system levels. Consequently, four key aspects in this process are: (1) validation metric: characterization of an appropriate validation metric for quantitative comparison of simulation and test data, (2) predictive capability and confidence: inference on the degree of validation at system-level, (3) scaling: quantitative characterization of the relationship between component-level and higher-level performance, and (4) decision: an acceptance criterion to determine effective strategies for improving the validation.

Validation Metric: Many different approaches have been examined in existing literature for characterizing an appropriate metric for the model validation under uncertainties. In most cases, a graphical comparison is employed to determine the degree of agreement between the simulation predictions and the actual observations. Classical statistical hypothesis testing has often been employed for comparison of two sets of random variables (Hills and Trucano, 2002; Dowding and Rutherford, 2003; Chen et al., 2004; Hills, 2006). The outcome of such a comparison is expressed in terms of the probability which can then be combined with error statistics to determine the degree of validation. The Bayesian hypothesis testing approach has been also applied to validation problem (Kennedy and O'Hagan, 2001; Zhang and Mahadevan, 2003; O'Hagan, 2006; Bayarri et al., 2007; Chen et al., 2008; Babuška et al., 2008; Rebba and Mahadevan, 2008). More specifically, Kennedy and O'Hagan (2001) define

model bias as the difference between the means of experimental and simulation data. Zhang and Mahadevan (2003) use the probability of Bayes factor exceeding a specified value as the decision criterion for the model acceptance/rejection. A direct comparison of mean values from simulation and experiment has also been used for the validation of simulation models (Coleman and Stern, 1997; Sprague and Geers, 1999; Oberkampf and Trucano, 2000; Oberkampf and Barone, 2006). Alternatively, probabilistic measures have also been used (Ferson et al., 2008; Ferson and Oberkampf, 2009; Roy and Oberkampf, 2011; Voyles and Roy, 2015).

Scaling: Some studies have also addressed the inference of the system-level validation starting with the component-level validation metric. A building block or hierarchical approach has been proposed for propagation of component level information to the system level through intermediate sub-system levels (AIAA Guide, 1998; Hasselman et al., 2002; Bayarri et al., 2005; Korb et al., 2013). In general, the amount of available experimental data decreases as one proceeds from lower to higher levels. Therefore, a Bayesian network (BN) can be employed very effectively to update the statistical information for all nodes when additional information becomes available within the Bayesian hypothesis testing framework (Mahadevan and Rebba, 2005; Rebba and Mahadevan, 2006). Effective use of Bayesian network requires availability of an explicit quantitative relationship between the component levels and the higher levels of the network. To do so, Mahadevan and Rebba (2005) utilize mechanistic equations to relate the higher-level output with lower-level input/output.

Uncertainty Modeling: For problems that could not be characterized by an analytical relationship, Rebba and Mahadevan (2006) construct a stochastic response surface between lower-level and higher-level data. Jiang and Mahadevan (2009) use a structural equation modeling approach to utilize the lower-level data for the higher-level model validation under uncertainty through a collective use of lower-level data, higher-level data, computational model, and latent variables. In order to address the acceptability of a model validation, Jiang and Mahadevan (2007) propose a decision-making methodology by considering a risk-benefit approach in which the risk/benefits of using the current model and the data support for the current model are evaluated with respect to the cost of acquiring new information for improving the model under the Bayesian hypothesis testing.

In the context of the various existing studies summarized above, the validation problem continues to be challenging one due to a few different reasons. First, the existing definitions of a quantitative validation metric need significant improvement especially for addressing validation problems that have large degree of uncertainties associated with them. Second, the existing studies are restricted to problems in which the system level simulation model is characterized mathematically. Such a mathematical description is neither available nor possible especially for evaluating the performance of nuclear systems subjected to external hazards. In addition to these restrictions, it is important to note that existing approaches do not identify whether or not an improvement in the validation of a given component or subsystem is important/critical with respect to system level performance.

This paper focuses on exploring a novel performance-based risk-informed validation approach that aspires to be rational, efficient, and quantitative in nature. The intent of the proposed approach is to provide a quantitative assessment of validation for a system-level simulation model based on component-level validation information. It uses performance-based criteria to judge the efficacy of a particular validation and a risk-informed framework to determine whether additional validation of a certain component or subsystem is needed or not. The applicability and effectiveness of the proposed approach is explored in the context of a structural system subjected to a natural hazard due to an earthquake. Yet, the approach is quite generic in nature and is applicable to a variety of validation problems.

2. Performance-based Probabilistic Risk Assessment (PRA)

In the current methodology, the overall risk (i.e. annual probability of occurrence or failure) for an individual hazard is evaluated by a convolution of hazard curve and the corresponding fragility as follows:

$$P_f = \int P_{f|\lambda} \cdot \left| \frac{dH(\lambda)}{d\lambda} \right| d\lambda \qquad (1)$$

in which λ is a hazard intensity parameter, $P_{f|\lambda}$ is the fragility curve, and $H(\lambda)$ represents hazard curve. The hazard curve expresses the probability of annual exceedance in a domain of the intensity measure used for characterizing the external hazard. The fragility curve for basic events is obtained by using empirical, experimental, and/or numerical simulation data

and represents the conditional probability of failure under each hazard's intensity. The system-level risk is calculated by employing either a series-parallel system as a simplistic representation of the system or by conducting a fault tree analysis in which the events are assumed to be statistically independent, mutually exclusive, and collectively exhaustive.

Probabilistic Hazard Analysis: In order to develop a hazard curve, the hazard is characterized in terms of an engineering design parameter. For example, probabilistic seismic hazard analysis (PSHA) focuses on quantifying uncertainties in the sources, size, distance, and ground motion characteristics of future earthquakes and incorporating this information to produce a distribution of possible ground motions that can occur at a site of interest. The end result of PSHA is represented by seismic hazard curves where the annual rates of exceedance are plotted against a ground motion intensity parameter such as peak ground acceleration (PGA) or spectral acceleration (SA). A detailed description of PSHA is given in McGuire (2002). The US Geological Survey (USGS, http://earthquake.usgs.gov/hazards/products/) provides hazard information and hazard curves at any site of interest within the US.

Performance-Based Fragility Assessment: The fragility of a structure, system, or component (SSC) is defined as the conditional failure probability, $P_{f|\lambda}$, to attain or exceed a specified performance function, G, under a given measure of specific intensity parameter λ. Mathematically,

$$P_{f|\lambda} = P\left(G < 0 \mid \lambda\right) \qquad (2)$$

G is a function of the random variables representing uncertainties in material properties, physical behavior, mechanistic models, and loading conditions. It can be described in a simplistic form as:

$$G(S,R) = S - R \tag{3}$$

where S represents the "Strength" or "Capacity" corresponding to the specified loading condition and R represents the "Response" or "Demand" corresponding to the given hazard intensity parameter. Eq. (3) can be written by various forms such as physics or mechanics based models, experimentally obtained data, empirical relations, simulations, or a combination of these. It can then be solved in many different ways such as Monte Carlo simulation, first/second order reliability methods, random vibration based approach, statistical inference approach, etc. In most implementations, the fragility curves are represented as the cumulative distribution function for a lognormal model.

System-Level Fragility using Fault Tree Analysis (FTA): A fault tree diagram is a graphical decomposition of an undesirable event representing system failure (denoted as top event TE) into intermediate events and basic events through the use of logical gates (AND and OR gates). The basic events are characterized by Boolean states that represent "failure" or "safe" states. The basic events are considered to be statistically independent as well. The basic events are connected through the logic gates to characterize intermediate events which are also connected through the logic gates.

To begin with, a qualitative evaluation is used to develop the logical expression for the TE. Boolean algebra is used to obtain the minimal cut-sets. The order of a minimal cut-set is the number of basic events that contribute to the particular minimal cut-set. For illustration purposes, let us consider the example of a simple fault tree shown in Fig. 1. In this figure, x1, x2, x3 and x4 represent four basic events. The IE1 and IE2 are the intermediate events produced through combination of basic events by logic gates. Therefore, we can write a logical expression for the top event as: $\mathrm{TE} = (\mathrm{x1} \cap \mathrm{x2}) \cup (\mathrm{x3} \cup \mathrm{x4})$. The corresponding Boolean algebra is $\mathrm{TE} = (\mathrm{x1} \cdot \mathrm{x2}) + (\mathrm{x3} + \mathrm{x4})$ and a total of 3 minimal cut-sets exist namely, x1·x2, x3, and x4. The minimal cut-sets x3 and x4 are of first order and the minimal cut-set x1·x2 is of second order. Finally, a quantitative analysis is conducted to compute the probability of occurrence of the TE and determine the importance measure for each minimal cut-set. The probability of occurrence of the TE is calculated by using following equation:

$$\begin{aligned} P(TE) &= P\left(\bigcup_{i=1}^{n} M_i\right) \\ &= \sum_{i=1}^{n} P(M_i) - \sum_{i<j=2}^{n} P(M_i M_j) + \sum_{i<j<k=3}^{n} P(M_i M_j M_k) \\ &\quad + \cdots + (-1)^{n-1} P(M_1 M_2 \cdots M_n) \end{aligned} \tag{4}$$

where M_1, M_2, …, M_n represents the minimal cut-sets and n is the total number of minimal cut-sets. The importance measure (*IM*) analysis calculates the contribution of the minimal cut-sets to the occurrence of TE and accordingly identifies the critical events. Various

methods for assessing the *IM*s are: Birnbaum, Criticality, Fussell-Vesely, Risk-Reduction Worth and Risk-Achievement Worth measures of importance (Modarres et al., 1999). In this study, the importance measure given by Fussell-Vesely (1975) is employed according to which:

$$IM = F\left(M_i\right) / F\left(\mathbf{M}\right) \qquad (5)$$

where F (**M**) is the total risk from all minimal cut-sets; F (M_i) is the risk from the cut-sets which contain minimal cut-set M_i. These *IM*s compute the overall percent contributions of minimal cut sets to the total risk.

3. Concept of Bayesian Network for PRA

Bayesian Network (BN): In contrast to a fault-tree, a Bayesian Network (BN), also referred to as a Bayesian Belief Network, is a more general form that can account for the statistical relationships among the events. It is a graphical representation of a set of conditionally independent assumptions and accordingly requires a joint probability distribution between random variables. This generality makes it a powerful tool for the structure/system reliability, risk management, accident analysis, artificial intelligence, etc. A Bayesian Network is a directed acyclic graph (DAG) which is created by using the nodes (or vertices) represented by circles, arrows (or arcs), and the conditional probability table (CPT). Each node defines either a discrete or a continuous random variable. An intermediate node serves as a parent as well as a child node. The nodes which have arrows directed to other nodes are parent nodes

and nodes that have arrows coming from other nodes are called as child nodes A node that does not have any arrow coming from another node is called as root node and it does not have any parent node. Arrows represent direct relationships between interconnected parent and child nodes. The CPTs assigned to nodes describe the quantitative relationships between interconnected nodes.

A BN analysis is performed based on the conditional probability as per Eq. (6) below and the conditional independence assumption, i.e. P(x,y|z) = P(x|z) P(y|z) if and only if $X \perp Y|Z$. The joint probability distributions can be expressed using conditional probability as:

$$P\left(X_1, X_2, \cdots, X_n\right) = \prod_{i=1}^{n} P\left(X_i \mid X_1, \cdots, X_{i-1}\right) \qquad (6)$$

The conditional independence assumption simplifies Eq. (6) further as:

$$P\left(X_1, X_2, \cdots, X_n\right) = \prod_{i=1}^{n} P\left(X_i \mid \text{Parent}\left(X_i\right)\right) \qquad (7)$$

Parent (X_i) is parent nodes for X_i; P(X_i | Parent (X_i)) is the CPT of X_i and n is the number of nodes in the network. For illustration, let us consider a simple network shown in Fig. 2 in which X_1, X_2, X_3 and X_5 are the root nodes. X_4 is the child node of X_1 and X_2, and parent node of X_6 and X_7. X_6 is the child node of X_3 and X_4. X_7 is the child node of X_4 and X_5.

A Bayesian network can also be used as an inference tool to evaluate beliefs of events when new information also called as “evidence” becomes available. The evidence is typically

represented by binary states: occurrence of event by “1” and non-occurrence by “0”. For evidence *e*, the joint probability of all the nodes can be inferred as

$$P\left(X_1, X_2, \cdots, X_n \mid e\right) = \frac{P\left(X_1, X_2, \cdots, X_n, e\right)}{P\left(e\right)} = \frac{P\left(X_1, X_2, \cdots, X_n, e\right)}{\sum_{X_1, \cdots, X_n} P\left(X_1, X_2, \cdots, X_n, e\right)} \qquad (8)$$

This equation can be adopted for two types of probabilistic reasoning - the predictive analysis as well as updating analysis.

Mapping algorithm: In general, it is not straightforward to create a Bayesian network directly. It is relatively much easier to create a fault tree. Therefore, a mapping algorithm is needed to transform a fault tree into a Bayesian network. The mapping involves two steps, graphical representation and numerical computation. First, all events in a fault tree - the basic, intermediate, and top events - are converted into the nodes of Bayesian network. The basic events map into the root nodes of a Bayesian network and the intermediate events map to child nodes of the root nodes. The top event of a fault tree maps into a child node of basic and intermediate events. For numerical computation, the probabilities of basic events in a fault tree are assigned to the marginal probabilities of root nodes in a Bayesian network. For the intermediate and top events of fault tree defined by logic gates, the CPTs are established at corresponding child nodes of Bayesian network. For illustration, let us consider the fault tree that is shown in Fig. 1 which is mapped into a Bayesian network as shown in Fig. 3. The CPTs of IE1 and IE2 nodes of BN which are represented as “AND” and “OR” gates in fault tree are given in tables located besides these nodes. In this figure, “0” and “1” represent non-

occurrence and occurrence of event, respectively. A detailed discussion of mapping algorithm is given in Bobbio et al. (2001). It must be recognized that an initial Bayesian network created by mapping from a fault tree consists of conditional probabilities that takes only a binary form. However, it can then be modified to a more general form by using non-binary values in the CPT or by creating arcs among the nodes to account for correlation of events. Even though each root node has only binary outcomes, the marginal probability can be characterized by an appropriate probability distribution. Once the root nodes are characterized by the probability distributions, the probability distributions for intermediate and top nodes are calculated by incorporating the CPT information.

4. Proposed Validation Metric: Overlapping Coefficient (OC)

In this section, we discuss the concept of overlapping coefficient which is used as a measure of agreement (or disagreement) between two probability distributions or two populations represented by such distributions (Inman and Bradley, 1989). The concept of overlapping coefficient was first introduced by Weitzman (1970) and it has been widely used in studies related to economics, sociology, and biology. Yet, its potential has not been fully exploited in engineering applications. The historical development of this index is described in detail by Bradley (1985). The overlapping coefficient can be calculated by evaluating the area that is common under two probability density functions (PDFs). Let $f_1(\mathbf{x})$ and $f_2(\mathbf{x})$ be PDFs defined on the n-dimensional real numbers R_n. For continuous variables, it is formally defined as

$$OC = \int_{R_n} \min\left(f_1(\mathbf{x}), f_2(\mathbf{x}) \right) d\mathbf{x} \tag{9}$$

For discrete variables, it is expressed as

$$OC = \sum_{\mathbf{x}} \min\left(f_1(\mathbf{x}), f_2(\mathbf{x}) \right) \tag{10}$$

The concept of overlapping coefficient for a simple univariate example is illustrated in Fig. 4. As shown in this figure, the OC is the shaded area and gives the degree by which the two PDFs agree/overlap with each other. Numerically, $0 \leq OC \leq 1$. If OC is "0", the distributions are disjoint. If OC is "1", the distributions are identical. Therefore, it can be employed quite effectively as a validation metric for various quantities especially while considering uncertainties in them. The use of OC as a validation metric can also help in characterizing an acceptance criterion to determine if the simulation model with a given OC is acceptable or not.

5. Concept of Response Surface

A response surface is a polynomial regression model developed to represent the data through a mathematical expression. A polynomial approximation for the data is typically developed using a Taylor series expansion of the independent variables in the data, i.e. an approximate relationship between the dependent variable (y) and the independent variables (x_i) represented by a quadratic polynomial model as:

$$y = \beta_0 + \sum_{i=1}^{n} \beta_i x_i + \sum_{i=1}^{n} \beta_{ii} x_i^2 + \sum_{i<j} \beta_{ij} x_i x_j \qquad (11)$$

where β_0, β_i, β_{ii}, and β_{ij} are the coefficients for variables and n is the number of variables. This quadratic model has $(n + 1)*(n + 2)/2$ coefficients for n variables. The coefficients are determined by minimizing the error between observed data of y and expected values of Eq. (11). A higher order polynomial with greater number of coefficients can appear to fit the model more accurately. However, calculation of larger number of coefficients in a higher order polynomial can cause ill-conditioning as well as result in what is termed as an over-fit. In the engineering applications, the concept of response surface has been utilized for computational efficiency in predictive analysis (Tatang et al., 1997). It has also been used in the structural reliability problems for improved efficiency in calculating the reliability indices (Wong, 1985; Bucher and Bourgund, 1990). In this manuscript, the motivation to use a response surface is derived from its ability to represent the relationships between the various variables that characterize the nodes in a Bayesian network especially for cases where a physics or mechanics based relationship is not explicitly known. Ability to express relationship among the events through response surface facilitates the development of the proposed performance-based validation framework.

6. Bayesian Updating

The fragility curve calculated from Eq. (2) can change due to availability of new data from empirical, experimental, or high fidelity simulations. Consequently, the fragility curve would

need to be updated. The Baye's theorem facilitates incorporation of additional data **d** into the current fragility model. The "prior" fragility curve $P_f^{prior}(\lambda;\boldsymbol{\theta})$ is updated to evaluate a "posterior" fragility curve $P_f^{post}(\lambda \mid \mathbf{d})$ by following equations:

$$P_f^{post}(\lambda \mid \mathbf{d}) = \int P_f^{prior}(\lambda;\boldsymbol{\theta}) f(\boldsymbol{\theta} \mid \mathbf{d}) d\boldsymbol{\theta} \tag{12}$$

$$f(\boldsymbol{\theta} \mid \mathbf{d}) = \frac{f(\mathbf{d} \mid \boldsymbol{\theta}) f(\boldsymbol{\theta})}{\int f(\mathbf{d} \mid \boldsymbol{\theta}) f(\boldsymbol{\theta}) d\boldsymbol{\theta}} \tag{13}$$

where $\boldsymbol{\theta}$ are the parameters of the defined probabilistic fragility model, $f(\boldsymbol{\theta} \mid \mathbf{d})$ is the posterior joint pdf, $f(\mathbf{d} \mid \boldsymbol{\theta})$ is the likelihood function, and $f(\boldsymbol{\theta})$ is the prior joint pdf of parameters of the fragility model. The likelihood function is formulated as Eq. (14) because the performance-based risk assessment approach allows a representation of the data as a binomial event with the probability of system failure taken as $P_f^{prior}(\lambda_i;\boldsymbol{\theta})$ and the probability of non-failure as $1-P_f^{prior}(\lambda_i;\boldsymbol{\theta})$.

$$f(\mathbf{d} \mid \boldsymbol{\theta}) = \prod_{i=1}^{k} \binom{n_i}{r_i} \left(P_f^{prior}(\lambda_i;\boldsymbol{\theta})\right)^{r_i} \left(1-P_f^{prior}(\lambda_i;\boldsymbol{\theta})\right)^{n_i-r_i} \tag{14}$$

where $\mathbf{d}$ is the k^{th} number of data as formatted in $\mathbf{d} = \left[\left[\lambda_1 \cdots \lambda_k \right]^T \quad \left[r_1 \cdots r_k \right]^T \quad \left[n_1 \cdots n_k \right]^T \right]$ with number of observed failure r_i out of total number of events n_i at a given $\lambda = \lambda_i$, and $\mathbf{\Pi}$ is the product of all k of $\lambda = \lambda_i$ levels.

For the likelihood function to incorporate multi-level discrete data within a fault tree or a Bayesian network, it can be expanded to a binomial pdf:

$$L(\mathbf{D}) \propto f(\mathbf{d_1} | \boldsymbol{\theta}_1) \cdots f(\mathbf{d_m} | \boldsymbol{\theta}_m) \tag{15}$$

where $\mathbf{d_m}$ is the discrete data which has same format like $\mathbf{d}$ at any level of events such as basic events, intermediate events or top events; $\boldsymbol{\theta}_\mathbf{m}$ are the parameters related to the fragility models in the corresponding event; m is the total number of data sets regarding the events; and $\mathbf{D}$ is the total data set consisting of $\mathbf{d_1}$ to $\mathbf{d_m}$. For higher dimension problems, solutions of Eqs. (12) and (13) can be mathematically intractable. Therefore, in this study we use Gibbs sampling algorithm to overcome this limitation. The implementation of Gibbs sampling is realized by using JAGS of R code (Plummer, 2003).

7. Proposed Validation Framework

In this section, we present the proposed model validation framework by combining the probabilistic risk assessment (PRA) based on a Bayesian network with the concept of overlapping coefficient (OC). The concept of OC is used as the quantitative measure for the validation metric. A Bayesian network to represent the system level PRA is used to develop

the inference on system-level validation metric starting with the component-level validation information. The relationships between lower-level and higher level data are characterized by mechanistic models or through a response surface if mechanistic models are not available. However, not all possible response surfaces are developed. Instead, an efficient strategy is used to develop these for only certain identified events. Identification of critical events is pursued in the context of system-level risk, i.e. Bayesian network based PRA is employed to determine a critical path and identify components/events that are critical with respect to desired performance when subjected to the specific hazard under consideration.

Fig. 5 illustrates the proposed method through a flowchart. First, the basic failure modes for a physical system are identified for characterizing the basic events and for developing a fault tree. To do so, the annual risk for each basic event is calculated by convolving hazard curve and the corresponding performance-based fragility curve using Eq. (1). Next, the fault tree is converted into a Bayesian network by implementing the mapping algorithm discussed in section 3. A systems analysis using the Bayesian network is conducted to determine the critical path with respect to system vulnerability. These steps are represented as the first stage of the proposed flowchart in Fig.5. In the next stage, overlapping coefficients of component level events in the Bayesian network are calculated based on the component-level simulation and experimental data. Then, the response surfaces between the component-level and upper-level responses are created especially if a mechanistic relationship is not directly known. The Bayesian network is used to propagate the component level fragility and risk information in conjunction with the response surfaces

to obtain the intermediate and system-level fragilities and risk. Both, the experimental data and simulation based component level fragilities and risk are propagated in the Bayesian network. This allows development of fragility curves for intermediate nodes as well as top nodes for both the cases of experimental and simulation based component fragilities. Finally, the two sets of curves at any given node are used to develop the OC for it. If new data becomes available or if simulation codes are enhanced at any level of events within the network, the OCs at all levels are updated by using Bayesian updating described in section 6. Lastly, a decision regarding the acceptability of the system level simulation is reached by a comparison of the calculated system-level OC with a predefined criterion. For example, one may state that the fidelity of the system-level simulation model should be at least *p* percent or greater.

8. Illustrative Application Examples

In this section, we present two simple examples that illustrate the application of proposed framework. As mentioned earlier, both these examples are based on structural performance of components and systems in a nuclear plant subjected to earthquake hazard.

8.1 Example 1: Coupled structure-equipment system

This example is a simple representation of a very realistic problem faced in a nuclear facility. Each plant has many digital control instruments such as relays, control switches, etc. which much continue to operate during and after an earthquake. The instruments are mounted on

what is called as an electrical cabinet or control panel which is located at many different locations inside a plant. Such instruments are typically qualified by a shake table test of the instrument and in many cases a test of the entire cabinet with instruments mounted on it. The behavior of such electrical cabinets and control panels (secondary system) depends significantly on their interaction with the building (primary system) supporting them especially when the natural frequencies of vibration for the two systems are close to each other, i.e. they are tuned to each other (Gupta and Gupta, 1997; Gupta and Choi, 2005; Gupta, 1992). The most simplistic representation of this structure-equipment system can be achieved through a single-degree-of-freedom (SDOF) primary and SDOF secondary system as shown in Fig. 6. The equation of motion for this 2-DOF system subjected to an earthquake ground motion can be written as

$$\mathbf{M}\cdot\ddot{\mathbf{u}}+\mathbf{C}\cdot\dot{\mathbf{u}}+\mathbf{K}\cdot\mathbf{u}=-\mathbf{M}\cdot\mathbf{u_b}\cdot\ddot{u}_g \qquad (16)$$

where $\mathbf{M} = [m_1, 0; 0, m_2]$ and $\mathbf{K} = [(k_1 + k_2), -k_2; -k_2, k_2]$ are the mass and stiffness matrices of the coupled structural system; **C** is the damping matrix constructed from the method of superposition in which all modal damping ratio follow certain damping ratio ξ; $\mathbf{u} = [u_1; u_2]$, $\dot{\mathbf{u}} = [\dot{u}_1; \dot{u}_2]$ and $\ddot{\mathbf{u}} = [\ddot{u}_1; \ddot{u}_2]$ are displacement, velocity and acceleration vectors of the coupled system relative to the fixed base of the primary system; Subscript 1 and 2 denote the primary and secondary system, respectively; $\mathbf{u_b} = [1; 1]$ is the static displacement vector of the coupled system and $\ddot{u}_g$ is the earthquake ground acceleration motion. Secondary systems

are in general much lighter than the primary systems and typical ratio of their masses (secondary to primary) is on the order of 0.001 or less. In this example, we take systems that are tuned to each other and have a mass ratio of 0.001. The properties of the coupled 2-DOF system considered in this study are given in Fig. 6. In general, the mass of both the primary and the secondary system can be determined with a fair degree of certainty and therefore it is considered to be a deterministic quantity. The stiffness on the other hand can exhibit significant uncertainty leading to a change in the degree of tuning between the two systems which in turn influences the performance of the cabinet/equipment significantly. Stiffness can be calculated from experimental data as well as formulated using principles of mechanics. For the purpose of this study, the uncertainty in stiffness of both the systems (k_1 and k_2) is expressed using a Gaussian distribution with their respective means and coefficients of variations (c.o.v.). The statistical characteristics for the experimental and mechanistic simulation based data considered in this study are given in Table 1. The damping ratio in both the systems is considered to be 2% and is assumed to be a deterministic constant in order to keep the problem at hand simple for facilitating the illustration of the proposed performance-based validation framework. The uncertainty in ground motion for a future earthquake is accounted for by considering 20 real ground motion records in accordance with the probabilistic seismic hazard assessment discussed earlier in this paper. Fig. 7 shows the response spectra at 2% damping for all the 20 earthquake records when they are scaled to a peak ground acceleration (PGA) of 1g. The figure also shows their mean and mean plus one standard deviation curves.

In the proposed performance-based framework, the failure is characterized using a performance function. The performance of cabinets is typically characterized using two different limit states. One for strength related failure which is characterized by the maximum relative displacement of the secondary system, i.e. d_{2max} = max($|u_2 - u_1|$). The other for the functional failure of instruments such as relays which is characterized in terms of the maximum absolute acceleration of secondary system, i.e. a_{2max} = max($|\ddot{u}_2 + \ddot{u}_g|$). The performance functions for these two failure modes can be written as:

$$g_1 = d_{2lim} - d_{2max} \tag{17}$$

$$g_2 = a_{2lim} - a_{2max} \tag{18}$$

where d_{2lim} and a_{2lim} are allowable limits for the maximum relative displacement of secondary system and absolute acceleration of secondary system, respectively. In this study, we take d_{2lim} = 0.2 m and a_{2lim} = 20g. Component failure event C1 corresponds to $g_1 < 0$ and component failure event C2 corresponds to $g_2 < 0$. The system failure event (S) occurs when either C1 or C2 occurs. Starting with these basic failure events, a fault tree is constructed for evaluating the system failure (S). It is assumed that the two basic events C1 and C2 are independent. One may argue that the events C1 and C2 can be correlated. Such a correlation cannot be accounted for in a fault tree. Therefore, the proposed framework relies on mapping the fault tree into a corresponding Bayesian network using the mapping algorithm discussed in this paper. The fault tree and the Bayesian network for this example are shown in Fig. 8.

While such a correlation can be considered by modifying the Bayesian network shown in Fig. 8, this study does not consider such a correlation for simplicity of this illustrative example. The Bayesian network as mapped from the fault tree cannot be used directly in this example (or other similar applications) because experimental data available in this validation process relates to the stiffness parameters which are not represented in the Bayesian network. Therefore, it becomes necessary to modify the Bayesian network by including the basic parameters through a hidden layer as shown in Fig. 9.

The modified Bayesian network can propagate the uncertainties or the overlapping coefficient at the hidden layer to upper level events. However, the relationship between the parameters in the hidden layer and the basic events C1 and C2 cannot be expressed through a conditional probability table (CPT) or a correlation. This relationship is highly dependent upon the particular system under consideration as well as on the earthquake hazard input. It is precisely this aspect that can be addressed by use of a response surface in the proposed framework. In this particular example, one can develop response surfaces for dependent variables d2max and a2max in terms of the independent variables k_1 and k_2. In the absence of any experimental or simulation data, response surfaces can be utilized for the inference on that data instead of numerically solving the equation of motion for this 2-DOF system, Eq. (16), for the 20 earthquakes records. A fourth order polynomial is used to represent the response surfaces which are shown in Fig. 10 along with the R^2 values. The value of R^2 is close to unity in both cases indicating that the 4^{th} order polynomial considered for the response surfaces has a good fit with the simulation data. It must be noted that if the

experimental and simulation data were available directly for events C1 and C2 in the Bayesian network, then a response surface would not have been needed.

Starting with the experimental and simulation data for k_1 and k_2, the response surfaces are used in conjunction with the performance functions for events C1 and C2 to develop fragility curves for each of these two basic events. For each event, one fragility curve can be developed corresponding to the experimental data for parameters in the hidden layer and the other corresponding to the simulation data for the parameters in the hidden layer. The fragility curves for C1 and C2 are then propagated through the Bayesian network to calculate the fragility curves for the system level failure event S as shown in Fig. 11. Finally, the two fragility curves which are cumulative distributions for any event (experimental and simulation based) are converted to their respective probability density functions which in turn then give the overlapping coefficient (OC) for the particular event. The overlapping coefficients for all the events in this example are also shown in Fig. 11. As seen in this figure, the system level OC is obtained at 0.80 or 80%.

The above example illustrates three important aspects in the proposed framework: (i) propagation and evaluation of the overlapping coefficient for various events using a performance-based approach implemented through a Bayesian network, (ii) the concept of including a hidden layer in the Bayesian network to relate the fundamental parameters to the basic events, and (iii) the need for developing response surfaces to represent the relationship between the parameters of hidden layer and the basic failure events.

8.2 Example 2: Building-piping system

The proposed framework and its application as illustrated in the previous example above can become computationally prohibitive for realistic systems if computations need to be performed for each and every event in the Bayesian network. Furthermore, it is desirable that a validation framework provides feedback by identifying critical components/events for which collection of additional information through experiments, field measurements, or conducting high fidelity simulations would help in improving the acceptability of system level simulation. The example described in detail below is intended to illustrate these two aspects.

In this example, we consider a system that comprises of a building structure, safety related equipment such as pump which is necessary to circulate the coolant, the piping system for circulating the coolant and pipe supports connecting the piping to the building. Let us consider that the a system failure is initiated by one or more of the four basic earthquake loading related failure modes: (i) excessive story drift for building structure (C1), (ii) failure of safety-related equipment (C2), (iii) failure of pipe supports (C3), and (iv) leakage at pipe joints (C4). These four basic events result in two intermediate events: (i) loss of circulation (IE1), and (ii) Loss of coolant (IE2). The system failure (S) is defined as an outcome of events IE1 and IE2, and occurs if at least one of the two intermediate events occurs. Since the concept of hidden layer is already illustrated through example 1 above, let

us assume that the experimental and simulation data is available directly for the four basic events and shown in Table 2.

The fault tree for the system failure is created and the risk for each event in the fault tree is calculated by convolution of hazard and fragility information in accordance with Eq. (1). The detailed information on the calculation of this risk for this problem is given in Part II of this thesis. Then, the fault tree is mapped into the Bayesian network using the mapping algorithm of section 3 and is shown in Fig. 12. Next, we propagate the probabilities of basic events through the Bayesian network to determine the probabilities of failure for the intermediate and system level risks. Subsequently, the critical path of the Bayesian network is identified and shown in Fig. 13. As seen in this figure, the critical event at component level simulation is identified as C4. Next, the overlapping coefficients (OCs) for the events on the critical path are calculated in the same way as explained in case of example 1 by using the fragility curves corresponding to the simulation as well as the experiment data. It must be noted that in this example, there is no need for developing a response surface because the probabilities of failure corresponding to experimental and simulation data is available directly for all the basic events. The OCs for the intermediate and system level events are given in Table 3. While the OCs are calculated and given for all intermediate events in this table, the OCs need to be calculated for only those events that lie on the critical path. This approach would reduce the computational effort needed in a Bayesian network of a real-life system.

As seen in Table 3, the OC for the system level event is only 0.24 which is relatively small thereby indicating a relatively low confidence in the validation/output of system level simulations. Therefore, additional tests/data is needed to improve the validation. One option is to conduct larger-scale experimentation or collect field measurements for intermediate level events. Based on the proposed framework, event IE2 lies on the critical path and therefore, it would be more appropriate to collect additional data for IE2 compared to event IE1. Let us consider that additional data collected for event IE2 is represented in the form of failure rate as shown in Table 4. Starting with the data given in Table 3, Bayesian updating is used to update and determine posterior values of OCs at all levels from component level to system level. The updated values of OCs are also given in Table 3. The system level fragility curves for the various cases (simulation, experimental-prior, and experimental-posterior) are shown in Fig. 14. As seen in this figure, availability of additional data reduced the differences in the experimental-posterior fragility curve and the simulation based fragility curve. Fig. 15 shows the results after updating in a comprehensive manner for the entire Bayesian network for this example. The OC for the system level improves even though it might still be considered to be unacceptable thereby requiring additional resources and strategies for improving the validation. One reason for this unacceptable performance seems to be related to extremely low value of OC for event C4 which lies on the critical path. Therefore, let us use the proposed approach to determine the improvement in system level OC due to an increase in the OC of event C4. If we consider that improvements in understanding the behavior of event C4 and an improvement in the simulation tools for

evaluating fragilities of C4 helps us improve the OC of event C4. Table 5 gives the improved values of the OCs for events starting with an improved value of the OC for C4. This is depicted graphically in Fig. 16. As seen in this table and the corresponding figure, the system level OC is equal to 0.82 and would be closer to a desired acceptance.

9. Conclusions

A novel approach is explored in this paper to quantitatively assess the validation of a system-level simulation based on the available information from component level validation. The proposed approach uses performance-based probabilistic risk assessment (PRA) as the basis for validation as well as for allocating resources towards improving the validation either by collecting additional data or by enhancing the accuracy of simulation tools. The approach builds upon characterizing the validation in terms of an overlapping coefficient which is described as the joint area under the experimentally obtained and simulation based probability density functions of basic parameters or events. The approach utilizes the power of Bayesian statistics by mapping a fault tree into a Bayesian network which allows consideration of non-Boolean relationships between events as well as allows consideration of correlated events in the network. Starting with the experimental and simulation based probability density functions of basic parameters or basic events, a Bayesian network is used to propagate the risk for the system. The fragilities and the risk associated with each intermediate event and the top event is calculated separately for both the experimental and simulated data. This set of curves are then used for evaluating the overlapping coefficient of

each event. The PRA based approach helps in identification of critical path thereby reducing the computational effort by focusing on only those events that lie on the critical path. Reliance on the events of critical path can also be used to determine the allocation of resources among different events for improving the validation at component or intermediate levels. When a validation between the experimental and simulation data is available for the basic parameters and not for the basic events directly in the network, a hidden layer is added below the basic events to relate the fundamental parameters to the basic events. The relationship between the hidden layer nodes and the basic event nodes can be defined by either a mechanistic model or a simulation based generation of response surface. Availability of new validation data, either through new experimental information or enhanced simulation tools, can be incorporated in a relatively straightforward manner by employing Bayesian updating to calculate posterior fragilities and the corresponding overlapping coefficients. The application of the proposed approach is illustrated through application examples.

Acknowledgements

This research was partially supported by the Center for Nuclear Energy Facilities and Structures at North Carolina State University. Resources for the Center come from the dues paid by member organizations and from the Civil, Construction, and Environmental Engineering Department and College of Engineering in the University.

References

AIAA, *Guide for the Verification and Validation of Computational Fluid Dynamics Simulations*, American Institute of Aeronautics and Astronautics, AIAA-G-077-1998, Reston, VA, 1998.

Babuška I, Nobile F, and Tempone R, "A systematic approach to model validation based on Bayesian updates and prediction related rejection criteria," *Computer Methods in Applied Mechanics and Engineering*, 197(29), 2517-39, 2008.

Bayarri MJ, Berger JO, Kennedy MC, Kottas A, Paulo R, Sacks J, Cafeo JA, Lin CH, and Tu J, "Bayesian Validation of a Computer Model for Vehicle Collision," National Institute of Statistical Sciences, *TR-163*, 2005,

Bayarri MJ, Berger JO, Paulo R, Sacks J, Cafeo JA, Cavendish J, Lin CH, and Tu J, "A framework for validation of computer models," *Technometrics*, 49(2), 138-154, 2007.

Bobbio A, Portinale L, Minichino M, and Ciancamerla E, "Improving the analysis of dependable systems by mapping fault trees into Bayesian networks," *Reliability Engineering & System Safety*, 71(3), 249-260, 2001.

Bradley EL, "Overlapping coefficient," *Encyclopedia of Statistical Science*, 6, New York, John Wiley, 546-547, 1985.

Bucher CG and Bourgund U, "A fast and efficient response surface approach for structural reliability problems," *Structural safety*, 7(1), 57-66, 1990.

Chen W, Baghdasaryan L, Buranathiti T and Cao J, "Model Validation via Uncertainty Propagation," *AIAA Journal*, 42(7), 1406-1415, 2004.

Chen W, Xiong Y, Tsui K-L and Wang S, "A Design-Driven Validation Approach Using Bayesian Prediction Models*," Journal of Mechanical Design*, 130(2), 021101, 2008.

Coleman HW and Stern F, "Uncertainties and CFD code validation," *Journal of Fluids*

Engineering, 119(4), 795-803, 1997.

Dowding KJ and Rutherford BM, "An approach to model validation and model-based prediction--polyurethane foam case study," Sandia National Laboratories, *No. SAND2003-2336*, 2003.

Ferson S and Oberkampf WL, "Validation of imprecise probability models," *International Journal of Reliability and Safety*, 3(1-3), 3-22, 2009.

Ferson S, Oberkampf WL, and Ginzburg L, "Model validation and predictive capability for the thermal challenge problem," *Computer Methods in Applied Mechanics and Engineering*, 197(29), 2408-30, 2008.

Fussell J, "How to Hand Calculate System Reliability and Safety Characteristics," *IEEE Transaction on Reliability*, 24(3), 1975.

Gupta A and Choi B, "Consideration of uncertainties in seismic analysis of coupled building piping systems," *Nuclear engineering and design*, 235(17), 2071-86, 2005.

Gupta A and Gupta AK, "Seismic response of tuned single degree of freedom secondary systems," *Nuclear engineering and design*, 172(1), 17-25, 1997.

Gupta AK, *Response spectrum method in seismic analysis and design of structures*, CRC press, 1992.

Hasselman TK, Wathugala GW, and Crawford J, "A hierarchical approach for model validation and uncertainty quantification," *Proceedings of Fifth World Congress on Computational Mechanics*, 2002.

Hills RG and Trucano TG, "Statistical Validation of Engineering and Scientific Models: A Maximum Likelihood Based Metric," Sandia National Laboratories, *SAND2001-1783*, Albuquerque, NM, 2002.

Hills RG, "Model validation: model parameter and measurement uncertainty," *Journal of Heat Transfer*, 128(4), 339-351, 2006.

Inman HF and Bradley EL, “The overlapping coefficient as a measure of agreement between probability distributions and point estimation of the overlap of two normal densities,” *Communications in Statistics-Theory and Methods*, 18(10), 3851-74, 1989.

Jiang X and Mahadevan S, “Bayesian risk-based decision method for model validation under uncertainty,” *Reliability Engineering & System Safety*, 92(6), 707-18, 2007.

Jiang X and Mahadevan S, “Bayesian structural equation modeling method for hierarchical model validation,” *Reliability Engineering & System Safety*, 94(4), 796-809, 2009.

Kennedy MC and O'Hagan A, “Bayesian Calibration of Computer Models,” *Journal of the Royal Statistical Society Series B-Statistical Methodology*. 63(3), 425-450, 2001.

Korb KB, Geard N, and Dorin A, “A Bayesian Approach to the Validation of Agent-Based Models,” *Ontology, Epistemology, & Teleology for Model. & Simulation (Andreas Tolk Ed.)*, 44, 255–269 , 2013.

Mahadevan S and Rebba R, “Validation of reliability computational models using Bayes networks,” *Reliability Engineering & System Safety*, 87(2), 223-32, 2005.

McGuire RK, “Probabilistic seismic hazard analysis and design earthquakes: closing the loop,” *Bulletin of the Seismological Society of America*, 85(5), 1275-1284, 1995.

Modarres M, Kaminskiy MP, and Krivtsov V, *Reliability engineering and risk analysis: a practical guide*, CRC press, 1999.

O’Hagan A, “Bayesian analysis of computer code outputs: a tutorial,” *Reliability Engineering & System Safety*, 91(10), 1290-1300, 2006.

Oberkampf WL and Barone MF, “Measures of agreement between computation and experiment: validation metrics,” *Journal of Computational Physics*, 217(1), 5-36, 2006.

Oberkampf WL and Trucano TG, “Validation methodology in computational fluid dynamics,” *AIAA paper*, 2549,19-22, 2000.

Plummer M, “JAGS: A program for analysis of Bayesian graphical models using Gibbs sampling,” *Proceedings of the 3rd international workshop on distributed statistical computing*, 124(125), Technische Universit at Wien, Austria, 2003.

Rebba R and Mahadevan S, “Computational methods for model reliability assessment,” *Reliability Engineering & System Safety*, 93(8), 1197-207, 2008.

Rebba R and Mahadevan S, “Model predictive capability assessment under uncertainty, *AIAA journal*, 44(10), 2376-84, 2006.

Roy CJ and Oberkampf WL, “A comprehensive framework for verification, validation, and uncertainty quantification in scientific computing,” *Computer Methods in Applied Mechanics and Engineering*, 200(25), 2131-44, 2011.

Sprague MA and Geers TL, “Response of empty and fluid-filled, submerged spherical shells to plane and spherical, step-exponential acoustic waves,” *Shock and Vibration*, 6(3), 147-57, 1999.

Tatang MA, Pan W, Prinn RG and McRae GJ, “An efficient method for parametric uncertainty analysis of numerical geophysical models,” *Journal of Geophysical Research: Atmospheres*, 102(D18), 21925-32, 1997.

Voyles IT and Roy CJ, “Evaluation of model validation techniques in the presence of aleatory and epistemic input uncertainties,” *17th AIAA Non-Deterministic Approaches Conference*, ARC, 1-16, 2015.

Weitzman MS, “Measures of overlap of income distributions of white and Negro families in the U.S.,” Tech Rep., 22, Bureau of the Census, U.S. GPO, Washington, DC., 1970.

Wong FS, “Slope reliability and response surface method,” *ASCE Journal of Geotechnical Engineering*, 111(1), 32-53, 1985.

Zhang R and Mahadevan S, “Bayesian Methodology for Reliability Model Acceptance,” *Reliability Engineering and System Safety*, 80(1), 95-103, 2003.

Table 1: Simulation and experiment data on stiffness of structural system

	PDF* type	Simulation data		Experimental data	
		Mean	c.o.v*	Mean	c.o.v
k_1 (N/m)	Normal	1e6	0.1	0.954e6	0.1
k_2 (N/m)	Normal	1e3	0.1	0.91e3	0.1

*PDF: probability density function; c.o.v: coefficient of variation

Table 2: Simulation and experiment data for fragility of building-piping structural system

	Simulation data			Experiment data		
	PDF type	Median	Std*	PDF type	Median	Std*
C1	Lognormal	2.9g	0.30	Lognormal	2.0g	0.50
C2	Lognormal	1.9g	0.30	Lognormal	1.6g	0.35
C3	Lognormal	1.5g	0.35	Lognormal	2.0g	0.50
C4	Lognormal	1.5g	0.30	Lognormal	0.5g	0.55

*Std: Lognormal Standard deviation

Table 3: Comparison of OCs with/without discrete data of IE1

	Overlapping coefficients	
	W/o discrete data of IE1	W/ discrete data of IE1
OC_{C1}	0.57	0.58
OC_{C2}	0.78	0.79
OC_{C3}	0.70	0.62
OC_{C4}	0.19	0.43
OC_{IE1}	0.64	0.65
OC_{IE2}	0.25	0.52
OC_{S}	0.24	0.48

Table 4: Discrete data in IE2 node

PGA	N_f * / *To**
1.0g	6/30
1.5g	15/30

*N_f: Number of failures, *To*: Total occurrence

Table 5: Overlapping coefficients for components satisfying criterion

	Overlapping coefficients
OC_{C1}	0.58
OC_{C2}	0.79
OC_{C3}	0.62
OC_{C4}	0.83
OC_{IE1}	0.65
OC_{IE2}	0.85
OC_{S}	0.82

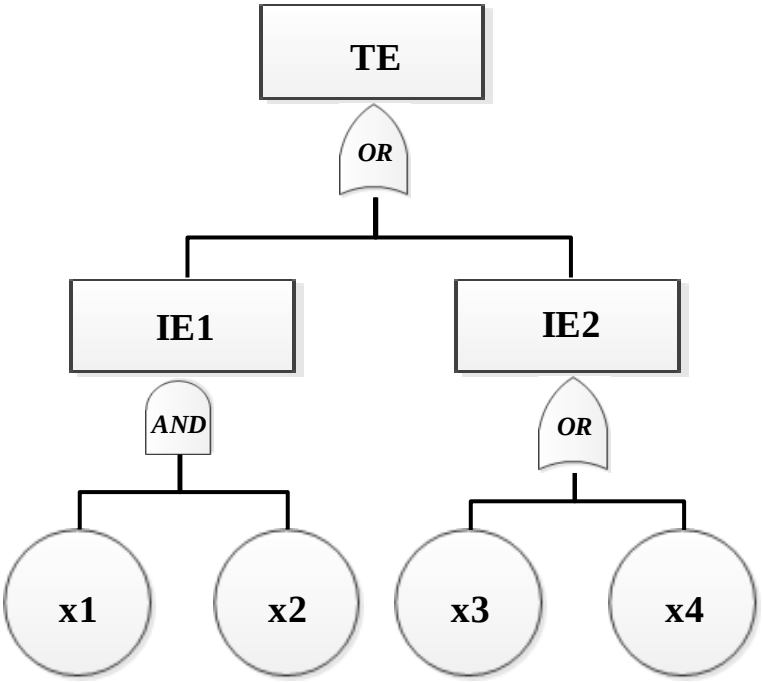

Fig. 1. An example of simple FT

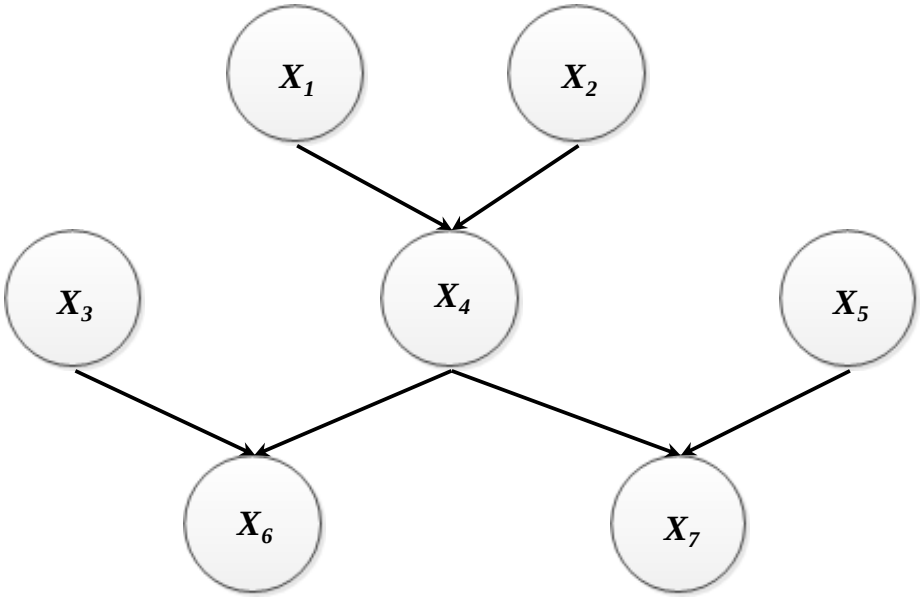

Fig. 2. An example of simple Bayesian network

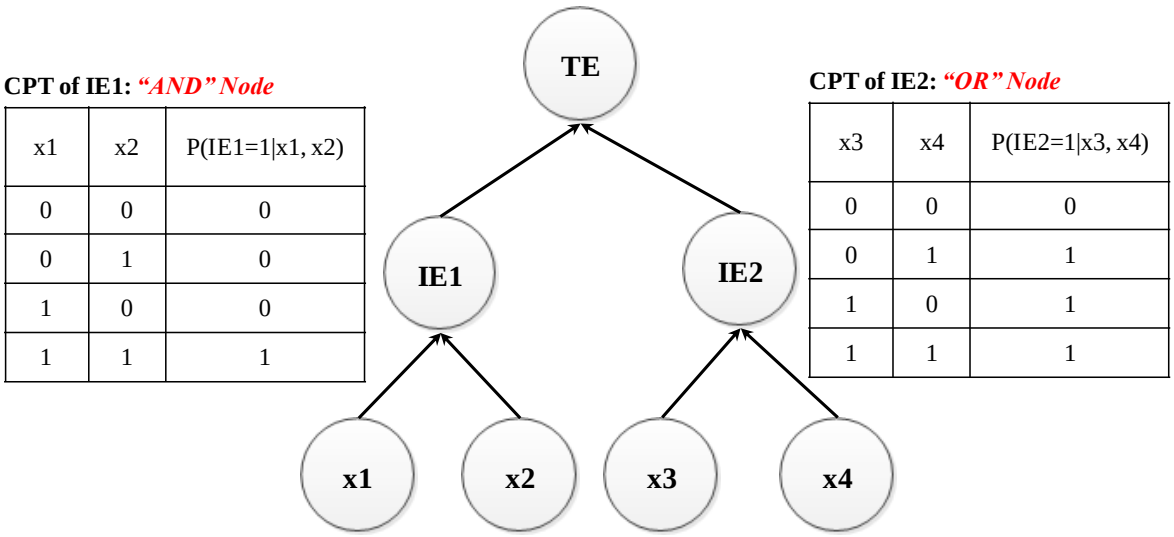

Fig. 3. BN for FT example of Fig. 1 using mapping algorithm

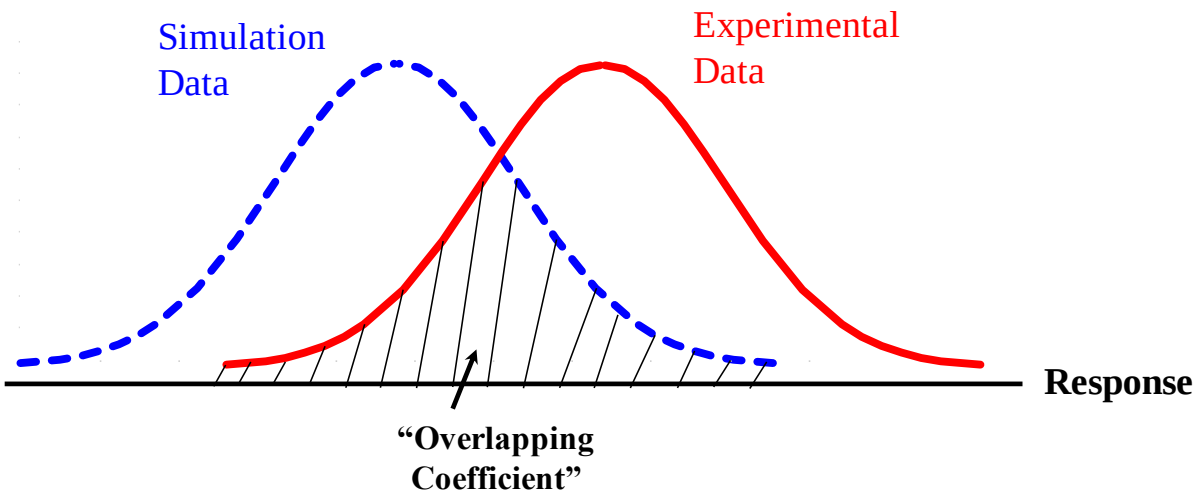

Fig. 4. Concept of overlapping coefficient

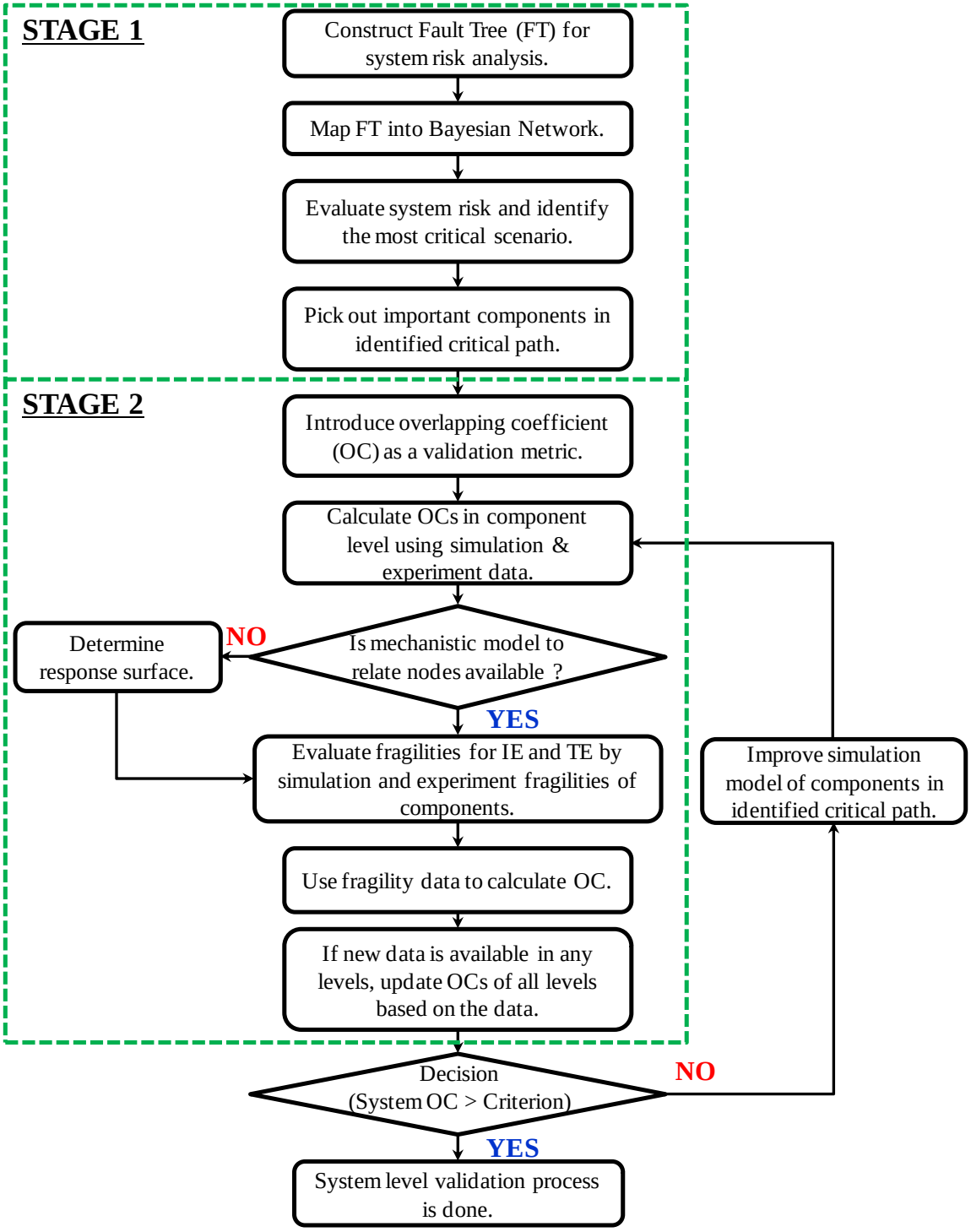

Fig. 5. Flowchart of proposed model validation method

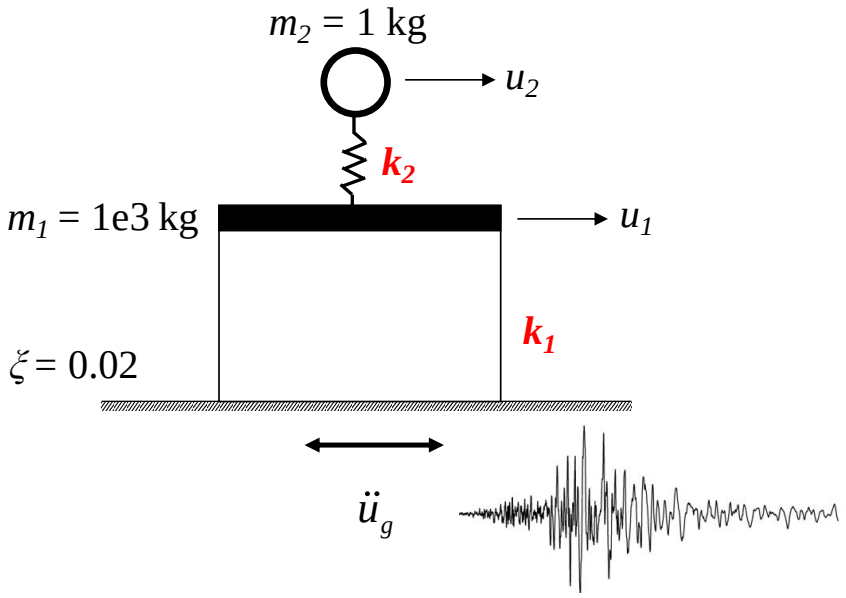

Fig. 6. Coupled TDOF structural system

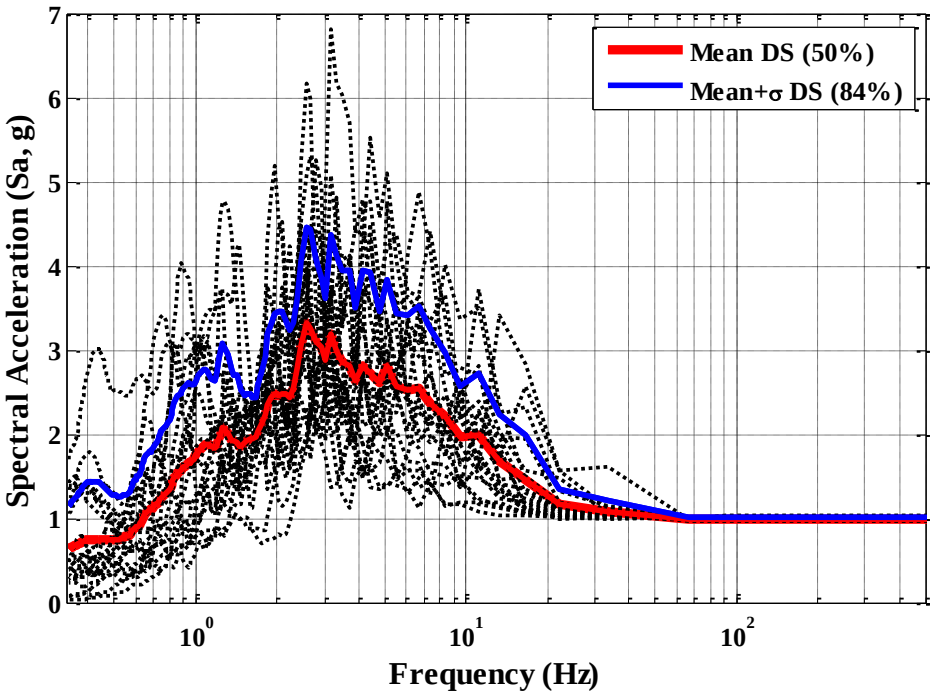

Fig. 7. Response spectra of 2% damped elastic SDOF system under 20 earthquake ground motions

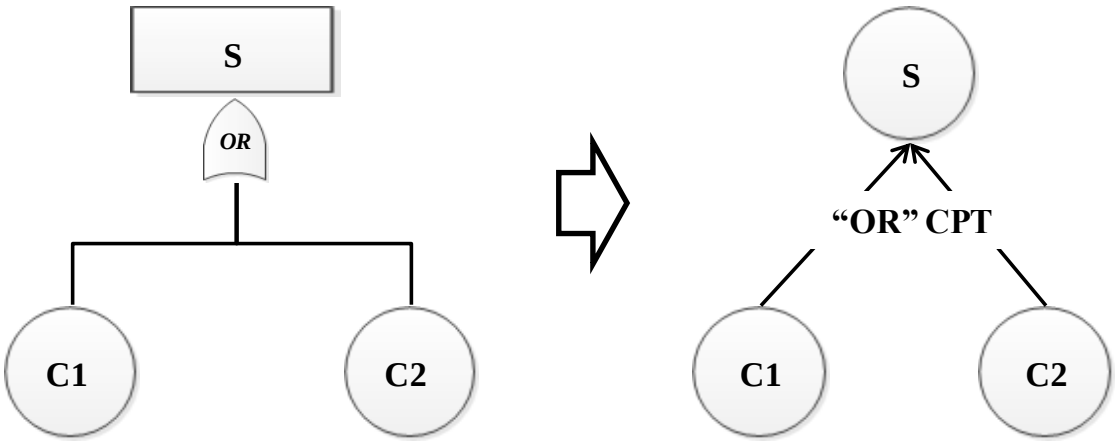

Fig. 8. FT and BN for system failure of coupled structure system (example 1)

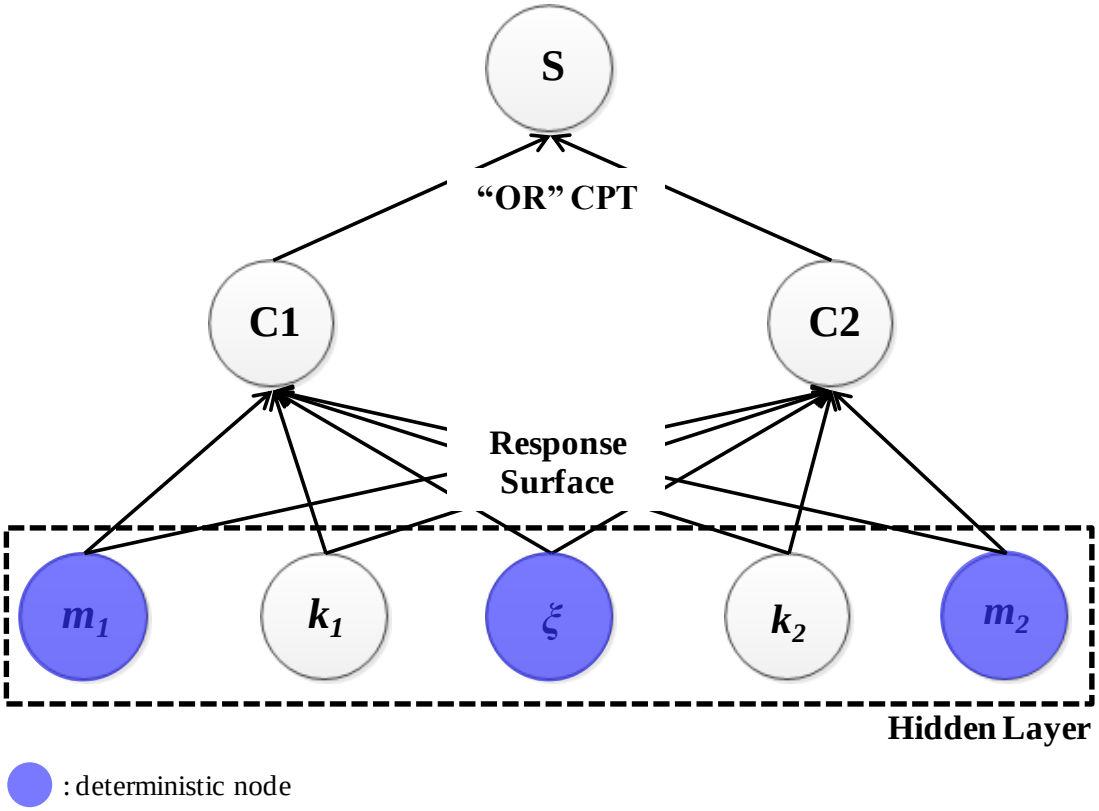

Fig. 9. Extended BN for system failure event of coupled structure system (example 1)

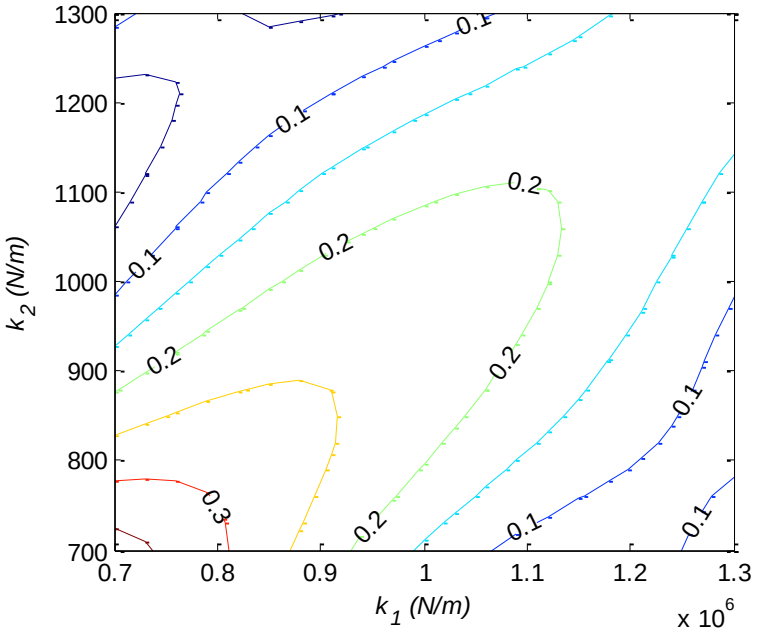

(a) d_{2max} (unit: m, R^2 = 0.9)

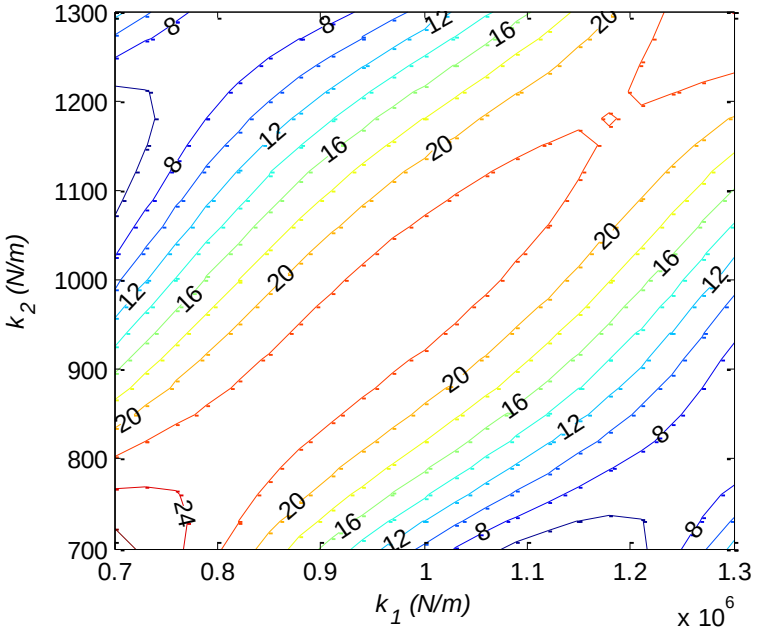

(b) a_{2max} (unit: g, R^2 =0.89)

Fig. 10. Response surface for d_{2max} and a_{2max} of coupled structural system under earthquake ground motions scaled to 1g PGA

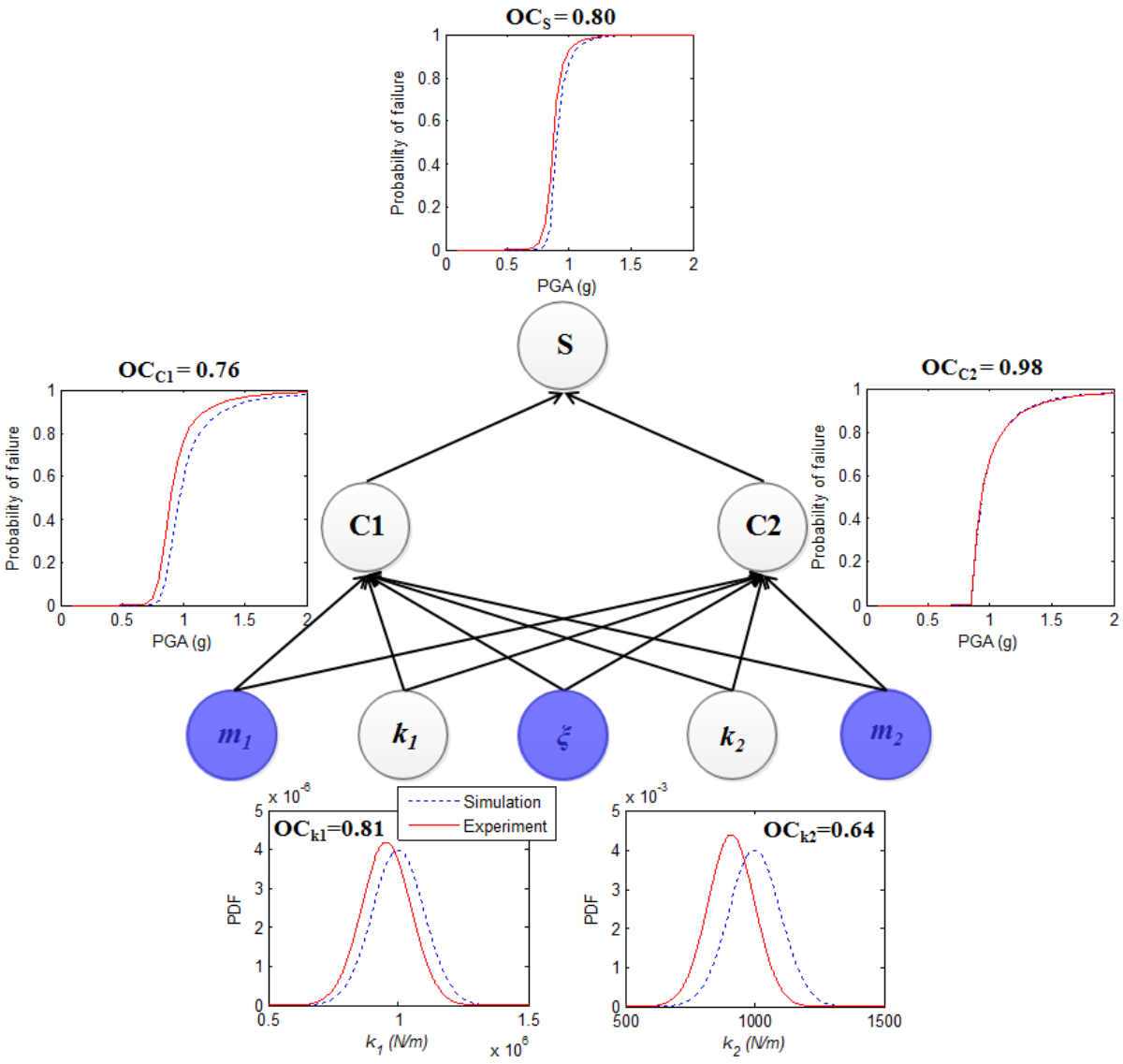

Fig. 11. OCs and corresponding distributions in extended BN structure (example 1)

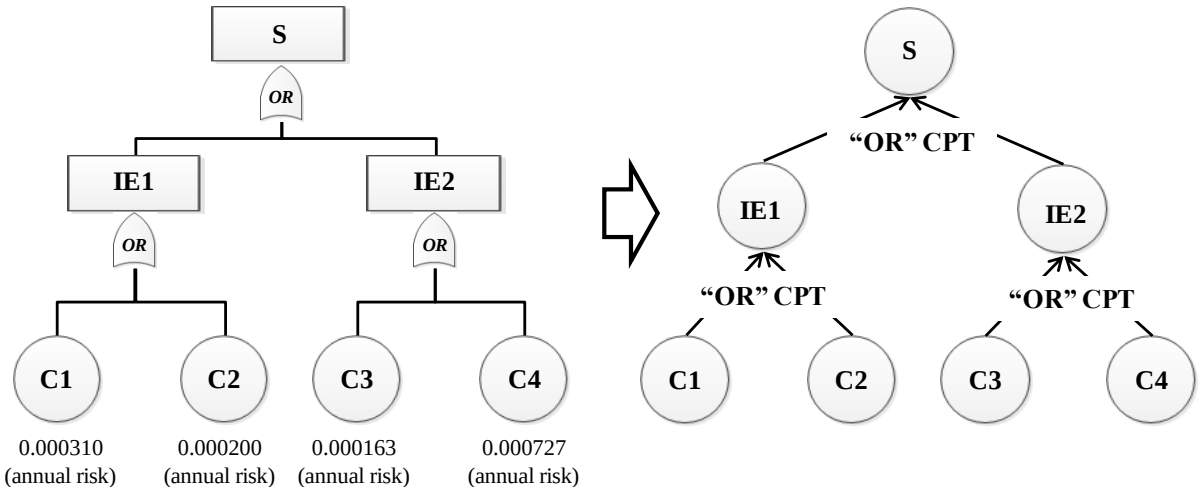

Fig. 12. FT and BN for system failure (example 2)

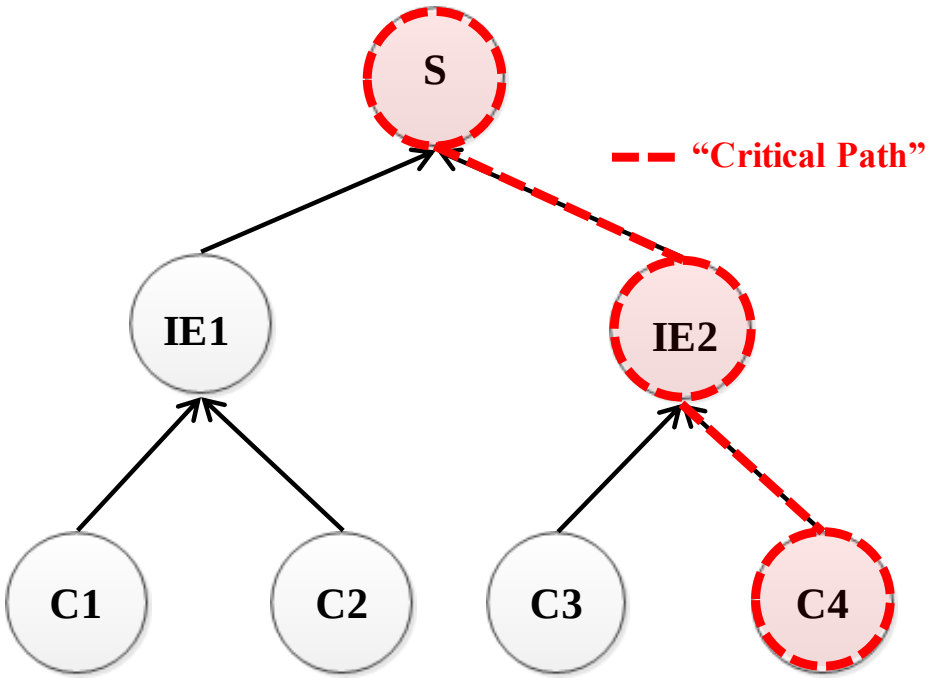

Fig. 13. Critical path within BN structure (example 2)

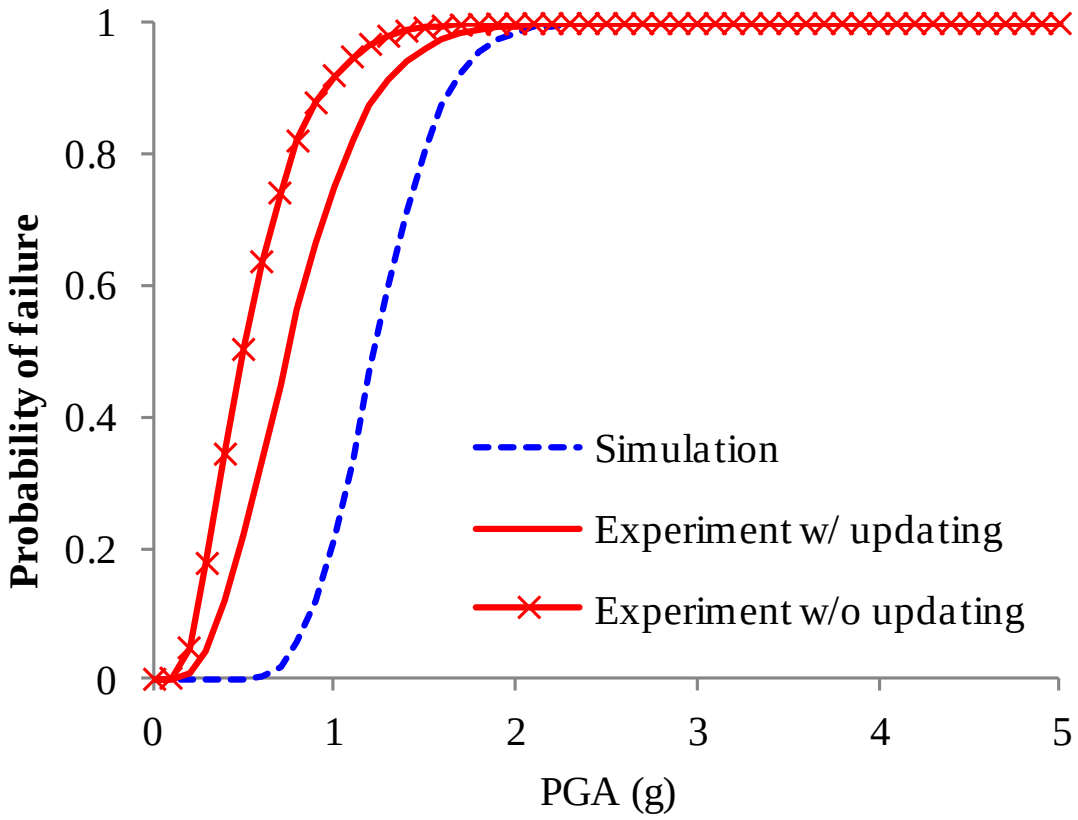

Fig. 14. Comparison of fragility curves of system failure with/without discrete data of IE2

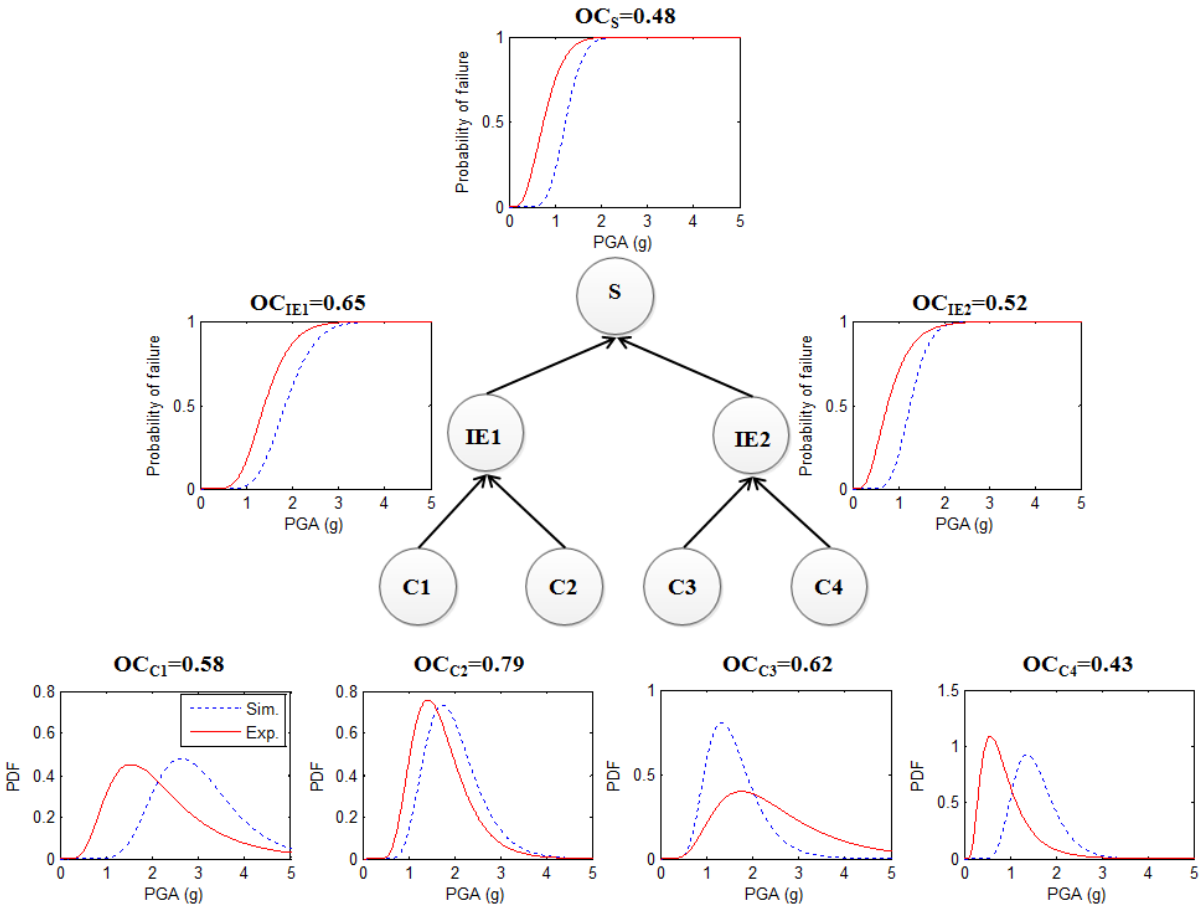

Fig. 15. OCs and corresponding distributions in BN structure (example 2)

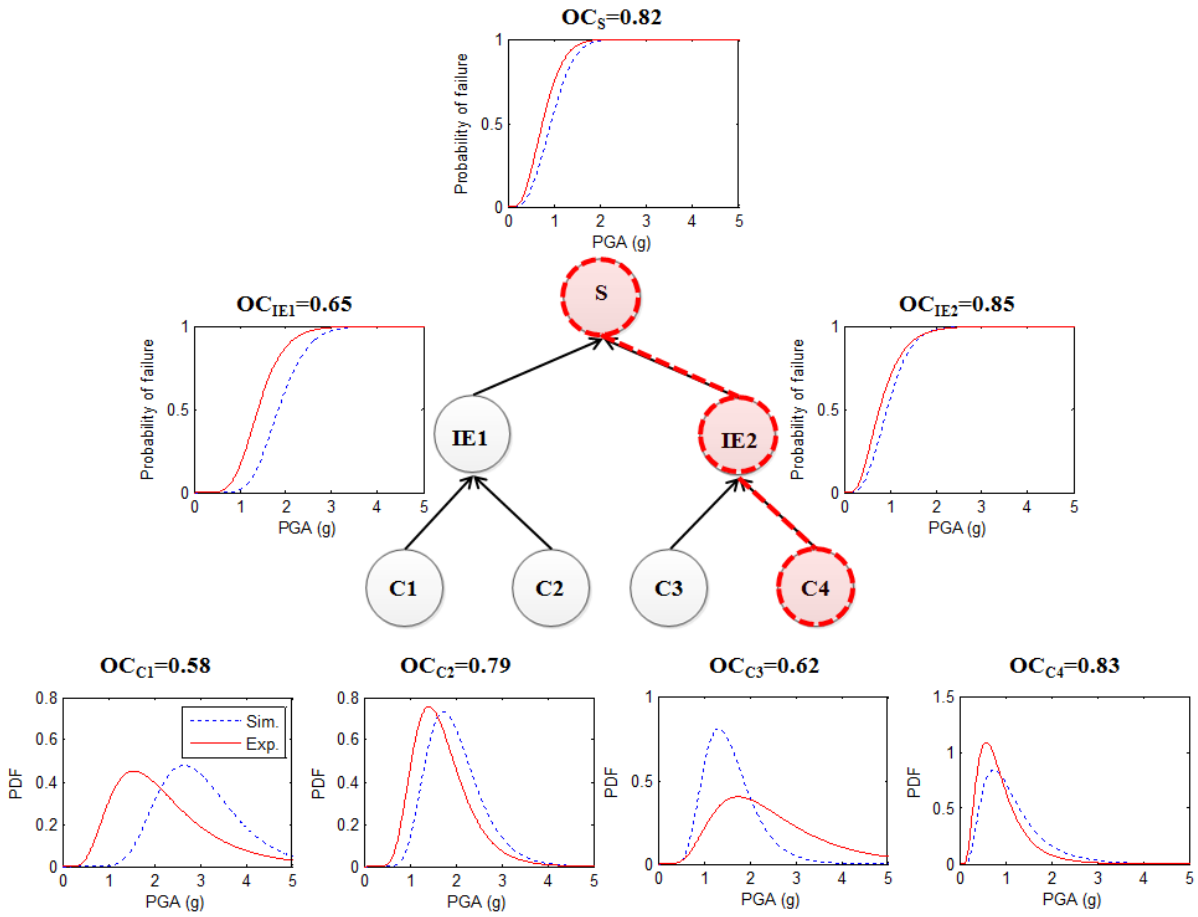

Fig. 16. OCs and corresponding distributions in BN structure satisfying criterion (example 2)

PART IV

EFFICIENT SEISMIC FRAGILITY ANALYSIS OF COUPLED SYSTEM USING EQUIVALENT ELASTIC LIMIT STATE CONCEPT AND BAYESIAN UPDATING

Shinyoung Kwag and Abhinav Gupta

ABSTRACT

Seismic response of secondary systems depends on their interaction with the primary systems supporting them. A conventional uncoupled analysis of secondary systems ignores this interaction and gives excessively conservative responses compared to those obtained from a seismic analysis of the coupled primary-secondary system. Furthermore, a coupled system becomes non-classically damped when the damping characteristics of the primary and secondary systems are different. Therefore, assessment of seismic fragility in secondary systems such as equipment and piping needs to be based on modeling the behavior of the complete coupled system. At the same time, nonlinear analysis of such coupled systems requires significant computational effort. Recently, Tadinada and Gupta (2016) presented an equivalent elastic limit state concept with an intent to reduce the computational effort needed in such an assessment and yet evaluate the seismic fragility without any loss of accuracy. This paper presents enhancements to the originally proposed approach. Modifications are proposed to allow consideration of hysteretic model for nonlinearity in the secondary system. The modified formulation also accounts for the effect of uncertainty in nonlinear characteristics and the effect of non-classical damping. Unlike the originally proposed formulation, the modified form accounts for the asymmetric variation of the equivalent limit state with respect to tuning ratio thereby improving the accuracy for detuned system that have positive values of tuning ratio. Fragilities calculated solely by using equivalent limit state concept are not necessarily accurate for tuned or nearly tuned systems. In such cases,

the fragilities from equivalent limit state concept can be used as prior fragilities in the context of Bayesian updating to obtain posterior fragilities by conducting only a limited number of nonlinear time history analyses. The posterior fragilities are shown to be very accurate when compared with the corresponding curves obtained by comprehensive nonlinear analyses.

1. Introduction

In a seismic probabilistic risk assessment (SPRA), the reliability of structures, systems and components (SSCs) is described in terms of the fragility which is commonly expressed by a curve that gives conditional probability of failure for a given seismic intensity parameters such as peak ground acceleration (PGA), spectral acceleration (SA), etc. Development of accurate and realistic seismic fragility curves often requires large amounts of empirical or experimental data as well as computationally intensive simulations. For large structural systems, experimental and experience data is either not available or it is available in very limited quantity. Therefore, engineers rely significantly on large scale simulations that involve conducting multiple time history analyses of the nonlinear systems. Depending upon the complexity of a simulation model and tractability of uncertainties in it, such an approach can become computationally prohibitive.

One example of a computationally intensive analysis relates to calculating fragilities of equipment or piping systems in critical industrial facilities such as nuclear power plants. Seismic response of such secondary systems depends on their interaction with the primary system on which they are supported. Historically, seismic analyses of equipment and piping systems are conducted by uncoupling them from the primary structure. The primary structure is analyzed to obtain the floor motions where secondary systems are attached to the primary systems. These floor motions are then used as input into an uncoupled model of the secondary system. Such conventional uncoupled analysis gives inaccurate responses which

are in general excessively conservative (Gupta and Gupta, 1995). An analysis of the coupled building-equipment or building-piping correctly accounts for: (i) the tuning between the modes of the primary and secondary systems, (ii) the mass interaction between the two systems, and (iii) the effect of non-classical damping. The concept of conducting a coupled analysis as well as its significance has been studied quite widely (Chen and Soong, 1988). USNRC conducted a benchmark program and developed many different benchmark problems for conducting such coupled analyses (USNRC, 2000). A fragility assessment should therefore be based on the analysis of coupled building piping system.

Ju and Gupta (2015) and Ju et al. (2016) present the results of detailed studies on calculating piping fragilities. They illustrate that the nonlinearities in a piping system are typically restricted to localized locations of joints between straight pipes and components such as Tee-joints. They evaluate piping fragilities by incorporating the experimental data on nonlinear behavior of piping joints into a system level building-piping model and conducting multiple time history analyses. Ju et. al. (2016) also considers nonlinearities in the building and study their influence on the piping fragility. However, such analyses require significant computational resources thereby making it almost impossible to implement such an approach into practice. Availability of an approach to calculate fragilities of secondary systems accurately through an equivalent linearization of the localized nonlinearity can be quite effective in overcoming such a limitation.

Many equivalent linearization methods have been studied and proposed in literature. These are reviewed in detail by by Proppe et al. (2003) and Crandall (2006). The existing methods can be broadly categorized into following types:

1) Equivalent viscous damping method (Jacobsen, 1930)
2) Elastic strain energy method (Veletsos and Newmark, 1960)
3) Empirical method (Gulkan and Sozen, 1974; Iwan, 1980; Kwan and Billington, 2003)
4) Stochastic linearization method (Caughey, 1963; Atalik and Utku, 1976; Wen, 1980)
5) Secant stiffness method (Deierlein and Hsieh, 1990; Chopra, 1995)
6) Equivalent elastic limit state (ELS) concept (Tadinada and Gupta, 2016)

Almost all these studies have focused on equivalent linearization of the primary system alone by minimizing the average error between the responses of nonlinear and the linearized system. In the seismic fragility analysis of the secondary systems, it is desirable that the equivalent linearization method minimizes the error between the maximum responses of interest instead of the average error. Tadinada and Gupta (2016) propose a novel concept of equivalent limit-state (ELS) to reduce the computational effort needed in such fragility studies. In this paper, we present several enhancements to the concept of equivalent limit-state. These can be enlisted as:

- Consideration of a more realistic model for the nonlinearities in the secondary system. The original study considers only an idealized bi-linear behavior with pinching effect to model the nonlinearities in the piping joints. An idealized bi-linear behavior is not necessarily appropriate for modeling the nonlinearities in some types of pipe joints as well as in the mounting arrangements of equipment (Gupta and Yang, 2002; Rustogi and Gupta, 2004).
- Accounting for the effects of uncertainties in the nonlinear model as well as the effects of non-classical damping in the development of the equivalent limit state.
- Modification to account for the asymmetric nature of the variation in equivalent limit-state with the tuning ratio (ratio that represented the degree of tuning between the frequencies of the primary and the secondary system). The equivalent limit-state for negative values of tuning ratio is not symmetric to that for positive values of tuning ratio.
- The applicability of the proposed modifications in the ELS concept is evaluated for various coupled systems.

It must be noted that the evaluation of seismic fragility using ELS concept is based on minimization of error between the response quantities of interest as evaluated from a nonlinear and a linearized system. The matching of the seismic fragility curve obtained from multiple nonlinear time history analyses with that obtained using the ELS concept is quite sensitive to the degree of localized nonlinearity and uncertainties in it for systems with tuning

ratio equal to zero (perfect tuning) or close to zero. Therefore, a probabilistic approach is adopted by incorporating Bayesian updating wherein the initial fragility curve obtained by the ELS concept is considered as the prior curve and updated to obtain a fairly accurate posterior fragility curve (Winkler, 2003; Ang and Tang, 2007) by conducting a very small number of computationally intensive nonlinear analyses.

2. Fundamental Background

2.1 Seismic fragility

The seismic fragility is defined as the conditional probability of failure or exceeding a specified failure limit state $G(.)$ for a given seismic intensity parameter. Mathematically,

$$P_f\left(x\right)\left(=P\left(\text{failure}\,|\,x\right)\right)=P\left(G\left(.\right)<0\,|\,x\right) \tag{1}$$

$$G=C-D \tag{2}$$

where $P_f\left(x\right)$ is the probability of failure given a seismic parameter x, C denotes the capacity of the system corresponding to the failure limit state, and D represents response demand at a given seismic intensity parameter. For simulation based evaluation of seismic fragility, a Monte-Carlo based approach is used to generate several discrete points of failure probability for a given seismic intensity parameter such as peak ground acceleration (PGA). Multiple time history analyses are conducted by normalizing each earthquake input motion to the same value of seismic intensity parameter, i.e. for $PGA = a_i$, we can write

$$P_f\left(a_i\right)=\frac{\sum 1\left(G\left(.\right)<0\,|\,a_i\right)}{n_i};\quad i=1,...,k \tag{3}$$

where 1(.) is the indicator function, a_i is the i^{th} level of PGA, and n_i is the number of simulations conducted at input ground motions having same level of PGA a_i. The seismic fragility curve is commonly assumed by many researchers (Kennedy et al., 1980; Shinozuka et al., 2000) to follow the log-normal cumulative distribution function (CDF).

$$P_f\left(PGA=a\right)=\Phi\left[\frac{\ln\left(a\right)-\ln\left(c\right)}{\beta}\right] \tag{4}$$

where $\Phi[\cdot]$ is the standard normal CDF, c is the median value of a, and β is the logarithmic standard deviation of a. These two parameters (the median and logarithimic standard deviation) of the log-normal CDF are determined by fitting them to the empirical, experimental and simulation data through the the maximum likelihood estimation or optimization method.

2.2 Equivalent elastic limit state (ELS) concept

The equivalent elastic limit state (ELS) is the optimal value V^* of the response quantity (displacement or rotation, etc.) that is considered as the failure limit state for the linearized system such that the seismic fragility evaluated from the linearized system is close to the seismic fragility for the nonlinear system. The linearization of the nonlinear system is performed by using same initial stiffness and damping coefficient of nonlinear system, but

adopting the different ELS V^* which is not the same as the nonlinear limit state D_{nl}. The concept of ELS for a SDOF system is illustrated in Fig. 1. The ELS V^* can be obtained by expressing the problem as an optimization problem in Eq. (5) where the failure probabilities from the linear system responses ${P_f}^l$ in Eq. (6) are close to failure probabilities of nonlinear system ${P_f}^{nl}$ in Eq. (7). The error between ${P_f}^l$ and ${P_f}^{nl}$ is represented as the root mean squared (RMS) error.

$$\underset{\{\text{Find } V^*\}}{\text{Minimize}}: \sqrt{\frac{1}{k}\sum_{i=1}^{k}\left({P_f}^{nl}\left(a_i; D_{nl}\right) - {P_f}^{l}\left(a_i; V^*\right)\right)^2} \tag{5}$$

$${P_f}^{l}\left(a; V^*\right) = P\left[v_{\max}\left(a\right) > V^* \mid PGA = a\right] \approx \sum_{i=1}^{N} 1\left(a \cdot v_{\max}^{i}\left(1g\right) > V^*\right) / N \tag{6}$$

$${P_f}^{nl}\left(a; D_{nl}\right) = P\left[u_{\max}\left(a\right) > D_{nl} \mid PGA = a\right] \approx \sum_{i=1}^{N} 1\left(u_{\max}^{i}\left(a\right) > D_{nl}\right) / N \tag{7}$$

where k is the number of PGA levels, N is the number of time history analyses at one level of PGA (or the number of different input ground motions), and $v_{max}(a)$ and $u_{max}(a)$ denote the random variables representing the peak displacement response under an earthquake of PGA = a in equivalent linear system and nonlinear system, respectively. Note that for a full description of seismic fragility curve using linear time history analyses, we need N responses at only a single PGA value as the responses at other PGAs can be acquired simply by scaling the values for the single PGA case. On the contrary, N times n (N x n) responses are needed to determine a fragility curve by using nonlinear time history analyses.

2.3 Bayesian updating

Bayesian statistics (Winkler, 2003; Ang and Tang, 2007) can incorporate newly available data $\mathbf{d}$ into an existing fragility model to improve the seismic fragility curve. In this method, the current (so called prior) fragility curve $P_f^{\,prior}(a;\boldsymbol{\theta})$ is updated into a modified (so called posterior) fragility curve $P_f^{\,post}(a\,|\,\mathbf{d})$ as follows:

$$P_f^{\,post}(a\,|\,\mathbf{d}) = \int P_f^{\,prior}(a;\boldsymbol{\theta}) f(\boldsymbol{\theta}\,|\,\mathbf{d})\, d\boldsymbol{\theta} \tag{8}$$

$$f(\boldsymbol{\theta}\,|\,\mathbf{d})\left(\propto f(\mathbf{d}\,|\,\boldsymbol{\theta})\, f(\boldsymbol{\theta})\right) = \frac{f(\mathbf{d}\,|\,\boldsymbol{\theta})\, f(\boldsymbol{\theta})}{\int f(\mathbf{d}\,|\,\boldsymbol{\theta})\, f(\boldsymbol{\theta})\, d\boldsymbol{\theta}} \tag{9}$$

where $\boldsymbol{\theta} = [c;\beta]$ are the two parameters of the lognormal fragility model, $f(\boldsymbol{\theta}\,|\,\mathbf{d})$ is the posterior joint probability density function (PDF), $f(\mathbf{d}\,|\,\boldsymbol{\theta})$ is the likelihood function, and $f(\boldsymbol{\theta})$ is the prior joint PDF of two parameters of the lognormal fragility model. The likelihood function is formulated representing the fragility data at each PGA in terms of a binomial event with a probability of failure $P_f^{\,prior}(a_i;\boldsymbol{\theta})$ and a corresponding probability of survival $1 - P_f^{\,prior}(a_i;\boldsymbol{\theta})$.

$$f(\mathbf{d}\,|\,\boldsymbol{\theta}) = \prod_{i=1}^{k} \binom{n_i}{r_i} \left(P_f^{\,prior}(a_i;\boldsymbol{\theta})\right)^{r_i} \left(1 - P_f^{\,prior}(a_i;\boldsymbol{\theta})\right)^{n_i - r_i} \tag{10}$$

where $\mathbf{d}$ is the k^{th} number of data as formatted in $\mathbf{d} = \left[\left[a_1 \cdots a_k \right]^T \quad \left[r_1 \cdots r_k \right]^T \quad \left[n_1 \cdots n_k \right]^T \right]$ with number of observed failure r_i out of total number observations n_i at a given PGA = a_i, and $\mathbf{\Pi}$ is the product for all k of PGA = a_i levels. The posterior PDF $f\left(\boldsymbol{\theta} \mid \mathbf{d}\right)$ is obtained numerically together with using Markov Chain Monte Carlo (MCMC). The MCMC helps in efficient generation of a sequence of points which are asymptotically distributed according to a target distribution. More specifically, Metropolis-Hastings algorithm (Metropolis et al., 1953; Hastings, 1970) is used in the present study.

3. Mathematical Modeling of Coupled System

3.1 Nonlinear hysteretic nonlinear model

The original concept of ELS as proposed by Tadinada and Gupta (2016) considers a bi-linear model with pinching to characterize the nonlinearities in the secondary system. In this paper, we enhance the originally proposed ELS approach by considering a hysteretic nonlinear behavior. Over the years, several mathematical models have been proposed to represent the nonlinear hysteresis behavior (Bouc, 1967; Wen, 1976; Jennings, 1964; Kaul and Penzien 1974; Bazant at al., 1983). Among these, the Bouc-Wen Model has been studied extensively and has been reconciled with the experimental data for many different applications such as the steel beam-column connection or structural steel element (Popov and Stephen, 1970; Charalampakis and Koumousis, 2008), seismic energy dissipators for RC panels (Sasani and Popov, 2001), RC columns (Park et al., 1986), electrical conductors (Filiatrault et al., 1999;

Song and Der Kiureghian, 2006), lead rubber bearing as a seismic isolator (Constantinou, 1985; Kwag and Ok, 2013), passive dampers (Yang et al., 1994), and a few others (Ismail et al., 2009). In addition to these applications, the simple differential equations used in the Bouc-Wen model provide flexibility to adjust its parameters for modeling the behavior of other applications that have nonlinear hysteresis characteristics. The model is shown in Fig. 2 in which the restoring force f_r is composed of the linear viscous elastic part and hysteretic part, and defined as:

$$f_r = c\Delta\dot{x} + \alpha k_i \Delta x + (1-\alpha) k_i y \tag{11}$$

where the parameter c is the viscous damping coefficient; k_i is the initial stiffness before yield; α (=k_f / k_i) represents the post-yield stiffness ratio when the post-yield stiffness is k_f; Δx is the displacement, $\Delta\dot{x}$ is the velocity; and y is the auxiliary variable representing inelastic behavior which can be written as:

$$\dot{y} = -\gamma \left|\Delta\dot{x}\right| y \left|y\right|^{n-1} - \beta\Delta\dot{x}\left|y\right|^{n} + A\Delta\dot{x} \tag{12}$$

where the parameter A controls the scale of the hysteresis loops and n determines sharpness of the hysteresis cycle at the transition from elastic to inelastic part. For example, it will represent bi-linear behavior when n approaches infinity. Parameters β and γ control the shape of the hysteretic loop.

3.2 Coupled system

The governing equation of motion for a m-DOF coupled system consisting of a p-DOF primary system and an s-DOF secondary system shown in Fig. 3 is given by Eq. (13). As shown in Fig. 13, the secondary system exhibits localized nonlinearity which is characterized by the Bouc-Wen nonlinear hysteretic model.

$$\left[M\right]_{m\times m}\left\{\ddot{u}\right\}_{m\times 1}+\left[C\right]_{m\times m}\left\{\dot{u}\right\}_{m\times 1}+\left[\overline{K}\right]_{m\times m}\left\{u\right\}_{m\times 1}+\left\{K_a\right\}_{m\times 1}y=-\left[M\right]_{m\times m}\left\{1\right\}_{m\times 1}\ddot{u}_g \tag{13a}$$

$$\begin{aligned}\left\{u\right\}_{m\times 1}^{T}&=\begin{bmatrix}u_1 & \cdots & u_p & u_{p+1} & \cdots & u_{p+s}\end{bmatrix}\\ \left\{\dot{u}\right\}_{m\times 1}^{T}&=\begin{bmatrix}\dot{u}_1 & \cdots & \dot{u}_p & \dot{u}_{p+1} & \cdots & \dot{u}_{p+s}\end{bmatrix}\\ \left\{\ddot{u}\right\}_{m\times 1}^{T}&=\begin{bmatrix}\ddot{u}_1 & \cdots & \ddot{u}_p & \ddot{u}_{p+1} & \cdots & \ddot{u}_{p+s}\end{bmatrix}\end{aligned} \tag{13b}$$

$$\left[M\right]_{m\times m}=diag\begin{pmatrix}m_1 & \cdots & m_p & m_{s1} & \cdots & m_{ss}\end{pmatrix} \tag{13c}$$

$$\left[C\right]_{m\times m}=\begin{bmatrix}\left[C_p\right]_{p\times p} & \left[0\right]_{p\times s}\\ \left[0\right]_{s\times p} & \left[C_s\right]_{s\times s}\end{bmatrix}+c_{s1}\left\{v\right\}\left\{v\right\}^{T}-c_{s1}\left\{r\right\}\left\{r\right\}^{T} \tag{13d}$$

$$\left[\overline{K}\right]_{m\times m}=\begin{bmatrix}\left[K_p\right]_{p\times p} & \left[0\right]_{p\times s}\\ \left[0\right]_{s\times p} & \left[K_s\right]_{s\times s}\end{bmatrix}+\alpha k_{s1}\left\{v\right\}\left\{v\right\}^{T}-\alpha k_{s1}\left\{r\right\}\left\{r\right\}^{T} \tag{13e}$$

$$\left\{K_a\right\}_{m\times 1}^{T}=-\left(1-\alpha\right)\left\{v\right\}^{T} \tag{13f}$$

where $\ddot{u}_g$ is the ground acceleration; $\{u\}, \{\dot{u}\}$ and $\{\ddot{u}\}$ are the displacement, velocity and acceleration vector of the coupled system; $[M]$, $[C]$ and $[\overline{K}]$ are the structural mass, damping, and stiffness matrices of coupled system; $[C_p]$ and $[C_s]$ are the damping matrices of the primary and the secondary system, respectively; $[K_p]$ and $[K_s]$ are the stiffness matrix of primary system and secondary system; $\{K_a\}$ is auxiliary stiffness vector induced by the localized nonlinear element; The vector $[v]^T$ and $[r]^T$ are defined as follows if the secondary system is assumed to be attached to the k^{th} primary system degree of freedom:

$$\{v\}_{m\times 1}^{T} = [0 \quad \cdots \quad 0 \quad 1 \quad 0 \quad \cdots \quad 0 \quad -1 \quad 0 \quad \cdots \quad 0] \tag{14}$$

$$[r]_{m\times 1}^{T} = [0 \quad \cdots \quad 0 \quad 1 \quad 0 \quad \cdots \quad 0] \tag{15}$$

where the non-zero entries of $[v]^T$ are at the k^{th} DOF for the primary system and $(p+1)^{th}$ DOF for the secondary system, and the non-zero entries of $[r]^T$ are at the k^{th} DOF of primary system.

The equation of motion given by Eq. (13a) can be rewritten as a second order ordinary differential equation (ODE) given by Eq. (16). Furthermore, the second order ODE in Eq. (16) written as a first order ODE representation given by Eq. (17a):

$$\{\dot{u}\} = [I]\{\dot{u}\}$$
$$\{\ddot{u}\} = -[M]^{-1}[\overline{K}]\{u\} - [M]^{-1}[C]\{\dot{u}\} - [M]^{-1}\{K_a\}y - \{1\}\ddot{u}_g \qquad (16)$$
$$\dot{y} = -\gamma|\dot{u}_b|y|y|^{n-1} - \beta\dot{u}_b|y|^n + A\dot{u}_b$$

$$\{\dot{Y}\} = f(t,\{Y\}) \qquad (17a)$$

$$\{Y\}_{(2m+1)\times 1}\left(=[Y_1 \sim Y_m \quad Y_{m+1} \sim Y_{2m+1} \quad Y_{2m+1}]^T\right) = \left[\{u\}^T_{m\times 1} \quad \{\dot{u}\}^T_{m\times 1} \quad y_{1\times 1}\right] \qquad (17b)$$

$$\{\dot{Y}\}_{(2m+1)\times 1}\left(=[\dot{Y} \sim \dot{Y}_m \quad \dot{Y}_{m+1} \sim \dot{Y}_{2m} \quad \dot{Y}_{2m+1}]^T\right) = \left[\{\dot{u}\}^T_{m\times 1} \quad \{\ddot{u}\}^T_{m\times 1} \quad \dot{y}_{1\times 1}\right] \qquad (17c)$$

$$\begin{Bmatrix}\dot{Y}_1\\ \vdots \\ \dot{Y}_m\end{Bmatrix} = [I]_{m\times m}\begin{Bmatrix}Y_{m+1}\\ \vdots \\ Y_{2m}\end{Bmatrix}$$
$$\begin{Bmatrix}\dot{Y}_{m+1}\\ \vdots \\ \dot{Y}_{2m}\end{Bmatrix} = -[M]^{-1}[\overline{K}]\begin{Bmatrix}Y_1\\ \vdots \\ Y_m\end{Bmatrix} - [M]^{-1}[C]\begin{Bmatrix}Y_{m+1}\\ \vdots \\ Y_{2m}\end{Bmatrix} - [M]^{-1}\{K_a\}Y_{2m+1} - \{1\}\ddot{u}_g \qquad (17d)$$
$$\dot{Y}_{2m+1} = -\gamma|Y_{m+1}|Y_{2m+1}|Y_{2m+1}|^{n-1} - \beta Y_{m+1}|Y_{2m+1}|^n + AY_{m+1}$$

where $[I]$ is the identity matrix and $\{Y\}$ is the state vector. Eq. (17a) can be solved by using the forth order Runge-Kutta algorithm.

4. Description of Equivalent Limit State Method

4.1 Efficiency

The primary motivation for developing an equivalent limit-state based approach to calculating seismic fragility lies in its efficiency by reducing the number of nonlinear time history analyses. To determine and illustrate the efficiency of this method, we consider a SDOF primary – SDOF secondary (2-DOF coupled) system. The configuration and properties for this system are given in Fig. 4 and Table 1. Seismic fragility curves are generated by considering total of 75 real earthquake records normalized to unit PGA (Gupta and Choi, 2005), and these motions are used for performing time history analyses of linear as well as nonlinear systems. Fig. 5 plots the response spectrum corresponding to each ground motion normalized to 1g, the mean response spectrum, and the mean plus one standard deviation response spectrum for 5% damping.

To begin with, the failure probabilities for nonlinear system $P_f{}^{nl}$ are calculated at twelve different PGA levels between 0.25g and 3g at an interval of 0.25g in accordance with Eq. (7). It takes a total of 900 nonlinear time history analyses (75 ground motion times 12 PGA level) to generate this curve. Then, equivalent limit state V^* is obtained by minimizing the error between failure probabilities for the nonlinear and the linearized system at all twelve PGA levels i.e. by solving Eq. (5) based on Eq. (17). The seismic fragility curve generated using a linear time history analyses requires only 75 analyses in accordance with Eq. (6). The root mean squared (RMS) error between the fragility curves calculated from

nonlinear and linear time history analyses is shown in Fig. 6. As seen in this figure, the optimal ELS V^* is evaluated as 0.2241m ($=3.735 \cdot u_y$) by solving Eq. (5). Fig. 7 illustrates the comparison between seismic fragility curves obtained from the 900 nonlinear time history analyses with that obtained from the 75 linear time history analyses in conjunction with ELS V^*.

The comparison presented above illustrates that ELS V^* for the secondary system is known a-priori, the computational effort reduces significantly without any appreciable loss in the accuracy of seismic fragility curve. Next, we develop an empirical equation for ELS V^* by conducting numerical simulations for a large number of different simplified coupled systems.

4.2 Empirical equation for ELS V*

Tadinada and Gupta (2016) proposed an empirical equation for ELS V^* that uses a Cauchy probability density function. As mentioned before, enhancements are needed in this empirical equation to account for:

- asymmetric nature of variation in V* with respect to tuning ratio.
- uncertainties in the nonlinear behavior of the secondary system
- effect of non-classical damping in coupled system.

In order to derive an empirical expression for ELS V^*, we consider simplified 2-DOF coupled systems with varying: (i) degrees of nonlinearities, (ii) tuning ratios η as defined by

Eq. (18), (iii) ductility (μ), and (iv) damping ratios (ξ) to account for non-classical damping. The nonlinear hysteretic behavior is varied by adjusting k_i , α and u_y of Bouc-Wen model under assumption of $A = 1$, $n = 1$, and $\beta = \gamma = 1/(2u_y)$. The tuning ratio is expressed as

$$\eta = \frac{f_p - f_s}{f_p + f_s} \tag{18}$$

where f_p and f_s are the fundamental natural frequency (Hz) of the primary and secondary system, respectively.

Specifically, as shown in Fig. 4 and Table 2, a total of 2,106 models are analyzed by varying different tuning ratios η, and nonlinear characteristics α and u_y for each ductility value μ (=2, 3, 5) and damping ratio of secondary system ξ_s (=0.02, 0.05). These systems are analyzed by normalizing the 75 earthquake ground motions to eight different PGA levels – four levels between 0.25g and 1g at an interval of 0.25g, and four levels between 1g and 3g at an interval of 0.5g. Therefore, a total of 1,263,600 nonlinear time history analyses (= 2,106 models x 8 PGAs x 75 ground motions) and 157,950 linear time history analyses (= 2,106 models x 1 PGAs x 75 ground motions) are conducted for developing the empirical expression for ELS V^*. It is assumed that the mass ratio between primary and secondary system is 0.001 and the damping ratio of primary system ξ_p is 0.02.

For developing the closed form equation of ELS V*, the kernel of a Cauchy probability density function is used as the basis, and other equivalent linearization concepts such as elastic strain energy method (Veletsos and Newmark, 1960) and secant stiffness

method (Deierlein and Hsieh, 1990; Chopra, 1995) are also incorporated. The Cauchy probability density function is used as the basis because the average trend of nonlinear simulation data in Fig. 8 follows the shape of a heavy-tailed probability density distribution in the domain of the tuning ratio. In elastic strain energy method, the equivalent elastic displacement is obtained by relating the peak displacement of an inelastic SDOF system with that of the corresponding elastic SDOF system using the concept of equal strain energy. In the secant stiffness method, the inelastic SDOF system is linearized into the elastic SDOF system by equivalent stiffness called secant stiffness and equivalent damping ratio which expresses the stiffness degradation and energy dissipation in a nonlinear system when the system is excited by its resonating frequency. The detailed explanation of these equivalent linearization methods is not provided in this paper for brevity. The empirical equation ELS V^* is obtained as follows:

$$\frac{V^*}{u_y} = f\left(\alpha, u_y, \eta, \mu, \xi_s\right) = \begin{cases} \eta < 0: & \dfrac{V^*}{u_y} = s \cdot \left(1.0 + \left(\dfrac{V_{SS}}{u_y} - 1.0 \right) \dfrac{1}{\left(1 + (18\eta)^2\right)} \right) \\ \eta \geq 0: & \dfrac{V^*}{u_y} = s \cdot \left(1.4\dfrac{V_{ESE}}{u_y} + \left(\dfrac{V_{SS}}{u_y} - 1.4\dfrac{V_{ESE}}{u_y} \right) \dfrac{1}{\left(1 + (10\eta)^2\right)} \right) \end{cases} \quad (19a)$$

$$s = 0.9 + 0.1 \cdot (1.5\mu - 2) \quad (19b)$$

$$V_{ESE} = u_y \sqrt{1 + (\mu - 1)\left(2 + \alpha(\mu - 1)\right)} \quad (19c)$$

$$V_{SS} = D_{nl}\sqrt{\frac{\left(\xi_s + \xi_{eq}\right)k_{\sec}}{\xi_s k_i}};$$
$$k_{\sec} = \frac{k_i u_y + \alpha k_i \left(D_{nl} - u_y\right)}{D_{nl}},\ \xi_{eq} = \frac{2}{\pi}\left(\frac{\left(\mu-1\right)\left(1-\alpha\right)}{\mu\left(1+\alpha\left(\mu-1\right)\right)}\right), D_{nl} = \mu \cdot u_y \quad \text{(19d)}$$

where s is scaling factor, V_{ESE} is equivalent elastic limit displacement calculated from elastic strain energy method when the nonlinear system is assumed to follow bi-linear hysteresis behavior., V_{SS} is equivalent elastic limit displacement computed from elastic secant stiffness method under the assumption that the nonlinear system follows bi-linear hysteresis behavior, k_{sec} is secant stiffness and ξ_{eq} is equivalent damping ratio for nonlinear hysteretic system. Fig. 8 compares the numerical simulation data and ELS V^* equation in the domain of η and V^*/u_y. The detailed process deriving the equation is presented in section 4.3.

The main limitation of the empirical equation developed above is that it uses data from a very simple 2-DOF representative coupled system. In addition, the comparison of the numerical values and the empirical equation in Fig. 8 shows that the problem is quite sensitive in the region around $\eta = 0$ and actual values can be different from that given by the empirical equation. These limitations can be overcome by using the method presented in the section 4.4.

4.3 Development of ELS V* equation

Tadinada and Gupta (2016) presented the ELS *V** equation based on the results using an idealized bi-linear behavior with pinching effect to model the nonlinearities in the piping joints as follows:

$$\frac{V^*}{u_y} = \frac{V_{ESE}}{u_y} + \left(\frac{V_{EVD}}{u_y} - \frac{V_{ESE}}{u_y} \right) \cdot \frac{1}{0.54\left(1+\left(15\eta/0.54\right)^2\right)} \tag{20a}$$

$$V_{EVD} = D_{nl}\sqrt{1+\frac{\xi_{eq}}{\xi}} \tag{20b}$$

where V_{EVD} is the equivalent elastic limit displacement obtained from the equivalent viscous damping concept (Jacobsen, 1930). The main drawbacks of this equation is that (1) it does not account for the different damping nature between the primary system and secondary system; (2) it does not consider the effect of stiffness degradation using the secant stiffness concept in the equivalent linearization process; (3) it assumes the ELS *V** variation to be symmetrical with respect to the tuning ratio η; (4) it does not use a scale factor to well describe the equation in the tuned ratio region and other ductility capacity value ranges. In this regard, the proposed equation should need some enhancement and improvement by dealing with these limitations.

Fig. 9 illustrates the difference between the equation of Tadinada and Gupta and the proposed equation by this study in μ = 2 and ξ_s = 0.02. The blue dotted line denotes the

original equation of Tadinada and Gupta. The red thick solid line shows the proposed equation by this study. The cross marks ("**x**") in the graph represent the ELS V^* data we obtained for this case. As shown in this figure, the equation of Tadinda and Gupta does not look quite well matching the obtained data. The reasons which bring about this difference are attributed to the characteristics of the equation.

So, as a first step to enhance this equation, let us consider the effect of stiffness degradation by using the secant stiffness concept. The green dashed line in Fig. 9 and Eq. (21) represent the enhanced equation accommodating the secant stiffness by using V_{SS} instead of V_{EVD} in Eq. (21a). As shown in this figure, the additional consideration of the stiffness degradation makes the equation be considerably close to the obtained data of the perfectly tuned region (η = 0). But, the enhanced equation acquired from the first step still cannot describe the obtained data in the tuned region, sufficiently.

$$\frac{V^*}{u_y} = \frac{V_{ESE}}{u_y} + \left(\frac{V_{SS}}{u_y} - \frac{V_{ESE}}{u_y} \right) \cdot \frac{1}{0.54\left(1 + \left(15\eta / 0.54\right)^2\right)} \qquad (21)$$

Thus, as a second step, let us use a scale factor to improve the accuracy in the tuned region. Eq. (22) represents the modified equation. The scale factor is multiplied only with the second term of right hand side of Eq. (21) since it is intended to have the scale effect be restricted to the tuned region. The scale factor is determined by minimizing errors between the equation and the data in the tuned region at all ductility capacity values. The obtained relation between ductility capacity μ and the scale factor s are $s = 0.15 \cdot \mu + 0.3$. The blue thin

solid line of Fig. 9 illustrates the scaled equation by Eq. (22). As we can see in this figure, the scale factor has the equation be more coming close to the obtained data in the tuned region. However, this improved equation in terms of the secant stiffness concept and the scale factor still cannot deal with issues of the unsymmetrical nature and scatter shape of the data.

$$\frac{V^*}{u_y} = \frac{V_{ESE}}{u_y} + s\left(\left(\frac{V_{SS}}{u_y} - \frac{V_{ESE}}{u_y}\right) \cdot \frac{1}{0.54\left(1+\left(15\eta/0.54\right)^2\right)}\right) \qquad (22)$$

Therefore, as a third step, let us take the unsymmetrical feature of the data into account by differentiating the asymptotic lines of the equation at $\eta \geq 0$ and $\eta < 0$ regions, and considering the data scatter shape by changing the factors in η. Fig. 10 specifically shows the different asymptotic lines at $\eta \geq 0$ and $\eta < 0$ well describing the data trend as red thick solid lines compared to the original asymptotic lines. From this figure and Fig. 9, it is observed that the proposed ELS V^*/u_y equation converges to the value of "$1.4 \cdot V_{ESE}/u_y$" as η goes to 1 and the proposed equation converges to the value of "1" as η goes to -1 while the equation of Tadinada and Gupta all converges to the value of "V_{ESE}/u_y" regardless of the data trend in η going to 1 or -1. Fig. 11 shows the curve shapes according to the change of the factors in η. The factors in η are respectively estimated as different values at $\eta \geq 0$ and $\eta < 0$ regions which can well delineate the data inclination. The obtained appropriate factors are specified as red solid line's boxes in Fig.11.

Finally, the trend of approximated asymptotic lines for the obtained data is changed under the different ductility capacity values. This can be observed in Fig. 8 of ELS V^* data in

all ductility capacity domain. So, in order to consider the changing nature of asymptotic lines in the different ductility capacities, the scale factor is multiplied to the entire form of equation and then, corresponding scale factor is re-decided. The identified relation between ductility capacity and scale factor in the changing form of equation are illustrated in Fig. 12. This figure shows all data and the predicted linear relation in the domain of ductility capacity μ and scale factor s. Consequently, the final improved equation incorporating the secant stiffness effect, scale factor, unsymmetrical data nature, and overall scatter shape of data is represented in the following Eq. (19a) and illustrated in Fig. 9 as a red thick solid line.

Then, in order to confirm the effectiveness of the improved equation, let us compare the fragility result using Eq. (20a) and Eq. (19a) for the example coupled structure of Fig. 4. In this case, the secondary system of example structure has the material properties corresponding to η = 0.6 and μ = 3. The reason we choose these parameters is that the equations are quite different in the tuned or asymptotic line regions. Fig. 13 compares fragility curves using the equation of Tadinada and Gupta which is Eq. (20a) and the proposed equation of Eq. (19a) by this study. As shown in this figure, we can see that the proposed equation gets more exact result than the Eq. (20a) does in comparison to the nonlinear analysis results. The more exact representation of ELS V^* by using Eq. (19a) can increase the accuracy of fragility result.

4.4 Seismic fragility assessment using ELS and Bayesian updating

Once an empirical expression is available for ELS V^*, seismic fragility can be obtained in relatively straightforward manner by conducting only a few linear time history analyses of the specific coupled system being evaluated. For facilitating the discussion in this manuscript, we use the term "ELS method" to refer to the process of calculating seismic fragility by using ELS V^* equation and linear time history analyses. As noted earlier, the ELS method by itself does not necessarily gives an accurate fragility curve especially for tuned or nearly tuned coupled system. Since the proposed method uses simple 2-DOF representative systems for developing the empirical equation, the differences between the curve obtained by this method and the true fragility curve of system are likely to increase with increasing complexity in the characteristics of the coupled system. Yet, the two curves are relatively close enough and the accuracy can be significantly improved if only limited information is available on the true fragility of the system. Additional information on true fragility can be obtained from either experimental data or by conducting a few nonlinear time history analyses. The additional information on true fragility even though limited in quantity can be used effectively in conjunction with Bayesian updating as given by Eq. (8). The fragility curve generated solely by using the ELS method is taken as the prior and limited number of nonlinear time history analyses is used as the data to update and generate the posterior curve. The complete process of using ELS method and Bayesian updating to generate the final fragility curve is explained through a flowchart in Fig. 14.

5. Application and Verification of Proposed Method

In this section, we illustrate the application of the proposed method and establish its accuracy by using three different coupled system configurations: 1) SDOF primary - SDOF secondary system, 2) MDOF primary - SDOF secondary system, and 3) MDOF primary - MDOF secondary system. The accuracy and efficiency of the proposed method are illustrated by comparing the seismic fragility curves obtained from using the ELS method by itself, the ELS method & Bayesian updating in conjunction with each other, and the comprehensive nonlinear time history analysis. The computational efficiency is illustrated by comparing the numbers of analyses needed for each case in all the three examples.

5.1 Example 1: Primary SDOF and secondary SDOF system

Eighteen (18) different models having tuning ratio η = -0.2, 0 and 0.6, damping ratio ξ_s = 0.02 and 0.05, and ductility μ = 2, 3 and 5 are selected for showing the effectiveness of the proposed method. The mass ratio between primary and secondary system, the post-yield stiffness ratio α and yield displacement u_y are assumed to be 0.001, 0.1, and 0.06 m, respectively. The 75 earthquake time histories normalized to 8 different PGA levels between 0 ~ 3g are used for developing seismic fragility curves. The physical properties of the models are given presented in Table 3.

Fig. 15 and Table 4 compare the seismic fragility curves for all 18 cases as obtained by using only linear time history analysis as per the ELS method by itself, the ELS method in conjunction with a few nonlinear time history analyses for Bayesian updating, and the

comprehensive nonlinear time history analysis approach. The calculated ELS V^* utilizing Eq. (19) for all 18 cases are given at the bottom of each fragility curve. As seen in Fig. 15 and Table 4, the seismic fragility curves obtained from the ELS method appears to be in good agreement with the corresponding curve obtained from the nonlinear time history analyses for all the detuned cases with η = 0.6 irrespective of the damping ratios and ductility values. Therefore, Bayesian updating is not needed. However, the seismic fragility curves obtained from the ELS method are somewhat different from those from the nonlinear time history analyses for both η = -0.2 and 0. For these cases, the seismic fragility curves from the ELS method used in conjunction with the Bayesian updating are very close to those obtained from the nonlinear time history analyses. The ELS method takes just 75 linear time history analyses, and the ELS method & Bayesian updating takes 75 linear time history analyses and 225(=75x3) nonlinear time history analyses while the nonlinear time history analysis approach for seismic fragility curve takes 600 (=75x8) nonlinear time history analyses.

5.2 Example 2: Primary MDOF and secondary SDOF system

A 9-DOF coupled system comprising of an SDOF secondary system connected to the fourth floor of the 8-DOF primary system is considered and is illustrated in Fig. 16. As in the case of example 1, eighteen (18) different models are considered with η = -0.2, 0 and 0.6, damping ratio ξ_s = 0.02 and 0.05, and ductility capacity μ = 2, 3 and 5. The ratio of the first modal effective mass of primary system and the mass of secondary system, the post-yield stiffness ratio α and yield displacement u_y are 0.0001, 0.1, and 0.06 m, respectively. The 75

earthquake time histories are normalized to 12 PGA levels between 0 ~ 3g for developing the seismic fragility curves. The properties and modal characteristics of the uncoupled systems are given in Table 5.

Fig. 17 and Table 6 compare the fragility curves for all 18 cases by using the three approaches. The calculated ELS V^* from Eq. (19) for all 18 cases are given at the bottom of each fragility curve. For the case of η = -0.2 and μ = 5, the median and logarithmic standard deviation for lognormal fragility model are not included in Table 6 because the fragilities in 0 ~ 3g PGA range are zero. The results shown in Fig. 17 and Table 6 are very similar in nature to those exhibited for the example 1 described earlier. The ELS method takes just 75 linear time history analyses where the ELS method when used in conjunction with Bayesian updating takes 75 linear time history analyses and 225(=75x3) nonlinear time history analyses. In comparison, the comprehensive nonlinear time history analysis approach takes 900(=75x12) analyses.

5.3 Example 3: Primary MDOF and secondary MDOF system

This example represents the most complex of all the examples considered in this study. A 10-DOF coupled system in which the secondary is a 2-DOF system which is connected to the fourth floor of the 8-DOF primary system as shown in Fig. 18. Once again, eighteen (18) different models are considered for η = -0.2, 0 and 0.6, damping ratio ξ_s = 0.02 and 0.05, and ductility μ = 2, 3 and 5. The ratio of the first modal effective mass of primary and secondary system, the post-yield stiffness ratio α and yield displacement u_y are taken as 0.0001, 0.1, and

0.06 m, respectively. The 75 earthquake time histories are normalized to 12 PGA levels within 0 ~ 3g. The physical properties and modal characteristics of the uncoupled models are given in Table 7. The results from different analyses are compared in Fig. 19 and Table 8. The observations from this set of results are same as in the case of previous two examples. The numbers of time history analyses needed for each case are also identical to those for example 2 described above.

6. Summary and Conclusions

This paper focuses on enhancements to an existing approach termed as equivalent limit state based methodology for evaluating the seismic fragility of secondary systems such as equipment and piping. The equivalent limit state concept focuses on arriving at a reasonably quick but accurate seismic fragility estimates which can be used as reliable prior information for a Bayesian updating framework. The Bayesian updating framework seeks to update the prior fragility using only limited results from actual nonlinear simulations or real-life experimental fragility data thus minimizing the total effort required in estimating the seismic fragility to a desired degree of accuracy. The equivalent elastic limit state is a modified representation of the failure capacity of secondary system such that the damage probabilities are close to that obtained from the actual nonlinear analyses.

Enhancements to the concept of equivalent limit-state are presented in this study. The original formulation for the empirical equation of equivalent limit state was developed using a bilinear model to represent the localized nonlinearities in secondary systems. Such

localized nonlinearities are typically exhibited at the joints of piping systems. However, the mounting arrangements in equipment and piping supports can often exhibit hysteretic behavior. Overall, three distinct enhancements are proposed:

- Consideration of a hysteretic model for the nonlinearities in the secondary system.
- Account for the effects of uncertainties in the nonlinear model and for non-classical damping. A coupled system becomes non-classically damped when the damping characteristics of the primary and secondary systems are different from each other.
- Account for the effect of asymmetric variation of the equivalent elastic limit state with respect to tuning ratio. The originally proposed formulation is symmetric and exhibits significant differences for systems in which tuning ratios are greater than zero.

Three different configurations of primary-secondary systems are used to illustrate the applicability and evaluate accuracy of the proposed approach. A total of 18 different models are created for each configuration by varying the tuning ratio, damping, and ductility values. It is shown that the proposed approach gives fragility curves that are close to those obtained from a comprehensive computationally intensive nonlinear time history analyses.

Acknowledgements

This research was partially supported by the Center for Nuclear Energy Facilities and Structures at North Carolina State University. Resources for the Center come from the dues

paid by member organizations and from the Civil, Construction, and Environmental Engineering Department and College of Engineering in the University.

References

Ang AH-S. and Tang WH, *Probability concepts in engineering: Emphasis on applications to civil and environmental engineering*, 2nd edition, Wiley, New York, 2007.

Atalik TS and Utku S, "Stochastic linearization of multi-degree-of-freedom non-linear systems," *Earthquake Engineering & Structural Dynamics*, 4(4), 411-420, 1976.

Bažant Z, "Endochronic inelasticity and incremental plasticity," *International Journal of Solid Structures*, 14, 691-714, 1978.

Bouc R, "Forced vibration of mechanical system with hysteresis," *Proceeding of 4th conference on Nonlinear Oscillation*, Prague Czechoslovakia, 1967.

Caughey TK, "Equivalent linearization techniques," *Journal of the Acoustical Society of America*, 35, 1706-1711, 1963.

Charalampakis AE and Koumousis VK, "Identification of Bouc–Wen hysteretic systems by a hybrid evolutionary algorithm," *Journal of Sound and Vibration*, 314(3-5), 571-585, 2008.

Chen Y and Soong TT, "Seismic response of secondary systems," *Engineering Structures*, 10(4), 218–228, 1988.

Chopra AK, *Dynamics of structures: : Theory and applications to earthquake engineering*, 4th Edition, Prentice Hall, Englewood Cliffs, New Jersey, 2012

Constantinou MC and Tadjbakhsh IG, "Hysteretic dampers in base isolation: random

approach," *ASCE Journal of Structural Engineering*, 111(4), 705-721, 1985.

Crandall SH, "A half-century of stochastic equivalent linearization," *Structural Control and Health Monitoring*, 13(1), 27-40, 2006.

Deierlein GG and Hsieh S-H, "Seismic response of steel frames with semi-rigid connections using the capacity spectrum method," *Proceedings of the 4th U.S. National Conference on Earthquake Engineering*, 2, 863–872, 1990.

Filiatrault A, Kremmidas S, Elgamal A, and Seible F, *Substation equipment interaction-rigid and flexible conductor studies*, Report SSRP-99/09, Division of Structural Engineering, University of California, San Diego, La Jolla, CA, 1999.

Gulkan P and Sozen MA, "Inelastic responses of reinforced concrete structures to earthquake motions," *Journal of the American Concrete Institute*, 71(12), 604–610, 1974.

Gupta A and Choi B., "Consideration of uncertainties in seismic analysis of coupled building piping systems," *Nuclear Engineering and Design*, 235, 2071-2086, 2005.

Gupta A and Gupta AK, "New developments in coupled seismic analysis of equipment and piping," *Transactions of the 13th International Conference on Structural Mechanics in Reactor Technology (SMiRT 13)*, Porto Alegre, Brazil, 1995.

Gupta A and Yang J, "Modified Ritz vector approach for dynamic properties of electrical cabinets and control panels," *Nuclear engineering and design*, 217(1), 49-62, 2002.

Hastings WK, "Monte Carlo sampling methods using Markov chains and their applications," *Biometrika*, 57(1), 97-109, 1970.

Ismail M, Ikhouane F, and Rodellar J, "The hysteresis Bouc-Wen Model, a Survey," *Archives of Computational Methods in Engineering*, 16(2), 161-188, 2009.

Iwan WD, "Estimating inelastic response spectra from elastic spectra," *Earthquake Engineering & Structural Dynamics*, 8(4), 375-388, 1980.

Jacobsen LS, "Steady forced vibrations as influenced by damping." *ASME Transactions*, 52(1), 169-181, 1930.

Jennings PC, "Periodic response of a general yielding structure," *ASCE Journal of the Engineering Mechanics Division*, 90(2), 131-163, 1964.

Ju BS and Gupta A, "Seismic fragility of threaded Tee-joint connections in piping systems," *International Journal of Pressure Vessels and Piping*, 132, 106-118, 2015.

Ju BS, Ryu Y and Gupta A, "Piping fragility evaluation: Interaction with high-rise building performance," *ASME Journal of Pressure Vessel Technology*, Accepted.

Kaul MK and Penzien J, "Stochastic analysis of yielding offshore towers," *ASCE Journal of the Engineering Mechanics Division*, 100(5), 1025-1038, 1974.

Kennedy RP, Cornell CA, Campbell RD, Kaplan S, and Perla HF, "Probabilistic seismic safety of an existing nuclear power plant," *Nuclear Engineering and Design* 59, 315-338, 1980.

Kwag S and Ok S-Y, "Robust design of seismic isolation system using constrained multi-objective optimization technique," *KSCE Journal of Civil Engineering*, 17(5), 1051-1063, 2013.

Kwan W-P and Billington SL, "Influence of hysteretic behavior on equivalent period and damping of structural systems," *ASCE Journal of Structural Engineering*, 129(5), 576–585, 2003.

Metropolis N, Rosenbluth AW, Rosenbluth MN, Teller AH, and Teller E, "Equations of state calculations by fast computing machines," *Journal of Chemical Physics*, 21(6), 1087-1092, 1953.

Park YJ, Wen YK, and Ang AH-S, "Random vibration of hysteretic systems under bi-directional ground motion," *Earthquake Engineering & Structural Dynamics*, 14, 543-547, 1986.

Popov EP and Stephen RM, *Cyclic loading of full-size steel connections*, UCB/EERC-70/03, Earthquake Engineering Research Center, University of California at Berkeley, 1970.

Proppe C, Pradlwarter HJ, and Schuëller GI, "Equivalent linearization and Monte Carlo simulation in stochastic dynamics," *Probabilistic Engineering Mechanics*, 18(1), 1-15, 2003.

Rustogi S and Gupta A, "Modeling the dynamic behavior of electrical cabinets and control panels: experimental and analytical results," *ASCE Journal of Structural Engineering*, 130(3), 511-9, 2004.

Sasani M and Popov EP, "Seismic energy dissipators for RC panels: Analytical studies," *ASCE Journal of Engineering Mechanics*, 127(8), 835-843, 2001.

Shinozuka M, Feng MQ, Lee J, and Naganuma T, "Statistical analysis of fragility curves," *ASCE Journal of Engineering Mechanics*, 126(12), 1224-1231, 2000.

Song J and Der Kiureghian A, "Generalized Bouc–Wen Model for Highly Asymmetric Hysteresis," *ASCE Journal of Engineering Mechanics*, 132(6), 610-618, 2006.

Tadinada SK and Gupta A, "Structural fragility of large-scale piping systems using equivalent elastic time-history simulations," *Structural Safety, submitted.*

USNRC, "Benchmark Program for the Evaluation of Methods to Analyze Non-Classically Damped Coupled Systems, NUREG/CR-6661 (BNL-NUREG52577), Washington DC, US, 2000.

Veletsos AS and Newmark NM, "Effects of inelastic behavior on the response of simple systems to earthquake ground motions," *Proceedings of the 2nd World Conference on Earthquake Engineering*, Tokyo, Japan, Vol. II, 895-912, 1960

Wen YK, "Equivalent linearization for hysteretic systems under random excitation," *ASME Journal of Applied Mechanics*, 47(1), 150-154, 1980.

Wen YK, "Method for random vibration of hysteretic system," *ASCE Journal of the*

Engineering Mechanics Division, 102(2), 249-263, 1976.

Winkler RL, *An Introduction to Bayesian inference and decision*, Probabilistic Publishing, 2nd edition, 2003.

Yang JN, Li Z and Vongchavalitkul S, "Stochastic hybrid control of hysteretic structures," *Probabilistic Engineering Mechanics*, 9(1-2), 125-133, 1994.

Table 1: Properties of 2-DOF coupled model

	m (kg)	k (N/m)	f (Hz)	α	u_y (m)	ξ	μ
Primary	32.2e3	1e7	3.1	-	-	0.05	-
Secondary	32.2	12,216	2.8	0.1	0.06	0.02	2

Table 2: Properties of 2-DOF coupled models for simulation

Primary (m_p = 32.2e3 kg, ξ_p = 0.05)	Secondary (m_s = 32.2 kg)				
f_p (Hz)	f_s (Hz)	α	u_y (m)	ξ_s	μ
2.4	0.5	0.05	0.01	0.02	2
3.0	1.0	0.10	0.06	0.05	3
3.6	1.4	0.15	0.12		5
	2.0				
	2.4				
	2.8				
	3.0				
	3.2				
	3.7				
	5.0				
	7.0				
	9.0				
	18.0				
Total number of coupled system: 3 x 13 x 3 x 3 x 2 x 3 = 2,106 systems					

Table 3: Properties of primary SDOF- secondary SDOF coupled models

	m (kg)	k (N/m)	f (Hz)	α	u_y (m)	ξ	μ
Primary	32.2e3	1.14e7	3	-	-	0.05	-
Secondary	32.2e	715 1.14e4 2.57e4	0.75 3 4.5	0.1	0.06	0.02 0.05	2 3 5

Table 4: Median value and log-standard deviation of seismic fragility curve for secondary system of primary SDOF – secondary SDOF coupled system using ELS only, ELS & Bayesian updating, and Nonlinear analysis approach in (a) ξ_s = 0.02 and (b) ξ_s = 0.05

(a) ξ_s = 0.02

		[η = -0.2]		[η = 0]		[η = 0.6]	
		c	β	c	β	c	β
[μ=2]	ELS only	1.326	0.296	0.704	0.456	0.295	0.663
	ELS & Bayesian	1.385	0.321	0.727	0.313	-	-
	Nonlinear	1.399	0.325	0.729	0.325	0.361	0.597
[μ=3]	ELS only	1.761	0.292	1.172	0.440	0.452	0.682
	ELS & Bayesian	1.785	0.327	1.207	0.323	-	-
	Nonlinear	1.796	0.333	1.189	0.329	0.538	0.601
[μ=5]	ELS only	2.541	0.255	2.070	0.453	0.847	0.661
	ELS & Bayesian	2.559	0.320	1.914	0.300	-	-
	Nonlinear	2.534	0.314	1.901	0.301	0.841	0.578

(b) ξ_s = 0.05

		[η = -0.2]		[η = 0]		[η = 0.6]	
		c	β	c	β	c	β
[μ=2]	ELS only	1.382	0.309	0.699	0.429	0.372	0.622
	ELS & Bayesian	1.554	0.322	0.813	0.315	-	-
	Nonlinear	1.554	0.327	0.808	0.321	0.394	0.589
[μ=3]	ELS only	1.758	0.318	1.191	0.405	0.590	0.556
	ELS & Bayesian	2.013	0.334	1.317	0.305	-	-
	Nonlinear	2.014	0.332	1.277	0.299	0.593	0.564
[μ=5]	ELS only	2.537	0.268	2.041	0.418	1.017	0.622
	ELS & Bayesian	2.811	0.296	2.125	0.278	-	-
	Nonlinear	2.799	0.274	2.101	0.256	0.934	0.551

Table 5: Properties of primary MDOF- secondary SDOF coupled models

		Level/Mode							
		1	2	3	4	5	6	7	8
Primary MDOF	m_i (e5 kg)	13.60	13.60	13.60	13.6	3.34	3.34	3.34	3.34
	k_i (e9 N/m)	13.40	13.40	13.40	13.40	3.34	3.34	3.34	3.34
	f_{pi} (Hz)	4	7.3	14.8	17.5	23.8	25.4	29.8	30.2
Secondary SDOF	m_{s1} (kg)	633							
	k_{s1} (e5 N/m)	0.25 4.0 9.0							
	f_{s1} (Hz)	1 4 6							

Table 6: Median value and log-standard deviation of seismic fragility curve for secondary system of primary MDOF – secondary SDOF coupled system using ELS only, ELS & Bayesian updating, and Nonlinear analysis approach in (a) $\xi_s = 0.02$ and (b) $\xi_s = 0.05$

(a) $\xi_s = 0.02$

		[η = -0.2]		[η = 0]		[η = 0.6]	
		c	β	c	β	c	β
[μ=2]	ELS only	2.790	0.283	1.423	0.489	0.403	0.649
	ELS & Bayesian	2.887	0.296	1.349	0.290	-	-
	Nonlinear	2.864	0.291	1.354	0.275	0.492	0.606
[μ=3]	ELS only	3.586	0.263	2.246	0.4452	0.644	0.607
	ELS & Bayesian	3.349	0.221	2.072	0.269	-	-
	Nonlinear	3.351	0.226	2.088	0.236	0.737	0.624
[μ=5]	ELS only	-	-	3.517	0.343	1.135	0.614
	ELS & Bayesian	-	-	3.221	0.192	-	-
	Nonlinear	-	-	3.166	0.171	1.136	0.619

(b) $\xi_s = 0.05$

		[η = -0.2]		[η = 0]		[η = 0.6]	
		c	β	c	β	c	β
[μ=2]	ELS only	2.876	0.318	1.510	0.429	0.525	0.575
	ELS & Bayesian	3.035	0.262	1.492	0.273	-	-
	Nonlinear	3.008	0.257	1.514	0.262	0.544	0.548
[μ=3]	ELS only	3.637	0.288	2.344	0.376	0.775	0.576
	ELS & Bayesian	3.468	0.174	2.271	0.247	-	-
	Nonlinear	3.435	0.167	2.263	0.228	0.779	0.616
[μ=5]	ELS only	-	-	3.710	0.274	1.340	0.592
	ELS & Bayesian	-	-	3.387	0.154	-	-
	Nonlinear	-	-	3.388	0.155	1.209	0.592

Table 7: Properties of primary MDOF- secondary MDOF coupled models

		Level/Mode							
		1	2	3	4	5	6	7	8
Primary MDOF	m_i (e5 kg)	13.60	13.60	13.60	13.6	3.34	3.34	3.34	3.34
	k_i (e9 N/m)	13.40	13.40	13.40	13.40	3.34	3.34	3.34	3.34
	f_{pi} (Hz)	4	7.3	14.8	17.5	23.8	25.4	29.8	30.2
Secondary SDOF	m_{si} (kg)	316	316						
	k_{si} (e5 N/m)	0.33 5.23 11.8	0.33 5.23 11.8						
	f_{si} (Hz)	1 4 6	2.6 10.5 15.7						

Table 8: Median value and log-standard deviation of seismic fragility curve for secondary system of primary MDOF – secondary MDOF coupled system using ELS only, ELS & Bayesian updating, and Nonlinear analysis approach in (a) $\xi_s = 0.02$ and (b) $\xi_s = 0.05$

(a) $\xi_s = 0.02$

		[η = -0.2]		[η = 0]		[η = 0.6]	
		c	β	c	β	c	β
[μ=2]	ELS only	3.537	0.262	1.619	0.489	0.519	0.561
	ELS & Bayesian	3.455	0.250	1.489	0.288	-	-
	Nonlinear	3.455	0.250	1.484	0.295	0.525	0.546
[μ=3]	ELS only	3.825	0.141	2.583	0.477	0.767	0.594
	ELS & Bayesian	3.691	0.165	2.294	0.247	-	-
	Nonlinear	3.630	0.157	2.261	0.244	0.801	0.588
[μ=5]	ELS	-	-	3.782	0.323	1.299	0.576
	ELS & Bayesian	-	-	3.449	0.161	-	-
	Nonlinear	-	-	3.376	0.145	1.244	0.581

(b) $\xi_s = 0.05$

		[η = -0.2]		[η = 0]		[η = 0.6]	
		c	β	c	β	c	β
[μ=2]	ELS only	3.565	0.266	1.599	0.441	0.606	0.546
	ELS & Bayesian	3.475	0.204	1.610	0.273	-	-
	Nonlinear	3.450	0.206	1.605	0.286	0.589	0.562
[μ=3]	ELS only	3.701	0.179	2.527	0.412	0.918	0.558
	ELS & Bayesian	3.889	0.150	2.406	0.250	-	-
	Nonlinear	3.800	0.150	2.397	0.240	0.833	0.608
[μ=5]	ELS only	-	-	3.713	0.283	1.605	0.536
	ELS & Bayesian	-	-	3.673	0.161	-	-
	Nonlinear	-	-	3.493	0.130	1.317	0.595

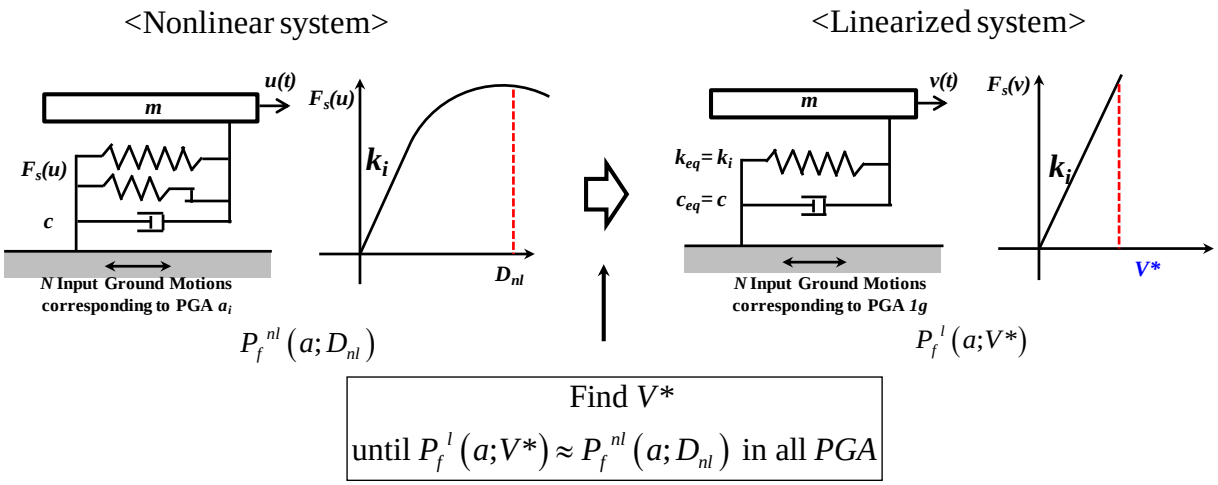

Fig. 1. ELS concept

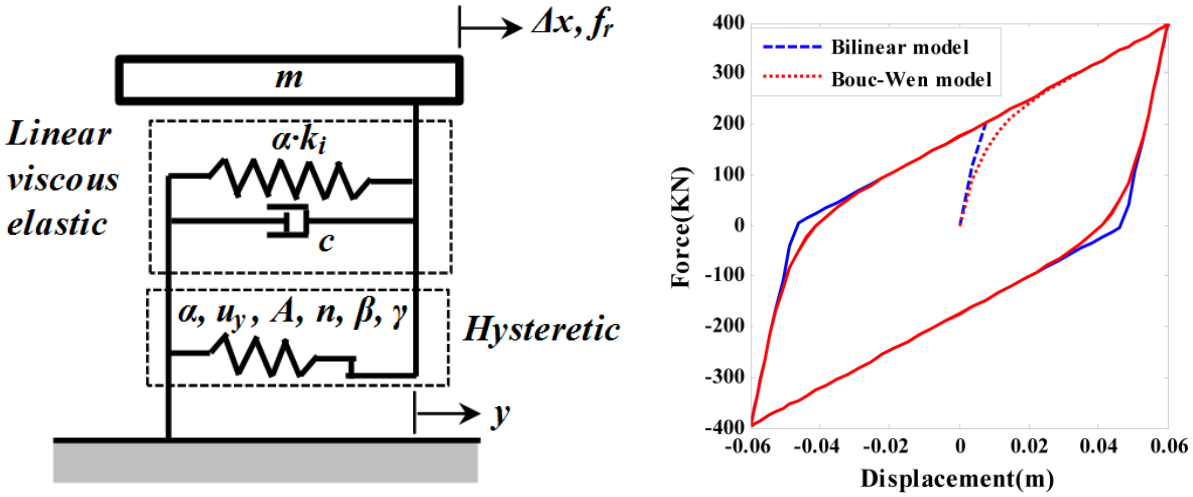

Fig. 2. Bouc-Wen hysteretic model

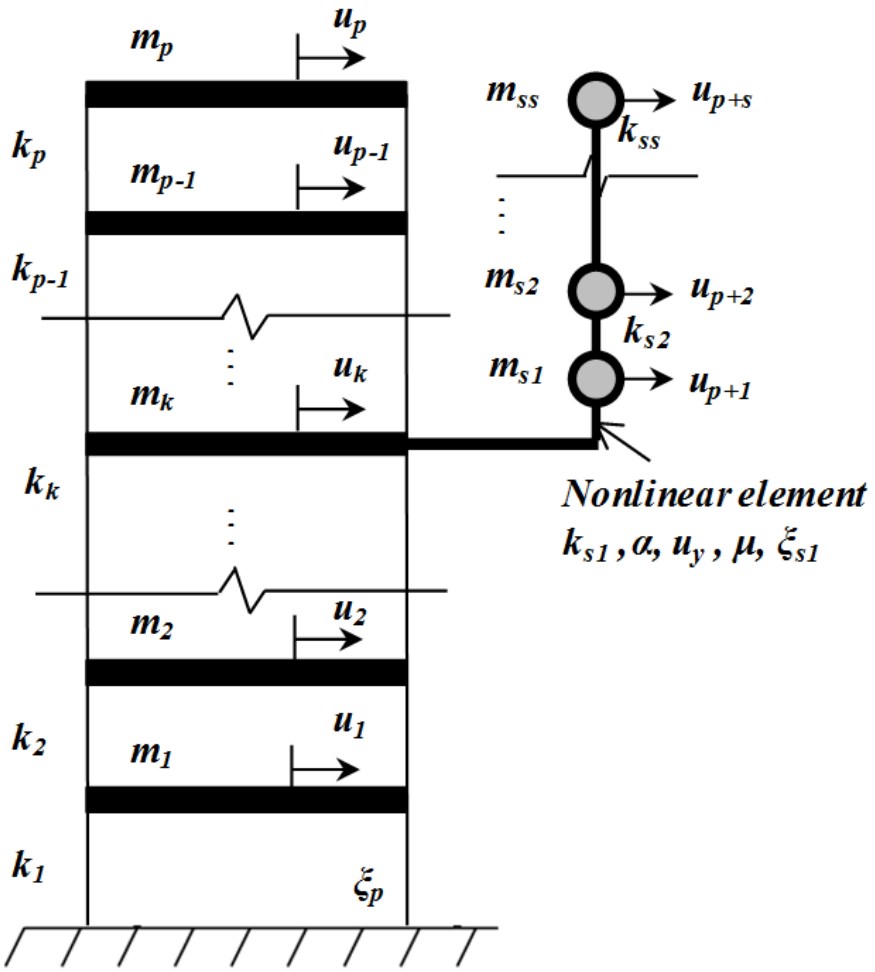

Fig. 3. $m(=p+s)$-DOF coupled system

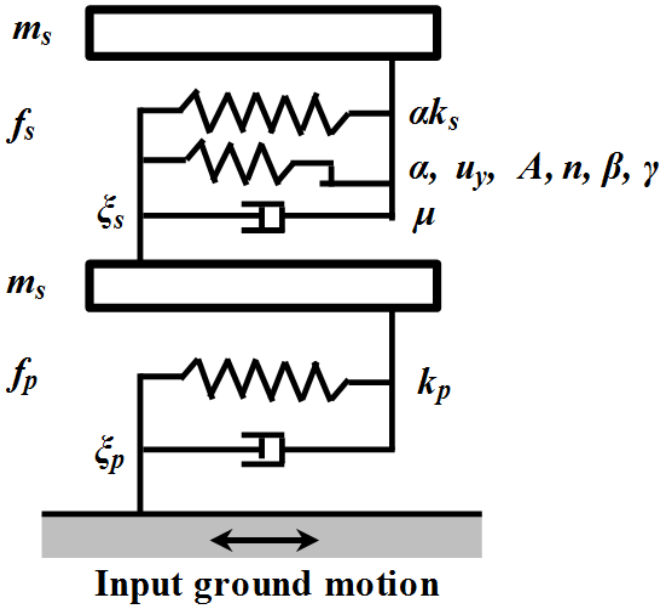

Fig. 4. Configuration and properties of 2-DOF coupled system

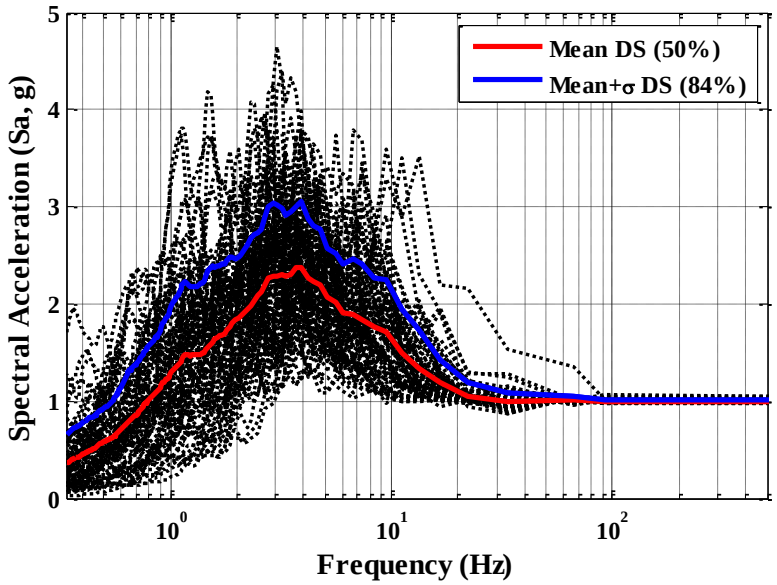

Fig. 5. Response spectra of the 5%-damped linear-elastic SDOF model under input ground motions normalized to 1.0g

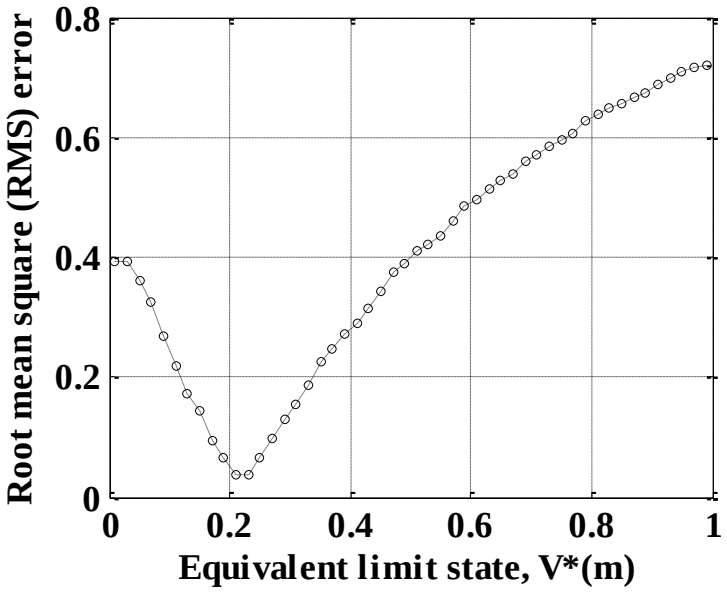

Fig. 6. RMS error between seismic fragility of linear and nonlinear system according to ELS *V**

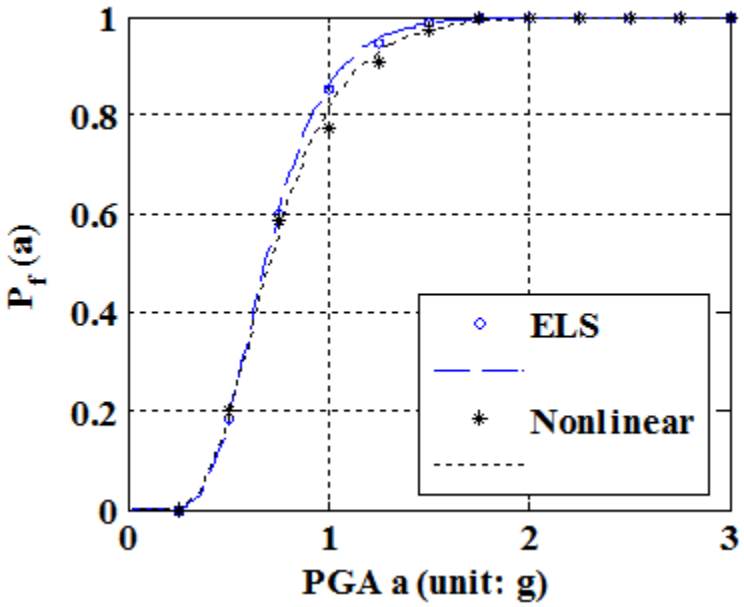

Fig. 7. Comparison between seismic fragility of nonlinear system and linear system using ELS *V**

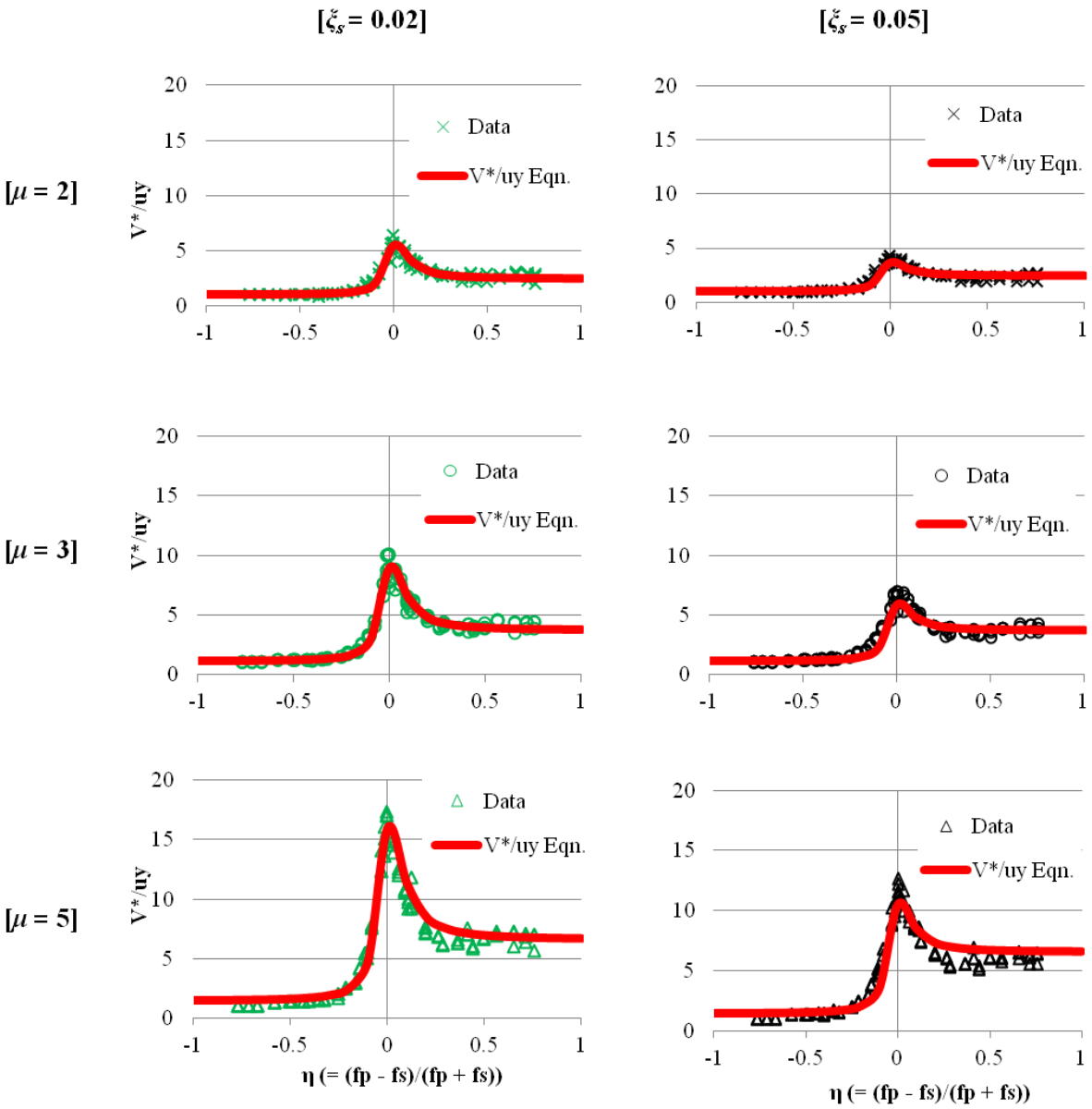

Fig. 8. Simulation data and ELS V* equation

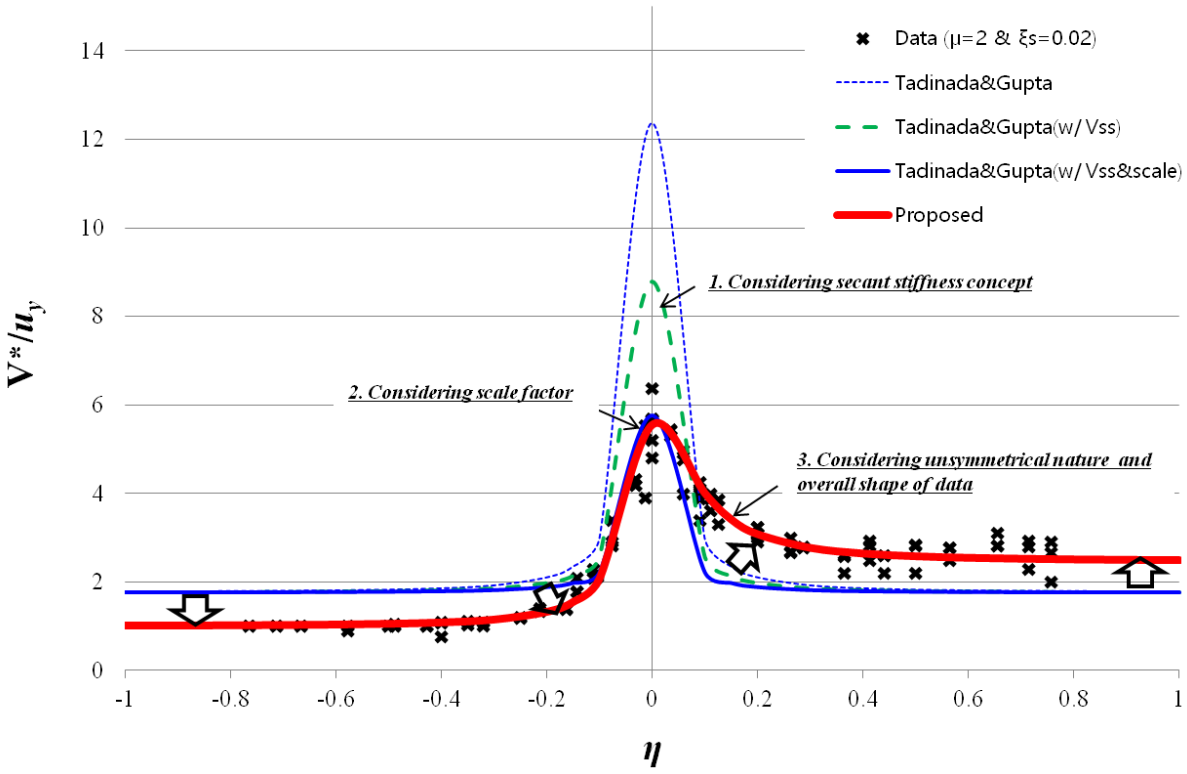

Fig. 9. ELS *V** curve using the equation of Tadinada and Gupta (2016) and the proposed equation by this study (μ = 2 and ξ_s = 0.02)

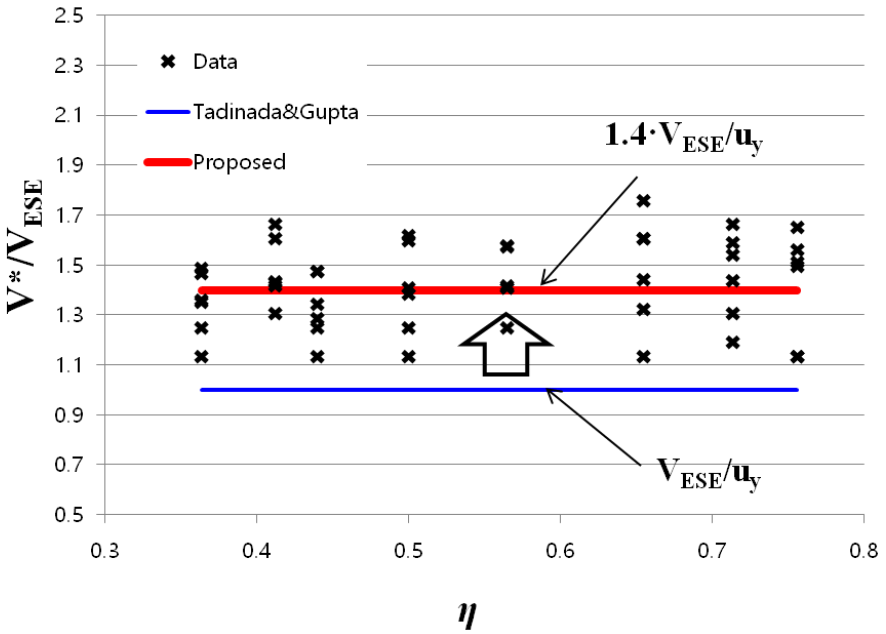

(a) $\eta \geq 0$

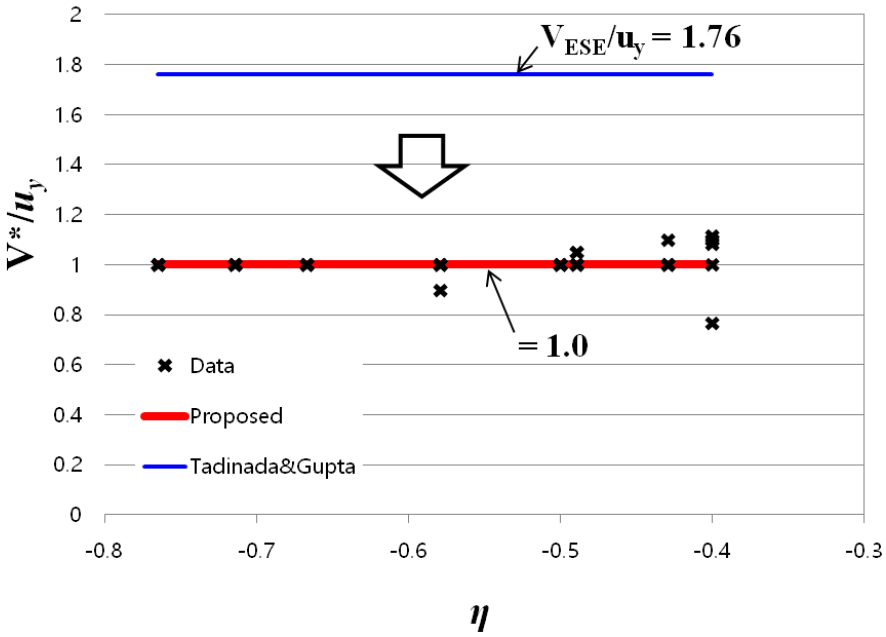

(b) $\eta < 0$

Fig. 10. Asymptotic lines for ELS V^* at $\eta \geq 0$ and $\eta < 0$

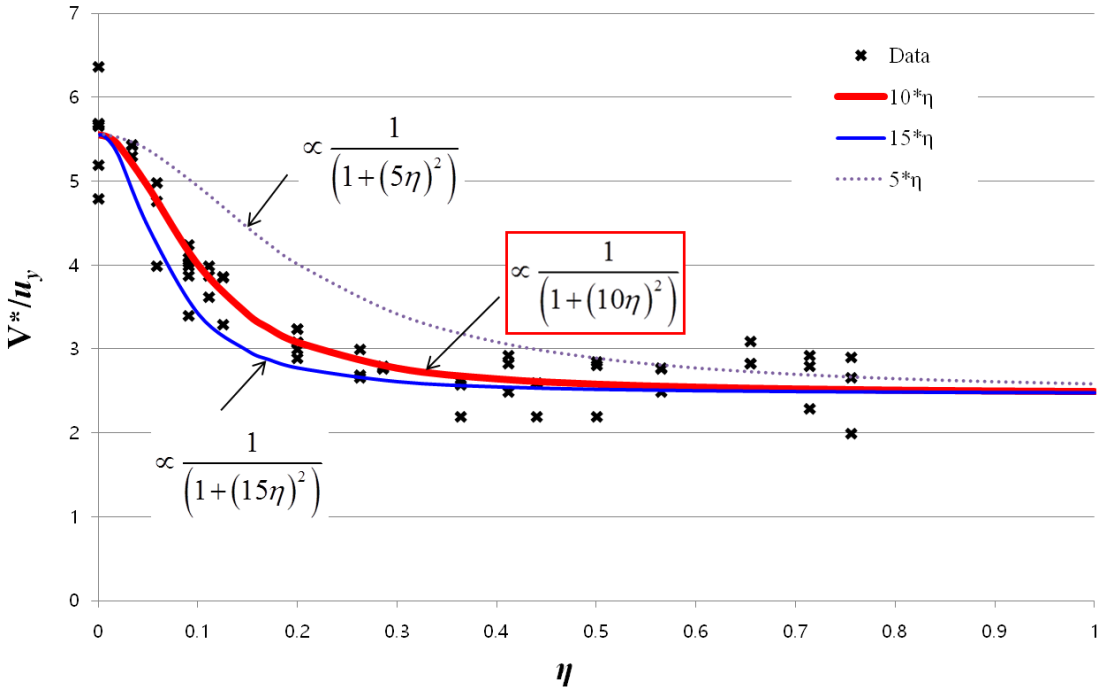

(a) $\eta \geq 0$

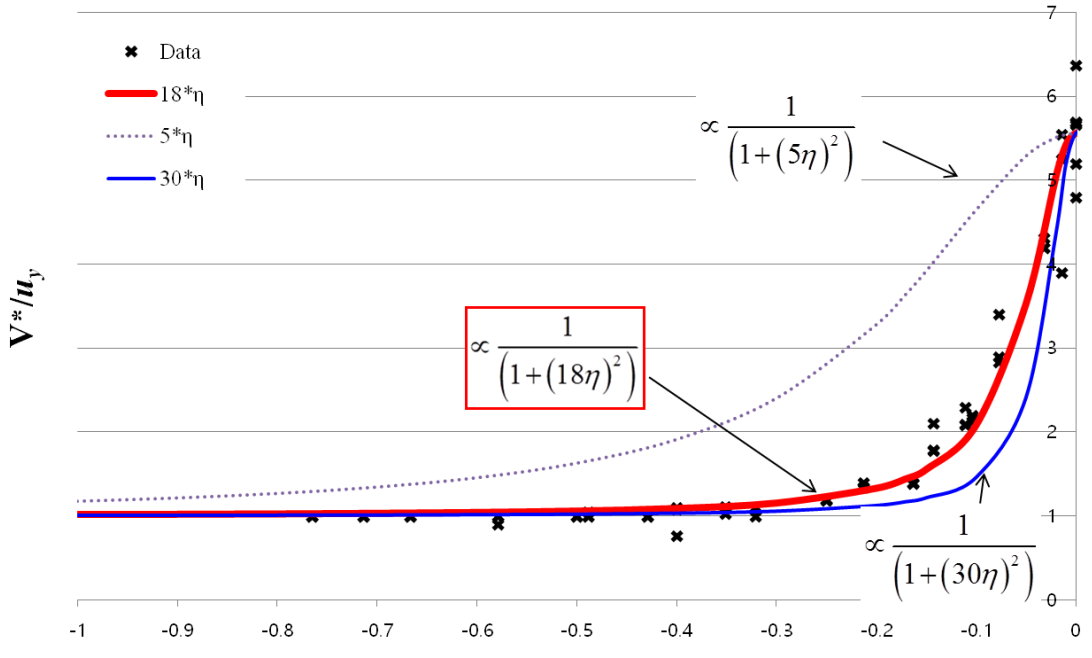

(b) $\eta < 0$

Fig. 11. Curve shapes for ELS V* according to the change of η

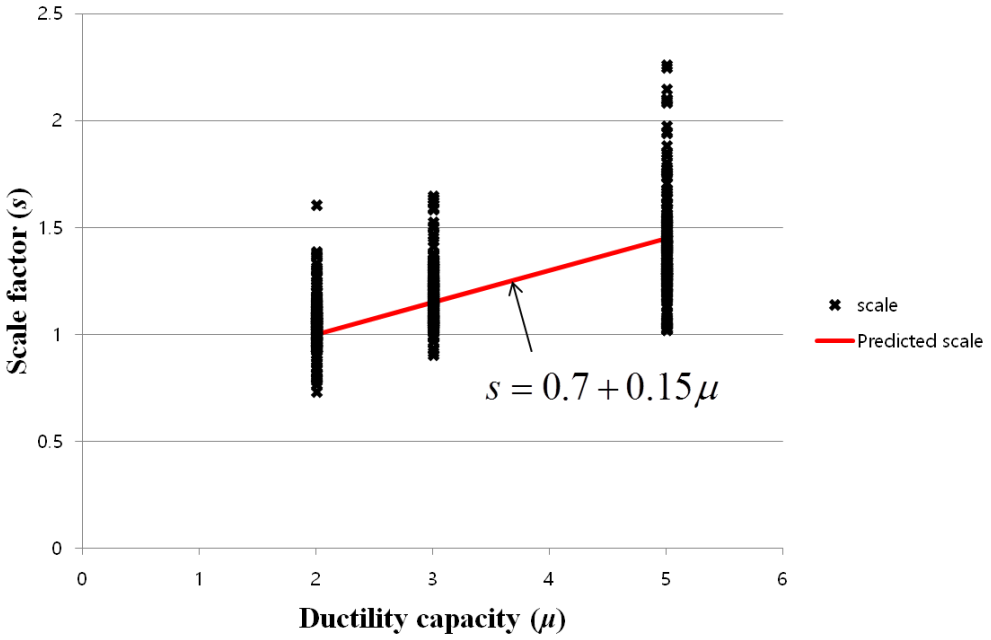

Fig. 12. Relation between ductility capacity and scale factor

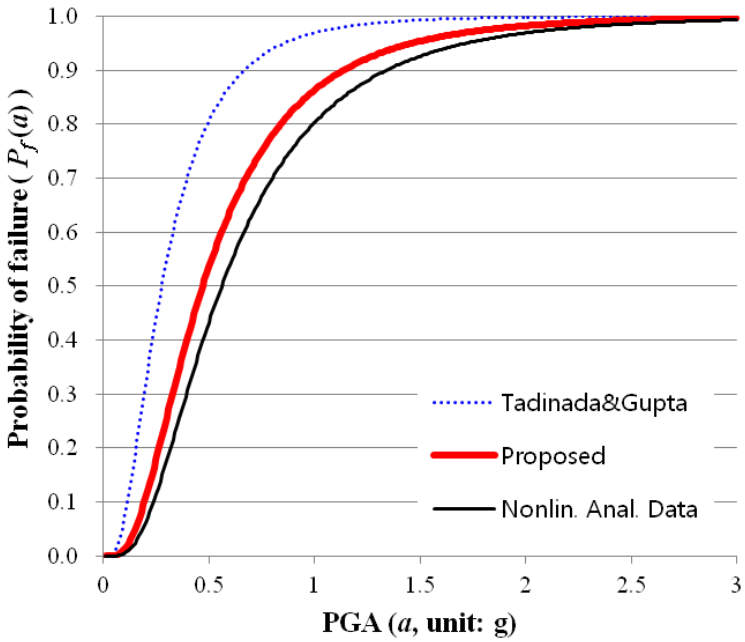

Fig. 13. Comparison of fragility curves using the equation of Tadinada and Gupta (2016) and the proposed equation by this study (μ = 3, ξ_s = 0.02, η = 0.6)

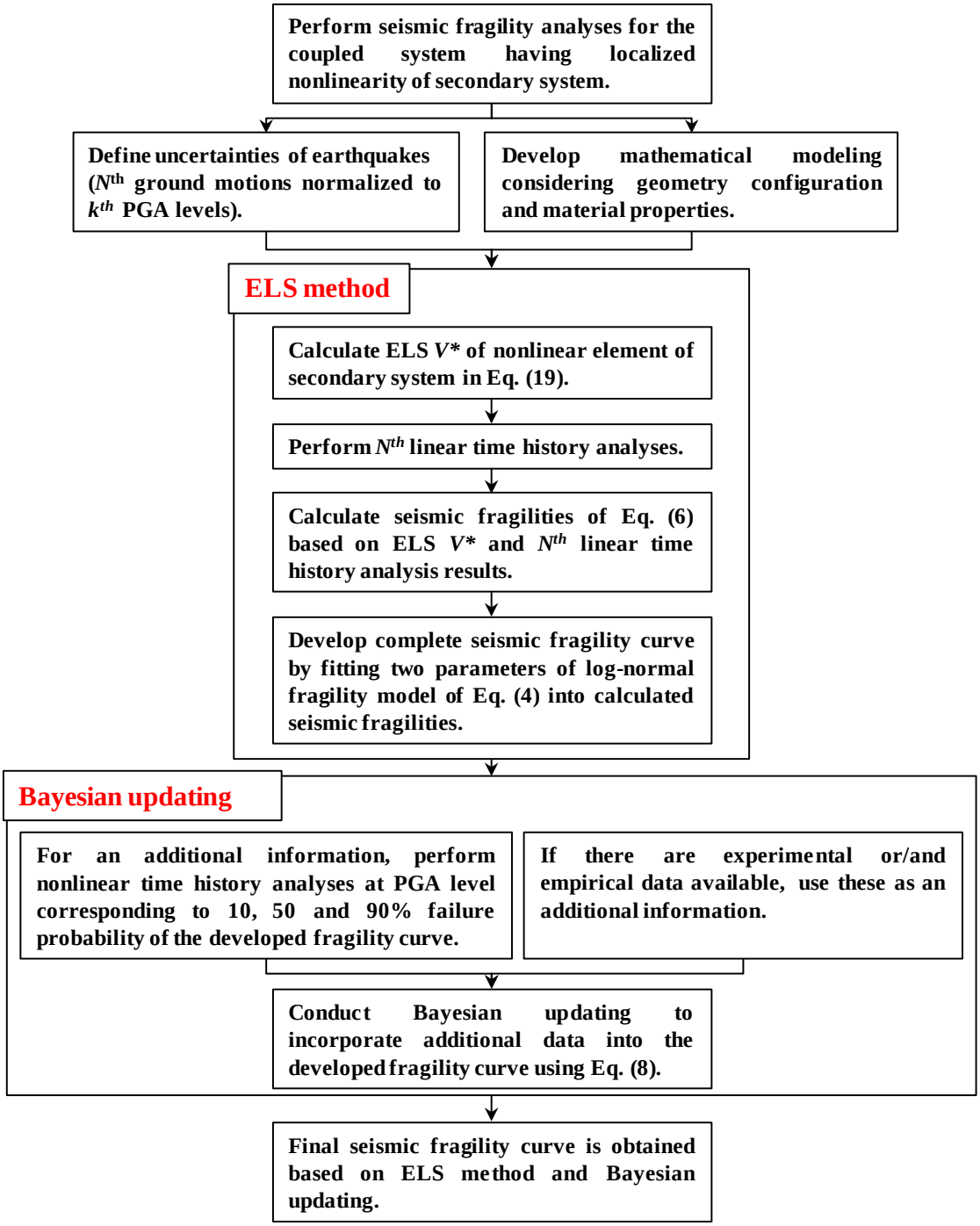

Fig. 14. Comprehensive procedure of seismic fragility analysis of the secondary system of coupled system using ELS method and Bayesian updating

	[η = -0.2]	[η = 0]	[η = 0.6]
[μ=2]	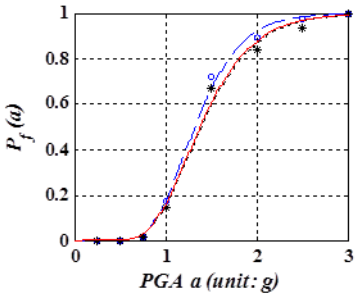 ELS V^* = 1.28 $\cdot u_y$	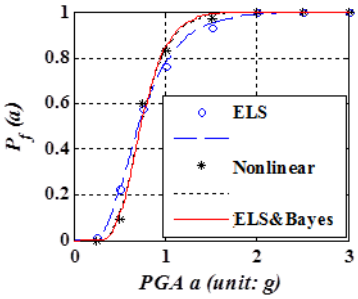 ELS V^* = 5.55 $\cdot u_y$	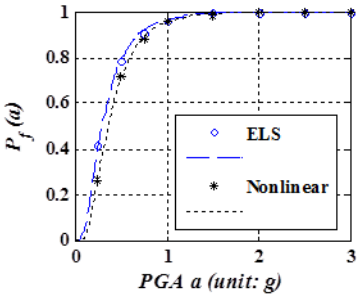 ELS V^* = 2.55 $\cdot u_y$
[μ=3]	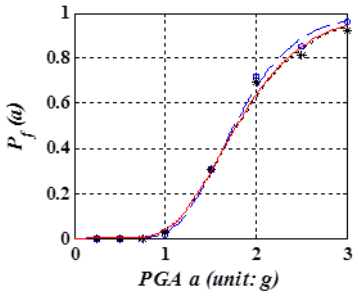 ELS V^* = 1.69 $\cdot u_y$	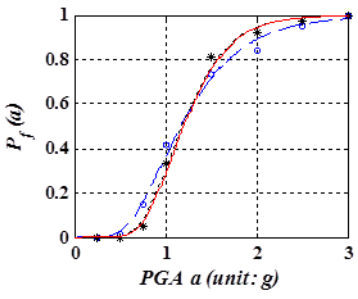 ELS V^* = 8.97 $\cdot u_y$	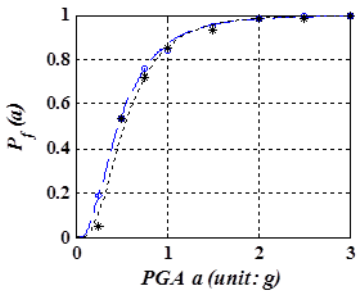 ELS V^* = 3.88 $\cdot u_y$
[μ=5]	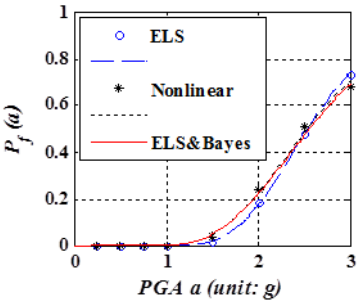 ELS V^* = 2.52 $\cdot u_y$	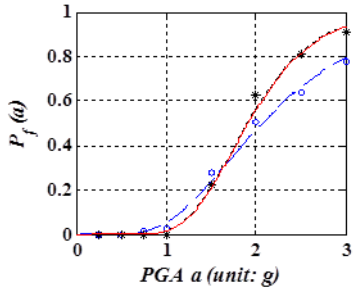 ELS V^* = 16 $\cdot u_y$	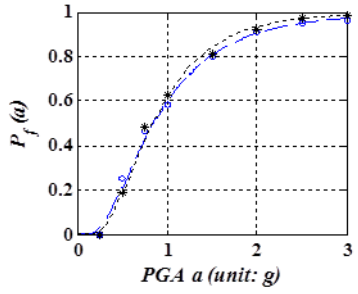 ELS V^* = 6.87 $\cdot u_y$

(a) ξ_s = 0.02

(Continued)

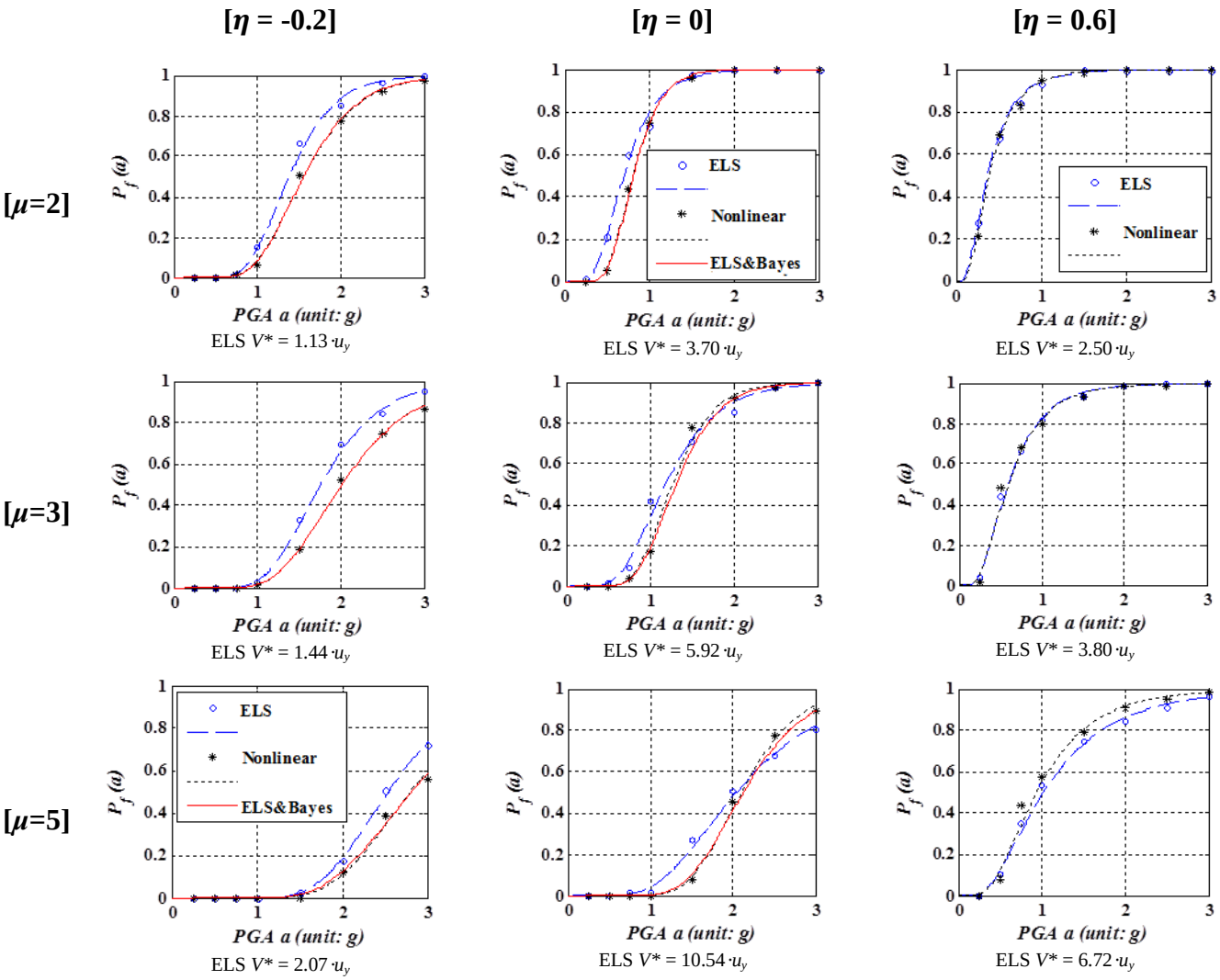

Fig. 15. Seismic fragility curve for secondary system of primary SDOF - secondary SDOF coupled system using ELS only, ELS & Bayesian updating, and Nonlinear analysis approach in (a) ξ_s = 0.02 and (b) ξ_s = 0.05

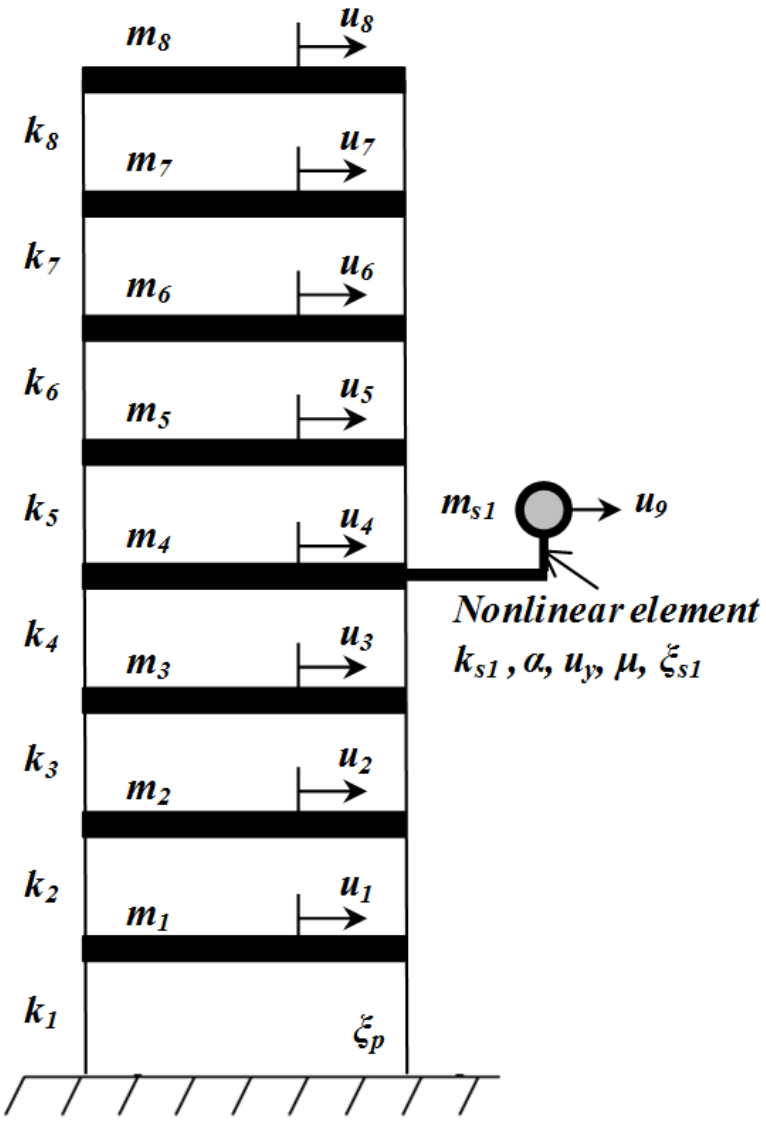

Fig. 16. Primary MDOF- secondary SDOF coupled model

	[η = -0.2]	[η = 0]	[η = 0.6]
[μ=2]	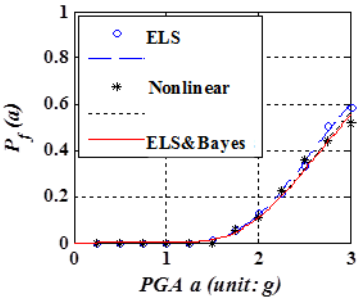 ELS V^* = 1.28 $\cdot u_y$	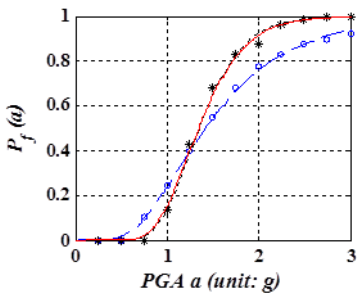 ELS V^* = 5.55 $\cdot u_y$	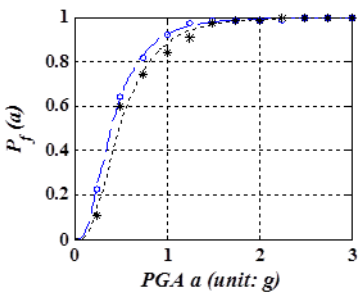 ELS V^* = 2.55 $\cdot u_y$
[μ=3]	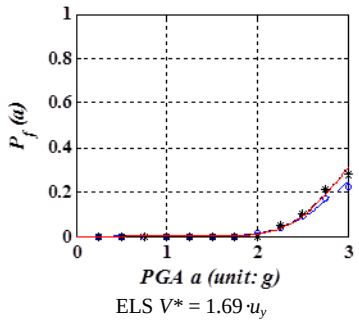 ELS V^* = 1.69 $\cdot u_y$	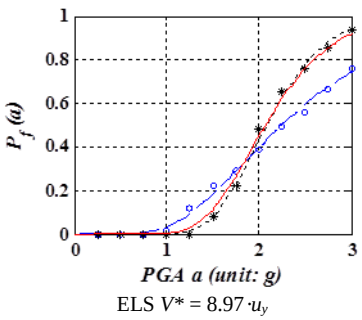 ELS V^* = 8.97 $\cdot u_y$	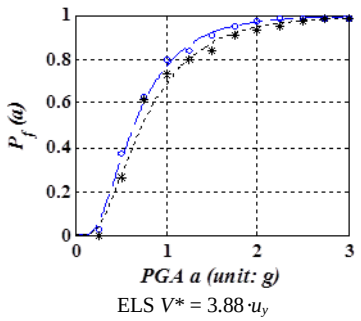 ELS V^* = 3.88 $\cdot u_y$
[μ=5]	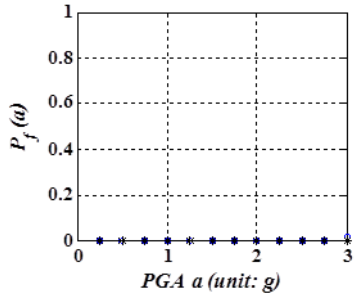 ELS V^* = 2.52 $\cdot u_y$	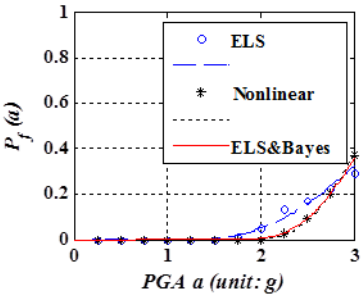 ELS V^* = 16 $\cdot u_y$	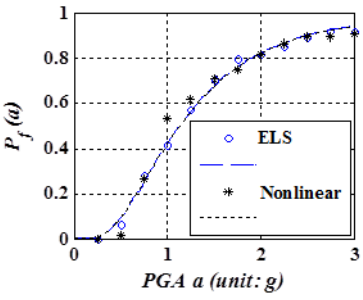 ELS V^* = 6.87 $\cdot u_y$

(a) ξ_s = 0.02

(Continued)

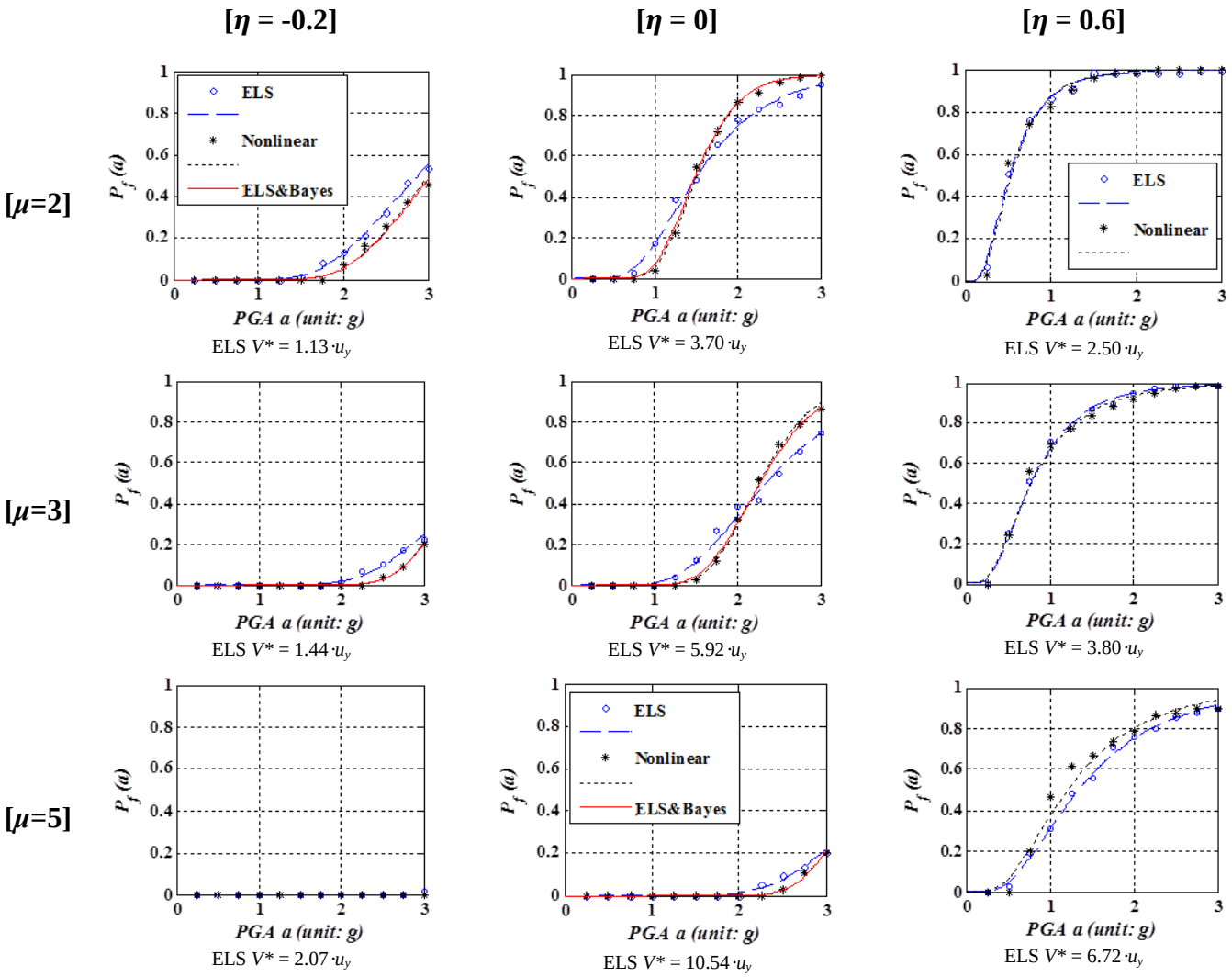

(b) ξ_s = 0.05

Fig. 17. Seismic fragility curve for secondary system of primary MDOF – secondary SDOF coupled system using ELS only, ELS & Bayesian updating, and Nonlinear analysis approach in (a) ξ_s = 0.02 and (b) ξ_s = 0.05

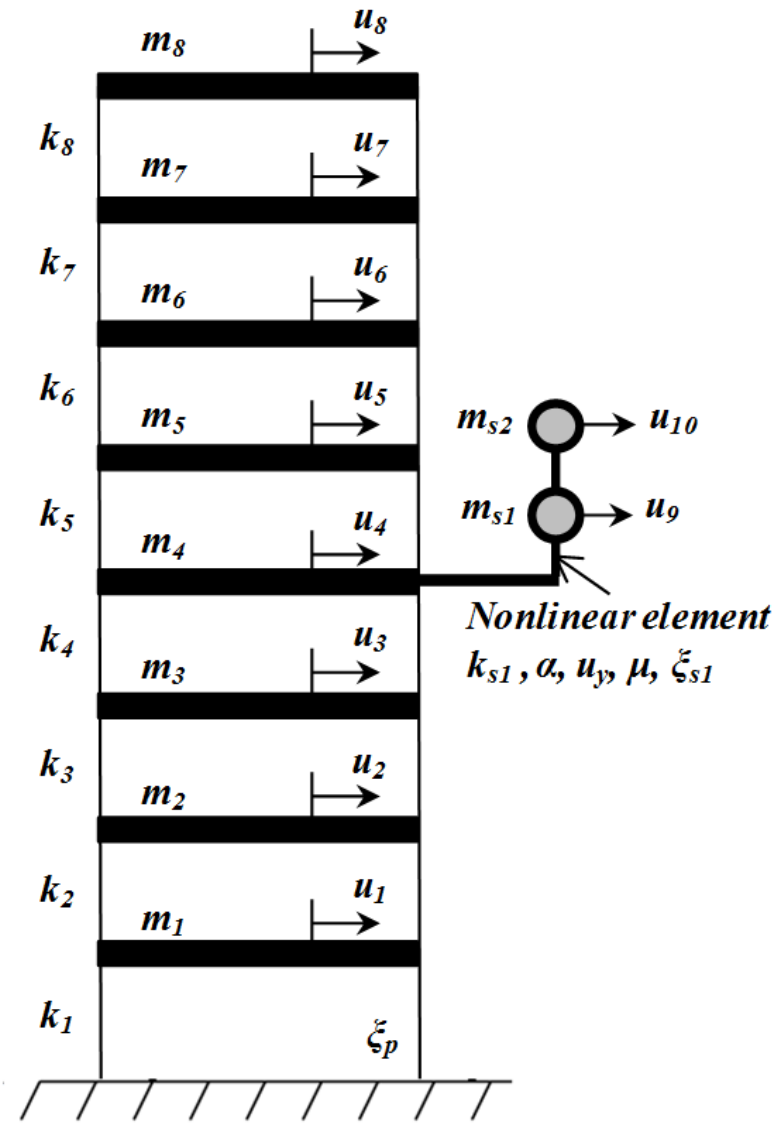

Fig. 18. Primary MDOF- secondary MDOF coupled models

	[η = -0.2]	[η = 0]	[η = 0.6]
[μ=2]	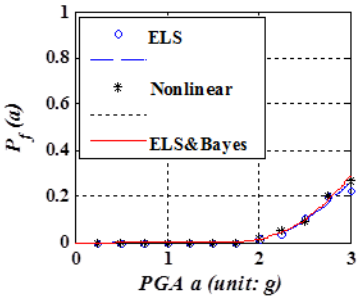 ELS $V^* = 1.28 \cdot u_y$	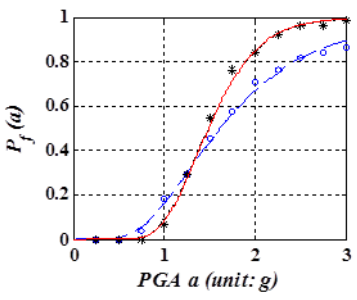 ELS $V^* = 5.55 \cdot u_y$	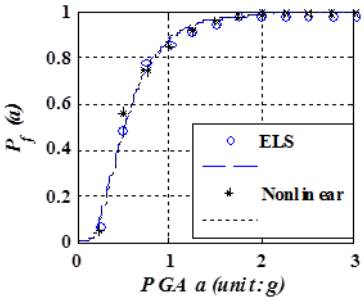 ELS $V^* = 2.55 \cdot u_y$
[μ=3]	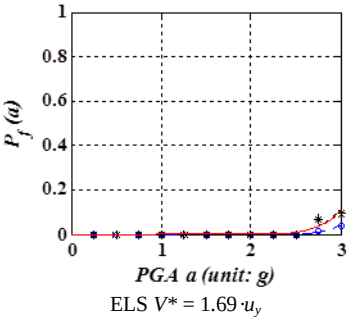 ELS $V^* = 1.69 \cdot u_y$	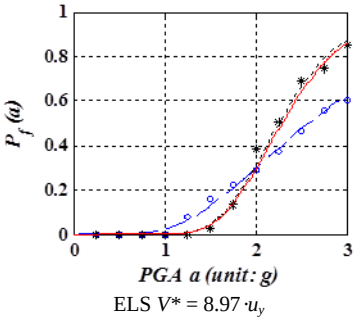 ELS $V^* = 8.97 \cdot u_y$	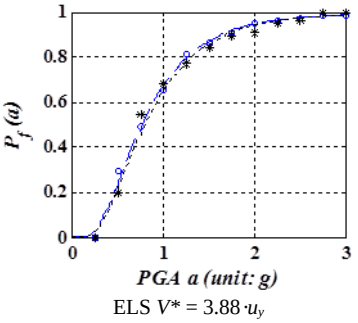 ELS $V^* = 3.88 \cdot u_y$
[μ=5]	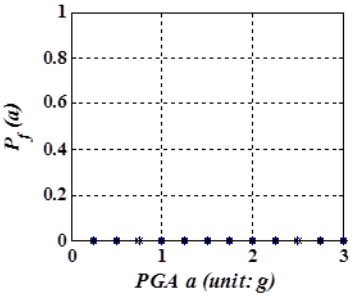 ELS $V^* = 2.52 \cdot u_y$	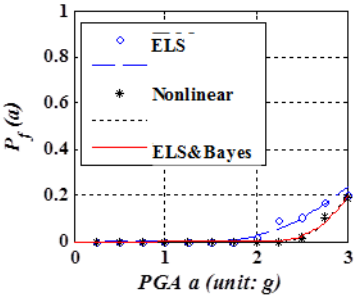 ELS $V^* = 16 \cdot u_y$	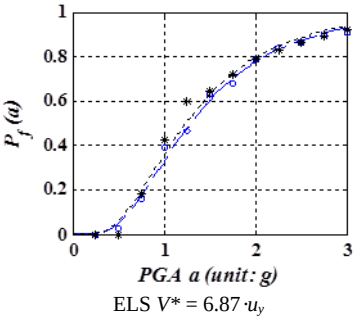 ELS $V^* = 6.87 \cdot u_y$

(a) ξ_s = 0.02

(Continued)

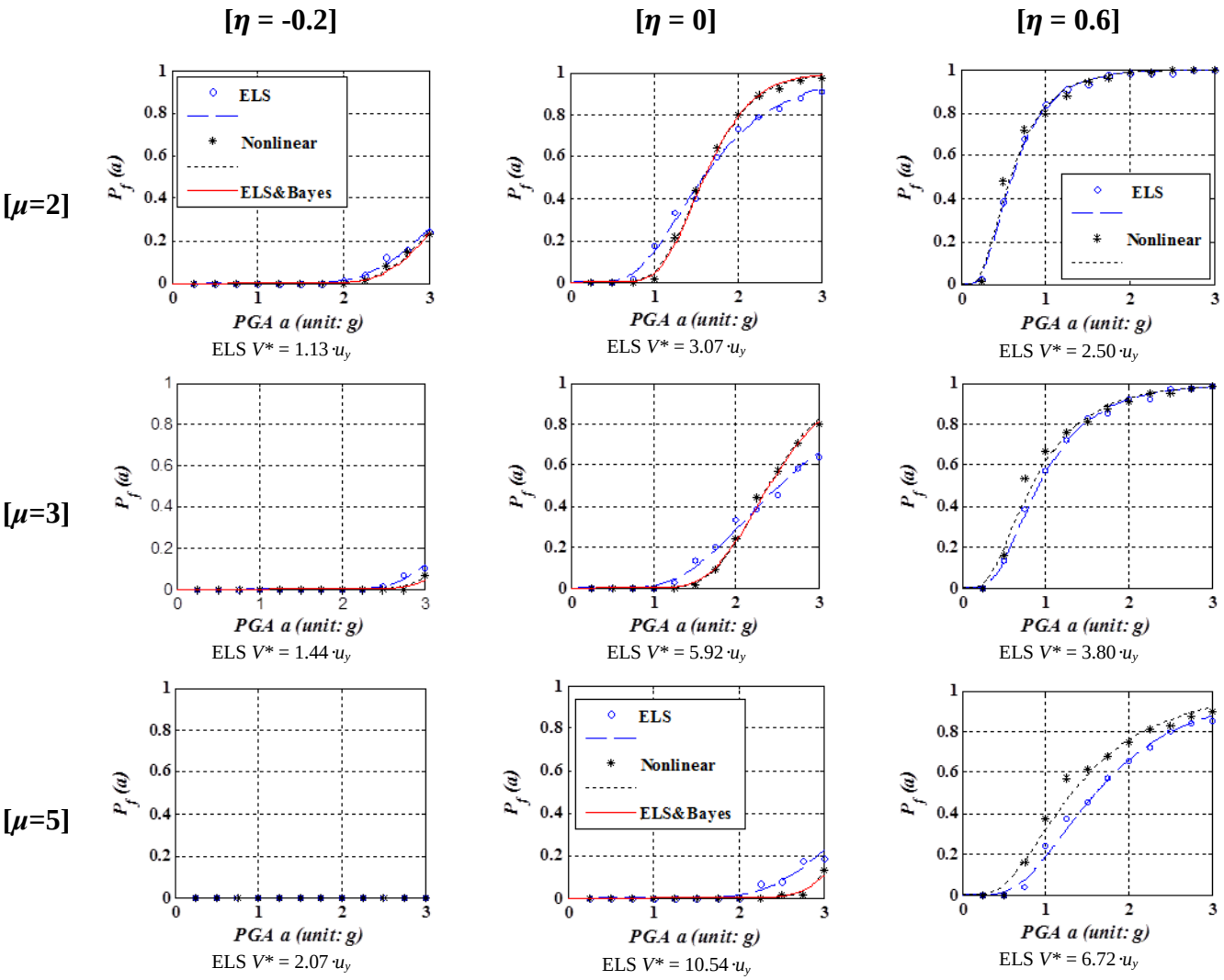

Fig. 19. Seismic fragility curve for secondary system of primary MDOF – secondary MDOF coupled system using ELS only, ELS & Bayesian updating, and Nonlinear analysis approach in (a) ξ_s = 0.02 and (b) ξ_s = 0.05

PART V

SIGNIFICANCE OF MULTI-HAZARD RISK IN DESIGN OF BUILDINGS UNDER EARTHQUAKE AND WIND LOADS

Shinyoung Kwag, Abhinav Gupta and John Baugh

ABSTRACT

Traditionally, external hazards are considered in the design of a building through the various combinations of loads prescribed in relevant design codes and standards. It is often the case that the design is governed by a single dominant hazard at a given geographic location. This is particularly true for earthquake and wind hazards, both of which impart time-dependent dynamic loads on the structure. Engineers may nevertheless wonder if a building designed for one of the two dominant hazards will satisfactorily withstand the other. Prior studies have indicated that in some cases, when a building is designed for a single dominant hazard, it does not necessarily provide satisfactory performance against the other hazard. In this paper, we propose a novel framework that builds upon performance-based design requirements and determines whether the design of a building is governed primarily by a single hazard or multiple hazards. It integrates site-dependent hazard characteristics with the performance criteria for a given building type and building geometry. The framework is consistent with the burgeoning area of probabilistic risk assessment, and yet can easily be extended to traditional, deterministically characterized design requirements as illustrated herein.

1. Introduction

Design and retrofit approaches for multi-hazard scenarios have received considerable attention in recent years. However, the concept of multi-hazard analysis is quite broad and the nature of existing studies varies across a wide spectrum of problems. In some cases, the focus is on hazards that either occur simultaneously or are closely correlated with one another, such as flooding and fires that are induced by the same seismic event. In other cases, multi-hazard studies relate to hazards that are not dependent or correlated but have a strong likelihood of occurrence at different points in the lifetime of a structure. Design and retrofit assessments for earthquake and extreme wind hazards fall within the latter category.

In the specific case of earthquake and wind loads, design and retrofit solutions are traditionally governed by the requirements of appropriate codes and standards that have historically accounted for multiple hazards through the guidance provided for load combinations. Since performance limit-states in the various codes and standards are the same for loads corresponding to different hazards, the final design is governed by only a single hazard that corresponds to higher loads. The basic premise is that each load combination attempts to account for a scenario that can occur simultaneously. In the United States, load combination requirements are prescribed by ASCE 7-05. More specifically, the two combinations involving earthquake and wind are (i) $1.2D + 1.0E + L + S$ and (ii) $1.2D + 1.6W + L + 0.5L_r$, respectively, where D = dead load, E = earthquake load, L = live load, S = snow load, L_r = roof live load, W = wind load. While it is quite evident that the load combination

for either earthquake or wind would dominate the design, recent studies have identified limitations of such an approach. Wen and Kang (2001) illustrate that, even if a single hazard (earthquake or wind) dominates the design loads, the less dominant hazard can contribute significantly to the overall design. Duthinh and Simiu (2009) and Crosti et al. (2010) additionally show that ASCE 7-05 requirements are not risk consistent. They illustrate that the overall risk for combined earthquake and wind loads in regions susceptible to both strong earthquakes and extreme winds can be more than twice that calculated by considering only a single dominant hazard. Consequently, these studies propose modifications to ASCE 7-05. Chen (2012) considers mid- to high-rise buildings in studying the inherent wind resistance of a building designed for earthquake loads as well as the inherent seismic resistance of a building designed for wind loads. The results indicate that certain solutions for ensuring safety against a single dominant hazard, such as wind, can create competing design objectives with respect to the other hazard, such as earthquake. Li et al. (2012) also show that design and retrofit strategies to improve a structure's performance for withstanding a single hazard can make the structure more vulnerable to other non-dominant hazards.

The fundamental basis for both earthquake and wind design is in finding the appropriate load path through the building and accounting for the dynamic nature of both loads. To do so, designers and engineers may ask if a building designed for one of the two hazards will also perform well for the other. AIA (1997) discusses this fundamental question and concludes that the answer is not necessarily so. The study observes that the true answer depends on a building's configuration height, load path for the given structural system, and

performance objectives. It also provides an interesting contrast between the two load cases, particularly in the ones calculated from building codes. In particular, earthquake loads calculated using the code provisions are shown to be much less than those typically exhibited during a major earthquake. Ductility of structural members and connections is utilized in the resistance of large earthquake loads, and is achieved through detailing requirements. In contrast, wind loads are much closer to the actual loads and wind pressures recorded at a geographic location, and there is no reliance on ductility. Consequently, a design in which inter-story drifts are governed by wind loads will not be able to provide sufficient ductility to withstand a large earthquake. This situation typically arises when buildings are located in regions with low-to-moderate seismicity and strong winds.

In a recent study, Unobe and Sorensen (2015) observe that different hazards can dominate performance in different limit states, addressing another aspect of the many possible multi-hazard scenarios. They illustrate that recurring moderate-to-high intensity winds can dominate performance with respect to fatigue, whereas the rare possibility of an earthquake during the lifetime of a structure can dominate the traditional design limit-states in shear, flexure, and/or drifts.

This trade-off between competing performance goals, such as those involving earthquakes and winds, has recently garnered considerable attention, and compels us to address multiple hazards in the assessment, design, construction, and retrofit of structures. However, there is in fact no framework available for the designer to determine whether the design of a particular building at a given site is governed by one or more hazards. In this

study, the development of such a framework is explored and a performance-based approach is proposed. The proposed approach makes use of (a) the site-dependent hazard intensity for a given site, (b) the building configuration/height, and (c) performance criteria that govern the design of the building for each individual hazard. The resulting framework can also be used to determine whether a particular building structure requires any retrofitting, especially in cases where both earthquake and wind hazards govern the design and performance of a building whose initial design may not have accounted for them as such. Here, we demonstrate the merits of the proposed framework through an application in which retrofit solutions are examined for two mid- to high-rise buildings located in close proximity to one another, as in a tight urban setting. Results of the analysis show that retrofit solutions differ significantly when evaluated under a multi-hazard scenario.

2. Performance Characterization

Structural performance is assessed through the use of limit states, which are characterized by design and serviceability thresholds, and limit states are expressed by performance functions, which can be described in the following form:

$$Z = g\left(L, R\right) = L - R \tag{1}$$

where L denotes the performance limit (capacity) of the structure and R represents response (demand) on the structure at a given hazard intensity measure. In general,

$$Z = g(X_1, X_2, ..., X_n) \tag{2}$$

where X_n represents probabilistically defined variables for the loads and the strength. The performance function g is a limit-state function that characterizes the failure criterion as:

$$\begin{aligned} g(-) < 0 &: \text{ Failure state} \\ g(-) = 0 &: \text{ Limit state} \\ g(-) > 0 &: \text{ Survival state} \end{aligned} \tag{3}$$

Performance functions are used to determine the safe or failure states from either a deterministic or probabilistic perspective. The probability of failure P_f is then given by the joint probability distribution of X_n's:

$$P_f = \int_{g(-)<0} ... \int f_{X_1, X_2, X_3, ..., X_n}(x_1, x_2 x_3 ..., x_n) dx_1, dx_2, dx_3 .... dx_n \tag{4}$$

where, $f_{X_1, X_2, X_3, ..., X_n}(x_1, x_2, x_3, ..., x_n)$ is the joint probability density function of the random variables.

The performance-based framework we propose is developed for a probabilistic characterization of the performance function, as above. However, limit states are often prescribed deterministically by codes and standards to ensure a minimum level of reliability in the design. Designers evaluate the demand for increasing values of the intensity measure and subsequently determine the value at which Eq. (1) becomes negative for a given capacity, again, as prescribed by relevant codes and standards. As a result, we extend the proposed

framework so that it accommodates deterministically characterized performance criteria. It must be noted that different measures are used to quantify the intensity of different hazards, leading to a completely independent characterization of Eq. (1) for different hazards, which cannot be directly compared or combined.

In general, multiple performance limit states exist and are examined in the design of a structure. Yet in most cases, the design is governed by a single performance limit state. Specifically, the performance of the building structure subjected to earthquake loading is typically governed by potentially excessive inter-story drift (characterizing the safety against side-sway collapse). ASCE 7-10 and IBC 2012 building codes specify the limit state for inter-story drift to be 1.5 % of the story height. Unlike for earthquakes, the design for high wind loading is not governed by the collapse of a building. Instead, it is typically governed by appropriate performance with respect to excessive vibrations, which is characterized in terms of the corresponding serviceability limit state. Tallin and Ellingwood (1985) state that the threshold of perception and annoyance for the acceleration intensity is approximately 0.005 g (0.049 m/s^2) ~ 0.015 g (0.147 m/s^2), and the limit for psychological well-being and the ability to perform routine tasks is about 0.04 g (0.39 m/s^2). For convenience, these limit states are adopted in this study. In general, the two limit states may be expressed as

$$g_1(IM_e) = \mathrm{L_e} - \mathrm{R_e}(IM_e) \tag{5}$$

$$g_2\left(IM_w\right) = \mathrm{L_w} - \mathrm{R_w}\left(IM_w\right) \tag{6}$$

where g_1 is the performance function for earthquakes, which is characterized in terms of the intensity measure for earthquake loading (IM_e); g_2 is a performance function for winds, which is characterized in terms of intensity measure for wind loading (IM_w); Re is the maximum inter-story drift (demand) of the structure under earthquake excitation; L_e is the performance limit (capacity) for earthquake loading, i.e., 1.5% of story height; R_w is the maximum acceleration (demand) of the structure under wind excitation; L_w is the performance limit (capacity) for wind loading, i.e., 0.04g (0.39 m/s^2). Characterizing performance is obviously the essential first step in the development of a performance-based multi-hazard risk assessment framework.

3. Proposed Framework

The proposed framework combines performance functions with the different intensity measures for multiple hazards in a spatial representation that is subdivided into distinct regions. These graphically depicted regions can then be used to evaluate the significance of each hazard at a given site. Consequently, one of the regions will correspond to sites at which more than a single hazard contributes significantly to the structure's performance.

Fig. 1 shows the proposed graphical framework. As seen in this figure, the starting point is to develop curves of a structure's performance with respect to the intensity measures for each individual hazard. In a probabilistic risk-assessment framework, such curves give the variation of P_f as calculated in accordance with Eq. (4) for a given performance function with the intensity measure for the particular hazard; these are referred to as "fragility curves."

As seen in the figure, two fragility curves are plotted with respect to the intensity measures. One curve corresponds to performance function g_1 for earthquakes and the other to g_2 for winds. The feasibility of a design is governed by an acceptable level of risk (or probability of failure), denoted by P_f^{allow}. Such a characterization of the acceptance criterion allows for risk-consistent design among multiple hazards. Safe designs are characterized by $P_f < P_f^{allow}$, whereas failure is characterized by $P_f > P_f^{allow}$. Also as seen in Fig. 1, the two fragility curves and the definitions of P_f^{allow} for each hazard are used to develop a third (central) plot, which we refer to as *risk space,* and each axis in this plot represents an intensity measure for one of the hazards. The P_f^{allow} value is then used to identify the corresponding intensity measure value ($IM_{1,L}$ and $IM_{2,L}$) in the fragility curve as the limiting boundary in risk space characterized by the corresponding intensity measures. These limiting boundary values, $IM_{1,L}$ and $IM_{2,L}$, are then used to identify four distinct regions in the risk space plot. The region that corresponds to $IM_1 > IM_{1,L}$ and $IM_2 > IM_{2,L}$ is the region in which both the hazards govern the design of the structure. At a given geographical location, the codes and standards can be used to determine the site-specific intensity measures for designing a structure. These two values for the two hazards are represented by a point ("x") in the risk space of Fig. 1, and its location determines whether the design of the particular structures at the given geographic location are governed by both hazards (region IV in Fig. 1) or a single hazard (regions II and III in Fig. 1).

The risk-consistent framework proposed above is developed while keeping in mind the actively evolving area of probabilistic risk assessment and reliability-based design.

Nevertheless, it can be easily converted into a deterministic form for consistency with current design codes and standards, as shown in Fig. 2, a modified form of the previous figure. As seen in Fig. 2, fragility curves are replaced with deterministically generated curves for g_1 and g_2 with respect to their intensity measures. The performance functions g_1 and g_2 are deterministic in nature as per Eq. (5) and (6), discussed earlier. The limiting values of intensity measures $IM_{1,L}$ and $IM_{2,L}$ in this form correspond to $g_1 = 0$ and $g_2 = 0$, respectively. The subsequent definition of risk space and identification of different regions remains identical to that of Fig. 1. Specifically, the four regions can be described as: I. sites at which the initial/current design is acceptable with respect to both the hazards when $g_1 > 0$ and $g_2 > 0$; II. sites governed by only earthquake hazard when $g_1 \leq 0$ and $g_2 > 0$; III. sites governed by only wind hazard when $g_1 > 0$ and $g_2 \leq 0$; IV. sites governed by both earthquake and wind hazards when $g_1 \leq 0$ and $g_2 \leq 0$.

4. Illustration of Proposed Framework

In this section, we illustrate the development and utilization of the proposed framework through a simple example that includes several selected geographic locations. To begin, a 20-story building is considered, and the illustration is then extended to 30-story and 40-story buildings. For simplicity, a square cross section of the building is considered with width B = 16 m and story height h = 4 m. The building is assumed to exhibit slenderness with a total height (H = 80 m) to width (B) ratio of 5. The mass of each floor is taken as 8e5 kg and the inter-story stiffness is taken as 1.4e9 N/m. The performance functions for this structure

become $g_1 = R_e - 0.06$ for an earthquake loading and $g_2 = R_w - 0.39$ for a wind loading by adopting Eq. (5) and Eq. (6). In order to outline the process of characterizing hazards and developing input loadings, three representative geographical locations are considered: (i) Los Angeles, CA (ii) Anchorage, AK and (iii) Charleston, SC. The primary reason for selecting these specific locations is that all three sites are vulnerable to seismic and wind hazards.

4.1 Characterization of earthquake hazard

The USGS (United States Geological Survey) and ASCE 7-10 provide seismic hazard intensity measures which are characterized in terms of the mapped hazard spectral accelerations at short period (S_S) and 1s period (S_1). ASCE 7-10 requires that the mapped hazard values (S_S and S_1) be multiplied by the site-specific soil amplification coefficients (F_a and F_v) and the design reduction factor (2/3) for characterizing the design hazard parameters (S_{DS} and S_{D1}). These parameters are then used to construct the design spectrum. If an acceleration time history is needed for analysis of structural responses, the design spectrum is used to develop corresponding motions by scaling the historical ground motions or artificially generating ground motions compatible with the design spectrum.

Next, we apply this process to characterize the seismic hazard at the three selected sites in this study. For Los Angeles, it is determined that S_S = 2.348g and S_1 = 0.823g. For Anchorage, S_S = 1.500g and S_1 = 0.676g, and for Charleston, S_S = 1.119g and S_1 = 0.355g. For comparison purposes, we consider the same soil site classification (class D) for the local soil profile. The soil amplification factors are F_a = 1 and F_v = 1.5 for Los Angeles, F_a = 1 and

F_v = 1.502 for Anchorage, and F_a = 1.052 and F_v = 1.609 for Charleston. The design hazard parameters with a soil site class D are calculated to be S_{DS} = 1.565g and S_{D1} = 0.823g for Los Angeles, S_{DS} = 1.000g and S_{D1} = 0.676g for Anchorage, and S_{DS} = 0.785g and S_{D1} = 0.400g for Charleston. Fig. 3 shows the design spectra calculated at these sites in accordance with ASCE 7-10 and represented by solid lines in the figure. For analysis purposes, the spectrum compatible artificial ground motions for each site are generated as described in Gasparini and Vanmarcke (1976). The response spectra calculated from the artificial ground motions are shown by the dashed lines in Fig. 3. The artificial time histories for each of the three sites are shown in Fig. 4.

4.2 Characterization of wind hazard

ASCE 7-10 gives wind speed maps for the entire United States that can be used to calculate the wind hazard. Static wind pressure is determined from the wind speed (V), which is considered to act as a three-second gust speed at 10 m above the ground in a particular exposure category. This information is then used to determine the importance factor (I), exposure coefficient (K_z), topographical factor (K_{zt}), and wind directional factor (K_d) in order to calculate the design velocity pressure (q_z) at height (z) as follows:

$$q_z = 0.613 K_z K_{zt} K_d V^2 I \left(N / m^2 \right) \tag{7}$$

Wind time history loadings can be developed by using the Kaimal spectrum as described below in Eq. (8) and (9).

$$\frac{fS_u(z,f)}{\sigma_u^2} = \frac{6.8 f_L}{(1+10.2 f_L)^{5/3}} \tag{8}$$

$$f_L = \frac{fL_H(z)}{U_H(z)} \tag{9}$$

where f is frequency; z is height; S_u is power spectral density; f_L is height dependent length scale of turbulence; σ_u is the standard deviation; L_H is length scale; U_H is wind velocity evaluated at the height. To take the correlation of all stories of the building into account, the defined spectrum should be updated by the following equation:

$$S_{rs} = \sqrt{S_{rr}(f) S_{ss}(f)} \cdot \exp\left[-f \frac{k_z |z_r - z_s|}{(1/2)\left[U_H(z_r) + U_H(z_s)\right]} \right] \tag{10}$$

where S_{rr} and S_{ss} are wind velocity spectra for stories r and s, respectively; S_{rs} is the off-diagonal wind velocity spectrum considering the correlation between stories r and s; k_z is the decay constant; z_r is the height of story r; z_s is the height of story s. The decay constant considering the cross correlation for obtaining off-diagonal spectra is typically taken as 10 when generating wind time history loadings. The transformation from the spectrum to a time history (Witting & Sinha, 1975; Dyrbye and Hansen, 1997; Zhou et al., 2003) can be performed in three steps: (1) the lower triangle matrix is obtained via Cholesky decomposition, (2) the FFT (Fast Fourier Transformation) function (X_p) having a phase angle following a normal distribution is generated at each floor, (3) the wind time histories (x_p) at

each floor are obtained by using the inverse FFT operation. The equations for X_p and x_p are as follows:

$$X_p(k\Delta f) = \sqrt{2 f_c N} \sum_{i=0}^{p} H_{pi}(k\Delta f)\zeta_{ik} \tag{11}$$

$$x_p(n\Delta t) = \frac{1}{N} \sum_{k=0}^{N} X_p(k\Delta f) exp\left(j \frac{2\pi kn}{N}\right) \tag{12}$$

where H_{pi} is the lower triangle matrix; ζ_{ik} is a complex Gaussian random variable having a mean of 0 and variance of 0.5; Δt is $1/(2 \cdot f_c)$; f_c is the Nyquist frequency.

Next, we apply the wind loading characterization described above to the three representative geographical locations considered in this study. To begin with, the basic wind speeds for the three sites of Los Angeles, Anchorage, and Charleston are taken as 38 m/s, 54 m/s, and 63 m/s, respectively, from the code-defined wind speed map. Other conditions of the exposure category, I, K_{zt} and K_d are taken as Exposure C, 1.0, 1.0, and 0.85, respectively. The value of K_z can be obtained from the code-defined shape along the height of the building structure. Based on these values and the simple 20-story building structure considered, the wind time history loadings are generated artificially for a total duration of 300 s at a time step of 0.5s. The power spectrum density (PSD) curves of $S_{20,20}$ are illustrated in Fig. 5. The average wind velocity distributions along the height of the 20-story building structure are specified in Fig. 6. Fig. 7 shows the wind time history loadings generated at the top floor of the 20-story building structure for each of the three sites.

4.3 Development of multi-hazard risk map

In this study, we consider the intensity measures for earthquake and wind (IM_1 and IM_2) as peak ground acceleration (PGA) and basic wind speed (Vs). For the 20-story building, the performance function is characterized as inter-story drift for earthquake, and acceleration for wind, in order to quantify functions g_1 and g_2. The performance functions are calculated at the three sites for a suite of IM_1 and IM_2 values, and corresponding interpolated curves for these performance functions are found by the regression analyses. The corresponding curves for g_1 versus PGA and g_2 versus Vs are shown in Fig. 8. As seen in these curves, the failure limits for each hazard intensity measure are found to be 0.54g ($IM_{1,L}$) for earthquake and 53 m/s ($IM_{2,L}$) for wind. With these values of $IM_{1,L}$ and $IM_{2,L}$, we now plot risk space and identify the four distinct regions of multi-hazard risk in Fig. 9. Finally, coordinates for the three sites (Los Angeles, Anchorage, and Charleston) are located in risk space to determine the significance of single versus multiple hazards in the design of this 20-story building. For instance, if this 20-story building is located at a site where the design levels are greater than 0.54g for earthquakes but less than 53 m/s for winds, then its design is governed by only the earthquake hazard. On the other hand, if the structure is located at a site where the design levels of both hazards are greater than 0.54g and 53 m/s, its design will be governed by both hazards.

Finally, we illustrate the changing nature of risk space as developed in the proposed framework by considering 30-story and 40-story buildings. The story height and slenderness

ratio for each building are taken to be the same as before, i.e., the story height is 4 m and slenderness ratio is 5. The same process is repeated for each building and the corresponding risk space plotted, with the results for all three buildings shown in Fig. 10. We observed that, as the total height of the building is increased, many more geographical locations fall under the region where $g_1 \leq 0$ and $g_2 \leq 0$, indicating an increased susceptibility to multiple hazards.

In the following section, we illustrate the changing nature of solutions under a multi-hazard scenario by looking at two buildings located in close proximity to one another. The example shows that the retrofit solutions for these buildings are very different depending on whether just earthquake or just wind hazards are considered, or whether they are considered together in combination.

5. Application: Alternative Solutions in a Multi-Hazard Scenario

For this application of the framework, we consider a 20-story building located in close proximity to a 10-story building in a tight urban setting. This particular example appears in the literature (Ni et al., 2001; Ok et al., 2008) in the context of earthquake design for adjacent buildings connected by supplemental damping devices. At the same time, the concept of connecting adjacent buildings by supplemental damping devices has also been presented as a possible approach for withstanding high winds (Gurley et al., 1994; Seto, 1996; Lee at al., 2012). Therefore, we examine the implications of a multi-hazard scenario for this example application.

Fig. 11 shows the configuration of two adjacent buildings connected by supplemental damping devices at different floor levels. The actual floor levels and the number of damping devices needed at each floor are investigated in determining the retrofit solution for these buildings. The buildings are assumed to be located at a geographical location that corresponds to an earthquake intensity measure similar to one in Los Angeles and a wind intensity measure similar to one in Charleston. With respect to supplemental damping devices, many different types are available and can be used, such as metallic, friction dampers, visco-elastic dampers, tuned-mass dampers, isolators, and MR-dampers. For the purpose of this study, we consider MR-dampers since Ok et al. (2008) use MR dampers in their study for earthquake loads. Similarly, Kim and Kang (2012) utilize MR dampers for high winds. Prior to evaluating design alternatives for a multi-hazard scenario with MR dampers, we present the numerical model for MR dampers that is used in conducting the analysis in the next section. The following section also presents a brief discussion of the design parameters used for characterizing the MR dampers.

5.1 Numerical model of MR damper

Several mechanical models have been proposed over the years to model MR damper behavior (Spencer et al., 1997). In this study, we adopt the experimentally validated model shown in Fig. 12 that uses a Bouc-Wen element and a viscous damper in parallel (Dyke et al., 1998). The restoring force in this model is expressed as shown below in Eq. (13). As seen in

this equation, the restoring force f_r is composed of a linear viscous elastic part and a hysteretic part:

$$f_r = c_0 \Delta\dot{x} + \alpha y \tag{13}$$

$$c_0(V) = c_{0a} + c_{0b} V \tag{14}$$

$$\alpha(V) = \alpha_a + \alpha_b V \tag{15}$$

where the parameters c_0 and α represent the viscous damping and inelastic coefficients, respectively; Δx is the nonlinear element-ended relative displacement; $\Delta\dot{x}$ is the nonlinear element-ended relative velocity; and y is the interior hysteretic variable, which is expressed as the first-order nonlinear differential equation given by Eq. (16):

$$\dot{y} = -\gamma \left|\Delta\dot{x}\right| y \left|y\right|^{n-1} - \beta \Delta\dot{x} \left|y\right|^{n} + A\Delta\dot{x} \tag{16}$$

where the parameter A controls the scale of the hysteresis loops and n determines the sharpness of the hysteresis cycle in the region of change from the elastic to the inelastic part; β and γ are parameters that control the shape of the hysteretic behavior (Barber and Wen, 1981).

In this study, we choose an MR damper of capacity approximately equal to 100 kN that has the following set of parameters characterizing its behavior based on experimental studies (Yi et al., 2001), i.e., c_{0a} = 0.88e2 N-s/cm, c_{0b} = 8.8e2 N-s/cm/V, α_a = 21744e2

N/cm, α_b = 99232e2 N-s/cm/V, γ= 3 cm^{-1}, β= 3 cm^{-1}, A = 1.2, and n = 1. Fig. 13 illustrates the force-velocity/displacement hysteretic behaviors of this particular MR damper model for six different input voltage values. The input voltage determines the maximum damping force and the energy dissipation. Therefore, the input voltage is a key parameter needed in determining the retrofit solution. The input voltage determines its force behavior, which in turn governs the number of dampers needed in a given design alternative.

Next, we describe the mathematical model that represents the equations of motion for two buildings coupled with MR-dampers. This mathematical model is needed for conducting an analysis with earthquake and wind loads.

5.2 Mathematical model for coupled buildings with MR dampers

Fig. 11 illustrates two adjacent buildings with n_1^{th} and n_2^{th} stories ($n_1 > n_2$) connected by m nonlinear hysteretic MR dampers along floors in the horizontal direction. Under earthquake and wind excitations, it is assumed that the coupled buildings remain linearly elastic, whereas the dampers experience nonlinear hysteretic behavior and transfer damper forces to the connecting floors of the buildings. The governing equations of motion for shear-type coupled building models ($N = n_1 + n_2$) are expressed as:

$$[M]\{\ddot{u}\} + [C]\{\dot{u}\} + [K]\{u\} + \{F_d\} = \{f\} \tag{17}$$

$$\{F_d\}_{N\times 1} = [C_0]_{N\times N}\{\dot{u}\}_{N\times 1} + [\mathrm{A}]_{N\times n_2}\{y\}_{n_2\times 1} \tag{18}$$

$$[M]_{N\times N}=\begin{bmatrix}\left[M^{(1)}\right]_{n_1\times n_1} & [0]_{n_1\times n_2}\\ [0]_{n_2\times n_1} & \left[M^{(2)}\right]_{n_2\times n_2}\end{bmatrix} \tag{19}$$

$$[C]_{N\times N}=\begin{bmatrix}\left[C^{(1)}\right]_{n_1\times n_1} & [0]_{n_1\times n_2}\\ [0]_{n_2\times n_1} & \left[C^{(2)}\right]_{n_2\times n_2}\end{bmatrix} \tag{20}$$

$$[K]_{N\times N}=\begin{bmatrix}\left[K^{(1)}\right]_{n_1\times n_1} & [0]_{n_1\times n_2}\\ [0]_{n_2\times n_1} & \left[K^{(2)}\right]_{n_2\times n_2}\end{bmatrix} \tag{21}$$

$$[C_0]_{N\times N}=\begin{bmatrix}diag[c_0]_{n_2\times n_2} & [0]_{n_2\times(n_1-n_2)} & -diag[c_0]_{n_2\times n_2}\\ [0]_{(n_1-n_2)\times n_2} & [0]_{(n_1-n_2)\times(n_1-n_2)} & [0]_{(n_1-n_2)\times n_2}\\ -diag[c_0]_{n_2\times n_2} & [0]_{n_2\times(n_1-n_2)} & diag[c_0]_{n_2\times n_2}\end{bmatrix} \tag{22}$$

$$[\mathrm{A}]_{N\times n_2}=\begin{bmatrix}-diag[\alpha]_{n_2\times n_2}\\ [0]_{(n_1-n_2)\times n_2}\\ diag[\alpha]_{n_2\times n_2}\end{bmatrix} \tag{23}$$

where [*M*], [*C*], and [*K*] represent the *N* x *N* dimensional mass, damping, and stiffness matrices of the coupled buildings, respectively; the superscripts (1) and (2) denote the n_1^{th} and n_2^{th} story buildings; $\{u\},\{\dot{u}\}$, and $\{\ddot{u}\}$ are the *N* x 1 dimensional displacement, velocity, and acceleration vectors; $\{F_d\}$ denotes the *N* x 1 dimensional force vector induced by nonlinear hysteretic MR dampers; $\{f\}$ denotes the *N* x 1 dimensional force vector caused

from external earthquake or wind excitations; [C_0] and [A] indicate the N x N dimensional damping and N x n_2 dimensional inelastic coefficient matrices, respectively. In order to obtain responses of the system with respect to the force vector, we represent the equation of motion given by Eq. (17) as the second-order ordinary differential equation (ODE) given by Eq. (24), and describe the second-order ODE of Eq. (24) by a first-order ODE representation of Eq. (25a):

$$\begin{aligned}
&\{\dot{u}\} = [I]\{\dot{u}\} \\
&\{\ddot{u}\} = -[M]^{-1}[K]\{u\} - [M]^{-1}[C]\{\dot{u}\} - [M]^{-1}[C_0]\{\dot{u}\} - [M]^{-1}[\mathrm{A}]\{y\} + [M]^{-1}\{f\} \\
&\{y\} = \left\{-\gamma|\Delta\dot{u}|y|y|^{n-1} - \beta\Delta\dot{u}|y|^{n} + A\Delta\dot{u}\right\}
\end{aligned} \quad (24)$$

$$\left\{\dot{Y}\right\} = f\left(t, \{Y\}\right) \quad (25a)$$

$$\{Y\}_{(2N+m)\times 1}\left(= \left[Y_1 \sim Y_N \quad Y_{N+1} \sim Y_{2N+1} \quad Y_{2N+1} \sim Y_{2N+m}\right]^T\right) = \left[\{u\}_{N\times 1}^T \quad \{\dot{u}\}_{N\times 1}^T \quad \{y\}_{m\times 1}^T\right] \quad (25b)$$

$$\left\{\dot{Y}\right\}_{(2N+m)\times 1}\left(= \left[\dot{Y} \sim \dot{Y}_N \quad \dot{Y}_{N+1} \sim \dot{Y}_{2N} \quad \dot{Y}_{2N+1} \sim \dot{Y}_{2N+m}\right]^T\right) = \left[\{\dot{u}\}_{N\times 1}^T \quad \{\ddot{u}\}_{N\times 1}^T \quad \{\dot{y}\}_{m\times 1}^T\right] \quad (25c)$$

$$\begin{Bmatrix} \dot{Y}_1 \\ \vdots \\ \dot{Y}_N \end{Bmatrix} = [I]_{N\times N} \begin{Bmatrix} Y_{N+1} \\ \vdots \\ Y_{2N} \end{Bmatrix}$$

$$\begin{Bmatrix} \dot{Y}_{N+1} \\ \vdots \\ \dot{Y}_{2N} \end{Bmatrix} = -[M]^{-1}[K]\begin{Bmatrix} Y_1 \\ \vdots \\ Y_N \end{Bmatrix} - [M]^{-1}[C]\begin{Bmatrix} Y_{N+1} \\ \vdots \\ Y_{2N} \end{Bmatrix} - [M]^{-1}[C_0]\begin{Bmatrix} Y_{N+1} \\ \vdots \\ Y_{2N} \end{Bmatrix} - [M]^{-1}[\mathrm{A}]\begin{Bmatrix} Y_{2N+1} \\ \vdots \\ Y_{2N+m} \end{Bmatrix} + [M]^{-1}\{f\} \quad (25d)$$

$$\begin{Bmatrix} \dot{Y}_{2N+1} \\ \vdots \\ \dot{Y}_{2N+m} \end{Bmatrix} = \begin{Bmatrix} -\gamma\left|\left(Y_{N+n_1+1} - Y_{N+1}\right)\right| Y_{2N+1}\left|Y_{2N+1}\right|^{n-1} - \beta\left(Y_{N+n_1+1} - Y_{N+1}\right)\left|Y_{2N+1}\right|^{n} + A\left(Y_{N+n_1+1} - Y_{N+1}\right) \\ \vdots \\ -\gamma\left|\left(Y_{N+n_1+m} - Y_{N+m}\right)\right| Y_{2N+m}\left|Y_{2N+m}\right|^{n-1} - \beta\left(Y_{N+n_1+m} - Y_{N+m}\right)\left|Y_{2N+m}\right|^{n} + A\left(Y_{N+n_1+m} - Y_{N+m}\right) \end{Bmatrix}$$

where $\{Y\}$ is the space-state vector. The detailed components of the state vector and the first-order ODE are described in Eq. (22b) to Eq. (22d). Eq. (25a) is solved using the forth-order Runge-Kutta algorithm.

Specifically for this study, n_1 = 20 and n_2 = 10. The properties of the 20-story building are the same as those described in section 4, and the building's performance is governed by both wind and earthquake loads as per the risk space of the proposed framework presented in section 4.3. The 10-story building has a square cross section with 8 m width (B), 4 m story height, and a slenderness ratio of 5. The mass of each floor is 8e5 kg and the inter-story stiffness is 1.4e9 N/m. The first five natural frequencies of the 20-story building structure are 0.51, 1.52, 2.54, 3.53, and 4.50 Hz, respectively. The first three natural frequencies of the 10-story building structure are 1.00, 2.96, and 4.86 Hz. The damping ratio for all modes of the buildings is assumed to be 2 %.

5.3 Alternative solutions for locating the dampers

Solutions for different numbers and voltages of dampers (types of dampers) are now evaluated with respect to performance requirements for both earthquake and wind loads. The intent is to illustrate that solutions obtained by considering only a single dominant hazard (whether earthquake or wind) are quite different from each other as well as from solutions obtained by considering both hazards in combination. Overall, the problem of arriving at the number of dampers, voltage requirements, and their floor locations is an optimization problem whose solutions would vary with the design constraints imposed by the designer. In this study we consider three different types of solutions by considering different constraints: (i) Case-1: dampers are located on all floors and their number does not change from floor to floor; (ii) Case-2: dampers are located on only a single floor; and (iii) Case-3: the most general case in which the number of dampers can vary from floor to floor. In all cases, the voltage requirements remain the same for all the dampers.

Case-1: In this scenario, a fixed number of MR dampers with the same input voltage are used to connect the buildings on all ten floors. The design variables are defined as the number of dampers on each floor and the specific value of the input voltage. It must be noted that these design variables decide the damper force characteristics and correspondingly the total cost of the dampers. As this problem is characterized by only two design variables, a graphical representation is simple and helps in understanding and assessing the possible alternatives. The responses for the coupled buildings with MR dampers as characterized by

Eq. (17) are computed numerically for both the earthquake and the wind time history loadings. Fig. 14 shows the contours of maximum inter-story drift under earthquake loading (R_e) and those of the maximum acceleration under wind loading (R_w) for the coupled building structures. The contours are plotted by varying the number of dampers at each floor as well as the input voltage for the dampers. We make three main observations from this figure: (1) The solution for "zero" dampers, the case in which the buildings are not connected by dampers, does not satisfy the performance requirements, thereby making it essential that the buildings be connected through dampers in order to withstand both the hazards. (2) There exists an optimal value of design variables, the number of dampers at each floor and the input voltage, which minimizes both R_e and R_w. Yet, the optimal design values are different under earthquake loading when compared to the corresponding values for the wind loading. (3) It is possible to obtain the optimal values of design variables that meet performance requirements for both the earthquake and the wind hazards and at the same time minimize the cost of dampers. For example, if the input voltage is assumed to be fixed at 2 V, then an optimum can be obtained as "3" which means 3 dampers at each of the 10 floors leading to a total of 30 dampers. It is apparent from Fig. 14 that this damper design can fulfill both performance requirements (red dashed lines) and minimize the total number of dampers. This optimal solution for the multi-hazard scenario is quite different from the optimal solutions obtained for the single individual hazards of earthquake or the wind.

Case-2: Klein and Healy (1987) conclude that buildings having different natural frequencies should be connected near the top to ensure appropriate utilization of control

devices, since the vibratory modes will most likely have nonzero amplitudes at the top. In our study, MR dampers are assumed to be installed between the 10^{th} floors of the two buildings, which is obviously the top floor of the 10-story building. The two design variables for this case are the number of dampers on the 10^{th} floor and the input voltage. Fig. 15 illustrates the contours for the R_e and R_w values of the coupled building structures with respect to the number of dampers and the input voltage. This figure is quite similar to Fig. 14 for Case-1 and the three main observations made in Case-1 also carry over to Case-2. A comparison of Case-1 and Case-2 shows that if the input voltage is fixed at 2 V, then the optimal number of dampers is "19" for Case-2 which is about one-third less than the total of 30 dampers needed in Case-1.

Case-3: As mentioned earlier, this case corresponds to allowing different numbers of dampers to be placed at different floors. Unlike the previous two cases, this case has more than two design variables, i.e., the total number of design variables is equal to the number of connected floors (to determine different number dampers needed at each floor) plus one additional variable for the input voltage. Therefore, there exists a total of 11 design variables in this scenario, which makes a graphical representation and determination of the potential solution quite difficult. Therefore, the problem is formulated as follows for a fixed input voltage value:

$$\begin{aligned} &\underset{\mathbf{x}}{\text{Minimize}} \quad f(\mathbf{x}) = \sum_{i=1}^{10} x_i \\ &\text{Subject to} \quad R_e \le L_e; \quad R_w \le L_w \end{aligned} \tag{26}$$

where $f(\mathbf{x})$ is a total number of dampers and x_i is the number of dampers installed at the i^{th} floor. This optimization problem is solved to determine the optimal distribution for the number of MR dampers that can satisfy performance requirements for both the earthquake and wind hazards as well as minimize the total number of the dampers, as shown in Fig. 16(c). For comparison purposes, Fig. 16 also gives the distributions of the number of MR dampers and corresponding maximum responses (R_e and R_w) obtained from the Case-1 and Case-2. As seen in this figure, the total numbers of MR dampers for the Case-2 and the Case-3 are not much different from each other. We attribute this to the fact that, for Case-3, most of the MR dampers are located on the two top floors of the 10-story building. These observations can be used to conclude that it is most desirable to locate the dampers as close to the top floors of a building as possible.

6. Summary and Conclusions

A performance-based framework is presented that determines whether the design and retrofit of given building types are governed by a single dominant hazard or instead by multiple hazards. While the study focuses on earthquake and wind hazards, the proposed framework is quite general in nature and can be applied to other external hazards as well. The performance criteria for each hazard can be different and can cover the various requirements of strength and serviceability. The framework is well suited for integration into the actively growing research area of probabilistic risk assessment. At the same time, we demonstrate that it can easily be converted to deterministically characterized performance criteria in accordance with

deterministic demand and capacity requirements as specified traditionally in the various building codes and standards. Application of the framework to three different geographic locations in the United States demonstrates the significance of location in multi-hazard risk assessment. In addition, the significance of multi-hazard design considerations is illustrated through explorations of alternative retrofit solutions in two adjacent buildings located in close proximity to each other, such as those encountered in a tight urban setting. The particular example considered for a retrofit solution has been studied by other researchers and involves connecting the buildings through supplemental damping devices. We observe that the number of dampers and their locations—as determined from multi-hazard design considerations—are very different from those determined for a single dominant hazard. A related observation is that a solution that might satisfy the performance requirements for an earthquake is not necessarily acceptable with respect to the performance requirements for wind and vice-versa. More generally, it is clear that the process of determining risk is highly dependent upon three primary concerns: performance criteria, building geometry, and geographic location.

Acknowledgements

This research was partially supported by the Center for Nuclear Energy Facilities and Structures at North Carolina State University. Resources for the Center come from the dues paid by member organizations and from the Civil, Construction, and Environmental Engineering Department and College of Engineering in the University.

References

AIA, *Buildings at Risk: Multihazard Design for Earthquakes, Winds and Floods*, The American Institute of Architects, NW Washington, DC, US, 1997.

ASCE, *Minimum design loads for buildings and other structures*, ASCE/SEI 7-05/-10, Reston, VA, US.

Barber TT and Wen YK, "Random vibration of hysteretic, degrading systems," *ASCE Journal of the Engineering Mechanics Division*, 107(6), 1069-1087, 1981.

Chen EY, *Multi-hazard design of mid- to high-rise structures*, M.S. thesis, Univ. of Illinois, Urbana-champaign, IL, 2012.

Crosti C, Duthinh D, and Simiu E, "Risk consistency and synergy in multihazard design," *ASCE Journal of Structural Engineering*, 137(8), 844-9, 2010.

Duthinh D and Simiu E, "Safety of structures in strong winds and earthquakes: multihazard considerations," *ASCE Journal of structural engineering*, 136(3), 330-3, 2009.

Dyke SJ, Spencer Jr BF, Sain MK and Carlson JD, "An experimental study of MR dampers for seismic protection," *Smart Materials and Structures*, 7(5), 693-703, 1998.

Dyrbye C, Hansen SO, *Wind Loads on Structures*, John Wiley & Sons Ltd, New York, 1997.

Gasparini DA, and Vanmarcke EH, "Simulated earthquake motions compatible with prescribed response spectra," *Civil Engineering Research Report R76-4*, Massachusetts Institute of Technology, Cambridge, USA, 1976.

Gurley K, Kareem A, Bergman LA, Johnson EA, and Klein RE, "Coupling tall buildings for control of response to wind," *Proceedings of 6th international conference (In: Schueller GI, Shinozuka M,Yao JTP, editors.)*, structural safety and reliability, Rotterdam, Netherlands, 1553-60, 1994.

IBC 2012, *International Building Code*, International Code Consortium.

Kim HS, and Kang JW, "Semi-active fuzzy control of a wind-excited tall building using multi-objective genetic algorithm," *Engineering Structures*, 41, 242-57, 2012.

Klein RE, and Healey MD, "Semi-active control of wind induced oscillations in structures," *Proceeding for 2nd International Conference on Structural Control*, Univ. of Waterloo, Ontario, Canada, Martinus Nijhoff Publishers, Dordrecht, Netherlands, 354-369, 1987.

Lee DG, Kim HS, and Ko H, "Evaluation of coupling–control effect of a sky-bridge for adjacent tall buildings," *The Structural Design of Tall and Special Buildings*, 21(5), 311-28, 2012.

Li Y, Ahuja A, and Padgett J, "Review of methods to assess, design for, and mitigate multiple hazards," *ASCE Journal of Performance of Constructed Facilities*, 26(1), 104–117, 2012.

Ni YQ, Ko JM, and Ying ZG, "Random seismic response analysis of adjacent buildings coupled with non-linear hysteretic dampers," *Journal of Sound and Vibration*, 246(3), 403-17, 2001.

Ok SY, Song J and Park KS, "Optimal design of hysteretic dampers connecting adjacent structures using multi-objective genetic algorithm and stochastic linearization method," *Engineering Structures*, 30(5), 1240-1249, 2008.

Seto K, "A structural control method of the vibration of flexible buildings in response to large earthquakes and strong winds," *Proceedings of the 35th Conference on Decision Control*, Kobe, Japan, 11–13 December, 658–663, 1996.

Spencer Jr BF, Dyke SJ, Sain MK, and Carlson JD, "Phenomenological model of magnetorheological damper," *ASCE Journal of Engineering Mechanics*, 123(3), 230-8, 1997.

Tallin A and Ellingwood B, "Wind induced lateral-torsional motion of buildings," *ASCE Journal of Structural Engineering*. 111(10), 2197-213, 1985.

Unobe ID and Sorensen AD, "Multi-hazard analysis of a wind turbine concrete foundation under wind fatigue and seismic loadings," *Structural Safety*, 57, 26-34, 2015.

Wen YK and Kang YJ, "Minimum building life-cycle cost design criteria. I: Methodology," *ASCE Journal of Structural Engineering*, 127(3), 330-337, 2001.

Wittig LE and Sinha AK, "Simulation of Multicorrelated Random Processes using the FFT Algorithm, *The Journal of the Acoustical Society of America*, 58(3), 630-633, 1975.

Yi F, Dyke SJ, Caicedo JM, and Carlson JD, "Experimental verification of multi-input seismic control strategies for smart dampers," *ASCE Journal of Engineering Mechanics*, 127(11), 1152–64, 2001.

Zhou Y, Kijewski T, and Kareem A, "Aerodynamic Loads on Tall Buildings: An Interactive Database," *ASCE Journal of Structural Engineering*, 129(3), 394-404, 2003.

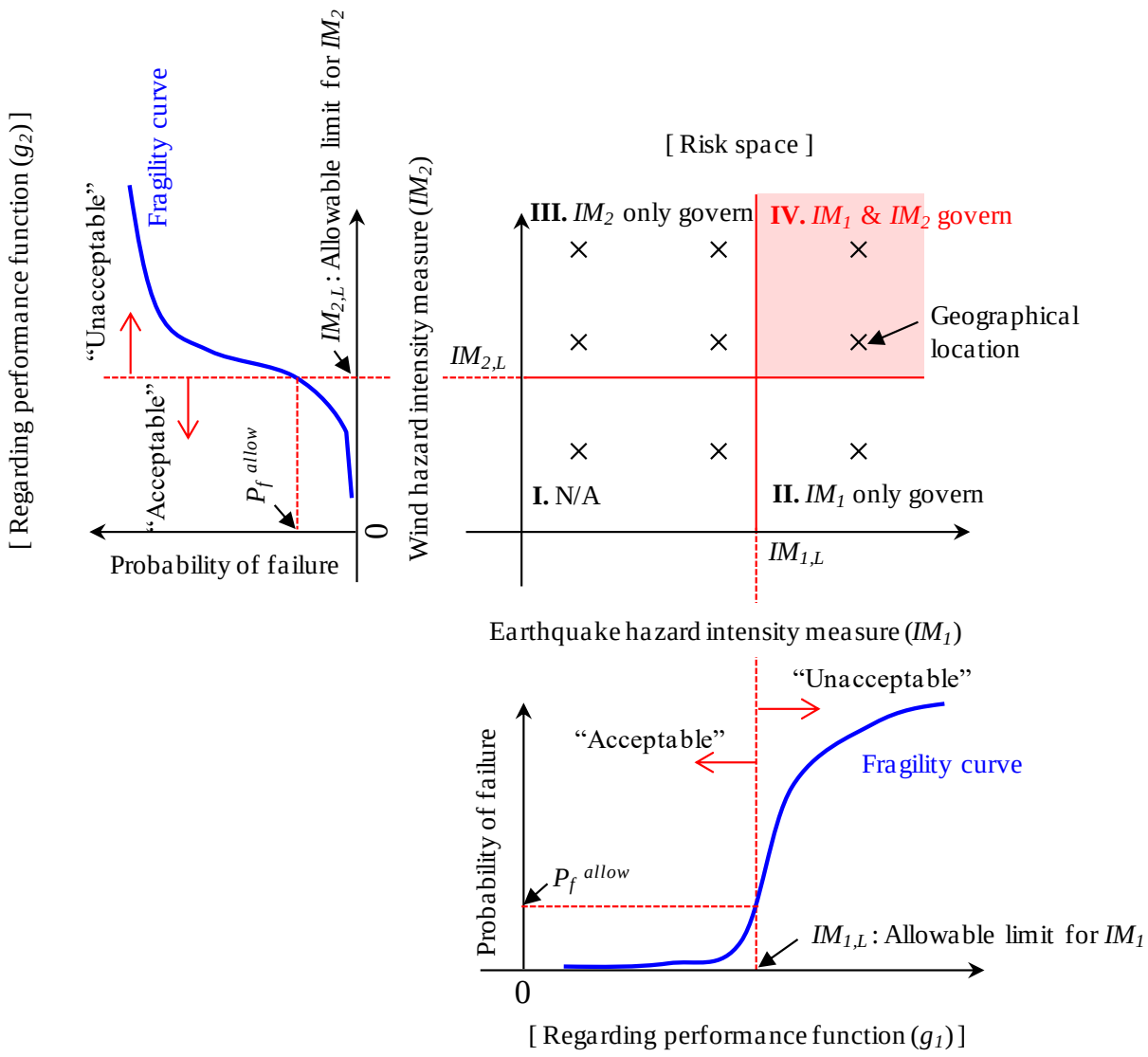

Fig. 1. Graphical representation of proposed framework: multi-hazard risk map

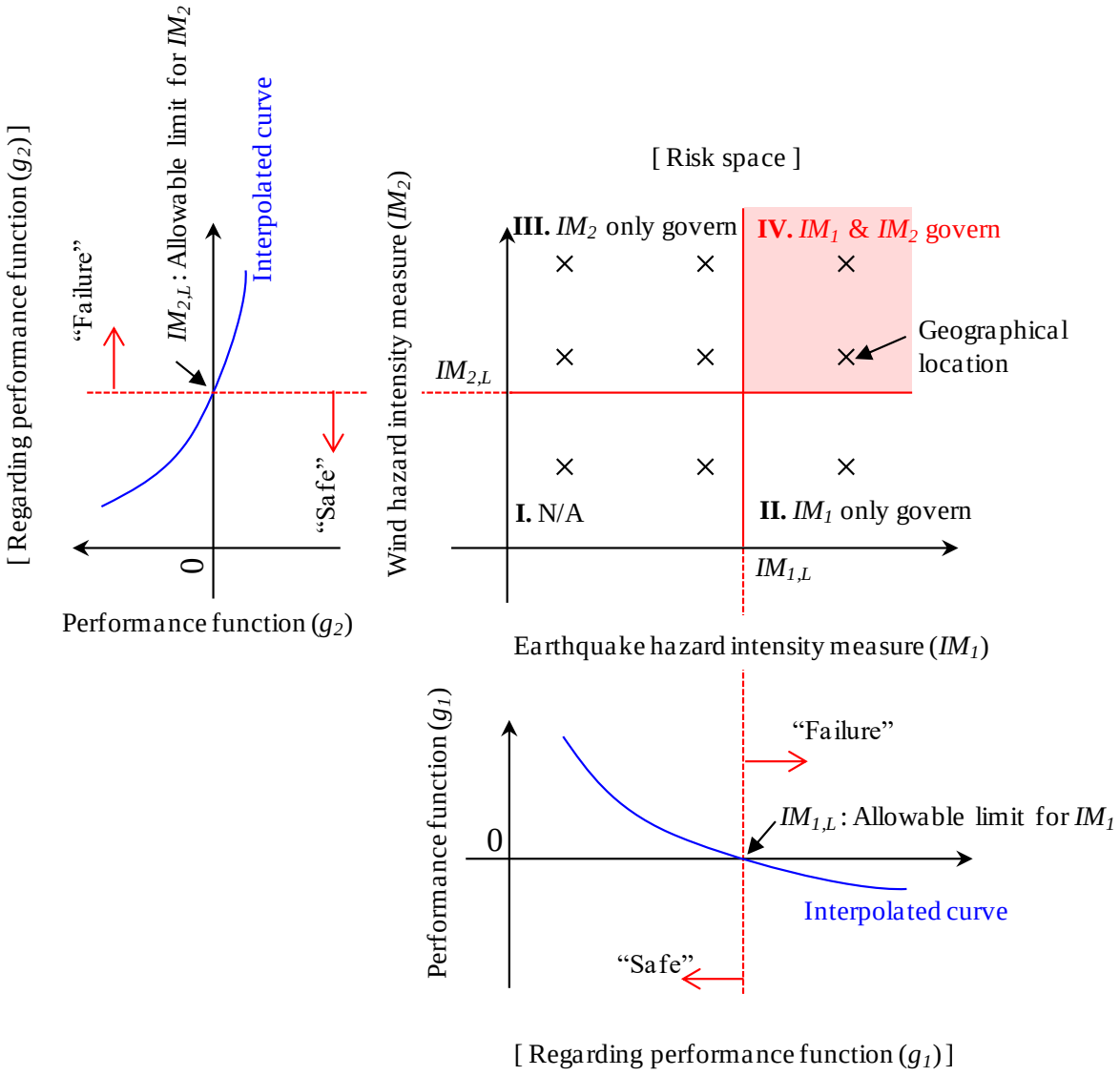

Fig. 2. Development of multi-hazard prone site map: deterministic form

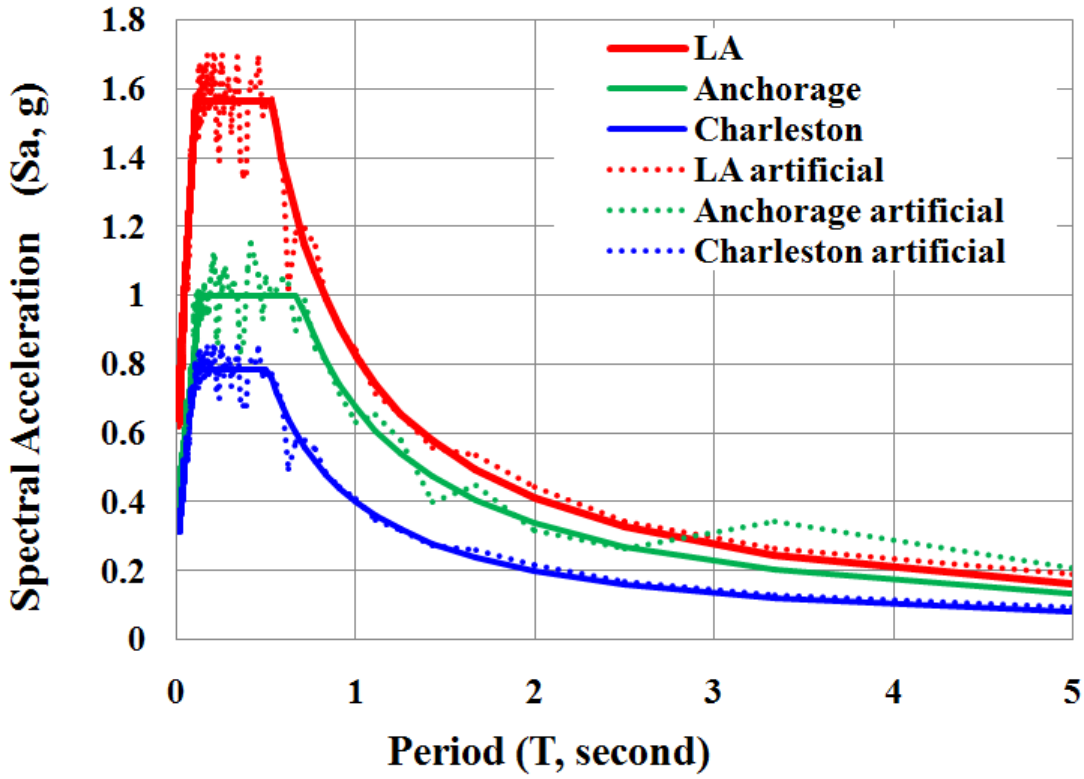

Fig. 3. Design spectra and compatible ground motions

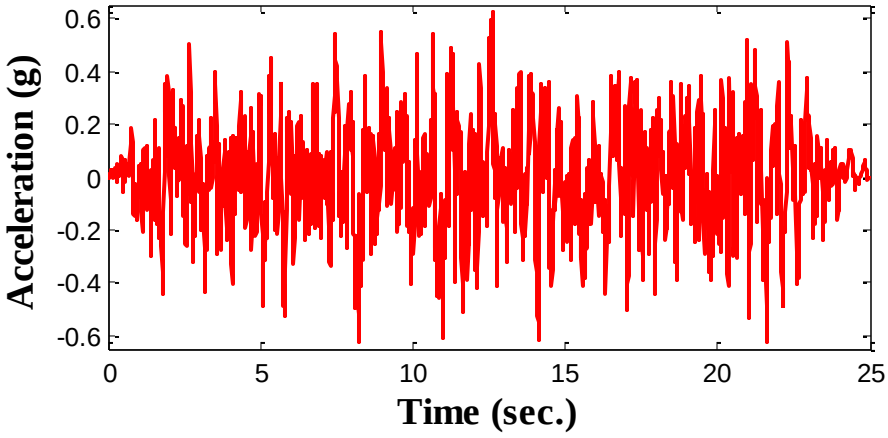

(a) LA

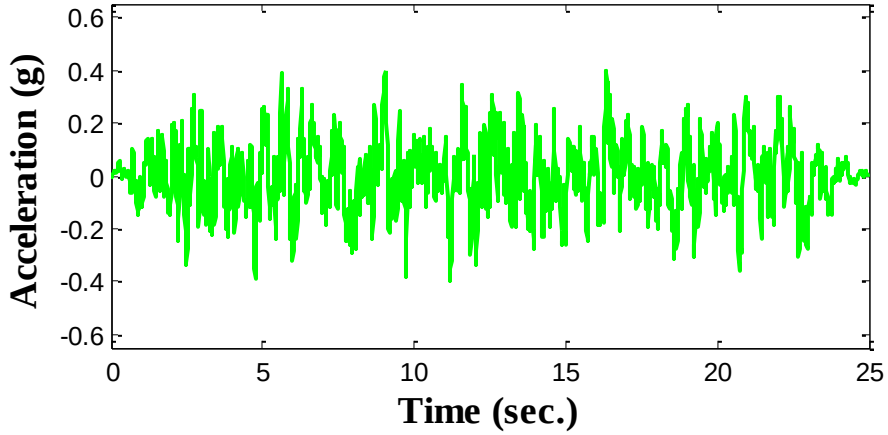

(b) Anchorage

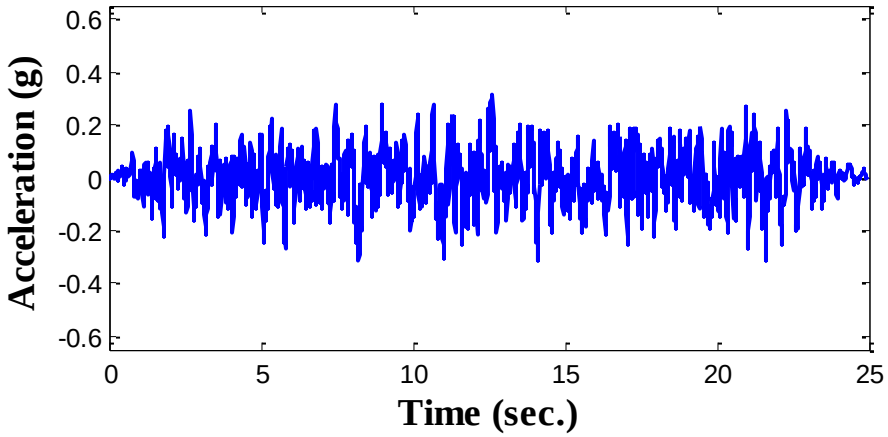

(c) Charleston

Fig. 4. Design spectra compatible ground motions

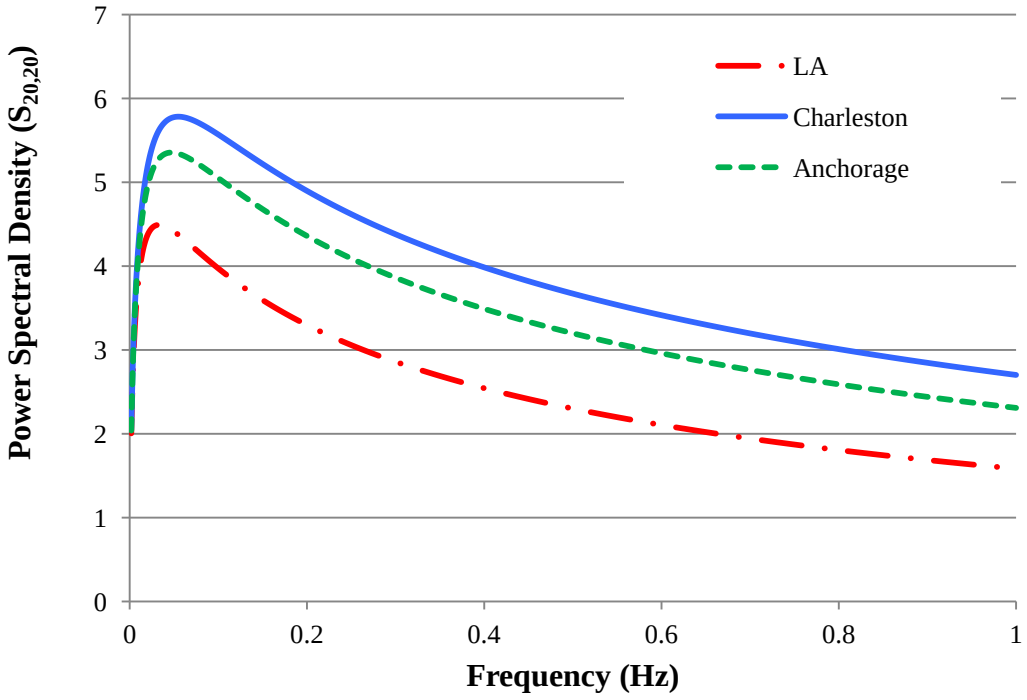

Fig. 5. PSD curves at the 20th floor of 20-story building ($S_{20,20}(f)$)

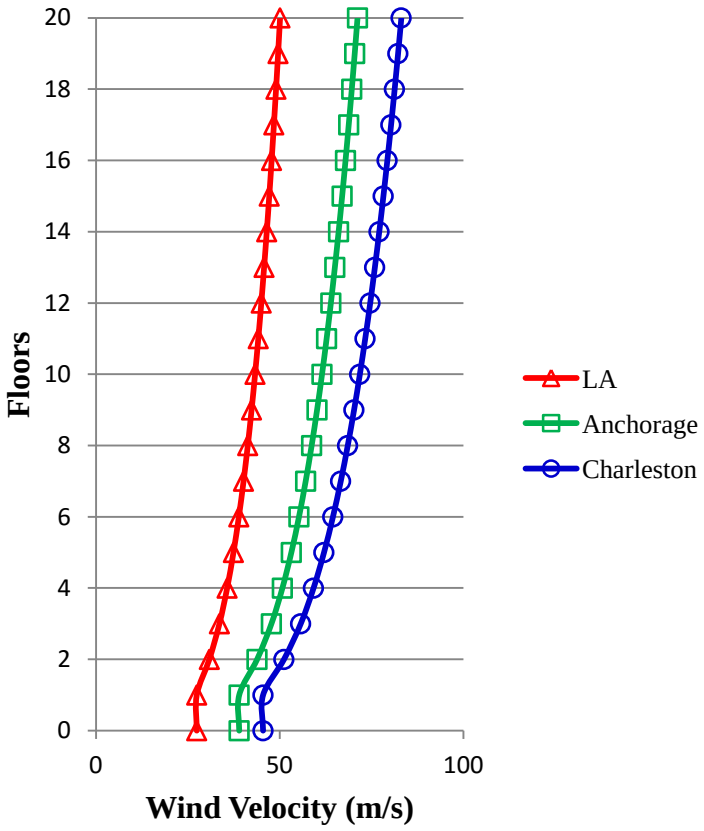

Fig. 6. Average wind velocity distribution along floors

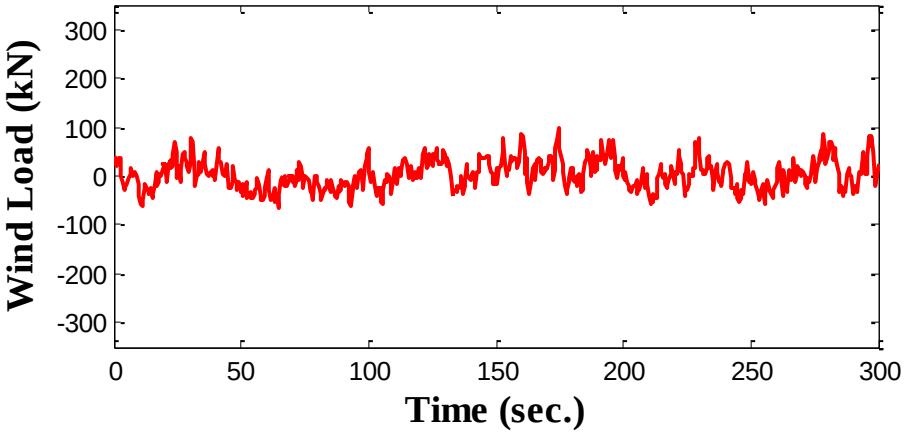

(a) LA

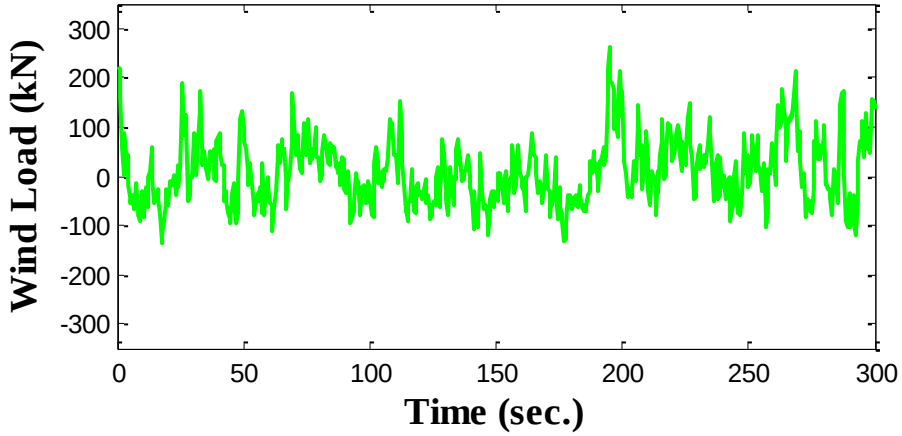

(b) Anchorage

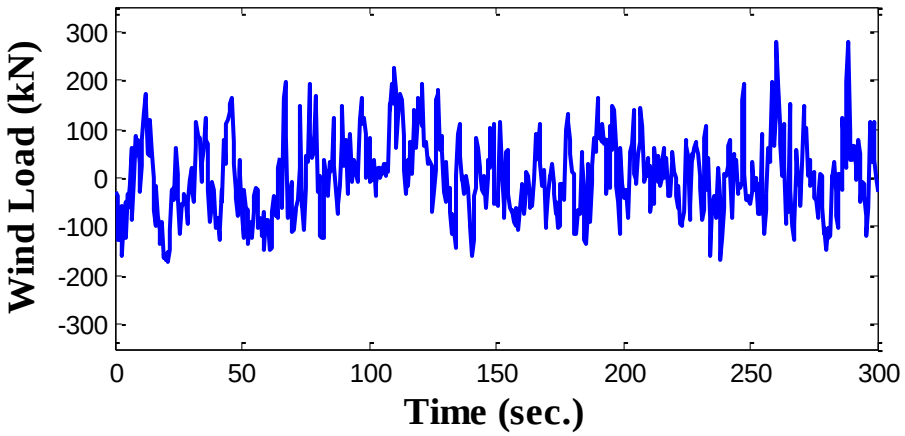

(c) Charleston

Fig. 7. Wind time history loadings at the top of the 20-story building

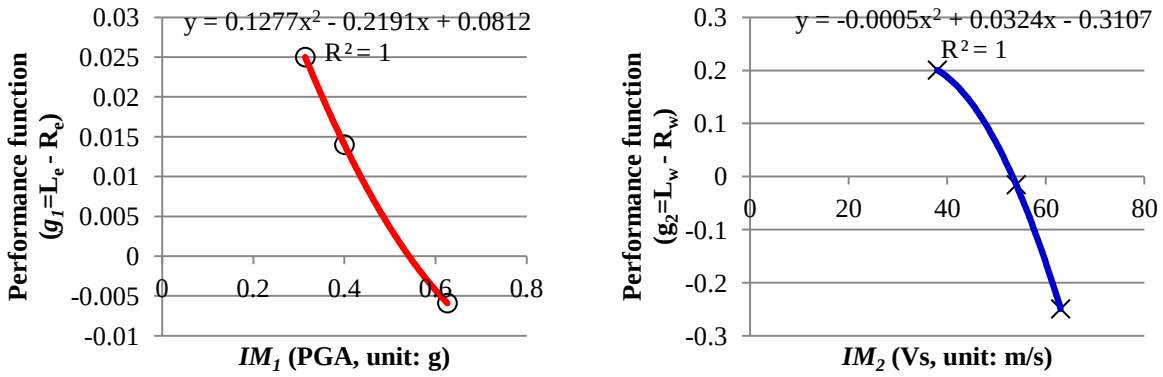

(a) EQ hazard (b) Wind hazard

Fig. 8. Evaluated performance function values of 20-story building structure and interpolated curves under two hazard intensity measures of EQ and Wind of three representative sites

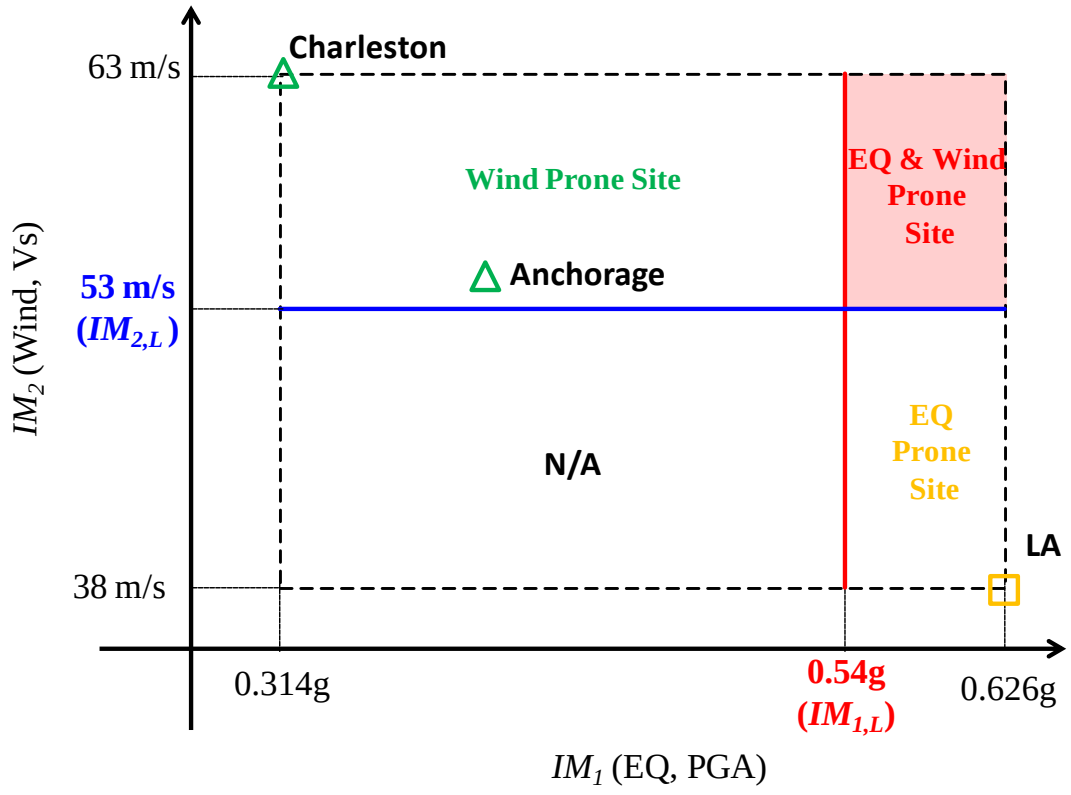

Fig. 9. Risk space: multiple hazard prone site map for 20-story building structure

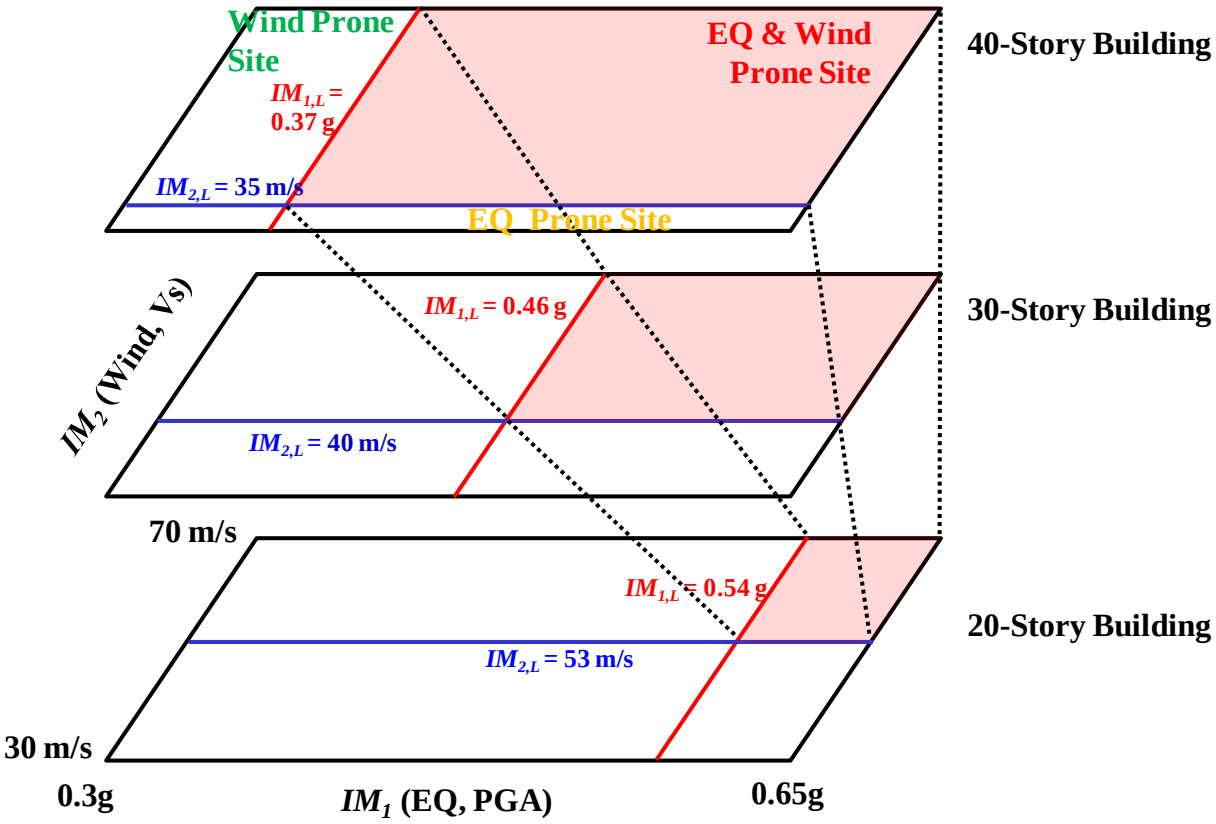

Fig. 10. Change of multi-hazard prone area according to total heights of building

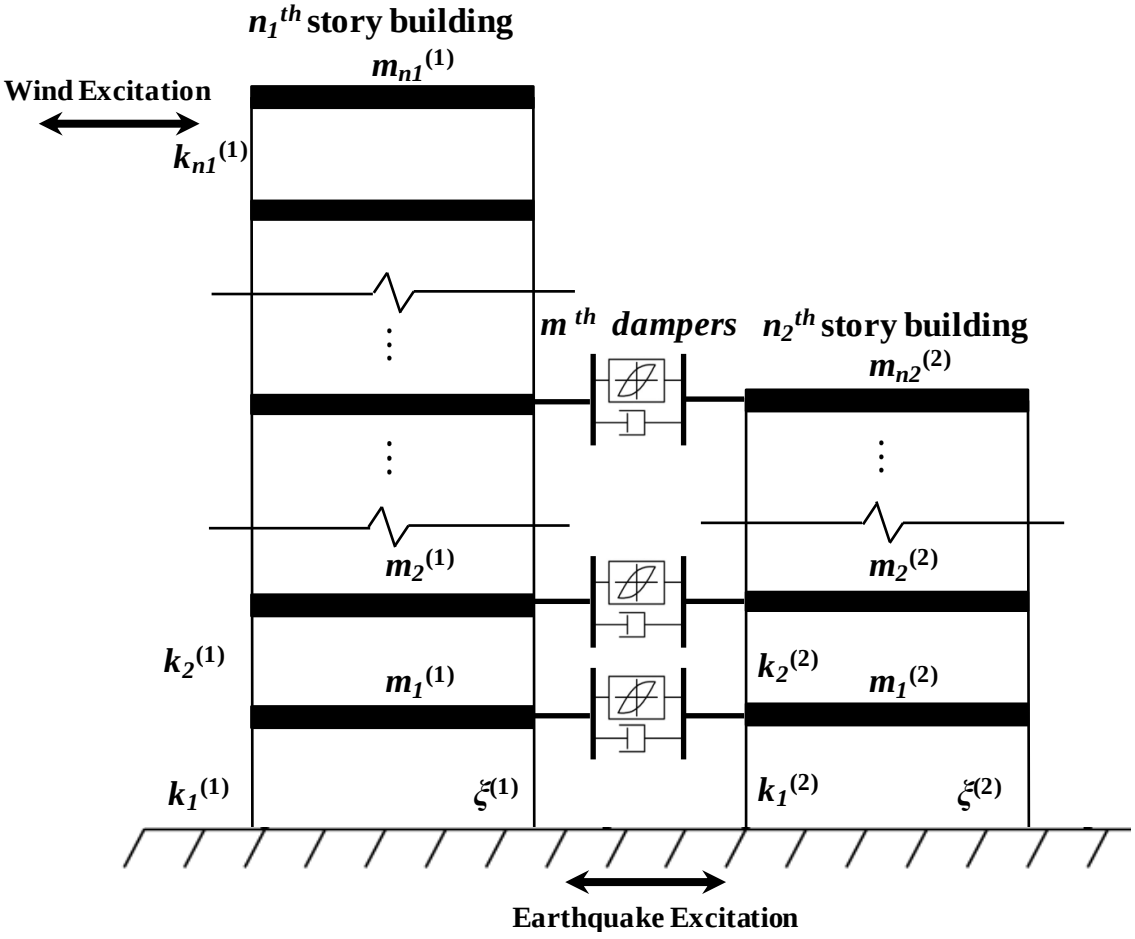

Fig. 11. Coupled buildings connected with nonlinear hysteretic MR dampers under earthquake and wind excitations

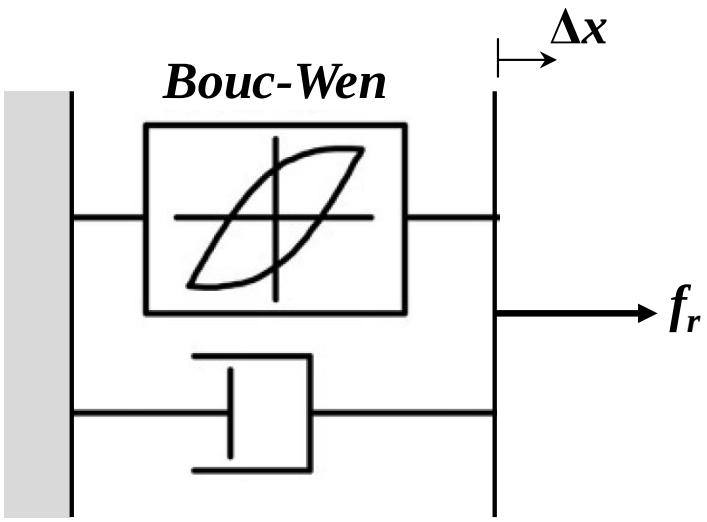

Fig. 12. MR damper mechanical model

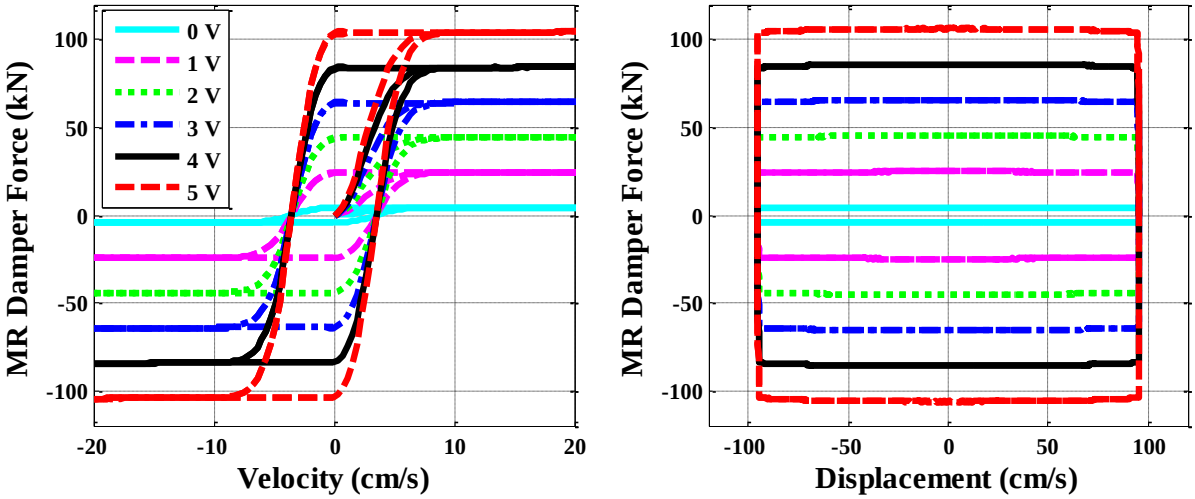

(a) Force v.s. Velocity **(b)** Force v.s. Displacement

Fig. 13. Nonlinear hysteretic behavior of the MR damper

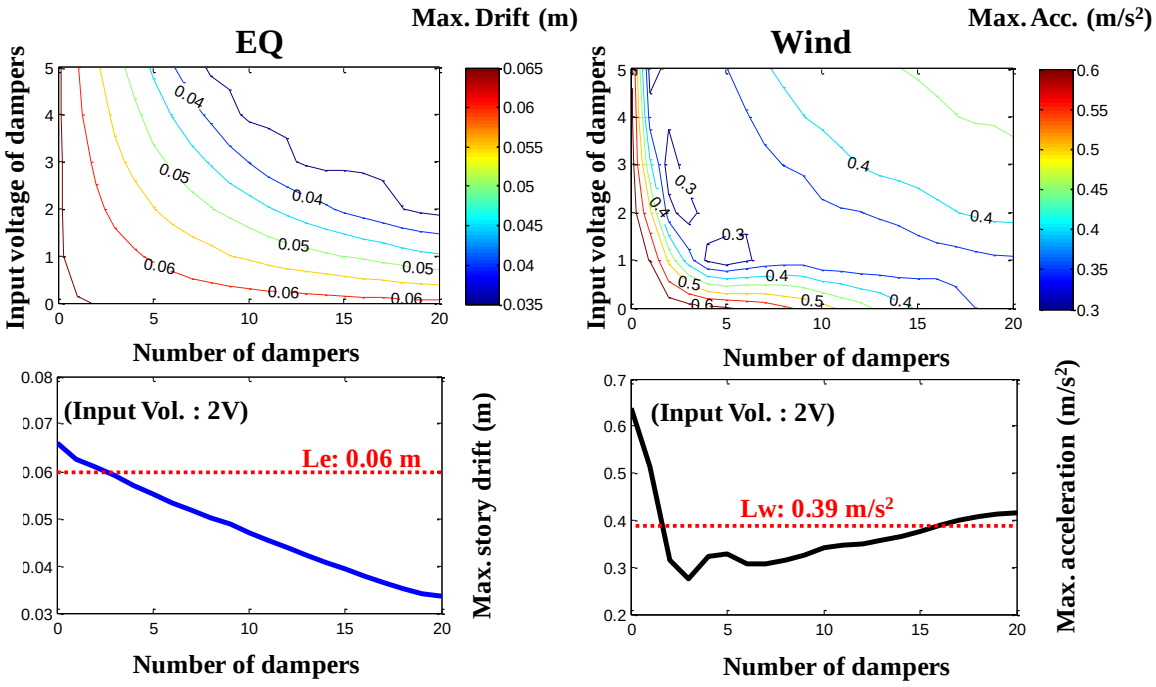

Fig. 14. Installing MR dampers at all floors uniformly (all floors)

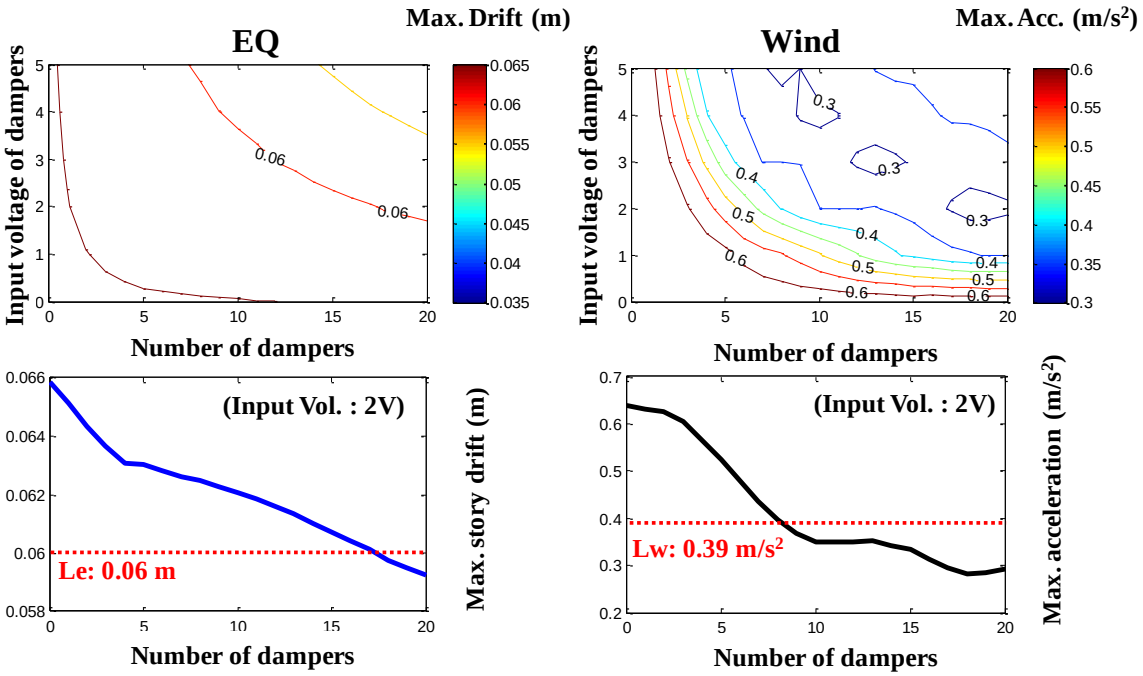

Fig. 15. Installing MR dampers at single floor (at the 10th floor or the top of 10-story building)

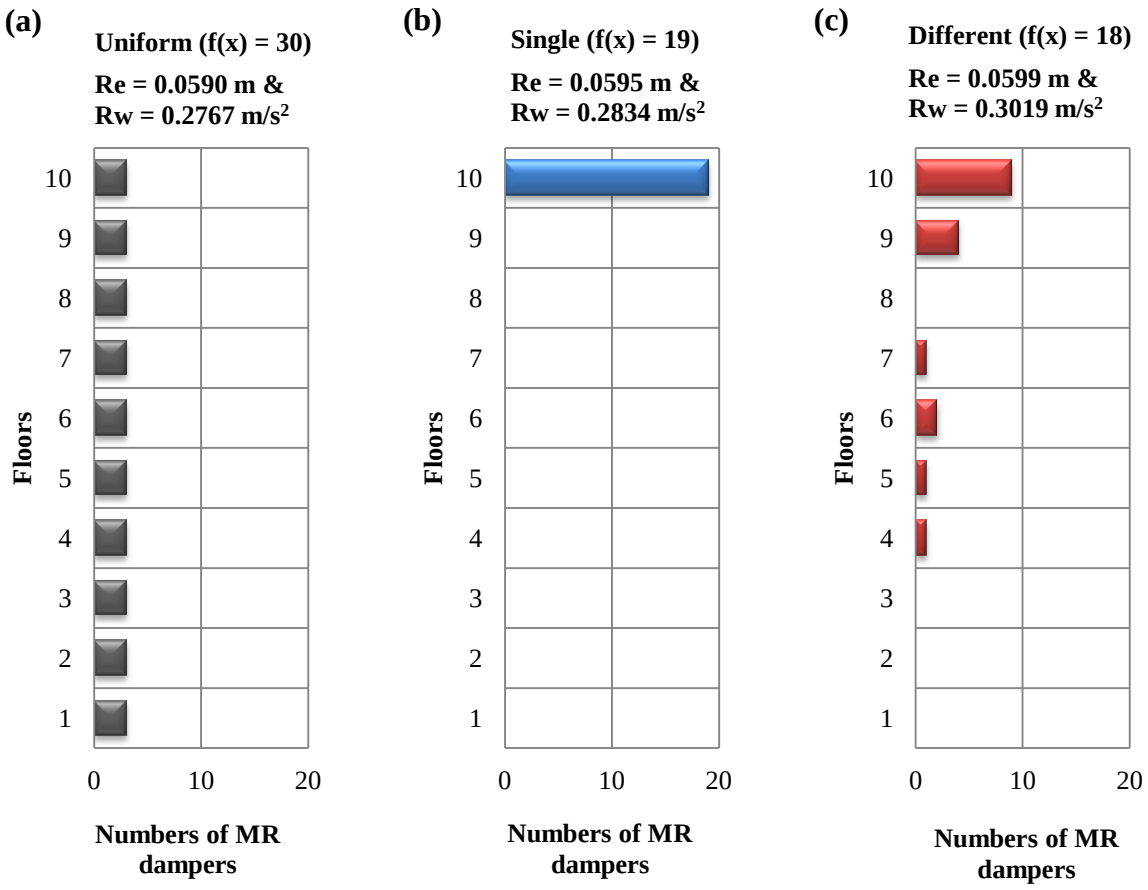

Fig. 16. Distribution of the numbers of MR damper along floors under a uniform 2 V input voltage signals: (a) uniformly installed at all floors (case 1); (b) installed at a single story (case 2); (c) differently installed at all floors (case 3)

PART VI

SUMMARY, CONCLUSIONS, AND RECOMMENDATIONS FOR FUTURE RESEARCH

1. Summary and Conclusions

This dissertation presents probabilistic approaches for effectively and efficiently dealing with external hazards in structures and systems. This thesis includes four main manuscripts that focus on describing the following key topics:

- Probabilistic risk assessment (PRA) framework for structural systems under multiple hazards using Bayesian statistics
- PRA based quantitative model validation approach.
- Efficient seismic fragility analysis method for coupled building-equipment-piping system using equivalent elastic limit state concept.
- Performance-based framework to determine the significance of multi-hazard risk in design of buildings under earthquake and wind loads

The summary and conclusions for each of these topics are given below.

1.1 Probabilistic risk assessment framework for structural systems under multiple hazards using Bayesian statistics

This part focuses on the development of a Bayesian framework for Probabilistic Risk Assessment (PRA) of structural systems under multiple hazards. The concepts of Bayesian network and Bayesian inference are combined by mapping the traditionally used fault trees into a Bayesian network. Unlike traditional fault tree analysis, such a mapping allows for consideration of dependencies as well as correlations between events. This is essential in risk

assessment for multi-hazard scenarios especially when correlated events are possible. Furthermore, Bayesian inference facilitates updating of prior information of all events based on new information or data that might become available from experimental studies, field observations, or high fidelity simulations. The primary conclusion of this study can be summarized as:

- The proposed Bayesian framework can consider statistical dependencies and correlations among different events and hazards in a relatively straightforward manner.
- Consideration of correlated events in the Bayesian framework allows appropriate treatment of multi-hazard scenarios.
- Applications to simple examples for single as well as multi-hazard scenarios illustrate that consideration of dependencies and correlations can result in a reduction of overall risk estimates both for mean as well as HCLPF values.
- Incorporation of Bayesian inference permits a novel approach for exploration of vulnerabilities beyond design events.
- The proposed approach for vulnerability beyond design basis assists in identification of events and the corresponding SSC that would lie on a critical path with respect to system level vulnerability.
- The critical path for vulnerability beyond design basis can be quite different from that corresponding to the design basis as calculated from a conventional PRA. Availability

of this information can be quite useful in managing the costs without compromising the safety by restricting additional studies on vulnerability to only those SSC that lie on the critical path.

1.2 Probabilistic risk assessment based model validation

A novel approach is explored in this part to quantitatively assess the validation of a system-level simulation based on the available information from component level validation. The proposed approach uses performance-based probabilistic risk assessment (PRA) as the basis for validation as well as for allocating resources towards improving the validation either by collecting additional data or by enhancing the accuracy of simulation tools. The approach builds upon characterizing the validation in terms of an overlapping coefficient which is described as the joint area under the experimentally obtained and simulation based probability density functions of basic parameters or events. The approach utilizes the power of Bayesian statistics by mapping a fault tree into a Bayesian network which allows consideration of non-Boolean relationships between events as well as allows consideration of correlated events in the network. Starting with the experimental and simulation based probability density functions of basic parameters or basic events, a Bayesian network is used to propagate the risk for the system. The fragilities and the risk associated with each intermediate event and the top event is calculated separately for both the experimental and simulation data. These two set of curves are then used for evaluating the overlapping coefficient of each event. The PRA based approach helps in identification of critical path

which helps in reducing the computational effort by focusing on only those events that lie on the critical path. Reliance on the events of critical path can also be used to determine the allocation of resources among different events for improving the validation at component or intermediate levels. When a validation between the experimental and simulation data is available for the basic parameters and not for the basic events directly in the network, a hidden layer is added below the basic events to relate the fundamental parameters to the basic events. The relationship between the hidden layer nodes and the basic event nodes can be defined by either a mechanistic model or a simulation based generation of response surface. Availability of new validation data, either through new experimental information or enhanced simulation tools, can be incorporated in a relatively straightforward manner by employing Bayesian updating to calculate posterior fragilities and the corresponding overlapping coefficients. The application of the proposed approach is illustrated through application examples.

1.3 Efficient seismic fragility assessment of coupled building-equipment-piping systems using equivalent elastic limit state concept

This part focuses on enhancements to an existing approach termed as equivalent limit state based methodology for evaluating the seismic fragility of secondary systems such as equipment and piping. The equivalent limit state concept focuses on arriving at a reasonably quick but accurate seismic fragility estimates which can be used as reliable prior information for a Bayesian updating framework. The Bayesian updating framework seeks to update the

prior fragility using only limited results from actual nonlinear simulations or real-life experimental fragility data thus minimizing the total effort required in estimating the seismic fragility to a desired degree of accuracy. The equivalent elastic limit state is a modified representation of the failure capacity of secondary system such that the damage probabilities are close to that obtained from the actual nonlinear analyses.

Enhancements to the concept of equivalent limit-state are presented in this study. The original formulation for the empirical equation of equivalent limit state was developed using a bilinear model to represent the localized nonlinearities in secondary systems. Such localized nonlinearities are typically exhibited at the joints of piping systems. However, the mounting arrangements in equipment and piping supports can often exhibit hysteretic behavior. Overall, three distinct enhancements are proposed:

- Consideration of a hysteretic model for the nonlinearities in the secondary system.
- Account for the effects of uncertainties in the nonlinear model and for non-classical damping. A coupled system becomes non-classically damped when the damping characteristics of the primary and secondary systems are different from each other.
- Account for the effect of asymmetric variation of the equivalent elastic limit state with respect to tuning ratio. The originally proposed formulation is symmetric and exhibits significant differences for systems in which tuning ratios are greater than zero.

Three different configurations of primary-secondary systems are used to illustrate the applicability and evaluate accuracy of the proposed approach. A total of 18 different models are created for each configuration by varying the tuning ratio, damping, and ductility values. It is shown that the proposed approach gives fragility curves that are close to those obtained from a comprehensive computationally intensive nonlinear time history analyses.

1.4 Significance of multi-hazard risk in design of buildings under earthquake and wind loads

A performance-based framework is proposed to evaluate if the design and retrofit of given building types are governed by a single dominant hazard or by a multi-hazard scenario. This study focuses solely on earthquake and wind hazards. However, the proposed framework is quite generic in nature and can be applied to other external hazards as well. The performance criteria for each hazard can be different and cover various different requirements of strength or serviceability. The proposed framework is well suited for integration into the actively growing research in the area of probabilistic risk assessment. At the same time, it is demonstrated that the proposed framework can easily be converted to deterministically characterized performance criterion in accordance with the deterministic demand and capacity requirements as specified traditionally in the various building codes and standards. Application of the proposed framework to three different geographical locations in the United States demonstrates the significance of a geographical location in a multi-hazard risk assessment. In addition, significance of multi-hazard design considerations is illustrated

through explorations of alternative retrofit solutions in two adjacent buildings located in close proximity to each other such as those encountered in a tight urban setting. The particular example considered for retrofit solution has been studied by many researchers in existing literature and considers connecting the two buildings through supplemental damping devices. It is observed that the number of dampers and their locations as determined from a multi-hazard design considerations are very different from those determined for a single dominant hazard. A related observation is that a solution that might satisfy the performance requirements for an earthquake is not necessarily acceptable with respect to the performance requirements for wind and vice-versa. It is also observed that appropriate risk assessment is highly dependent upon three primary considerations namely the performance criteria, building geometry, and geographical location within a multi-hazard risk scenario.

2. Recommendations for Future Research

Based on the experience gained in conducting this research, a few recommendations for future work on these topics are summarized below.

- The sensitivity of the total system risk to the correlations among basic events and components can be investigated for a more comprehensive identification of the critical components.
- The proposed framework would allow exploration of a top-down approach to allocate overall risk-goals among different subsystems and components.

- The applicability of the proposed approach for quantitative model validation needs to be assessed for more complex systems as well as for other hazards such as flooding.
- Accuracy and efficiency of equivalent limit-state concept needs to be evaluated for realistic primary-secondary systems such as building-equipment and building-piping system.
- Equivalent limit state concept can be evaluated for applicability to other types of nonlinear models such elasto-plastic, Takeda type model, Ramberg-Osgood model, flag shaped model and so on.
- Statistical nonlinear regression analysis or machine learning algorithms can be employed in order to increase the accuracy of equivalent limit state concept.
- Performance based multi-hazard risk framework is applied to design of tall buildings subjected to earthquake and wind loading. A similar approach can be developed for seismic and flooding scenario including correlated hazards.